

AN EVALUATION OF THE SEDIMENTOLOGY AND  
THE INFLUENCE OF GRAIN SIZE AND FACIES ON  
PERMEABILITY FOR THE WHITE ROSE A-17  
CORED INTERVAL, WHITE ROSE OILFIELD,  
OFFSHORE EASTERN NEWFOUNDLAND

CENTRE FOR NEWFOUNDLAND STUDIES

---

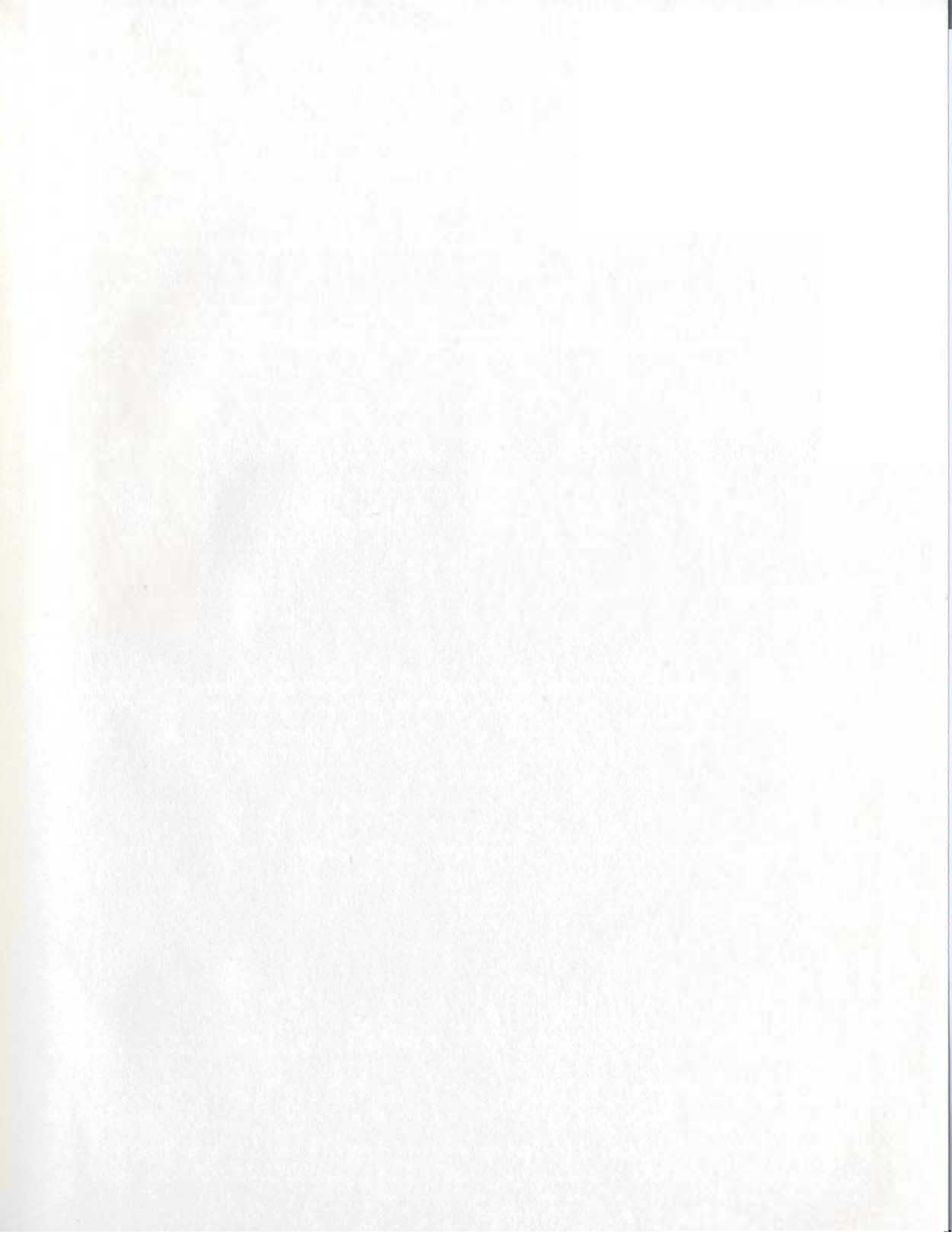
**TOTAL OF 10 PAGES ONLY  
MAY BE XEROXED**

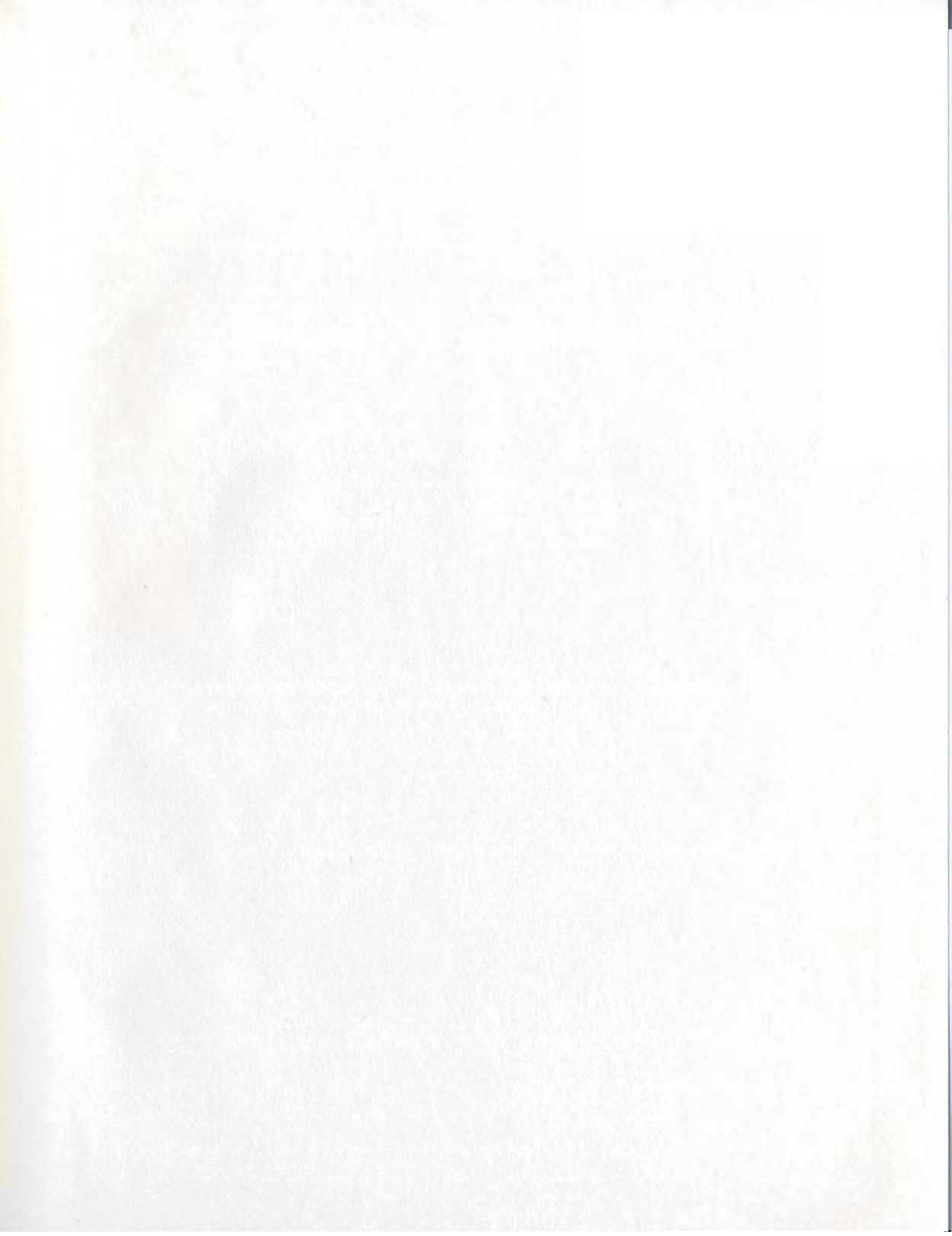
(Without Author's Permission)

MARK PETER FERRY











**An Evaluation of the Sedimentology and the Influence of Grain Size and  
Facies on Permeability for the White Rose A-17 Cored Interval, White  
Rose Oilfield, Offshore Eastern Newfoundland**

By  
Mark Peter Ferry

A thesis submitted to the School of Graduate Studies  
in partial fulfillment of the requirements  
for the degree of  
Master of Science



Department of Earth Sciences  
Memorial University of Newfoundland  
March 2005

## **ABSTRACT**

The A-17 cored interval from the Cretaceous Ben Nevis Formation of the White Rose oilfield, located approximately 350 km ESE of St. John's NL, consists of 106.25 m of predominantly shallow-marine shoreface deposits of which fine- to very fine-grained low angle cross-stratified and massive sandstones form the main hydrocarbon-bearing intervals. The principal focus of this thesis is to test aspects of the depositional model currently in use by industry geologists, and on the reservoir scale, investigate the influence of the sedimentology on reservoir fluid flow. Addressing these issues might assist in the future exploration and/or development of the White Rose oilfield.

To address these issues, grain size, sedimentary contacts, diagenetic and shelly components, and facies are described, classified, coded and/or quantified. These sedimentological data are integrated along with closely-spaced probe permeameter measurements into an extensive database, permitting direct comparison between sedimentological and permeability data.

Core from the White Rose A-17 well can be divided into 9 facies and displays 4 principal types of contacts/boundaries. Fine- to very fine-grained, low angle cross-stratified sandstone and structureless sandstone are the most abundant facies types, whereas planar laminated, moderately inclined cross-stratified, pervasively calcite-cemented, and shell-bearing sandstones are much less abundant. Bioturbated, very fine-grained sandstone and siltstone is restricted to the uppermost 5-6 m of the core. The most common contact type is erosive, followed by abrupt and cementation contacts. Erosive contacts represent bed boundaries; abrupt contacts represent internal surfaces within

beds. Gradational boundaries are uncommon and typically represent a decrease in grain size or the upward reduction of bioclastic material. Neither facies nor contacts/boundaries appear to be well organized vertically in the core.

The A-17 cored interval is interpreted to represent deposition in a high-energy, storm-dominated, middle to lower shoreface environment. This is based on the abundance of well sorted, very fine-grained quartzose sandstones, repeated fining-upward grain-size trends, a predominance of low-angle, gently curved, convex-up laminations, structureless beds, numerous erosional contacts overlain by transported bioclastic debris, rare mud and siltstone laminae, and limited biogenic structures.

Over the entire cored interval horizontal probe permeability measurements to air (kha) do not correlate well with grain size. Only in selected cases can linear correlations be established. Each grain size is typically associated with a range of permeabilities; these ranges generally increase with increasing grain size. Changes in permeability across contacts and intervals can occur without changes in grain size; however, where there are grain size changes there is a wide range of changes in permeability. The highest mean permeability and highest overall permeabilities occur in well sorted, clean, structureless sandstones. The lowest permeabilities occur in pervasively calcite-cemented sandstones. In addition to bioturbation and bioclastic material, poor sorting due to the presence of variable amounts of silty and carbonaceous debris appears to reduce permeability.

Results of this study demonstrate that for the White Rose A-17 cored interval, and potentially the south Avalon pool, a middle to lower shoreface depositional model is appropriate. Additionally, for indurated sandstones such as those represented in the White



Rose A-17 core, grain size may be used as a predictor of maximum permeability for given reservoir facies. However, because most facies have overlapping grain-size-permeability distributions, prediction of facies using grain size and permeability is likely not possible. To more accurately determine the controls on permeability, other factors such as cementation should be incorporated from petrographic and image analysis studies.

## **ACKNOWLEDGEMENTS**

First and foremost, I would like to acknowledge my thesis supervisors, Dr. R.N. Hiscott and Dr. R. Meyer, for their advice, encouragement and patience. Without their help this thesis would not have been possible. I would also like to thank these two individuals for nurturing my interests in sedimentology and giving me the opportunity to assist them in a number of sedimentology related courses.

I would like to express my gratitude to Dr. A. Pulham for suggesting this thesis project and for providing me with the opportunity to go to southwest Ireland and southwest Utah on sedimentology/stratigraphy related field trips. Both were valuable experiences that will never be forgotten.

Husky Energy is kindly thanked for providing the White Rose A-17 core, core photos, and probe permeametry data.

Many thanks to the faculty and staff of the Earth Sciences Department, especially Dr. A. Aksu for his assistance and encouragement during the course of this thesis.

I am grateful to the School of Graduate Studies for providing me with financial assistance in the form of a Graduate Student Fellowship. In addition, the Pan Atlantic Petroleum Systems Consortium (PPSC) graciously provided me with the funding necessary to complete this thesis.

An extended thanks goes to my two good friends, Michelle Spila and Sherif Awadallah, for their unprecedented help, encouragement and patience.

Last, and by no means least, I would like to acknowledge my parents, Peter and Donna Ferry, for their love and encouragement over the past two and a half years. I love you both very much.



## LIST OF TABLES

Table 2.1 Grain size comparator categories (letter and micrometer format) and the revised micrometer format used for this thesis.....	30
Table 2.2 Contact and Transitions and their codes.....	39
Table 2.3 Brief Description of facies and their corresponding numeric codes .....	41
Table 3.1 A brief summary of the facies identified in the White Rose A-17 core, the percentage of the core that they occupy, and their process interpretations .....	85
Table 3.2 Transition matrix for the nine facies identified in the White Rose A-17 core .....	86
Table 3.3 Transition matrix for the nine facies, the three types of erosive, and the three types of abrupt contacts .....	87
Table 4.1 Summary of the sorting values for the seven analyzed thin-sections.....	163
Table 4.2 Examples used to demonstrate the broad range of permeabilities and different average permeabilities for sandstones of the same grain size between the different units.....	165

## LIST OF PLATES

Plate 3.1 Examples of gently to moderately undulatory non-inclined erosive contacts as observed in the White Rose A-17 core.....	71
Plate 3.2 Examples of gently to moderately undulatory inclined erosive contacts as observed in the White Rose A-17 core.....	72
Plate 3.3 Examples of gently to highly curved, convex-up erosional contacts as observed in the White Rose A-17 core .....	74
Plate 3.4 Examples of very gently to moderately undulatory non-inclined abrupt contacts as recognized in the White Rose A-17 core .....	75
Plate 3.5 Examples of very gently to moderately undulatory inclined abrupt contacts as recognized in the White Rose A-17 core .....	77
Plate 3.6 Examples of gently to highly curved convex-up abrupt contacts as recognized in the White Rose A-17 core.....	78
Plate 3.7 Examples of cementation contacts as recognized in the White Rose A-17 core .....	80
Plate 3.8 Examples of cementation contacts between Facies 5 and Facies 6 as recognized in the White Rose A-17 core.....	81
Plate 3.9 Examples of gradational transitions as recognized in the White Rose A-17 core .....	83
Plate 3.10 Examples of Facies 1 - Fine- to very fine-grained structureless sandstone.....	89
Plate 3.11 Examples of Facies 2 - Very fine- to fine-grained planar laminated sandstone.....	94
Plate 3.12 Examples of Facies 3 - Low angle cross-stratified fine- to very-fine grained sandstone.....	99
Plate 3.13 Examples of Facies 3 - Low angle cross-stratified fine- to very fine-grained sandstone.....	100

## LIST OF PLATES (Continued)

Plate 3.14 Examples of Facies 4 Type 1- Moderately inclined, cross-stratified fine- to very fine-grained sandstone .....	107
Plate 3.15 Examples of Facies 4 Type 2 - Moderately inclined very fine-grained cross-stratified sandstone with abundant carbonaceous and silty debris.....	108
Plate 3.16 Examples of Facies 5 - Pervasively calcite-cemented sandstone .....	112
Plate 3.17 Examples of Facies 6 - Pervasively calcite-cemented sandstone with abundant shelly material .....	116
Plate 3.18 Examples of Facies 7 - Shell-serpulid -and siderite-bearing sandstone .....	119
Plate 3.19 Examples of Facies 8 - Shelly sandstone.....	123
Plate 3.20 Examples of Facies 9 - Bioturbated very fine-grained sandstone and siltstone.....	126



## TABLE OF CONTENTS

ABSTRACT .....	ii
ACKNOWLEDGEMENTS .....	v
TABLE OF CONTENTS .....	vii
LIST OF FIGURES .....	x
LIST OF TABLES .....	xiii
LIST OF PLATES .....	xiv
CHAPTER1: GRAND BANKS, JEANNE d’ARC BASIN AND WHITE ROSE FIELD.1	
1.1 Introduction .....	1
1.2 Regional Setting and Geology .....	1
1.3 Evolution of the Grand Banks and its Basins .....	3
1.4 Jeanne d’Arc: Location, Structure, and Stratigraphy .....	8
1.5 White Rose field: Location, Structure, and Stratigraphy .....	10
1.6 Exploration History of the White Rose field .....	18
1.7 Remaining Problems in Understanding the Reservoir Geology of the White Rose Field, and Thesis Objectives .....	21
1.9 Thesis Outline .....	23
CHAPTER 2: METHODS AND DATA TYPES .....	24
2.1 Introduction .....	24
2.2 Choice of the A-17 Well: Location, Thickness and Reservoir Facies .....	24
2.3 Types of Data Collected and Methods.....	27
2.3.1 Grain Size .....	28
2.3.1.1 Rationale for Measuring Grain Size .....	28
2.3.1.2 Method of Grain Size Measurement .....	29
2.3.1.2 Calibration of the Grain Size Card .....	29
2.3.1.3 Grain Size Subdivisions.....	31
2.3.1.4 Location of Grain Size Measurements, Measurement Repeatability, Measurements Accuracy, and Sorting .....	32
2.3.2 Fossils and Diagenetic Components .....	34
2.3.3 Contacts and Other Transitions .....	35
2.3.4 Facies .....	40
2.4 Probe Permeametry .....	40
2.5 X-Radiography.....	42
CHAPTER 3: SEDIMENTOLOGY OF THE WHITE ROSE A-17 CORE .....	43
3.1 Introduction .....	43
3.2 Grain Size and Grain-Size Trends .....	43
3.2.1 Grain Size .....	43
3.2.2 Grain-Size Trends .....	47
3.2.2.1 First Order Grain-Size Trends .....	47
3.2.2.2 Interpretation and Implications .....	50
3.2.2.3 Second Order Grain-Size Trends .....	50
3.2.2.4 Interpretation and Implications .....	65

## TABLE OF CONTENTS (Continued)

3.2.2.5 Third Order Grain-Size Trends .....	66
3.2.2.6 Interpretation and Implications .....	68
3.3 Contacts and Transitions .....	69
3.3.1 Introduction .....	69
3.3.2 Erosive Contacts .....	70
3.3.3 Abrupt Contacts .....	73
3.3.4 Cementation Contacts .....	76
3.3.5 Gradational Transitions .....	82
3.4 Facies .....	84
3.4.1 Introduction .....	84
3.4.2 Description of Facies 1 .....	88
3.4.2.1 Process Interpretation for Facies 1 .....	91
3.4.3 Description of Facies 2 .....	93
3.4.3.1 Process Interpretation for Facies 2 .....	95
3.4.4 Description of Facies 3 .....	98
3.4.4.1 Process Interpretation for Facies 3 .....	102
3.4.5 Description of Facies 4 .....	106
3.4.5.1 Process Interpretation for Facies 4 .....	111
3.4.6 Description of Facies 5 .....	111
3.4.6.1 Process Interpretation for Facies 5 .....	114
3.4.7 Description of Facies 6 .....	115
3.4.7.1 Process Interpretation for Facies 6 .....	117
3.4.8 Description of Facies 7 .....	118
3.4.8.1 Process Interpretation for Facies 7 .....	122
3.4.9 Description of Facies 8 .....	122
3.4.9.1 Process Interpretation of Facies 8 .....	125
3.4.10 Description of Facies 9 .....	125
3.4.10.1 Interpretation for Facies 9 .....	128
3.5 Depositional Environment .....	131
3.5.1 Previous Interpretations .....	131
3.5.2 Interpretation Developed for this Thesis .....	135
3.5.3 Problems with the Depositional Model .....	140
CHAPTER 4: LINKS BETWEEN GRAIN SIZE, FACIES, AND PERMEABILITY .....	142
4.1 Introduction .....	142
4.2 Permeability: Definition, Importance, and Controls .....	142
4.2.1 Definition .....	142
4.2.2 Importance .....	144
4.2.3 Controls .....	144
4.2.3.1 Compaction and Cementation: Their Affect on Permeability .....	146
4.2.3.2 Textural Controls on Permeability .....	147
4.2.3.2.1 Grain Size and Permeability .....	147

## TABLE OF CONTENTS (Continued)

4.2.3.2.2 Sorting and Permeability .....	148
4.2.3.2.3 Grain Shape, Fabric, and Permeability .....	149
4.2.3.3 Sedimentary Structures and Permeability .....	150
4.2.3.4 Depositional Environments and Permeability .....	151
4.3 Permeability: Description of the A-17 Core Data and its Relation to Grain Size	153
4.3.1 Introduction .....	153
4.3.2 Permeability Data .....	154
4.3.3 Permeability and its Relation to Grain Size .....	157
4.3.3.1 For the Entire Cored Interval .....	157
4.3.3.2 For the Three Units .....	162
4.3.3.3 For Small-Scale Intervals .....	167
4.4 Parallel and Unrelated Changes in both Grain Size and Permeability Across Contacts and Gradational Transitions .....	171
4.5 Relationships between Grain Size, Permeability, and Facies .....	176
4.5.1 Permeability-Grain-Size Relationships for Facies in the White Rose A-17 Core... .....	177
4.5.2 Permeability-Grain-Size Relationships for Facies in the Lower and Middle Parts of the A-17 Core .....	180
4.5.3 Distribution of Permeabilities for Each Facies .....	182
4.5.4 Interpretation of the Permeability Data for Each Facies .....	186
CHAPTER 5: CONCLUSIONS, RECOMMENDATIONS, AND IMPLICATIONS....	195
5.1 Introduction .....	195
5.2 Inventory of the Main Conclusions .....	196
5.2.1 Sedimentology and Depositional Environments .....	196
5.2.2 Sedimentology and its Relation to Permeability .....	197
5.3 Recommendations for Future Studies .....	201
5.4 Implications for the Future Development and/or Exploration of the White Rose Field .....	203
REFERECES CITEED .....	205
APPENDIX A (CD with Excel File of the White Rose A-17 Core Sedimentological and Permeability Data) .....	215
APPENDIX B (Logs with Sedimentological and Permeability Data).....	216



## LIST OF FIGURES

Figure 1.1 Rift basins of the Grand Banks and the Precambrian and Paleozoic basement highs that separate them.....	2
Figure 1.2 Lithostratigraphy of the Jeanne d’Arc Basin .....	5
Figure 1.3 Configuration and location of significant discoveries within the Jeanne d’Arc Basin .....	9
Figure 1.4 Major structural elements that delimit the Jeanne d’Arc Basin .....	11
Figure 1.5 Regional Composite-Marker Time-Structure Map, at or near the base of the Ben Nevis reservoir .....	12
Figure 1.6 Structural cross-section through the south White Rose field .....	13
Figure 1.7 Generalized stratigraphy of the White Rose field .....	15
Figure 2.1 List of Symbols for the White Rose A-17 cored interval litholog .....	25
Figure 2.1 (Cont’d) Generalized litholog of the White Rose A-17 cored interval .....	26
Figure 3.1 Grain-size distribution for the White Rose A-17 core.....	45
Figure 3.2 Cumulative % grain size for grains measured in the White Rose A-17 core.....	46
Figure 3.3 Smoothed grain-size profile for the White Rose A-17 core.....	48
Figure 3.4 Plot of Grain size (microns, at fixed standard values) vs. Depth (meters) .....	49
Figure 3.5 Histogram of bed thickness for the White Rose A-17 core.....	51
Figure 3.6 Grain size vs. Depth from 2950-2940 m .....	53
Figure 3.7 Grain size vs. Depth from 2960-2950 m .....	54
Figure 3.8 Grain size vs. Depth from 2970-2960 m .....	55
Figure 3.9 Grain size vs. Depth from 2980-2970 m .....	56

## LIST OF FIGURES (Continued)

Figure 3.10 Grain size vs. Depth from 2990-2980 m .....	57
Figure 3.11 Grain size vs. Depth from 3000-2990 m .....	58
Figure 3.12 Grain size vs. Depth from 3010-3000 m .....	59
Figure 3.13 Grain size vs. Depth from 3020-3010 m .....	60
Figure 3.14 Grain size vs. Depth from 3030-3020 m .....	61
Figure 3.15 Grain size vs. Depth from 3030-3040 m .....	62
Figure 3.16 Grain size vs. Depth from 3040-3047 m .....	63
Figure 3.17 Histogram displaying the frequency of thickness for the 566 intervals in the White Rose A-17 core.....	67
Figure 3.18 Grain size ( $\mu\text{m}$ ) vs. Depth (m) for facies 1, 2, and 3.....	90
Figure 3.19 Bedform stability diagram.....	97
Figure 3.20 Conceptual bedform phase diagrams for variable current type, current velocity, and grain size .....	105
Figure 3.21 Grain size ( $\mu\text{m}$ ) vs. Depth (m) for facies 4, 5, and 6.....	109
Figure 3.22 Grain size ( $\mu\text{m}$ ) vs. Depth (m) for facies 7, 8, and 9.....	121
Figure 3.23 Shoreface settings and position of characteristic shallow-marine ichnofacies .....	129
Figure 3.24 Schematic of a shoreline cross-section used to illustrate the proximal to distal relationships of HCS beds.....	138
Figure 4.1 An interpretation of the effects of various controls on porosity and permeability .....	145
Figure 4.2 Permeability frequency distribution for the White Rose A-17 cored interval with all data, and minus permeabilities from Facies 5 and Facies 6 .....	155

## LIST OF FIGURES (Continued)

Figure 4.3 Frequency distribution of the logarithms of all permeabilities greater than or equal to mD.....	156
Figure 4.4 Vertical permeability profile for the White Rose A-17 cored interval .....	158
Figure 4.5 Vertical permeability profile and vertical grain size profiles for the White Rose A-17 cored interval set side by side for comparison .....	159
Figure 4.6 Grain size ( $\mu\text{m}$ ) vs. Permeability mD for the White Rose A-17 cored interval .....	161
Figure 4.7 Grain size ( $\mu\text{m}$ ) vs. Permeability mD for the lower (L), middle (M), and upper (U) units of the White Rose A-17 core .....	164
Figure 4.8 Selected intervals to demonstrate the apparent close relationship between grain size and permeability.....	168
Figure 4.9 Grain size ( $\mu\text{m}$ ) vs. Permeability mD cross plots for the four small-scale intervals selected to demonstrate the apparent close relationship between grain size and permeability .....	170
Figure 4.10 lots of change in Grain size ( $\mu\text{m}$ ) vs. change in Permeability mD across erosive and abrupt contacts and gradational boundaries.....	173
Figure 4.11 Grain size ( $\mu\text{m}$ ) vs. Permeability mD cross plots for Facies 1, 2, 3, 4, 7, 8, and 9.....	178
Figure 4.12 Grain size ( $\mu\text{m}$ ) vs. Permeability mD cross plots for Facies 1, 2, 3, 4 and 8 for the middle and lower units .....	181
Figure 4.13 Permeability frequency distributions for Facies 1, 2, 3, 4, 7, 8, and 9 with 95 % confidence limits about their means .....	184
Figure 4.14 Grain size ( $\mu\text{m}$ ) vs. Permeability mD for Facies 4 (Type 1) and (Type2).....	189
Figure 4.15 Grain size ( $\mu\text{m}$ ) vs. Permeability (mD) cross plot for Facies 7.....	192

# **CHAPTER 1**

## **GRAND BANKS, JEANNE d'ARC BASIN, AND WHITE ROSE FIELD**

### **1.1 Introduction**

The goal of this chapter is to provide an overview of the evolution and geology of the Grand Banks and its basins, with emphasis on the structure and stratigraphy of the Jeanne d'Arc Basin and, in the easternmost part of the Jeanne d'Arc basin, the White Rose field. Topics specific to the White Rose field which are addressed include the exploration history of the field, the development of the field, and remaining problems in understanding the reservoir geology. This latter topic leads into the thesis objectives. The final section of this chapter outlines the topics covered in the thesis chapters.

### **1.2 Regional Setting and Geology**

The broad continental margin off Newfoundland's east coast encompasses an area of approximately 36,000 square kilometers, and is host to a series of northeast-trending, interconnected Mesozoic rift basins separated by Precambrian and Paleozoic basement highs (Figure 1.1). Development of the rift basins and the continental margin around the Grand Banks is inherently linked to break-up of the Pangaeian Supercontinent and sequential south to north opening of the North Atlantic Ocean. Various authors (Haworth and Keen, 1979; Hubbard et al., 1985a; Tankard and Welsink, 1987; Enachescu, 1987) note that the development, geometry and distribution of basins on the Grand Banks was controlled in part by the Mesozoic extension direction and the pre-existing tectonic fabric

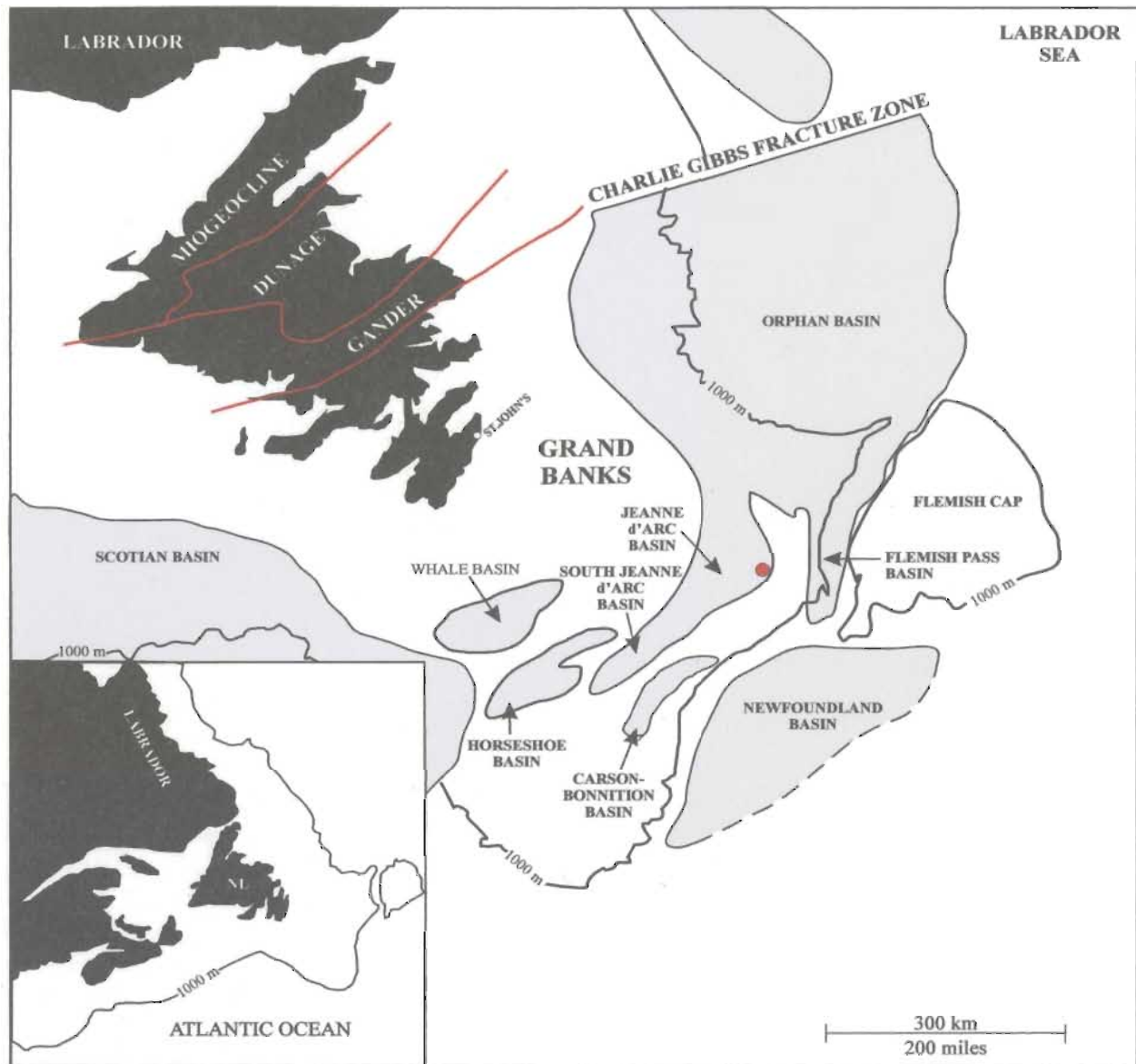


Fig.1.1. Mesozoic rift basins of the Grand Banks and the Precambrian and Paleozoic basement highs that separate them. Rift basins are in gray and basement highs are in white. Red circle indicates the approximate position of the White Rose field. Modified from Keen et al. (1987).

in the Avalon and Meguma zones. A tectonic history of the break-up of Pangea and opening of the Atlantic Ocean is preserved in the thick sequences of strata in the rift basins of the Grand Banks (Enachescu, 1987).

### **1.3 Evolution of the Grand Banks and its Basins**

Three rifting episodes affected the Grand Banks region beginning in the Late Triassic, ceasing by mid-Cretaceous time (Haworth and Keen, 1979; Enachescu, 1987). Each phase of extension was followed by a prolonged period of thermal and/or fault-induced subsidence as expressed by thick limestone and shale successions that extend across the basins (McAlpine, 1990).

The initial rift phase, termed the Tethys rift (Jenkyns, 1980; Lemoine, 1983; Bernoulli, 1984), began in the Late Triassic and ceased by mid-Pliensbachian (mid-Early Jurassic) time. Extension occurred in a northwest-southeastward direction, forming a series of northeast-southwest-trending rift basins. The trend of these basins on the Grand Banks is parallel with tectonostratigraphic elements of the Avalon Zone of the Appalachian Orogen exposed on Newfoundland (Grant et al., 1986).

During the first rift episode, continental red beds and restricted marine evaporite deposits filled the newly developed extensional basins. These deposits belong to the Eurydice and Argo formations respectively. By the end of this first rifting phase, nearly all the present-day troughs and basins had been initiated and the southern Grand Banks transform margin was established (Enachescu and Dunning, 1994).

Following this initial rift phase, a thermal subsidence phase ensued, beginning in the mid-Pliensbachian and ending in Kimmeridgian time. It was during this time that a broad epicontinental sea occupied the Grand Banks and thick accumulations of shale and limestone were deposited. In the Jeanne d'Arc basin, a strong, mid-Jurassic seismic marker, the Whale Member of the Downing Formation, was deposited. This widespread limestone reflects the stability of the basin at this time. Approaching the end of this thermal subsidence phase, important source rocks belonging to the Egret Member of the Rankin Formation (Figure 1.2) were deposited in restricted, silled, anoxic basins. These calcareous, organic-rich, oil-prone shales are the principal proven source rocks for the Hibernia, Terra Nova and the White Rose fields (McAlpine, 1990).

A second episode of extension began at the end of the Jurassic (Kimmeridgian time), rejuvenating existing rift basins and opening new depositional areas on the Grand Banks. In the Jeanne d'Arc Basin, the prominent Kimmeridgian Unconformity (Figure 1.2) reflects the beginning of this renewed episode of rifting. Extension was directed east-west leading to the separation of Iberia from Newfoundland by the late Early Cretaceous, thus establishing the eastern limit of the Grand Banks (Keen et al., 1987). This second rift episode is known as the North Atlantic rift (Keen and Barret, 1981; Jansa et al., 1979; Wade, 1981; McWhae, 1981; Storetvedt, 1985). This event is believed to have been an important source of siliciclastic input into the Jeanne d'Arc Basin. Sediment for three of the four main reservoirs was provided during this time. These are the Jeanne d'Arc, Hibernia, and Catalina Formations (Figure 1.2).



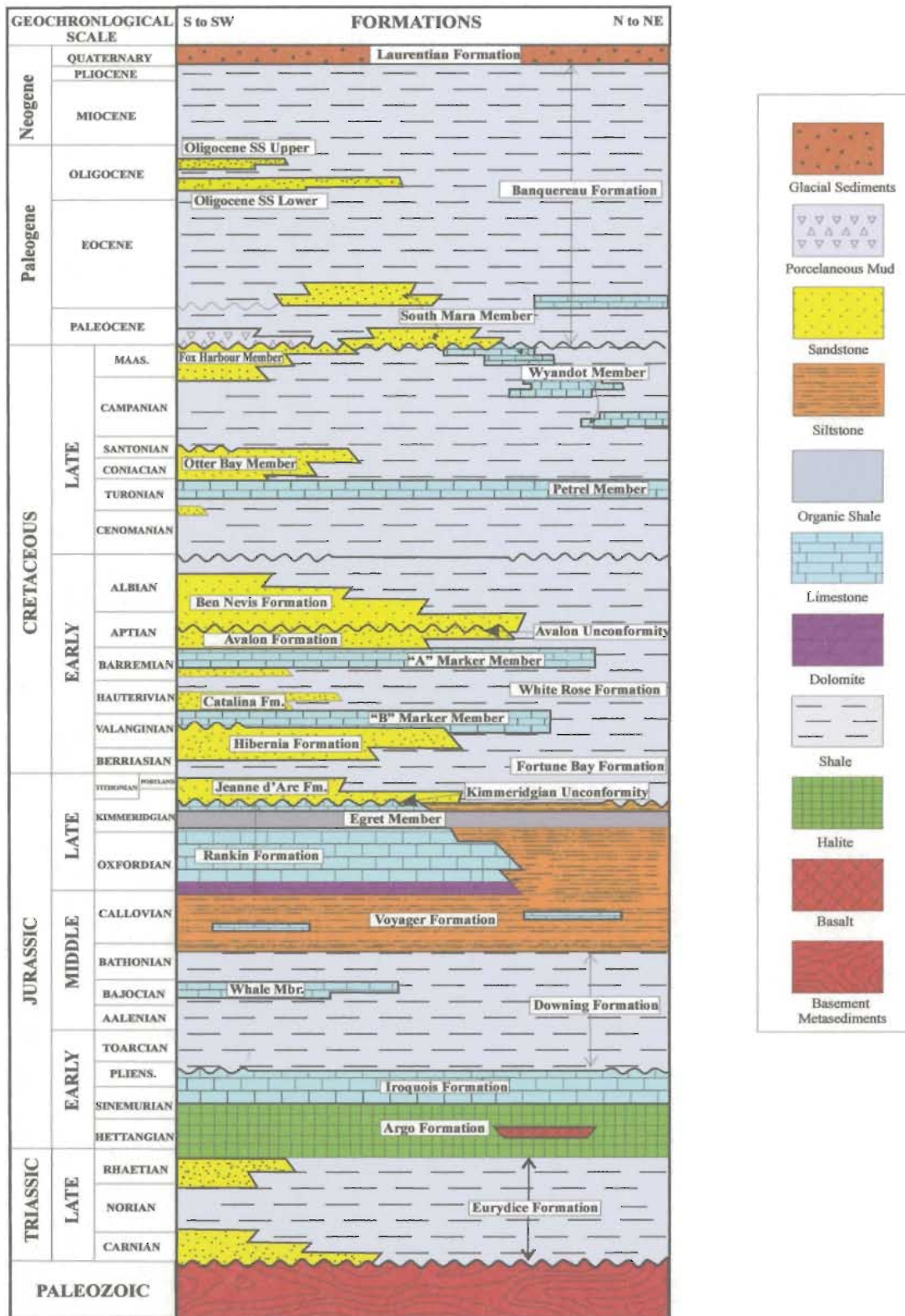


Fig.1.2. Lithostratigraphy of the Jeanne d'Arc Basin. Modified from Sinclair (1988).

Beginning in the mid-Early Cretaceous, a second phase of thermal subsidence began. In the Jeanne d'Arc Basin, this is expressed by thick successions of shale assigned to the White Rose Formation (Figure 1.2), punctuated by laterally persistent limestones, signifying a return to basin stability. The "B" Marker, a limestone unit found above the Hibernia Formation, and the "A" Marker, found below the Avalon Formation (Figure 1.2), provide excellent regional stratigraphic and seismic markers.

A third and final episode of structural deformation to affect the Grand Banks began in Aptian-Albian time. Extension was directed northeast-southwest leading to the separation of North America from Greenland-Northwest Europe and establishment of Newfoundland's northeastern continental margin (Masson and Miles, 1984; Srivastava and Tapscott, 1986). During this time, a number of northwest-southeast-trending normal faults severely fragmented the basins and intervening basement highs (Husky Energy, 2004). This third rift episode appears to be associated with a period of uplift and erosion, producing a prominent unconformity or series of unconformities, collectively termed the Avalon Unconformity (Jansa and Wade, 1975). The hiatus represents as much as 50-60 million years of erosion over the southern and central Grand Banks, and as various authors point out (Keen et al., 1987) the Avalon Unconformity is laterally equivalent to a number of unconformities and intervening stratigraphic units in basins flanking the Avalon uplift. In the south, the Avalon unconformity is underlain by Middle Jurassic to basal Lower Cretaceous strata, and overlain by 1-2 km of Upper Cretaceous and younger sedimentary rocks and strata (Keen et al., 1987). In the north, the Avalon Unconformity is less easily identified, as it is not an angular unconformity and is more deeply buried

under post-rift sediments of Late Cretaceous and younger age. Uplift and erosion of the broad regional arch on the southern Grand Banks (Avalon Uplift) during the Late Jurassic to Early Cretaceous is believed to have been an important source of siliciclastic input into the Jeanne d'Arc Basin. By the end of the second rift phase, the present-day configuration of the Grand Banks and its basins was in place (Keen et al., 1987).

During Cenomanian time, a third and final thermal subsidence phase began and the whole Grand Banks area subsided as an intact block (Tankard and Welsink, 1987). Marine shale, chalky limestone, shelf sandstone and turbidite sequences of the Dawson Canyon, Wyandot, and Banquereau formations (Figure 1.2) were deposited during the Late Cretaceous to Paleogene and Neogene on the subsiding passive margin (Keen et al., 1987). At the top of the Cretaceous section there is a regional unconformity indicating a marked relative sea-level drop, which resulted in the deposition of submarine fans (South Mara Member sandstones) at the toe of the Late Cretaceous slope (DeSilva, 1994). Throughout the Paleogene and Neogene, low sediment influx, long-term subsidence and tilting led to the deposition of a structurally undisturbed marine succession, typical of the drift phase of a passive margin (McAlpine, 1990). In the Jeanne d'Arc Basin, mainly marine shales and minor chinks of the Banquereau Formation characterize the Tertiary. However, two regressive sandstone units appear to signify the return to shallow marine and paralic environments in the Oligocene (Pemberton et al., 2001). Since the Tertiary, most sediment on the Grand Banks has been glacio-marine in origin.

#### **1.4 Jeanne d'Arc Basin: Location, Structure and Stratigraphy**

Of the nine basins that occupy the Grand Banks, it is the Jeanne d' Arc Basin that has proven most prospective for oil accumulation and entrapment; thus it is of great interest to oil companies. To date, all major oil and gas discoveries off Newfoundland's east coast are restricted this basin (Figure 1.3) (DeSilva, 2004). The Jeanne d'Arc Basin is located approximately 300 km east-southeast of St. John's Newfoundland (Figure 1.1), and encompasses an area of approximately 10,500 km<sup>2</sup> (Husky Energy, 2004). The Jeanne d'Arc Basin is one of the largest, and is the deepest of all the interconnected basins found beneath the Grand Banks (Keen et al. 1987; Tankard and Welsink, 1987). Upwards of 14 km of syn-rift fill are contained within the basin (Figure 1.3). The basin is an asymmetrical half graben, narrow in the south and widening towards the north, forming an elongate trough oriented north-northeast (Driscoll and Hogg, 1995). Major tectonic elements, active during the development of the basin, now form its boundaries. To the west, the Jeanne d'Arc Basin is limited by the Bonavista Platform and by the Murre Fault that separates the basin and the platform (Figure 1.4). In the east it is bounded by the Central Ridge Complex, and to the south by the Avalon Uplift (Figure 1.4). Internally the basin is characterized by a series of trans-basinal fault trends (Sinclair et al., 1992). A majority of these faults terminate below or at the Albian-Cenomanian unconformity, indicating that structural development was essentially complete by the Late Cretaceous (Grant et al., 1986).

The thick succession of sedimentary strata contained within the Jeanne d'Arc Basin is host to three key sandstone reservoirs. These are the Upper Jurassic (Tithonian)

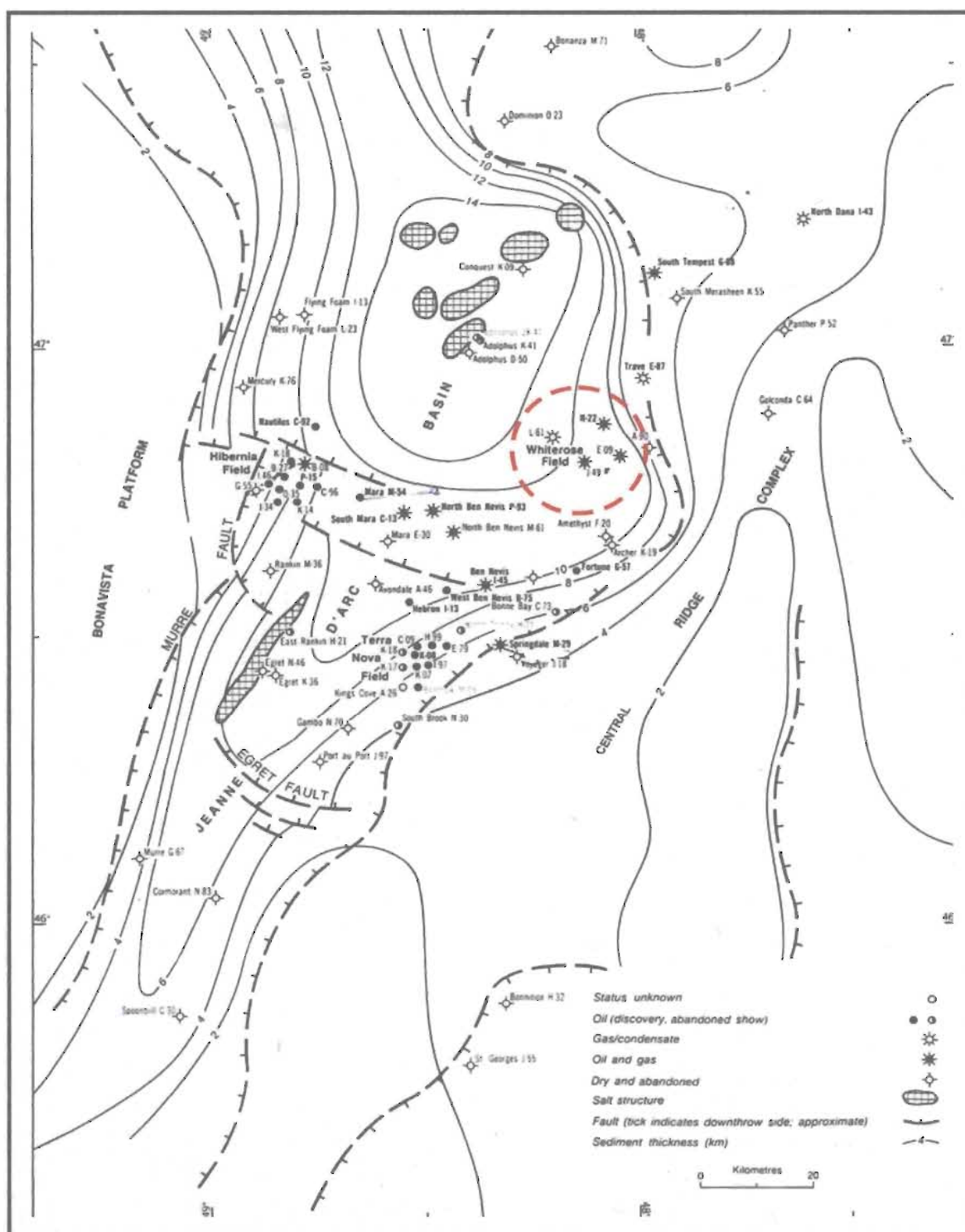


Fig.1.3. Configuration and location of significant discoveries within the Jeanne d'Arc Basin. Figure also displays the position of major faults, salt structures, and sediment thickness in kilometers. White Rose field is encompassed by the dashed circle. After Keen et al. (1987).

Jeanne d'Arc Formation, the Lower Cretaceous (Berriasian to Valanginian) Hibernia Formation and the mid-upper Lower Cretaceous (Aptian-Albian) Ben Nevis Formation (see Figure 1.2). Production at White Rose will be from a thick succession of fine to very fine-grained sandstones of the Ben Nevis Formation (Sinclair, 1995a).

### **1.5 White Rose Field: Location, Structure and Stratigraphy**

The White Rose field is situated on the northeastern flank of the petroliferous Jeanne d'Arc Basin, approximately 350 km ESE of St. John's (Figure 1.1), and approximately 50 km equidistant from both the Hibernia and Terra Nova fields, in 120 m of water (Figure 1.4). Structurally, the field is complicated (Figure 1.5). It is cored by salt at depth and consists of numerous rotated fault blocks (Husky Energy, 2004). It owes its current configuration to extensional tectonics and halokinesis, which are intimately linked to the three rift episodes responsible for the development of the Grand Banks and its basins. Three main structural features surround the field. To the east it is the basin-bounding Voyager Fault Zone; to the north is the White Rose Diapir, and to the south is the Amethyst Ridge (Figure 1.5) (Husky Energy, 2004). Structurally, the field is located in a highly faulted area on the hanging wall of the Voyager Fault above the White Rose Diapir and Amethyst Ridge (Figure 1.5) (Husky Energy, 2004). Three sets of faults oriented northwest–southeast, north–south and northeast–southwest dissect the area (Figure 1.5). Sealing faults separate three pools, which comprise the field.

During the third episode of rifting, imbricates of the Voyager Fault created a series of tilted fault blocks in the southern part of the field (Figure 1.6). The faults that



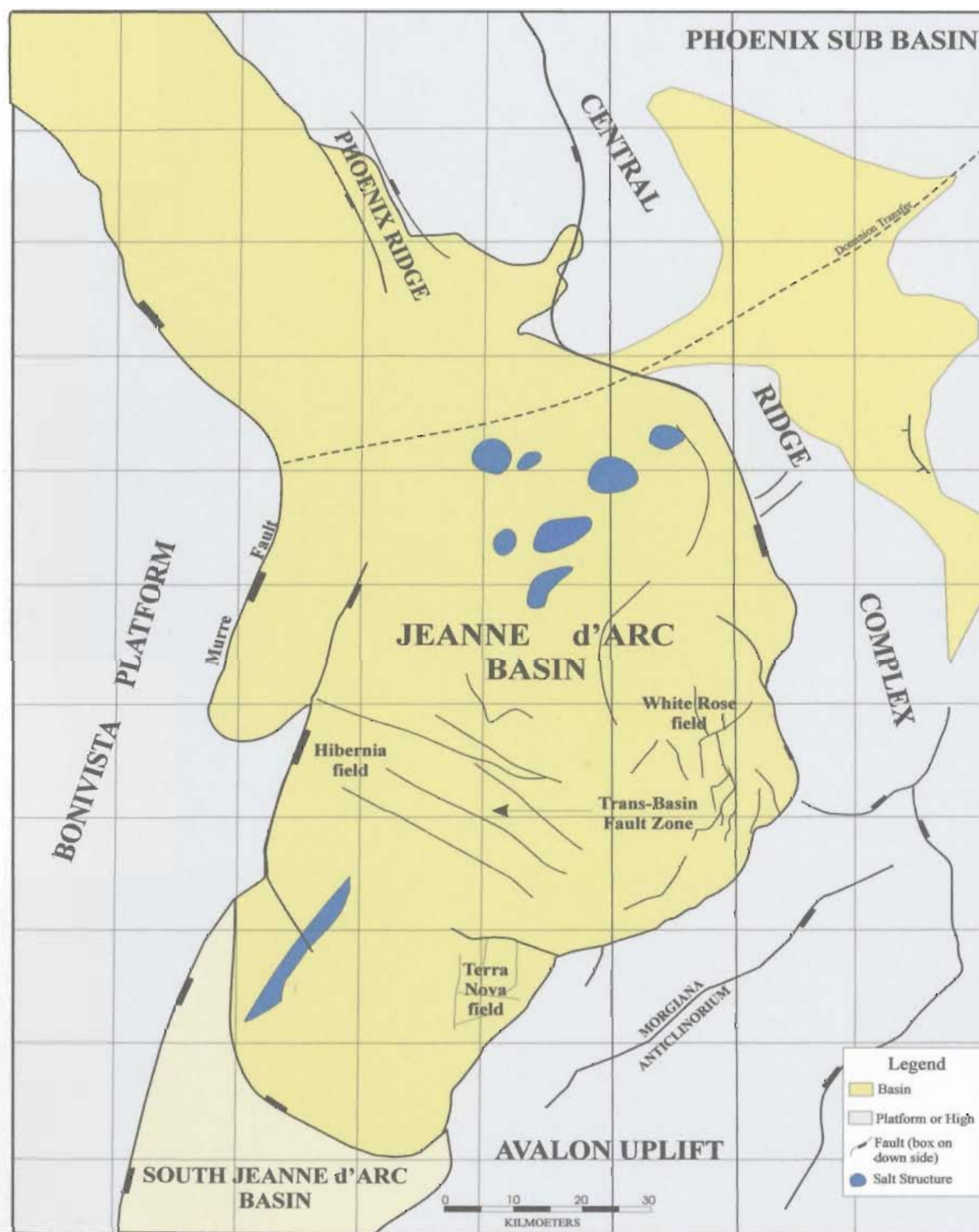


Fig.1.4. Major structural elements that delimit the Jeanne d'Arc Basin and the locations of the Hibernia, Terra Nova and White Rose fields. Modified from Husky Energy (2003).



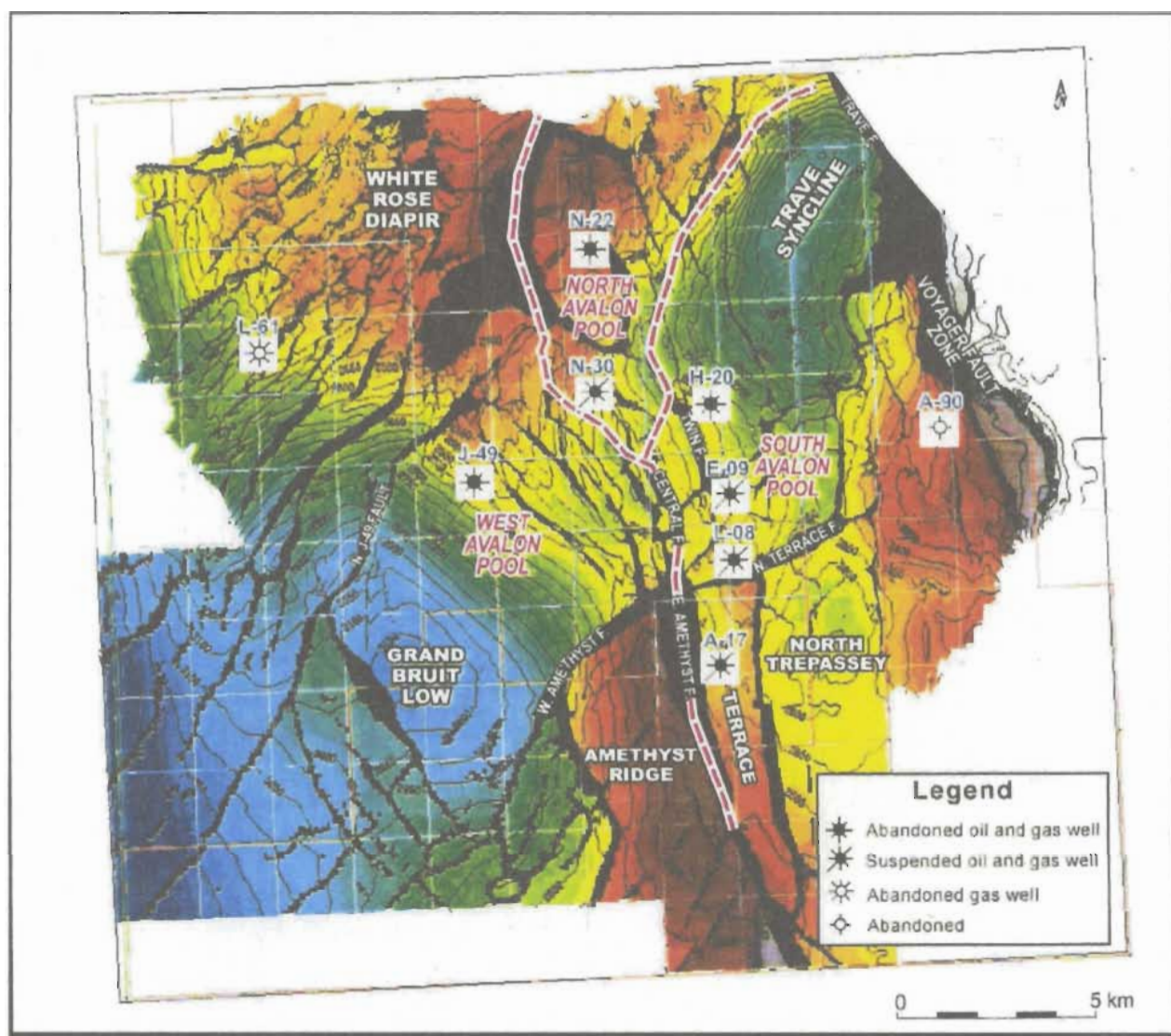


Fig.1.5. Regional Composite-Marker Time-Structure Map, at or near the base of the Ben Nevis reservoir. The major structural features surrounding the White Rose field are shown (F=Fault). Note the series of north to south, northwest to southeast and northeast to southwest faults that dissect the field. The location of the Trave E-87 well is not shown. After Husky Energy (2003).

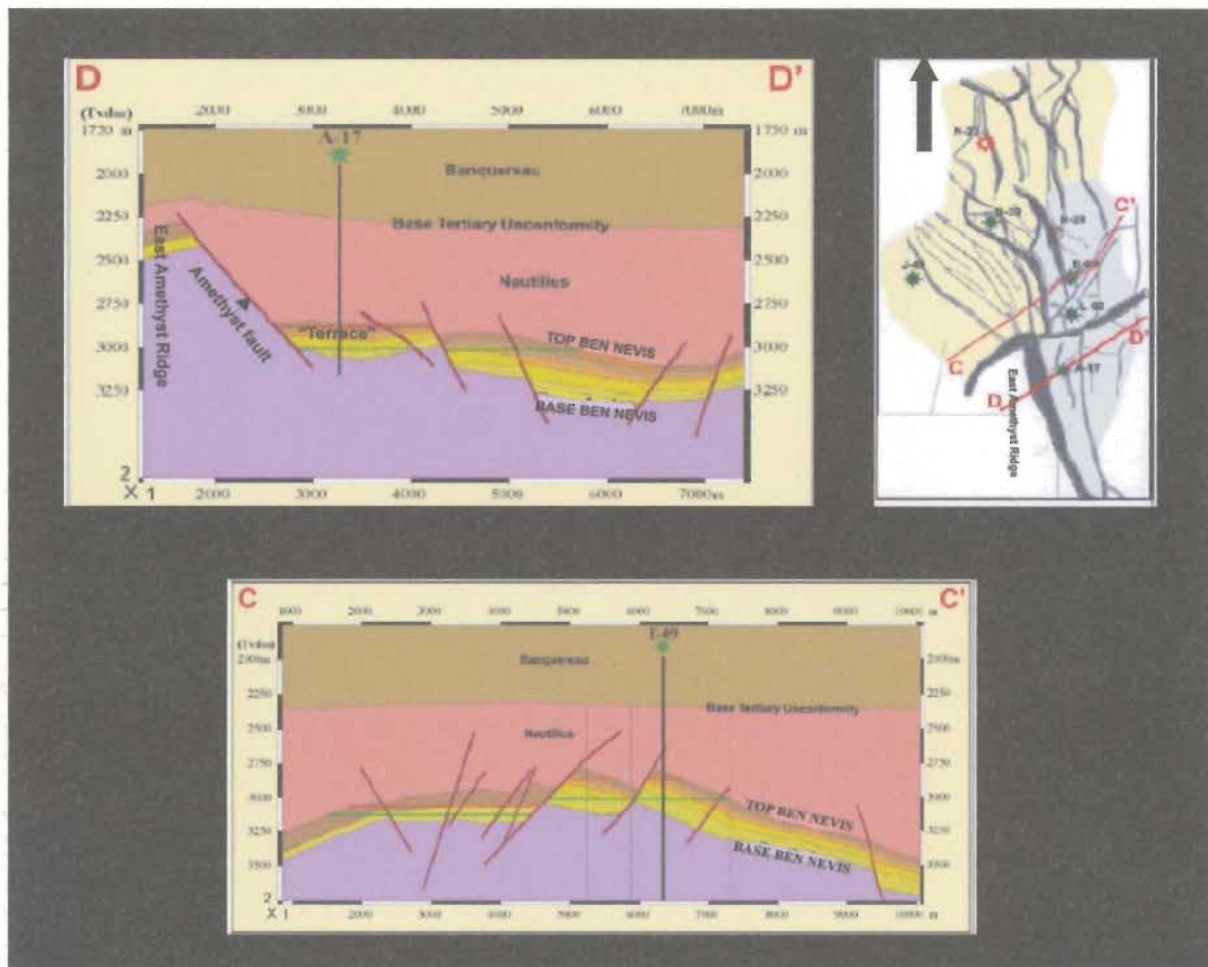


Fig.1.6. Structural cross-sections through the south White Rose field, highlighting the numerous rotated fault blocks and position of the Ben Nevis Formation; the principal reservoir interval at White Rose. Note the position of well A-17 on the “terrace” (upper left) - a rotated fault block on the hangingwall of the Amethyst Fault. Additionally, note the position of well E-09 (center), the discovery well at White Rose. Inset map (upper right) shows the location of both cross-sections. Modified from Husky Energy (2001).

bound these blocks are growth faults. During this faulting, the Aptian Ben Nevis reservoir sandstones were deposited. The thickest amounts of sediment accumulated on the down-thrown fault-blocks.

In the White Rose area, Upper Jurassic to Paleogene and Neogene rocks have been penetrated in a number of the exploration and delineation wells. The following is a review (see Husky White Rose website) of the stratigraphic section encountered in the White Rose area (Figure 1.7), beginning with the oldest strata penetrated.

Rocks of the Upper to Middle Jurassic Voyager Formation (Bathonian to Oxfordian in age) are the oldest rocks to have been penetrated in the White Rose area. They were encountered in the White Rose N-22 well in the northern part of the field. Unconformably overlying the Voyager Formation is the Oxfordian to Kimmeridgian Rankin Formation. In the White Rose area, the Rankin Formation consists of an assortment of shales and siltstones with minor limestones and sandstones. The Egret Member, which belongs to the Rankin Formation, is the main source rock for the Hibernia, Ben Nevis, and White Rose fields. It was penetrated in the A-90 well. A coeval section was penetrated towards the base of the N-22 and E-09 wells; however, source rocks were not encountered. Unconformably above the Rankin Formation lies the Late Jurassic, Kimmeridgian to Portlandian Fortune Bay Formation. It is a basinal, shaly, time-equivalent of the Jeanne d'Arc Formation. It consists predominantly of silty marine shale, and has been penetrated in the White Rose N-22 and J-49 wells where it unconformably overlies the Rankin Formation. It was also found at the bottom of the A-

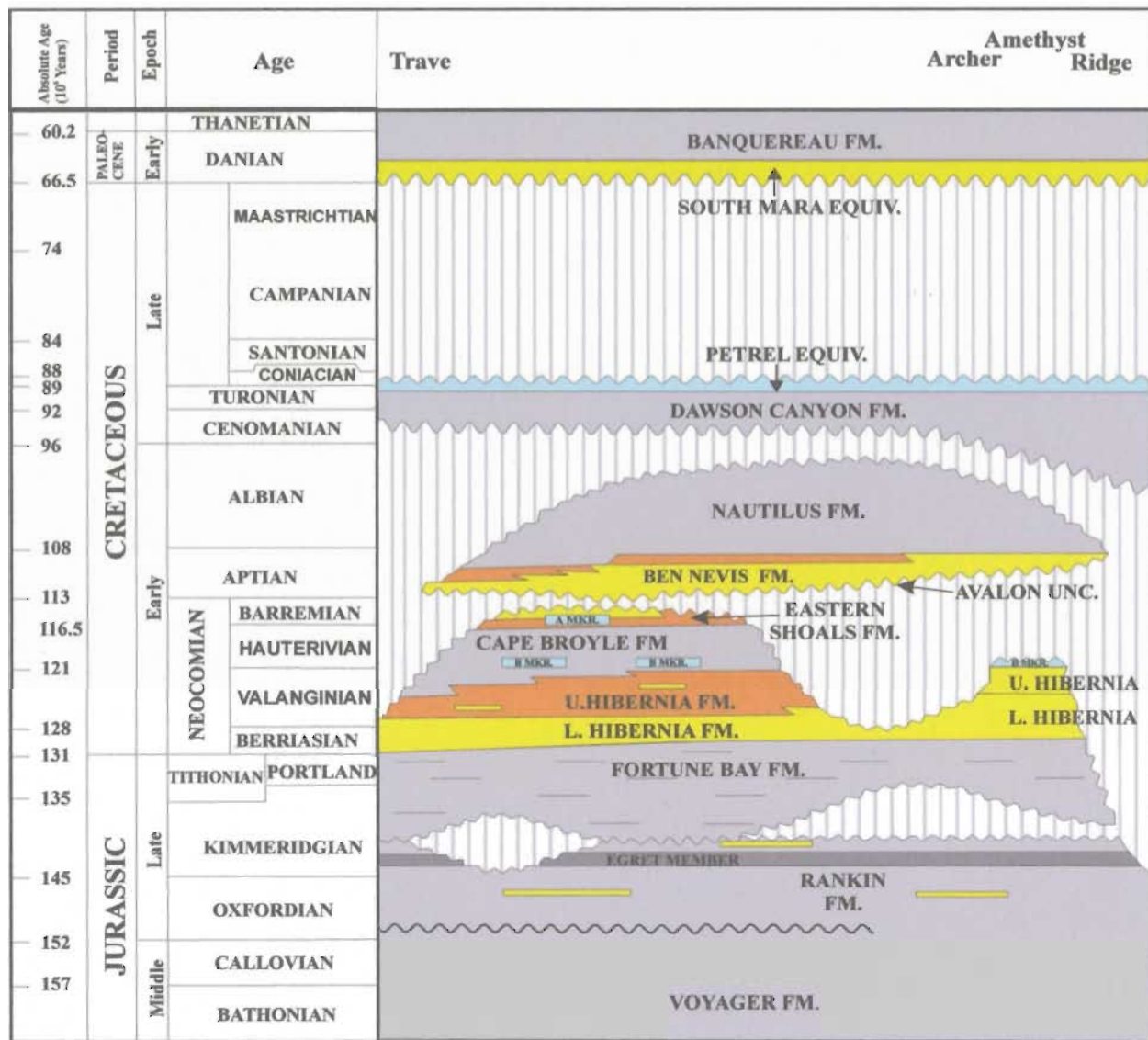


Fig.1.7. Generalized stratigraphy of the White Rose field. Modified from Husky Energy (2001). Colors used to represent lithologies are equivalent to those used in Figure 1.2 (i.e. gray = shale, yellow = sandstone, orange = siltstone, blue = limestone). Note that all lithologies in each formation/member are not represented here. In most cases only the principal lithology type is represented by a color. See text for details.



17 well. The Fortune Bay Formation is interpreted to represent deposition during a major transgression in the Late Jurassic.

Conformably overlying the Fortune Bay Formation is the Hibernia Formation. Rocks of the Hibernia Formation are the oldest Cretaceous rocks in the White Rose area. They are Berriasian to Valanginian in age and have been penetrated in the White Rose A-17, E-09, N-22, and J-49 wells. In the White Rose area, the Hibernia sandstones form a regressive succession, which can be separated into an upper and lower member, with a distinct basal unit. The upper member is poorly developed and consists of non-reservoir-quality siltstone and sandstone. It decreases in thickness to the north. The lower member consists of fine- to medium-grained, light gray/brown and slightly silty sandstones. It was deposited primarily as a prograding shoreface as part of an overall regional regressive package. The gross thickness of the Hibernia Formation ranges from 272 m in the White Rose J-49 well to 86 m in the A-17 well where it has been largely eroded, beneath the Avalon Unconformity. Overlying the Hibernia Formation is the Neocomian Cape Broyle Formation. The Cape Broyle Formation represents a regional transgressive package of marine shale with minor siltstone. The regionally correlative B Marker, found throughout most of the Jeanne d'Arc Basin, is poorly developed in the White Rose area due to erosion. It is present in the N-22 and E-09 wells but is eroded in the White Rose A-17 and Trave E-87 wells. Reservoir-quality rocks are not present in the Cape Broyle Formation at White Rose.

The Cape Broyle Formation is succeeded by the Hauterivian to Barremian Eastern Shoals Formation. Throughout much of the White Rose field the Eastern Shoals

Formation unconformably underlies the Ben Nevis Formation, but elsewhere it is eroded beneath the Avalon Unconformity. The White Rose E-09, L-08, N-30, N-22, L-61, and the J-49 wells all penetrate the Eastern Shoals Formation. In the N-22 and J-49 wells it is comprised of interbedded shale, siltstone and sandstone. The A marker, another regionally extensive marker in the Jeanne d'Arc Basin is preserved in the J-49 and L-61 wells only; in other wells it is eroded by the Avalon Unconformity.

Above the unconformity is the Aptian Ben Nevis Formation. This is the primary reservoir in the White Rose field. It is dominated by fine- to very fine-grained sandstone, siltstone, and shale. The Ben Nevis Formation generally represents a marginal marine shoreface succession throughout most of the White Rose field. It is 0-400 m thick. The main sandstone accumulations are located in the southeastern portion of the field within the E-09, L-08, and A-17 wells (South Avalon pool), where the formation is 350 m thick. In the White Rose A-90 and Trave E-87 wells, the Ben Nevis Formation is absent. It is in unconformable contact with the Eastern Shoals Formation and separated from it by the Avalon Unconformity.

Conformably overlying the Ben Nevis Formation is the mostly Albian Nautilus Formation. It has been penetrated by all the wells in the White Rose area, but is not present to the north in the Trave E-87 well. Though the Nautilus Formation conformably overlies the Ben Nevis Formation, they are laterally equivalent where the Nautilus Formation "shales out". In the White Rose area, the Nautilus Formation consists of gray siltstone and shale with minor sandstone and is of non-reservoir quality.

The Cenomanian to Coniacian Dawson Canyon Formation unconformably overlies the Nautilus Formation and consists primarily of marls and calcareous shales, and ranges from 100 to 500 m thick in the White Rose field. At the top of the Dawsons Canyon Formation is the Petrel Member. It consists of a thin, light gray to brown argillaceous limestone.

The youngest rocks in the White Rose area belong to the Paleogene and Neogene Banquereau Formation, including its South Mara equivalent. The Banquereau is a thick (~2500 m) shale succession, with coarser clastics at its base. It represents deposition during the final stage of thermal subsidence.

## **1.6 Exploration History of the White Rose Field**

Exploration of the White Rose field spans nearly two decades, commencing in the mid nineteen eighties. In November of 1984, the drilling and testing of the White Rose N-22 exploration well marked the initial discovery, encountering both oil and gas (C-NOPB, 2001). N-22 was drilled on the southeastern flank of the White Rose diapir in what is now termed the West Avalon pool (Figure 1.5). Following the initial discovery, two more wells, J-49 and L-61, were drilled in 1985-86. Results were encouraging, as both oil and gas were once more encountered. Exploration wells J-49 and L-61, like N-22, were both drilled in the larger White Rose domal area and results were promising. In 1987-1988, discovery well E-09 was drilled (Figures 1.5 and 1.6). It encountered approximately 90 m of net oil pay (NOP) and tested 5108 bopd (Husky Energy, 2004). E-09 is thought by many to be the primary discovery well at White Rose. Unlike previous

exploration wells, E-09 was drilled into a structurally separate culmination on the southern flanks of the White Rose complex (Husky Energy, 2004) and was the first well to be drilled in the southern Avalon pool.

After the successful drilling and testing of well E-09, delineation well A-90 was drilled to the immediate east in another elevated fault block (Figures 1.5 and 1.6). No oil-bearing sandstones were encountered. The well completely missed the Cretaceous Ben Nevis reservoir sandstones and bottomed in highly deformed Jurassic strata (Husky Energy, 2004). The failure of A-90 to encounter reservoir sandstones is attributed to a poor understanding of reservoir distribution. No wells were drilled between 1989 and 1999. Husky and its partners returned to active exploration of the Grand Banks in 1995, with the intention of acquiring new sets of seismic data over the White Rose field.

The summer of 1997 saw renewed activity in the White Rose area and a state-of-the-art seismic survey was completed. Processing allowed the unconformable nature of the base of the reservoir and the position of the reflector associated with the top of the Ben Nevis Formation near the E-09 well to be properly imaged for the first time (Husky Energy, 2004). Additionally, stratigraphic markers such as the Base Tertiary and Kimmeridgian unconformities encountered at both the Hibernia and Terra Nova fields were also imaged. Both the A and B limestone units, which make excellent seismic markers elsewhere in the basin, appear to be only locally present in the White Rose area (Husky Energy, 2004).

Based on the success of the 1997 seismic survey, a three-well delineation program was conducted in the summer of 1999. Well N-30 was drilled downdip from the N-22



well (see Figure 1.5) in the north part of the White Rose structure (Husky Energy, 2004). Results from this well helped to define the extent of the hydrocarbon pool first encountered by the N-22 well. Wells A-17 and L-08 were drilled south of the initial discovery in rotated fault blocks which are imbricates of the larger Voyager Fault Zone. Each of the three wells encountered over 100 m net oil pay (NOP), further highlighting the economic potential of the field. In the spring of 2000, another well, H-20, was drilled to delineate the northern limit of the South Avalon Pool. Two more wells were drilled in 2003 in the South Avalon pool, encountering significant thickness of reservoir sandstone, as in White Rose A-17 well (Enachescu, personal communication, 2004).

Pressure data and fluid contacts (separate oil/water and gas/oil contacts) indicate that the Ben Nevis Formation in the White Rose field is divided into three separate pools, each with an associated gas cap (C-NOPB, 2001). These are the West, North and South Avalon pools (Figure 1.5). Faults and structural closure associated with the faults separate the pools.

The West Avalon pool is penetrated only by well J-49 (Figure 1.5). A series of northwest-southeast-trending elongate faults divide the area into a number of narrow fault blocks making the trap structural. The North Avalon pool is delineated by two wells, N-22 and N-30. Two sets of faults oriented mainly north-northwest to south-southeast and north-northeast to south-southwest dissect the area (Figure 1.5). The most significant pool, the South Avalon pool, has been defined by the H-20, E-09, L-08 and A-17 wells (C-NOPB, 2001). The pool is limited by faults to the east, west, and south with a stratigraphic limit to the north between E-09 and H-20 where the reservoir sandstones

pinch out (Husky Energy, 2004). Based on core interpretation, the South Avalon pool reservoir sandstones are interpreted as middle to lower shoreface deposits, and the West and North Avalon pools as shelf deposits (e.g. Husky Energy exploration geologists, 2004). Development in the White Rose area is focused principally in the Southern Avalon pool where over 100 m of net oil pay has been encountered in each of the four wells that delineate the field (see Figure 1.5). The area of the pool is  $\sim 40 \text{ km}^2$ .

### **1.7 Remaining Problems in Understanding the Reservoir Geology of the White Rose Field, and Thesis Objectives**

The White Rose field, Jeanne d'Arc Basin, comprises a Cretaceous, sandstone-rich reservoir up to several 100's of meters thick that exhibits a limited range of sandstone textures and sedimentary structures. There are no sedimentological reports in the public domain regarding these rocks, so the following comments reflect information in confidential reports (e.g. Plint (1999)) or transmitted to the author by Husky Energy geologists.

The key reservoir facies are moderate to well sorted, fine- to very fine-grained, quartz arenite sandstones (Husky Energy, 2004). These predominantly show low-angle to horizontal laminations, can be structureless, and have very low to moderate amounts of bioturbation. Silt and mudstone interbeds are very rare and vertical facies successions are not obviously developed and/or recognized. Thus, the reservoir facies at White Rose seem poorly organized. Additionally, the cored section does not fit any established depositional facies model. This is problematic since facies models are typically used, or

are relied upon heavily, in the pursuit for and development of hydrocarbon resources (Walker and James, 1992). One of the main functions of a facies model is its ability to be used as a predictor in new geological situations (Walker and James, 1992). As an example, if the cored section from the White Rose A-17 well was to be part of a paleo-shoreline system, models which incorporate shorelines could be used to predict the distribution and/or geometry of such a system.

Current consensus recognizes an overall shallow marginal-marine setting for the Ben Nevis in the White Rose field; however, the depositional model for the reservoir facies is uncertain (Husky Energy, 2004). As well, the extent to which the sedimentology, specifically grain size and facies relate to permeability is not known. Reducing uncertainty on the depositional model and establishing if any combination of the sedimentological fabrics within the key reservoir facies type has a value in predicting permeability (or vice versa) would assist in the future development of the White Rose field.

This thesis project therefore has three main objectives:

- 1) To describe, classify, and quantify the variety of sedimentary textures, boundaries, and facies within the White Rose A-17 cored interval;
- 2) To interpret the sedimentology of the White Rose A-17 cored interval;
- 3) To compare the sedimentological data with probe permeability data to determine the extent to which these datasets correlate.

## **1.8 Thesis Outline**

This thesis consists of five chapters intended to elucidate the sedimentology of the Ben Nevis Formation in the White Rose A-17 well, and to investigate the relationships(s) between the sedimentology and permeability. The chapter topics are explained below:

- 1) Chapter 2 describes the methods and data types used in the study. Descriptions of how data types were collected and their relevance to the study are explained.
- 2) Chapter 3 documents and interprets the sedimentology of the White A-17 core. Its primary focus is on grain size, grain size trends, sedimentary contacts and boundaries, facies descriptions, facies interpretations, and the proposal of a depositional model.
- 3) Chapter 4 investigates the relationships between the sedimentological data and permeability data.
- 4) Chapter 5 delivers the major findings of the thesis, makes some recommendations for potential additional work on White Rose cores and for similar types of studies, and provides a list of the implications/applicability of these findings with respect to the A-17 cored interval and the White Rose field in general.

## **CHAPTER 2**

### **DATA TYPES AND INDIVIDUAL METHODS**

#### **2.1 Introduction**

The aim of this chapter is to familiarize the reader with the methods used to collect the range of data needed to address the thesis objectives. The data are subsequently used to explain depositional processes and to correlate reservoir textures and fabrics with probe permeability measurements. The principal method of data collection involved logging 106.25 m of core from the White Rose A-17 well. Probe permeability data were collected by Core Labs Inc. in Calgary and provided to the author by Husky Energy. All of the sedimentological and permeability data can be found in Appendix A on a compact disc.







#### **2.2 Choice of the A-17 Well: Location, Thickness and Reservoir Facies**

The White Rose A-17 well is a vertical well, and was drilled into a small ( $\sim 10 \text{ km}^2$ ) fault block directly east of the East Amethyst Ridge in the southeastern portion of the White Rose field (Figure.1.6). The angle of the bedding in the fault block is relatively low, ranging from  $\sim 0$  to  $8^\circ$  (Petro-Canada geologists, personal communication, 2005). Because the bedding is not horizontal, the dip angles of contacts and laminations recorded for this thesis are not true dips – they are apparent only. However, that being said, all dip angles are thought to be relatively low.








The cored section of 106.25 m (Figure 2.1) is mostly sandstone of Aptian age, and is typical of the reservoir facies in the South Avalon pool. The key reservoir facies are

## List of Symbols


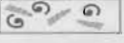
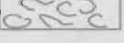

### Physical Sedimentary Structures

Abrupt Contacts	
Erosive Contacts	
Massive Bedding	
Planar Stratification	
Very Low to Low Angle Cross Stratification	
Moderately Inclined Cross Stratification	

### Trace Fossils

Asterosoma	
Chondrites	
Ophiomorpha	
Paleophycus	
Planolites	
Rhizocarallium	
Thalassinoides	

### Bioclasts

Bivalve Fragments	
Gastropods	
Oyster Fragments	
Serpulid Worm Tube Fragments	

### Diagenetic Features



Authigenic Siderite	
Pervasive Calcite Cementation	

Fig. 2.1. List of symbols for the litholog of the White Rose A-17 cored interval

Scale: 1cm = 1.6m

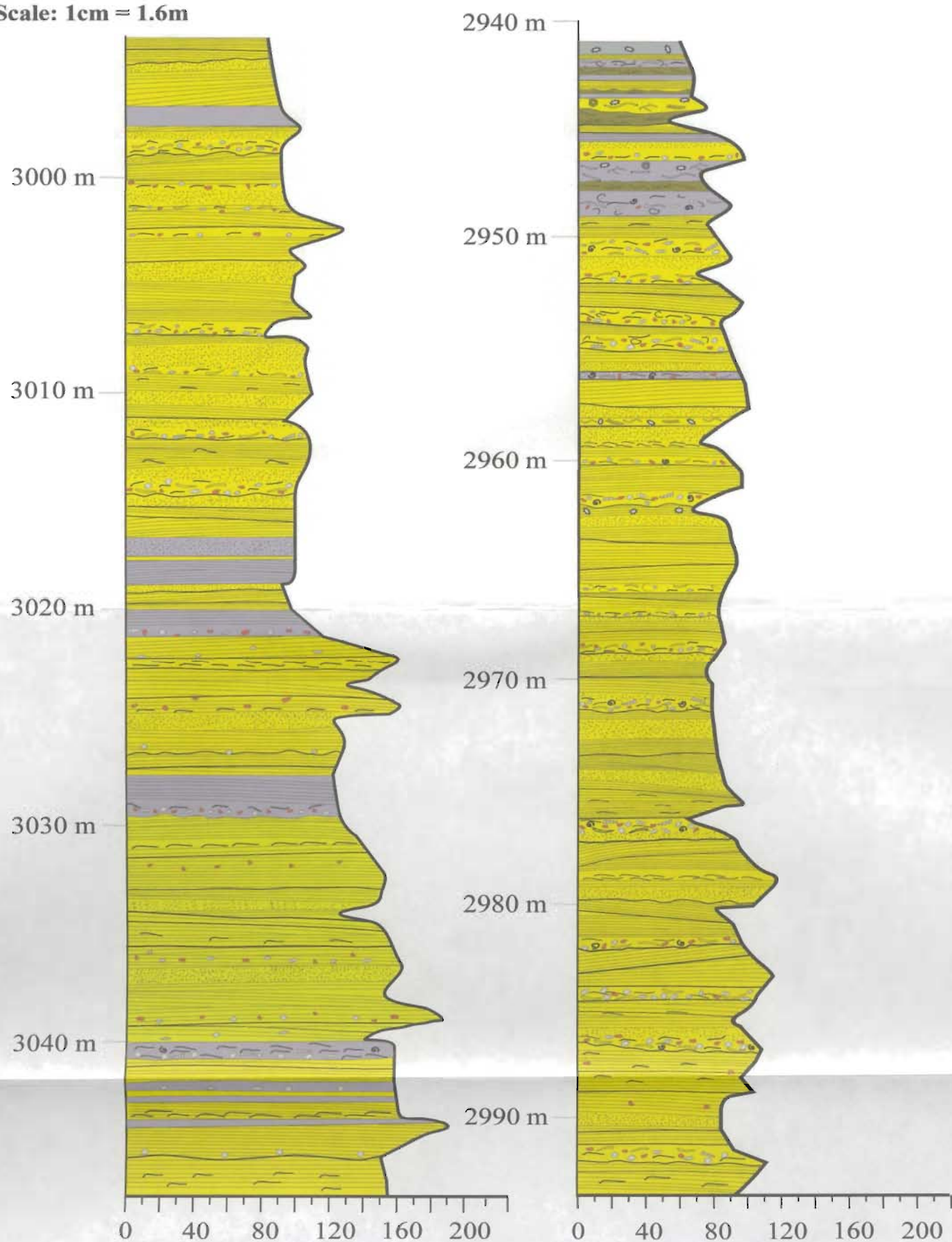


Fig. 2.1. Generalized litholog of the White Rose A-17 cored interval

well sorted, very fine grained sandstones that exhibit predominantly low-angle to horizontal lamination, can be structureless and have very low to moderate amounts of bioturbation (Figure 2.1). Fine-grained mudstone interbeds are extremely rare and vertical facies sequences are not obviously developed and/or recognized. Transported clasts of biogenic and sedimentary origin can be associated with bedding contacts, especially where these are erosive (Figure 2.1).

The cored section was chosen specifically because it is located in a proven hydrocarbon pool and because it presents a challenging set of sedimentological properties. The large pre-existing petrophysical dataset available in A-17 allows the inter-relationships between texture and permeability to be evaluated.

### **2.3 Types of Data Collected and Methods**

The methods of data collection for this thesis differ from those conventionally employed when logging oilfield cores. This is because the lithology of the cored section is almost homogeneous. The key reservoir facies have a limited range of texture, physical sedimentary structures, and appearance (Figure 2.1). Similarly, changes associated with these features are particularly subtle. In an attempt to overcome these difficulties, core features were either semi-quantified or were coded. An inventory of important features against depth was entered into an Excel® spreadsheet designed to allow a straightforward synthesis and evaluation of the data.

A thorough examination of the core revealed that the following features could be either semi-quantified or coded:



- 1) Grain-size - semi-quantified
- 2) Fossils and diagenetic components - semi-quantified
- 3) Contacts and other transitions - coded
- 4) Facies - coded

The following sections provide justification for, and describe in full, the methods used to semi-quantify and code features observed in the core.

### **2.3.1 Grain-Size**

#### **2.3.1.1 Rationale for Measuring Grain Size**

Acquiring grain-size data is a primary objective of this thesis. The reason for this is two-fold:

- 1) Initial inspection of the core revealed that the range of grain-size is extremely limited, and vertical grain-size trends are either absent or ill-defined. Establishing the existence of subtle differences in grain-size and vertical trends is considered to be crucial to the interpretation of the depositional history.
- 2) Grain size (in unconsolidated sands) is a major factor controlling permeability. However, the extent to which grain size and permeability are correlatable in consolidated sandstones, and in particular, this core, has not been demonstrated. Assessing the relationship between grain size and permeability was considered to be a valuable approach to help explain reservoir properties.

For these two reasons, the decision was made to assign numerical values to grain sizes which would allow for plotting of the data.

### **2.3.1.2 Method of Grain Size Measurement**

Grain sizes were measured using a Canadian Stratigraphic grain-size comparator card positioned adjacent to core slabs under the 40x objective of a Wild Leitz binocular microscope.

Initial examination of the core revealed that sand grains are restricted to the very fine-grained and fine-grained size classes. These grain sizes occupy the four finest grain-size divisions on the grain-size comparator card: upper fine, lower fine, upper very fine, and lower very fine. These four categories were deemed insufficient, however, to capture the subtle differences in grain-size that were presumed to exist in the core. Therefore, because each grain-size division on the comparator card displays a range of sizes of imaged grains, it was itself subdivided into lower, middle and upper parts with each part assigned a corresponding value in microns (Table 2.1).

To reiterate, because a principal aim of this thesis is to compare grain size to permeability, a larger number of grain sizes than those available on the comparator card were required.

### **2.3.1.3 Calibration of the Grain Size Card**

Before sand-sized grains in the core were measured, it was first necessary to measure the range of sizes of grains, in microns, imaged on the comparator card for each of the four divisions. This was accomplished by placing the comparator card under the 40x objective of a Nikon Eclipse E600 POL® petrographic microscope. A sufficient number of measurements (approximately 100 for each division) confirmed that the range

<b>Grain Size Comparator</b> Size of grains in letter format for the four finest card swatches	<b>Grain Size Comparator</b> Size of grains in micrometers for the four finest card swatches	<b>Revised Comparator Scale</b> Midpoints of size classes used for this thesis
fU – fine Upper	177-250 $\mu\text{m}$	190 $\mu\text{m}$ 214 $\mu\text{m}$ 238 $\mu\text{m}$
fL – fine Lower	125-177 $\mu\text{m}$	134 $\mu\text{m}$ 151 $\mu\text{m}$ 168 $\mu\text{m}$
vfU – very fine Upper	88-125 $\mu\text{m}$	94 $\mu\text{m}$ 107 $\mu\text{m}$ 119 $\mu\text{m}$
vfL- very fine Lower	62-88 $\mu\text{m}$	66 $\mu\text{m}$ 75 $\mu\text{m}$ 84 $\mu\text{m}$

Table.2.1. Grain size comparator categories (letter and micrometer format) and the revised micrometer format used for this thesis. The first and second columns display the conventional divisions as seen on most grain size comparator cards. The third column shows the twelve grain-size values assigned to spot measurements in core.

of sizes of grains, in microns, imaged in each of the lowermost four divisions on the comparator card were reasonably valid. The maximum and minimum sizes of imaged grains for each division were found to differ by  $\pm 5$  microns compared to stated values. Imaged grains on the far left of each division are the smallest in the range while those imaged on the far right of each division are the largest. Between these end members, there is grain size grading, and in the middle of each division, a value close to the average occurs.

#### **2.3.1.4 Grain Size Subdivisions**

The sizes, in microns, assigned to the lower, middle, and upper parts of each division on the card were obtained by dividing the micron range into three equal parts and then selecting the arithmetic mid-point of each part as the value to be recorded. To clarify this procedure, the following example is provided. The range in microns for the finest class on the comparator card is 62-88  $\mu\text{m}$ . Now,  $88-62 \mu\text{m} = 26 \mu\text{m}$ , and  $26/3 = \sim 8.7 \mu\text{m}$ . The three parts of this division therefore have micron boundaries of 62-70.7  $\mu\text{m}$ , 70.7-79.3  $\mu\text{m}$  and 79.3-88  $\mu\text{m}$ , with midpoint values of  $\sim 66.3 \mu\text{m}$ , 75  $\mu\text{m}$ , and  $\sim 83.7 \mu\text{m}$ . These are then rounded off to integer values (Table 2.1). This procedure gives upper and lower possible values for the sand in each size category that are entirely within the range provided on the comparator card. Using this procedure avoids overlapping values from one division to the next. Note that the actual range, in microns, for successive grain-size divisions increases with the absolute size. This is because the scale used on comparator cards is logarithmic.

In total, twelve values (expressed in microns) are used to represent the grain-size of the sandstones in the core. It is important that the reader understand that these values are not absolute – they are only relative estimates of the actual sizes.

Because silt-sized grains are not imaged on the grains-size comparator card, assigning values to them is quite subjective. Nevertheless, best estimates were made by placing core slabs underneath the 40x objective of a Wild Leitz microscope and using the smallest grain size division on the comparator card as a reference. The values assigned to silt-sized particles are based on those as defined by Folk and Ward (1957). They are 23,28,36, and 46  $\mu\text{m}$ .

#### **2.3.1.5 Location of Grain Size Measurements, Measurement Repeatability, Measurements Accuracy and Sorting**

Grain sizes were measured above and below each contact, gradational transition, and break in the core at depths equal to the nearest probe permeameter measurement. This procedure led to the collection of 1176 grain-size measurements. The distance between each grain size and probe permeameter measurement was typically less than one half of a centimeter and never exceeded one centimeter. To ensure that replicate grain-size measurements were unbiased, measurements were taken at different times throughout the analysis of the core. To ensure accuracy, grain size determinations were made ~20-30 times at each measurement depth. Replicate grain size measurements were found to differ by (at most) ~ 5  $\mu\text{m}$  for the 2 finest classes and by ~ 10  $\mu\text{m}$  for the two

coarser grain size classes from individual measurements. It is very important to restate that these grain size measurements are relative estimates only – they are not absolute.

In addition to grain-size measurements, grain-size sorting was measured on selected samples (seven thin-sections) to determine its relationship with permeability. These selected samples represent facies 1, 2, 3, and 4, and each of the cores three units as discussed in chapter 3. Facies 5 and 6 were not chosen because they are pervasively calcite-cemented (~ 0 mD horizontal permeability). Facies 7, 8, and 9 were not chosen because they have bimodal sorting (bioclasts and silt-sized grains). Each of the three units were chosen because they appeared to have differing degrees of cementation (visual estimation).

To determine sorting values, the following steps were implemented. First, digital images of thin-sections selected from the various facies and units were taken using a Nikon DXM1200F digital camera mounted on top of the Nikon Eclipse E600 POL petrographic microscope. Digital images were taken while viewing thin-sections under 10x magnification. Second, enhancements and adjustments to the digital images were made using Nikon ACT-1 digital picture software. Third, the digital images were imported into the Simple PCI- Image Analysis software. Fourth, the long axis diameter of eighty to one hundred quartz grains from each of the thin-sections was measured. Fifth, sorting values were calculated in an Excel® spreadsheet using the formula of Folk and Ward (1957). The formula is as follows:

$$\text{Sorting} \quad \sigma \phi = \frac{\phi_{84} - \phi_{16}}{4} + \frac{\phi_{95} - \phi_5}{6.6}$$

where

$\sigma$  = sorting

$\phi$  = the grain size in phi units at the  $n$ th percentage frequency

Terms used to describe sorting values obtained from the Folk and Ward (1957) formula are:

$\phi$ less than 0.35	very well sorted
0.35-0.50	well sorted
0.50-0.71	moderately well sorted
0.71-1.00	moderately sorted
1.00-2.00	poorly sorted
greater than 2.00	very poorly sorted

### 2.3.2 Fossils and Diagenetic Components

A variety of shells (principally bivalve fragments), serpulid worm tubes and authigenic siderite are widely present in the core. Additionally, there are a number of pervasively calcite-cemented zones. These cemented zones are typically coincident with shell-hash horizons. Throughout the core, the fossils and diagenetic minerals can occur either together or separately. For this thesis, the abundance of each feature is reported using an ordinal scale. The ordinal scale has a minimum value of zero and a maximum value of three. Zero implies a feature is completely absent. The number one implies that a feature is of low abundance; the number two is used where a feature is moderately abundant, and the number three indicates that a feature is very abundant. Measurements with ordinal scales are ordered in the sense that higher numbers represent greater abundance. However, the points on each ordinal scale not imply equal difference in abundance. It is important to state that allowances for cross sections through bioclasts

were not made; therefore, in some cases, the ordinal values assigned to report the abundance of bioclasts might be high.

### **2.3.3 Contacts and Transitions**

In this study, the word “contact” is used for any sharp and distinct surface, whereas the word “transition” is used if a change in core properties is gradational. Particular attention was paid to the variety of contacts and transitions recognized in the core. Nevertheless, the nature of some of these contacts and transitions remain uncertain. For example, in several instances it is unclear whether contacts signify true bed boundaries, amalgamation surfaces, or simply the foresets of cross-bedding. This uncertainty stems from the lithologic homogeneity and limited width of the core. In this thesis, erosive contacts are termed bed boundaries; these typically coincide with a noticeable increase in grain-size or the presence of bioclastic material. All other sharp and distinct surfaces, which are not clearly erosive, are inferred to be internal bed boundaries. Such surfaces may represent the boundaries between amalgamated beds or stratification within very low angle cross beds. They sometimes bound the top of distinct shell accumulations and on rare occasions, they separate unbioturbated and bioturbated lithologies.

Contacts and gradational transitions may be important for the following reasons:

- 1) Facies and textural changes in the core are subtle. The assumption is that the best places to observe measureable amounts of change are across contacts and zones of lithologic change.



- 2) The type, nature, and spatial distribution of a majority of the contacts and transitions had not been previously documented.
- 3) A principal aim of this thesis is to uncover the relationship between grain-size and permeability. This relationship can most readily be tested for grain sizes and permeability values recorded adjacent to and across contacts and other transitions, where the most pronounced changes are expected to occur. Contact type is expected to influence changes in these parameters.

In total, 639 contacts and gradational transitions (including 90 breaks in core continuity) were documented in the core from the White Rose A-17 well. These can display a range of geometries. The criteria used to distinguish between each type are described below.

- 1) Erosive contacts: A contact is erosive if it truncates a minimum of one laminae or bed or if there is significant evidence to suggest that the character of the above zone is distinctly different from that below (e.g. grain-size increases or distinct facies change). In numerous instances, erosive contacts are associated with and are overlain by an assortment of shells and/or serpulid worm-tube debris. Changes in facies (both the same and different facies) across erosive contacts are typically more evident than are changes across abrupt contacts.
- 2) Abrupt contacts: Abrupt contacts are sharp, but show no evidence for truncation. Changes in core features, particularly grain-size, are less pronounced across abrupt contacts than across erosive contacts. Abrupt contacts are less frequently

overlain by shell and serpulid debris than erosive surfaces. Abrupt contacts are not necessarily bed boundaries.

- 3) Cementation Contacts: Cementation contacts either separate pervasively calcite-cemented sandstones from more porous sandstones, or they separate cemented zones with abundant shelly debris from less fossiliferous but still cemented sandstone. In the latter case, the contact is within calcite-cemented rock. A majority of the contacts separating more porous sandstone from pervasively cemented sandstone are presumed to have no sedimentological significance: however, there are a few that are erosive, but for the purpose of this study they are not considered in detail.
- 4) Gradational transitions: the term “gradational contact” is inherently contradictory. Therefore, these textural or facies changes are referred to as gradational transitions. In the core, these transitions most typically occur where fragments of shells and serpulid worm tubes (of varying abundance) gradually diminish upward away from underlying (or rarely overlying) contacts, or where shell fragments aligned with stratification cease to be present. They also occur over sections in the core where there is a noticeable change in grain-size not marked by a distinct boundary, and between unbioturbated and bioturbated intervals. By convention, a gradational transition was recognized at the position in the core (a), which separates shell-bearing sandstone from sandstone containing no shells, (b) where the maximum amount of grain-size grading in a section of core is achieved, and (c) above or below bioturbated zones.

Contacts and gradational transitions are non-quantifiable features. However, assigning codes to them facilitates classification and tabulation of the frequency of occurrence of each type. Contacts and transitions were recorded using a one-or two-digit numeric code. These codes do not indicate such things as the absolute change in grain-size or the amount of overlying shell and/or serpulid debris nor do they capture changes in facies. It is worth noting that contacts and transitions were recorded wherever there was any noticeable change in core properties. Table 2.2 lists each contact type, the different geometries, and resultant codes.

When describing grain-size trends in Chapter 3, the terms ‘bed’ and ‘interval’ are used frequently. These are distinguished by their contacts. All erosive contacts are defined as first-order boundaries, whereas abrupt contacts are defined as second-order surfaces. The term ‘bed’ is used for deposits bounded by two first-order bed boundaries. The term ‘interval’ is used for deposits bounded either by two second-order surfaces, or by one second-order and one first order surface. This distinction is made because ‘beds’ are more likely the deposits of separate events preceded and followed by scour and erosion, whereas ‘intervals’ might have been emplaced by pulses of current activity during longer depositional episodes. In total, there are 61 beds without any internal second-order surfaces. The remaining 261 beds contain at least one internal second-order surface, and combined account for 566 intervals. This means that many beds contain several intervals and second-order surfaces.

Contact and other Boundary Types	First Digit	Erosive Subtypes	Code
Erosive contact	1	Erosive, very gently to moderately undulatory and non-inclined	11
Abrupt contact	2		
Gradational transition	3	Erosive, very gently to moderately undulatory and inclined	12
Cementation contact	4		
Discontinuities	5	Erosive, gently to highly curved and convex-up	13
Geometrical Variations	Second Digit	Abrupt Subtypes	Code
Very gently to moderately undulatory and non-inclined	1	Abrupt, very gently to moderately undulatory and non-inclined	21
Very gently to moderately undulatory and inclined	2	Abrupt, very gently to moderately undulatory and inclined	22
Gently to highly curved and convex-up	3	Abrupt, gently to highly curved and convex-up	23

Table.2.2.Contact and boundary types, subtypes, and their codes.

### **2.3.4 Facies**

A facies is defined as a body of rock characterized by a particular combination of lithology, physical and biological structures that bestow an aspect (“facies”) different from the rocks above, below and laterally adjacent (Walker, 1992). Facies and facies associations provide guidance for the selection of probable depositional settings through comparison with modern analogues having the same characteristics. Distinctly different facies are not obvious in the cored section from the White Rose A-17 well, and facies associations are not obviously developed. Nevertheless, in an attempt to better understand the organization of these deposits, subtly different facies are assigned numeric codes. Each facies is assigned a one-digit number. In total, 9 facies are recognized (Table 2.3). This procedure has two main advantages: 1) Assigning codes to facies and entering them into a spreadsheet provides an easy way of accessing and sorting data, and 2) permeability measurements can be directly compared between facies.

### **2.5 Probe Permeametry**

The permeability data used in this thesis were collected using a frame-mounted PDPK-200 probe permeameter, based on a non-steady-state, pressure-decay technique described by Jones (1992). This instrument is designed to make a large number of rapid, localized, non-destructive permeability measurements on the face of core slabs (Goggin, 1988). To obtain permeability measurements, slabs of core are placed beneath the probe tip, the device releases a known tank volume of gas (air in this case) to the sample (core slab), tank pressure is recorded as a function of time, and the slope of the pressure-decay

<b>Facies</b>	<b>Numeric Code</b>
Homogeneous sandstone	1
Planar laminated sandstone	2
Low angle cross-stratified sandstone	3
Moderately inclined cross-stratified sandstone	4
Pervasively calcite-cemented sandstone	5
Pervasively calcite-cemented sandstone with abundant shelly material	6
Shell-serpulid- and siderite-bearing sandstone	7
Shelly sandstone	8
Bioturbated sandstone and siltstone	9

Table.2.3. Brief description of facies (left), and their corresponding numeric codes (right).

curve yields an instantaneous flow-rate function that is substituted in to the appropriate form of Darcy's equation (Jones, 1992). Solving Darcy's equation for 'k' yields a permeability value. For this thesis 1176 probe permeameter measurements are utilized.

## **2.4 X-radiography**

To determine if "structureless" beds/intervals in the White Rose A-17 core are devoid of stratification a number of X-rays were taken. Core segments, which appeared homogeneous, were X-rayed using an industrial Picker X-ray source (model 6321). Placing cores on a specially designed aluminum plate prevented dark-edge effects produced by overexposure at core edges. Best results were obtained when core segments were exposed for ~ 2 minutes at a voltage of 60 kV and a current of 50 mA. Standard developing procedures were used.

## **CHAPTER 3**

### **SEDIMENTOLOGY OF THE WHITE ROSE A-17 CORE**

#### **3.1 Introduction**

Previous studies on White Rose cores are limited, and have not been done in significant detail. The principal goal of this chapter is to provide a thorough account of the sedimentology of the White Rose A-17 cored interval and provide insight into its significance. Specifically this chapter has four goals:

- 1) To provide a comprehensive record of the textural data, describe and discuss grain-size trends, and provide insight into their significance;
- 2) To present and describe the four principal contact and transition types observed in the core, variations in their geometry and discuss their significance;
- 3) To present and describe the variety of facies recognized in the core, discuss the vertical organization of facies, and provide process interpretations for each facies, and
- 4) To hypothesize the most probable depositional setting(s) for the cored interval.

#### **3.2 Grain Size and Grain-Size Trends**

##### **3.2.1 Grain Size**

This section is primarily concerned with presenting and discussing the grain size and grain-size trends in the A-17 core. A total of 1176 grain sizes were measured and recorded above and below the 639 contacts and transitions; including 79 breaks in the core and 11 styrofoam inserts where samples had been previously taken for other studies.



The discrepancy between the number of grain-size measurements and boundaries (i.e.  $639 \times 2 = 1278$ ) is attributed to three factors: 1) grains could not be measured above and below the base and top of the core because rock was not present (2 grain sizes), 2) grains could not be measured above and below breaks where core had been extracted for special core analysis and replaced by styrofoam (22 grain sizes), and 3) seventy-eight boundaries share a single grain-size measurement because they were closely spaced and only one permeability measurement was present in the zone of core between them, which is where grains were measured.

Grain size in the White Rose A-17 core ranges from a minimum of  $\sim 23 \mu\text{m}$  to a maximum of  $214 \mu\text{m}$ , with an average grain size of  $\sim 107 \mu\text{m}$  (Figure 3.1). The equivalent phi values are  $\sim 5.44 \phi$  and  $\sim 2.22 \phi$  for the range, and  $\sim 3.22 \phi$  for the average (Figure 3.2). Grains are primarily very fine-grained and are well sorted (Figure 3.2).

Before measurements were taken, it was evident that fine-grained sandstone is common towards the base and siltstone towards the top; however, smaller-scale grain-size trends were not obvious. Though sand-sized grains are restricted to the fine- and very fine-grained size classes, there is a considerable amount of variation within these classes. These variations were captured by using a large number of possible grain-size values (Table 2.1).

Grain-size trends are presented and discussed at three scales, these are first, second, and third order grain size trends. To best highlight these trends, a number of grain size logs will be shown. The first order grain-size trend is at the scale of the entire cored interval, second order grain-size trends are at the bed-set scale, which is typically a few

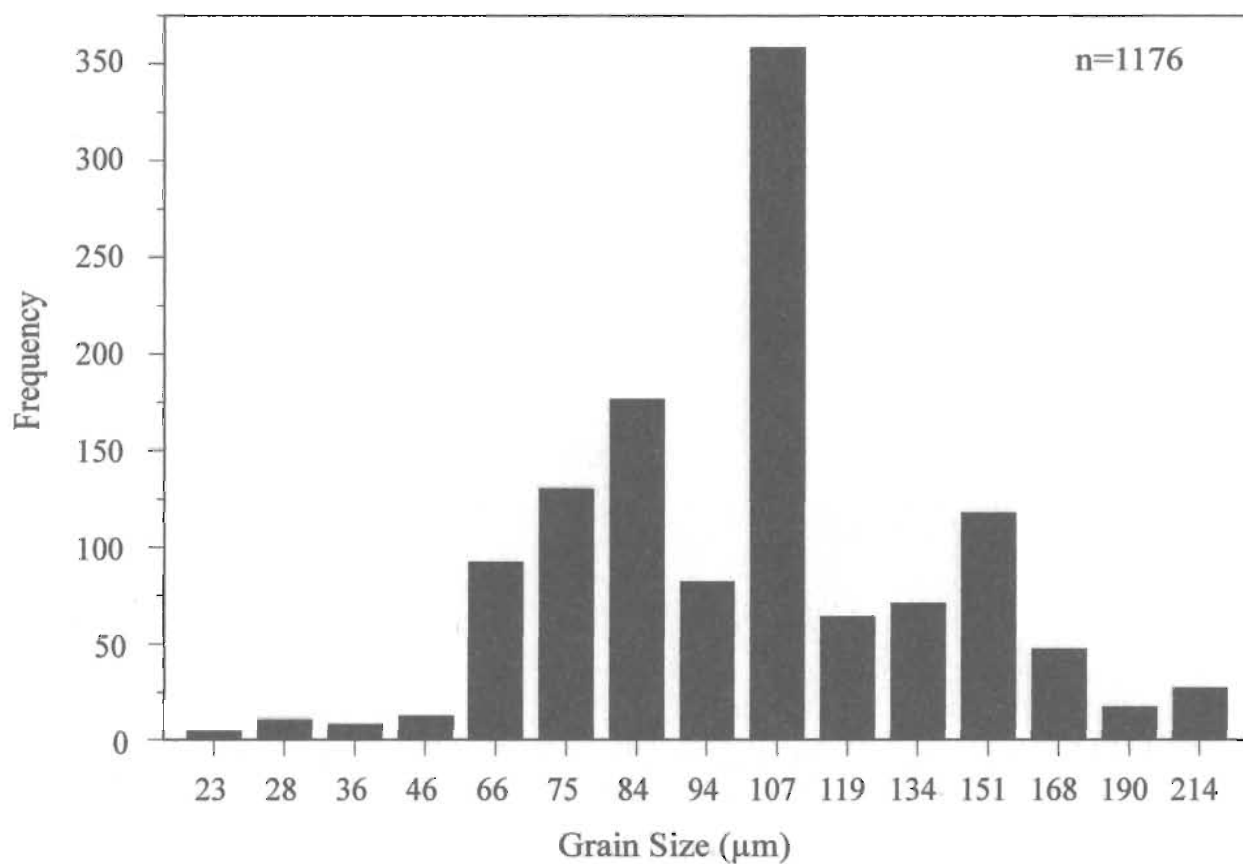


Fig.3.1. Grain-size distribution for the White Rose A-17 core. Grains were measured (where possible) above and below all contacts, boundaries, and breaks in the core. In total, 1176 grain sizes were measured, averaging 107  $\mu\text{m}$  or very fine-grained.

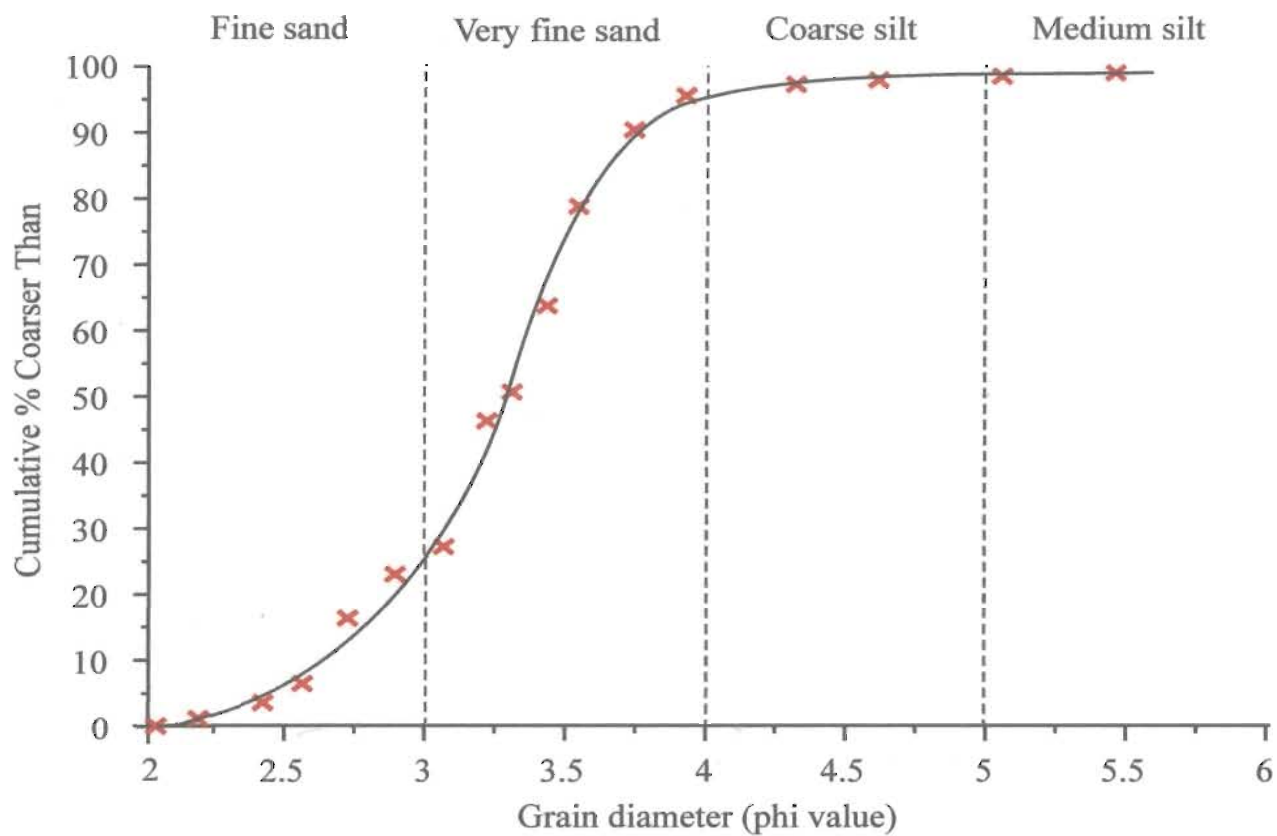


Fig.3.2. Cumulative % grain size for grains measured in the White Rose A-17 core. Red x's mark the appropriate phi values (x-axis), and their cumulative percentage (y-axis). The steepness of the curve indicates that the grains are well sorted. Approximately 70% of the measured grains are very fine-grained sand.

meters, and third order grain-size trends are at the bed/interval scale which are typically less than one meter.

### **3.2.2 Grain-Size Trends**

#### **3.2.2.1 First Order Grain-Size Trends**

First order grain-size trends occur at the scale of the entire cored interval (Figures 3.3 and 3.4). Overall, the cored interval fines upward. Internally, it is characterized by a large number of grain-size fluctuations. On grain size alone, the cored interval can be segmented into three units. The lower unit, representing the lowermost 27 m from 3047-3020 m, consists mostly of fine-grained sandstone with rare very fine-grained sandstone, and only a minute fraction of carbonaceous and silt-sized material. Above this lower unit, over a zone of two meters from 3020-3018 m, the most significant and noticeable change in grain size occurs (Figures 3.3 and 3.4). The decrease in grain size is approximately 60-65  $\mu\text{m}$ . Above this point, grain size rarely reverts to fine sand size (Figures 3.3 and 3.4).

The middle unit encompasses ~75 m of the core, and extends from ~3020-2945 m depth (Figures 3.3 and 3.4). This unit is composed almost exclusively of very fine-grained quartz sandstone with rare silt-sized particles. Throughout the bulk of this unit, the general trend remains is an overall fining-upward one; however, meter-scale grain-size fluctuations are frequent, but their magnitudes are small. These smaller trends are discussed in the next section.

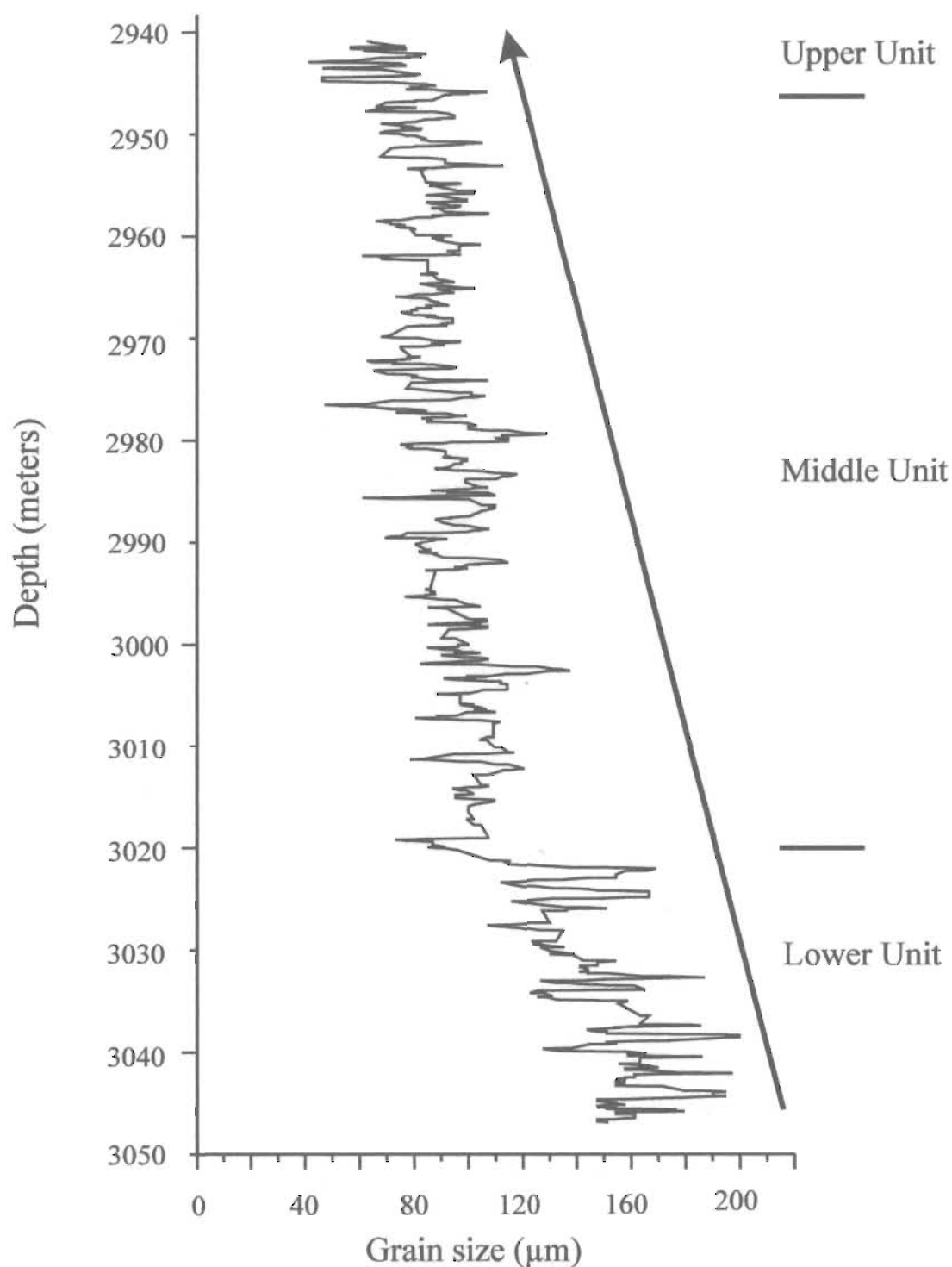


Fig. 3.3. Smoothed grain-size profile for the White Rose A-17 core. From base to top, the interval displays an overall fining-upward grain-size trend (also depicted by arrow). Values used in the construction of this grain-size profile were obtained by running a moving average over every five grain sizes with averages placed at the midpoint.

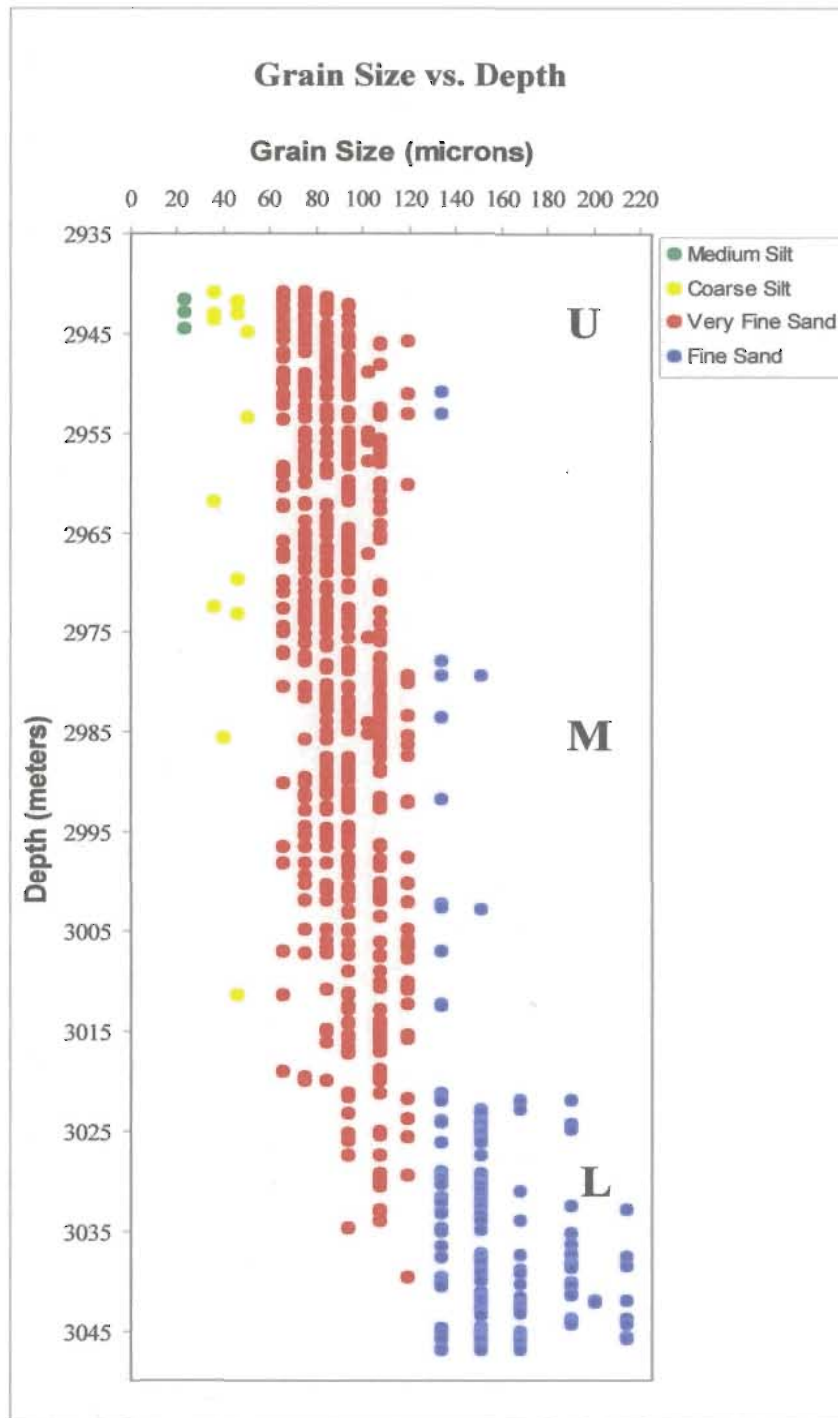


Fig.3.4. Plot of Grain size (microns, at fixed standard values) vs. Depth (meters). Blue dots representing fine-grained sandstones are mainly restricted to the lowermost 25 m of the core (L), red dots representing very fine-grained sandstones dominate the middle part of the core (M), and siltstones both coarse (yellow) and medium (green) are primarily restricted to the uppermost 5-6 m of the core (U).

The middle unit is succeeded by a 5-6 m upper unit, which consists of very fine-grained sandstone and siltstone (Figures 3.3 and 3.4). This upper unit is the only unit in the core composed of more than one lithology.

### **3.2.2.2 Interpretation and Implications**

The overall fining-upward grain-size trend represented in the A-17 core reflects a gradual decrease in the amount of energy in the depositional system and may suggest a change in the depositional environment, from one in which fine- and very fine-grained sand was dominant to one in which very fine-grained sand and silt were dominant. This overall fining-upward grain-size trend might also be a function of sediment supply and/or sediment availability.

### **3.2.2.3 Second Order Grain-Size Trends**

Second order grain-size trends refer to grain-size trends that occur at the bed and/or bed-set scale. They span beds that consist of a number of intervals that fine, coarsen or remain the same upwards, and in some instances a number of beds or bed-sets that do the same. These units typically comprise less than one meter of core, but may be as thick as two meters. In total, there are 322 beds in the A-17 core; they range from ~ 2.5 cm to 197.5 cm in thickness, and average ~75 cm thick (Figure 3.5). Because the plot of grain size versus depth for the entire core (Figures 3.3 and 3.4) does not reveal medium-scale trends with any degree of detail, the grain-size log was subdivided into a number of segments that were individually enlarged. Aside from the lowermost segment,



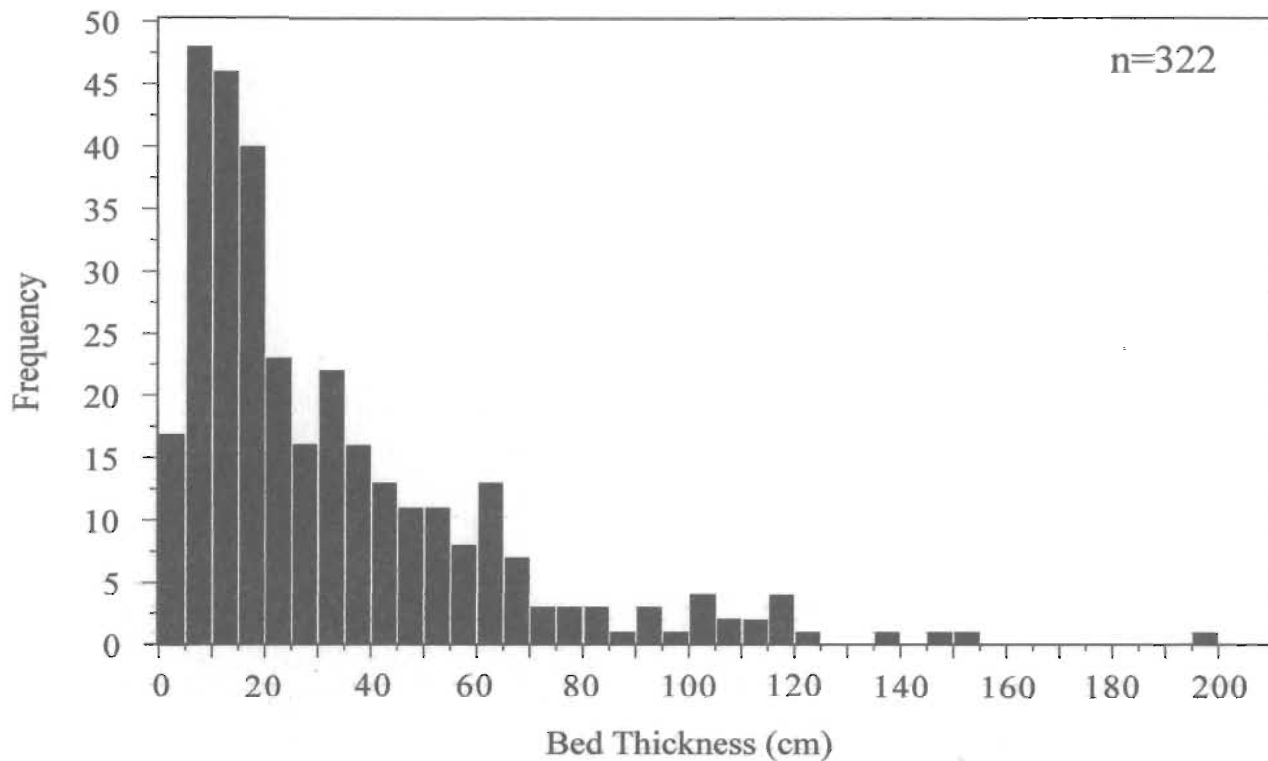


Fig. 3.5. Histogram of bed thickness for the White Rose A-17 core. Beds range from a minimum of 2.5 cm to a maximum of 197.5 cm, and average approximately 75 cm thick. Bed thicknesses appear to have a log-normal distribution (cf. Drummond and Wilkinson, 1996). Class width is 5 cm with data plotted at midpoints.

which is 7 m thick (3047-3040m), each segment represents 10 m (Figures 3.6-3.16). This was thought to be a suitable scale to display second order grain-size trends. Any smaller, and the number of logs becomes too great for visual comparisons and some trends are missed; any greater and some of the details are missed. Only the most general trends are symbolized by the use of arrows. Arrows are simply a means of showing that grain size has a tendency to change. The word 'general' is emphasized because these trends do not imply that grain size consistently decreases, increases or stays the same vertically; rather, it has a tendency to vary in one way.

Arrows set adjacent to just one bed signify that the bed consists of a number of smaller intervals that either fine, coarsen or generally remain the same upwards. Arrows set adjacent to a number of beds signify that the beds have an overall tendency to fine, coarsen or remain generally the same upwards. For comparative purposes, grain-size logs which show all surfaces (left side of Figures 3.6-3.16) are shown beside grain-size logs that use data above and below bed boundaries only (right side of Figures 3.6-3.16). This is done primarily to visually show why some beds are considered to show grain-size trends and why others are grouped together into bed-sets to show trends. Only the most obvious bed-scale and bed-set-scale trends are highlighted by the use of arrows.

There are three types of second order grain-size trends. They are as follows:

- 1) Fining-upward trends;
- 2) Coarsening-upward trends;
- 3) Static trends.

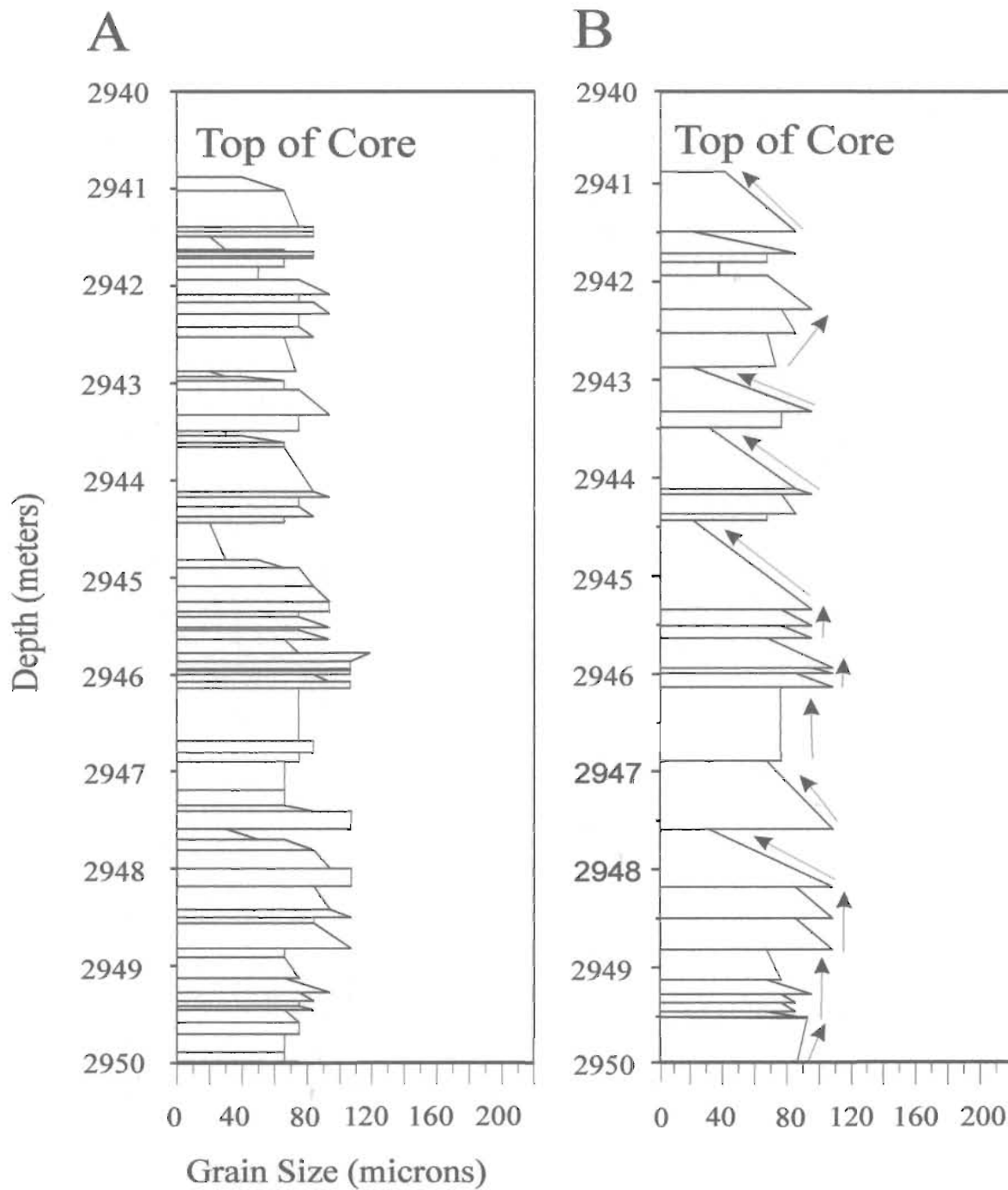


Fig.3.6. Grain size vs. Depth from 2950-2940 m. Log on left (A) represents the positions of all contacts and tops of transitions between 2950-2940 m while the log on the right (B) marks only bed boundaries. Arrows are used to show the general tendency for grain size to increase, decrease or remain the same vertically.

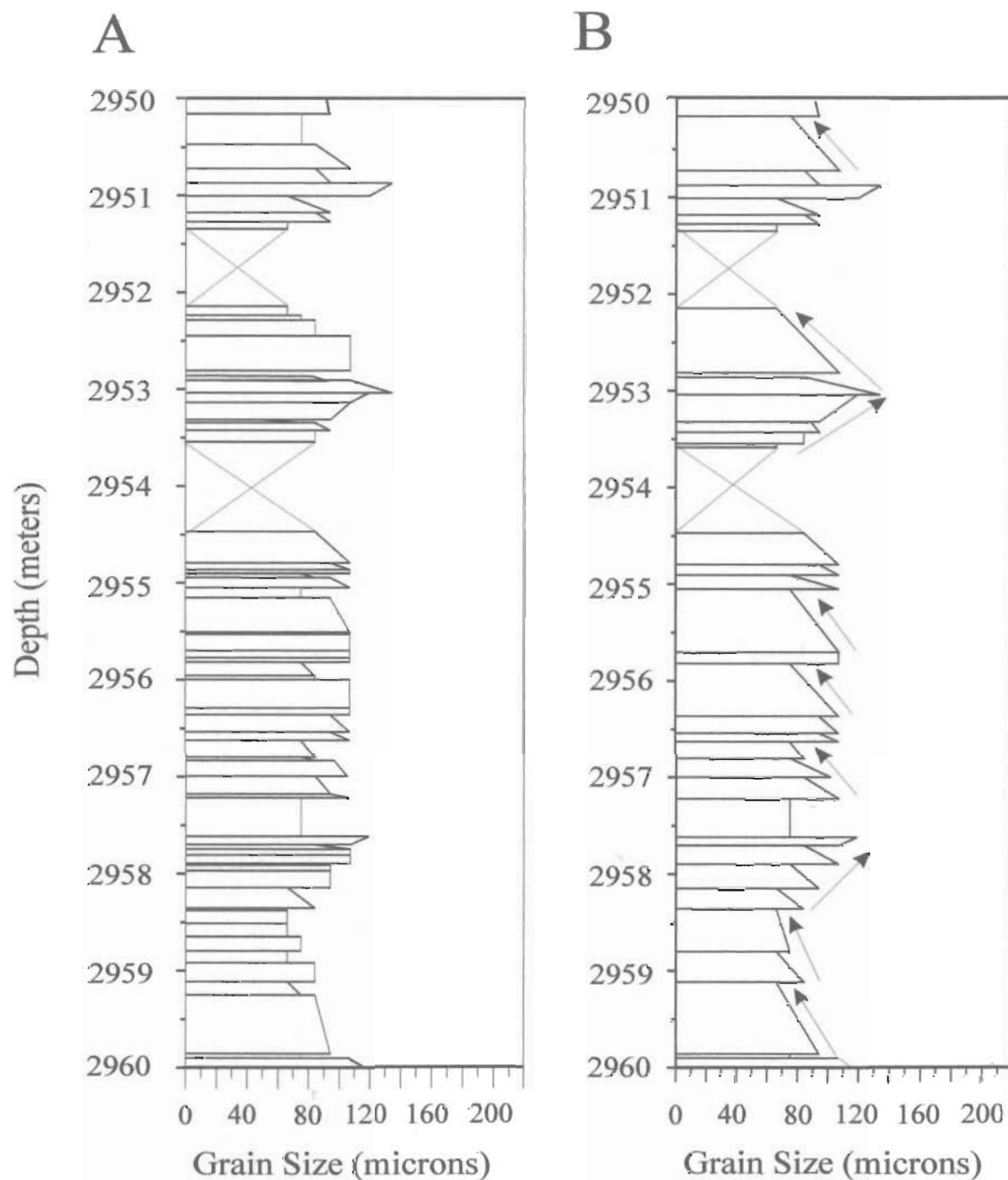


Fig.3.7. Grain size vs. Depth from 2960-2950 m. Log on left (A) represents the positions of all contacts and tops of transitions in the core between 2960-2950 m while the log on the right (B) marks only bed boundaries. Arrows are used to show the general tendency for grain size to increase, decrease or remain the same vertically.

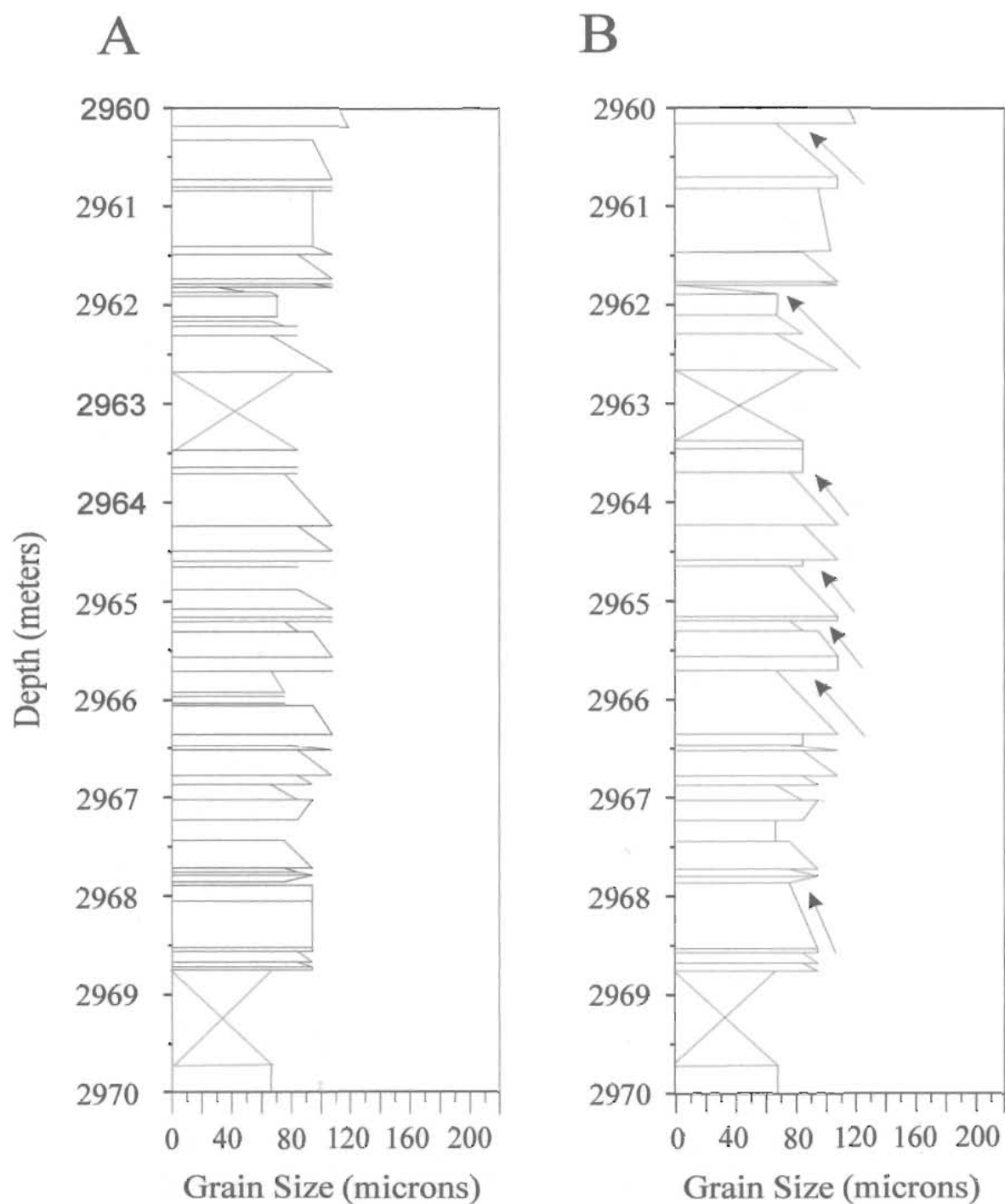


Fig.3.8. Grain size vs. Depth from 2970-2960 m. Log on left (A) represents the positions of all contacts and tops of transitions between 2970-2960 m observed in the core while the log on the right (B) marks only bed boundaries. Arrows are used to illustrate the general tendency for grain size to increase, decrease or remain the same vertically.

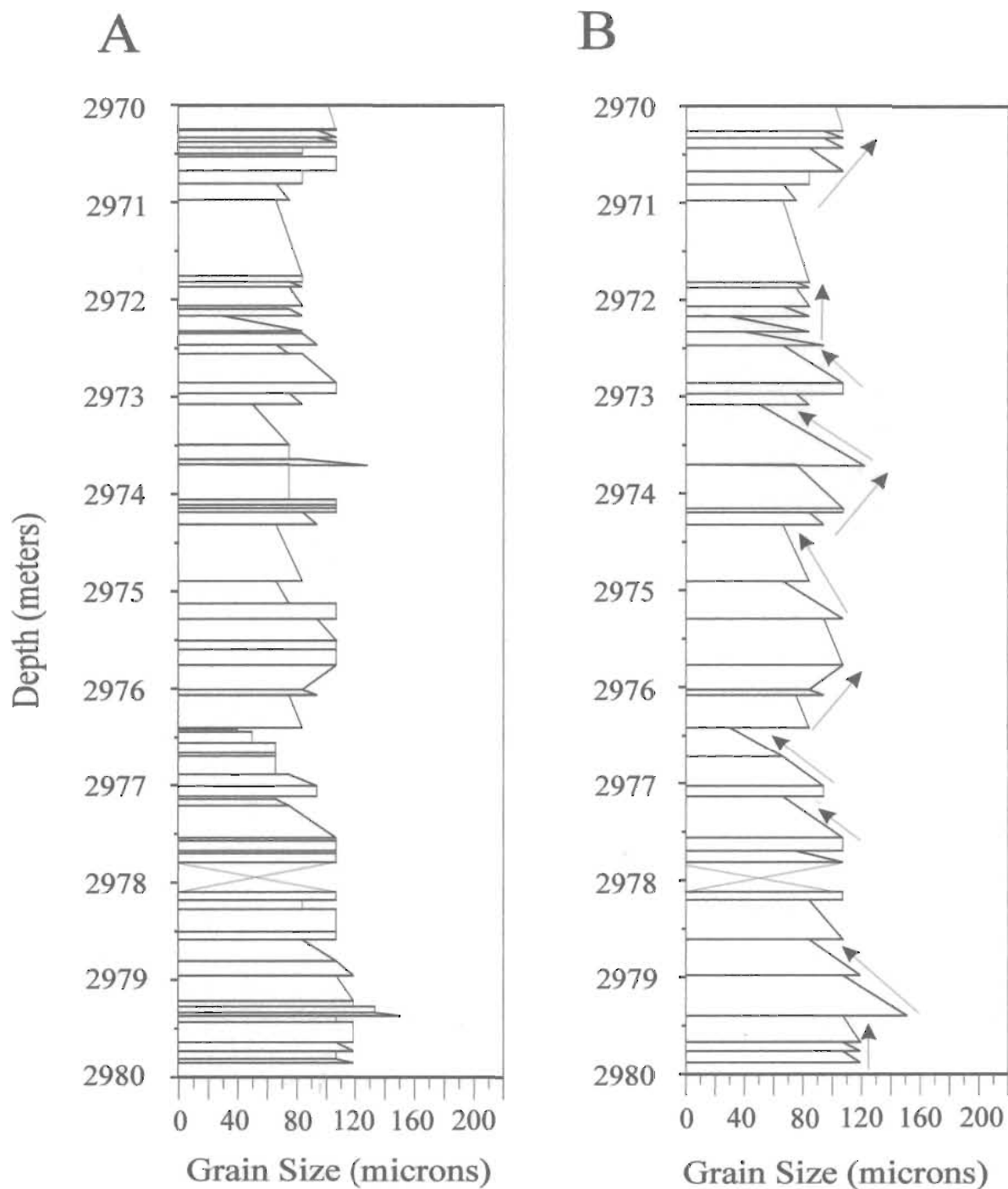


Fig.3.9. Grain size vs. Depth from 2980-2970 m. Log on left (A) represents the positions of all contacts and tops of transitions recorded between 2980-2970 m while the log on the right (B) marks only bed boundaries. Arrows are used to show the general tendency for grain size to increase, decrease or remain the same vertically.

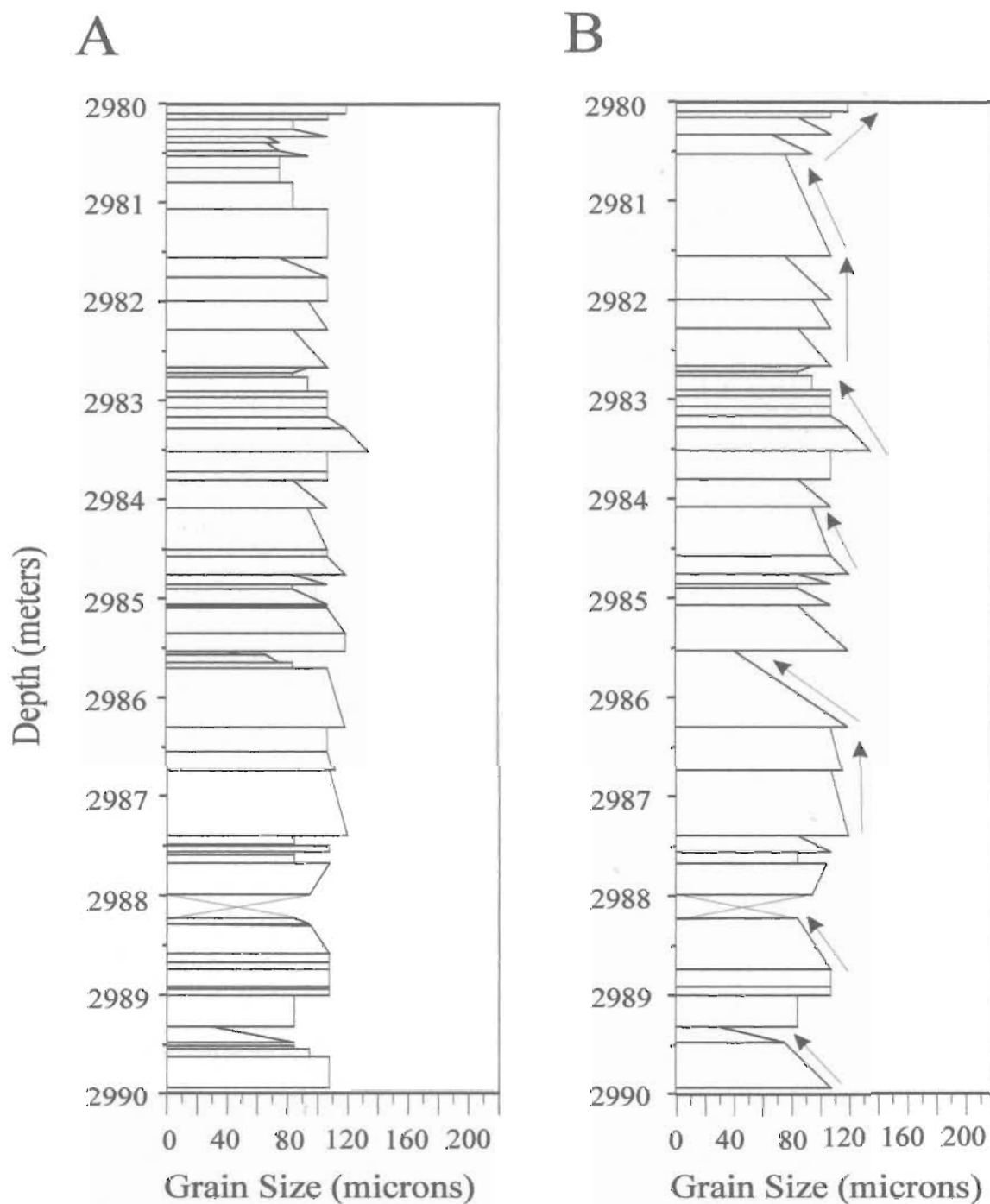


Fig.3.10. Grain size vs. Depth from 2990-2980 m.. Log on left (A) represents the positions of all contacts and tops of transitions between 2990-2980 m observed in core while the log on the right (B) marks bed boundaries only. Arrows are used to show the general tendency for grain size to increase, decrease or stay the same vertically.



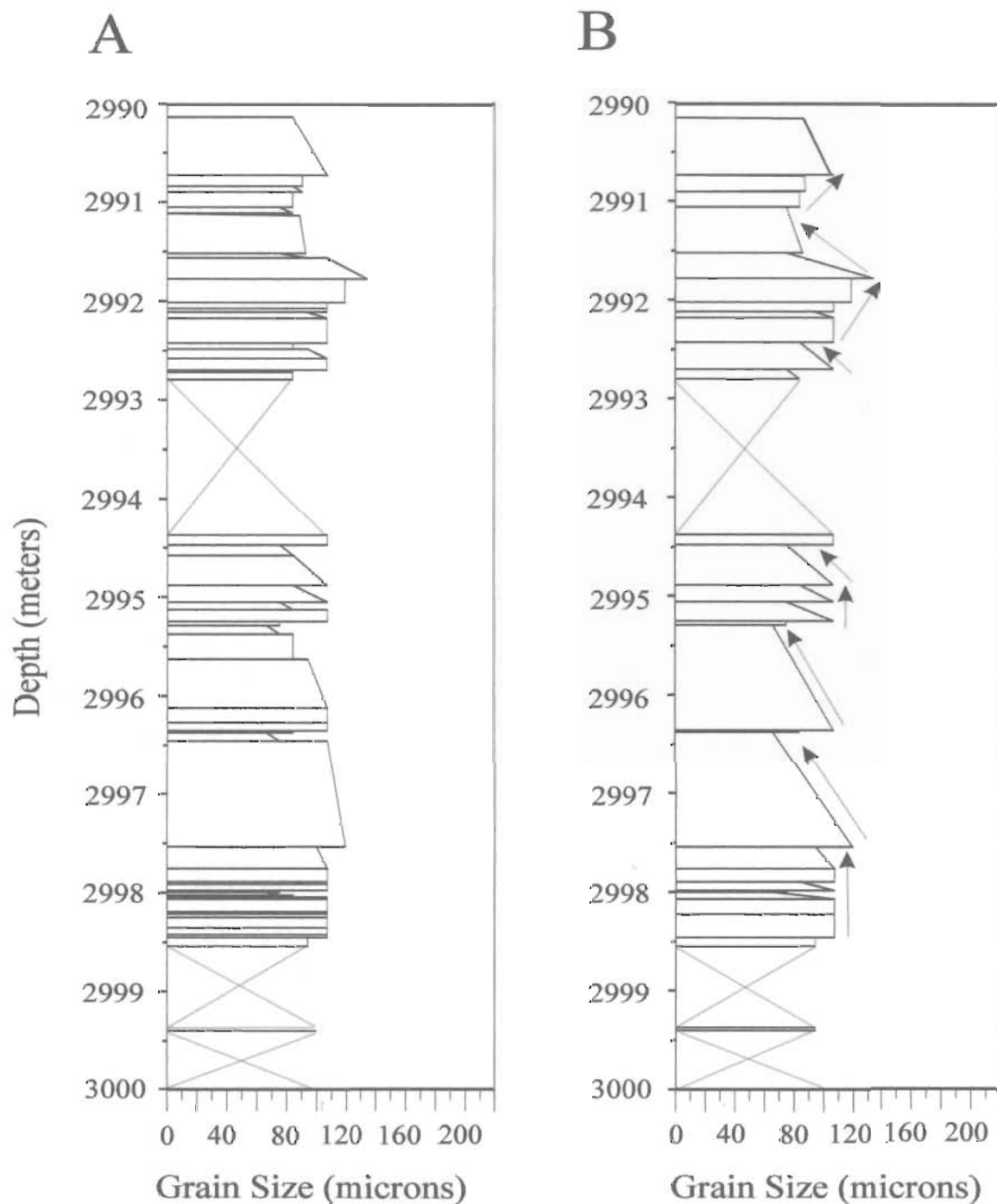


Fig.3.11. Grain size vs. Depth from 3000-2990 m. Log on left (A) represents the positions of all contacts and tops of transitions recorded between 3000-2990 m while the log on the right (B) marks only bed boundaries. Arrows are used to show the general tendency for grain size to increase, decrease or remain the same vertically.

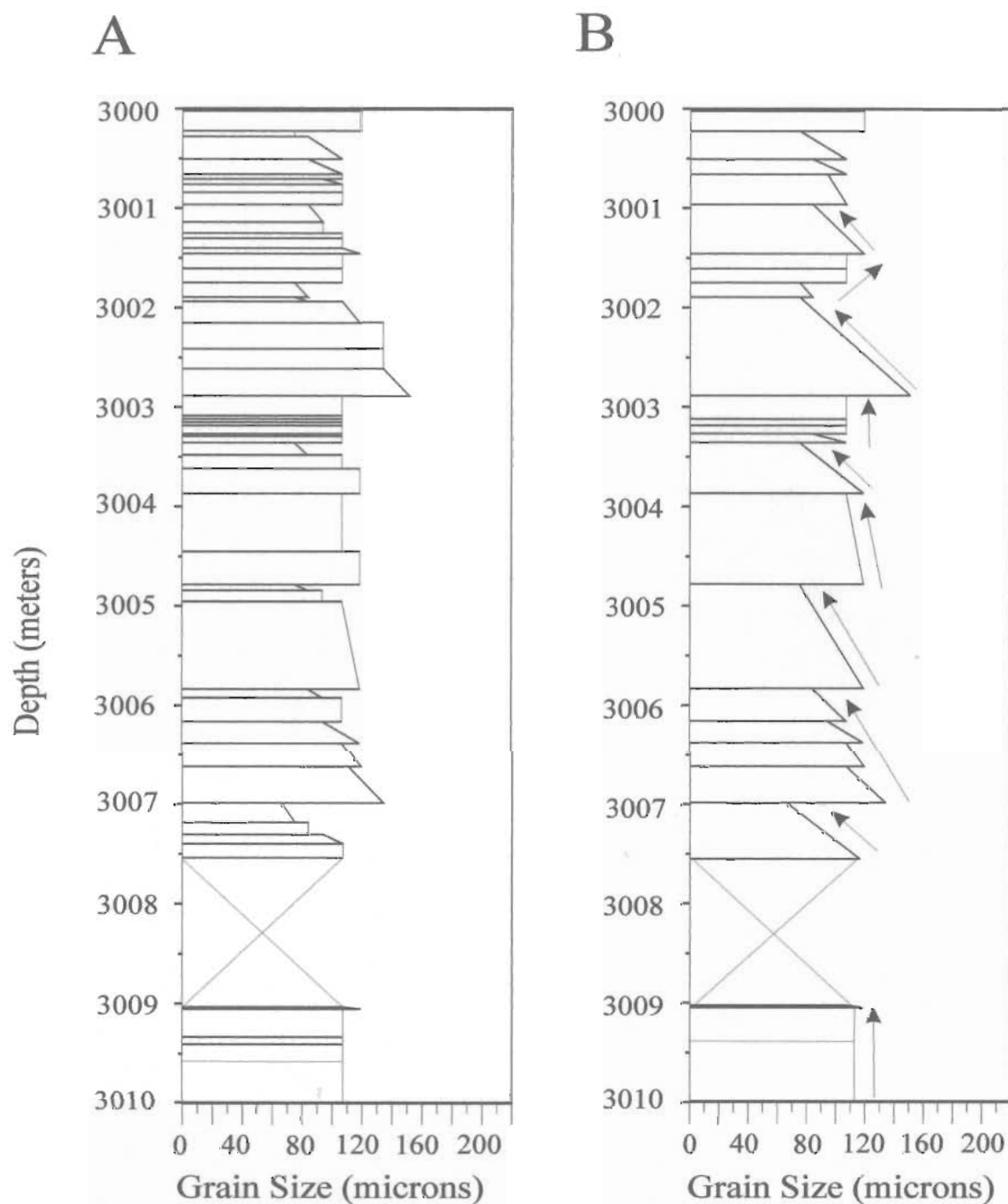


Fig.3.12. Grain size vs. Depth from 3010-3000 m. Log on left (A) shows the positions of all contacts and tops of transitions recorded between 3010-3000 m while the log on the right (B) shows the positions of bed boundaries only. Arrows are used to show the general tendency for grain size to increase, decrease or remain the same vertically.

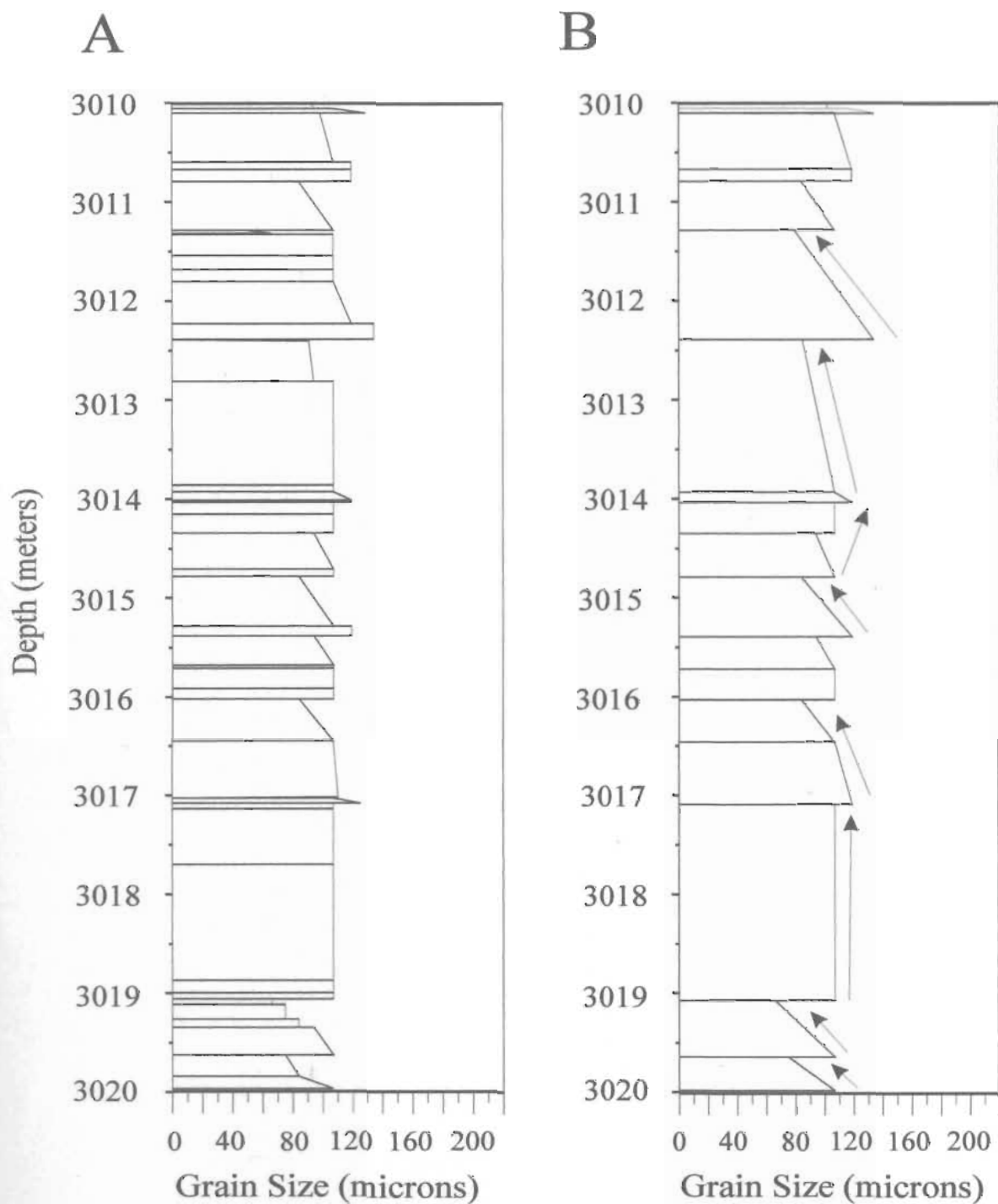


Fig.3.13. Grain size vs. Depth from 3020-3010 m. Log on left (A) represents the positions of all contacts and tops of transitions recorded between 3020-3010 m while the log on the right (B) marks only bed boundaries. Arrows are used to show the general tendency for grain size to increase, decrease or remain the same vertically.

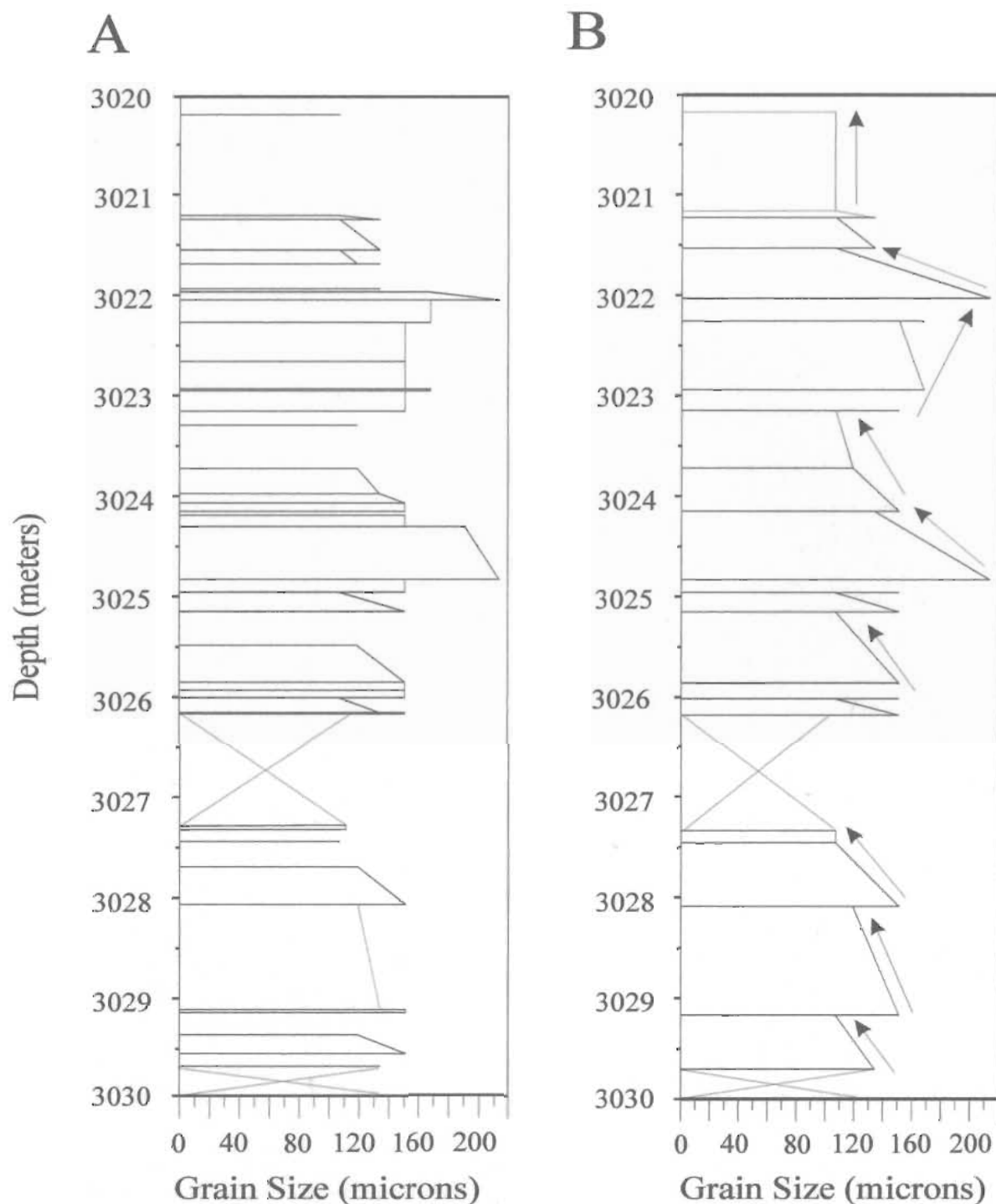


Fig.3.14. Grain size vs Depth from 3030-3020 m. Log on left (A) represents the positions of all contacts and tops of transitions between 3030-3030 m while the log on the right (B) marks bed boundaries only. Arrows are used to show the general tendency for grain size to increase, decrease or remain the same vertically.

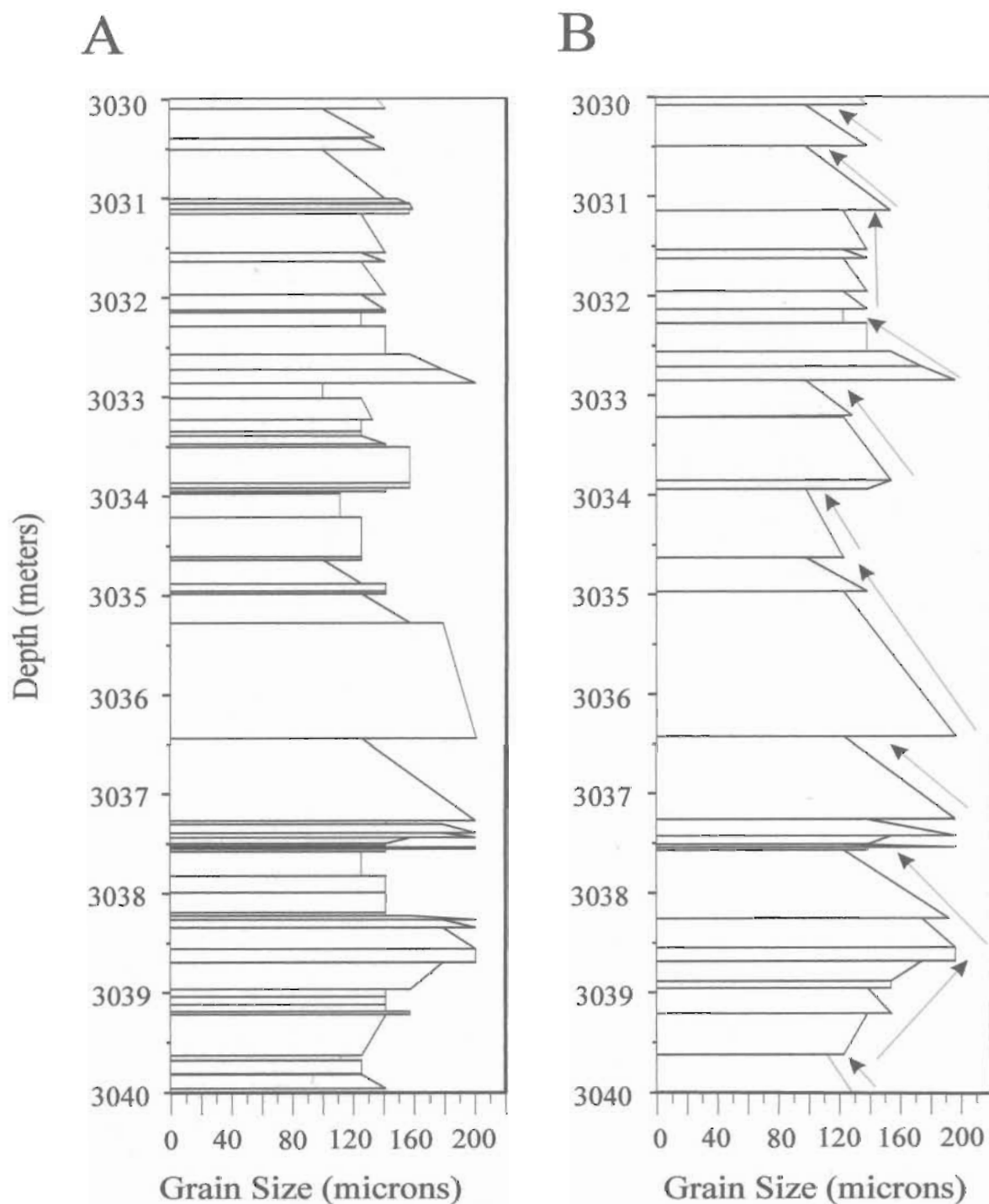


Fig.3.15. Grain size vs. Depth from 3040-3030 m. Log on left (A) represents the positions of all contacts and tops of transitions observed between 3040-3030 m in the core while the log on the right (B) marks only bed boundaries. Arrows are used to show the general tendency for grain size to increase, decrease or remain the same vertically.

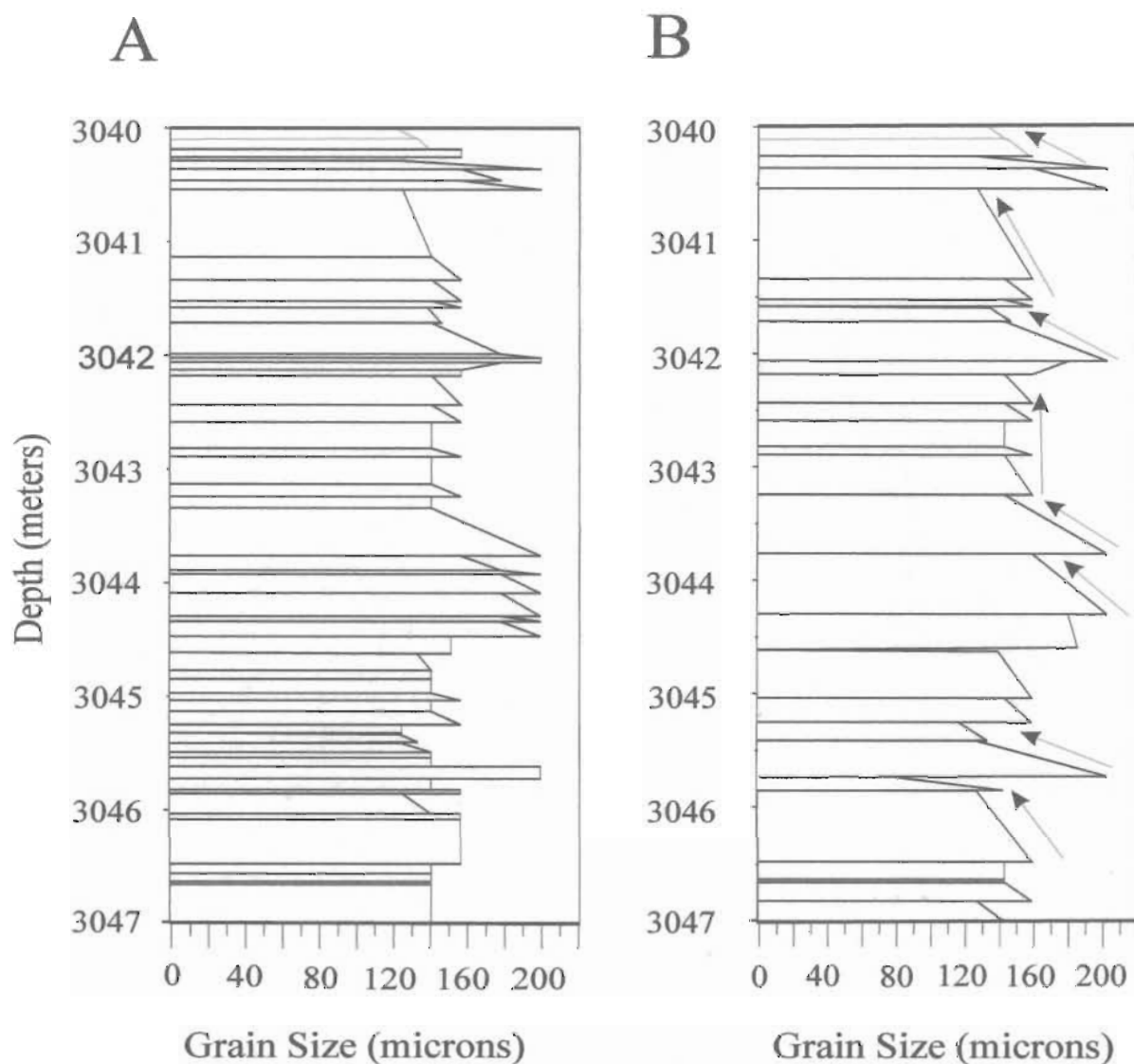


Fig.3.16. Grain size vs. Depth from 3047-3040 m. Log on left (A) represents the positions of all contacts and tops of transitions observed in the core between 3047- 3040 m while the log on the right (B) marks only bed boundaries. Arrows are used to show the general tendency for grain size to increase, decrease or remain the same vertically.

The bulk of the core consists of fining-upward grain-size trends. These fining-upward trends range from 30 cm to 1.75 m, averaging  $\sim 75$  cm in thickness (refer to Figures 3.6-3.16). Fining-upward grain-size trends may encompass one bed (i.e., normal grading) or a number of beds. Beds exhibit grain-size trends if they consist of a number of intervals that have a tendency to fine upward. In most instances, the term 'compound normally graded bed' is the best phrase to describe their architecture because they consist of a number of ungraded to normally graded intervals. Very rarely do these beds contain reversely graded intervals. Fining-upward grain-size trends spanning more than one bed are more common than those spanning single beds. The grain-size changes through intervals with fining-upward trends range from a minimum of  $\sim 20 \mu\text{m}$  to a maximum of  $120 \mu\text{m}$ , averaging  $\sim 75 \mu\text{m}$ .

Second in abundance to the fining-upward trends are coarsening-upward trends. These trends are much less common than fining-upward ones. Intervals of these trends range from  $\sim 20$  cm to 1.2 m, and average  $\sim 70$  cm thick. These trends are comprised largely of a succession of normally graded beds, less commonly ungraded and normally graded beds, and rare inverse and non-graded to normally graded beds. Nowhere in the core are coarsening-upward trends represented by a single inversely graded bed. The grain-size increase over coarsening-upward trends ranges from a minimum of  $20 \mu\text{m}$  to a maximum of  $100 \mu\text{m}$ , and averages  $\sim 50 \mu\text{m}$ .

Static trends are defined as those trends which show no significant vertical increase nor decrease in grain size. They represent sections of the core which consist of a succession of normally graded, and non graded to normally graded beds. They are the

least common of the medium-scale trends. They range from 50 cm to 2.0 m, and average ~90 cm thick. Reversely graded beds are absent from these trends.

#### **3.2.2.4 Interpretation and Implications**

Single normally graded beds, and compound normally graded and ungraded to normally graded beds that form fining-upward grain-size trends, imply cyclic net decreases in the amount of energy in the depositional system. These trends (from base to top) might represent different sub-environments with specific energy regimes; however, the fining-upward trend does not imply that the sediment source changed. This is substantiated by the fact that grain sizes have little absolute variation from base to top of such trends, and the mineralogy is nearly constant.

The coarsening-upward trends consist of combinations of normally graded, ungraded, and rarely reversely graded beds. These suggest a net increase in energy from base to top. They might signify different sub-environments but are not thought to indicate a change in the sediment source for the reasons given above. The rarity of these trends might imply that progressive increases in energy through time were less common than progressive decreases. Note however, that in the middle unit, there is no net increase or decrease. This is because each progressive fining trend ends with a bed with markedly greater grain size.

Static trends imply no significant medium-scale net increases or decreases in energy in the depositional system. They also strongly suggest that the sediment available during their deposition was essentially uniform in size.



### 3.2.2.5 Third Order Grain-Size Trends

Third order grain-size trends are a property of the smallest units and characterize what have been defined as intervals. Intervals are parts of beds and are therefore within-bed trends. There are 566 intervals in the White Rose A-17 core. Intervals range from 0.7 cm to 190 cm, averaging 30 cm thick (Figure 3.17). These intervals are most commonly ungraded.

There are 332 ungraded intervals representing ~44.25% of the core. These intervals range from 1-117 cm thick with a mean thickness of ~14 cm. Because of their abundance, they appear to be distributed uniformly. In a number of cases, (refer to Figures 3.6-3.16) they stack vertically and are the building blocks of the fining and coarsening trends. They also (in combination and with normally graded intervals) constitute a number of the normally graded beds, which therefore are effectively step-wise graded.

Second in frequency to the ungraded intervals are normally graded intervals. There are 216 such intervals representing ~41.5% of the core. These intervals are on average 19 cm thick and range from 1.3 -116 cm. Grain-size change over these intervals ranges from a minimum of ~10  $\mu\text{m}$  to a maximum of 80  $\mu\text{m}$ , averaging 18  $\mu\text{m}$ . Normally graded intervals appear to have no preferred distribution in the core.

Reversely graded intervals are the least abundant of all intervals. There are only 18 such intervals, which represent ~3.6% of the core. Reversely graded intervals range from 4.6 to 90 cm, and average ~9 cm thick. These intervals are most commonly found in the lowermost 20 m and uppermost 40 m of core, where they form parts of thicker

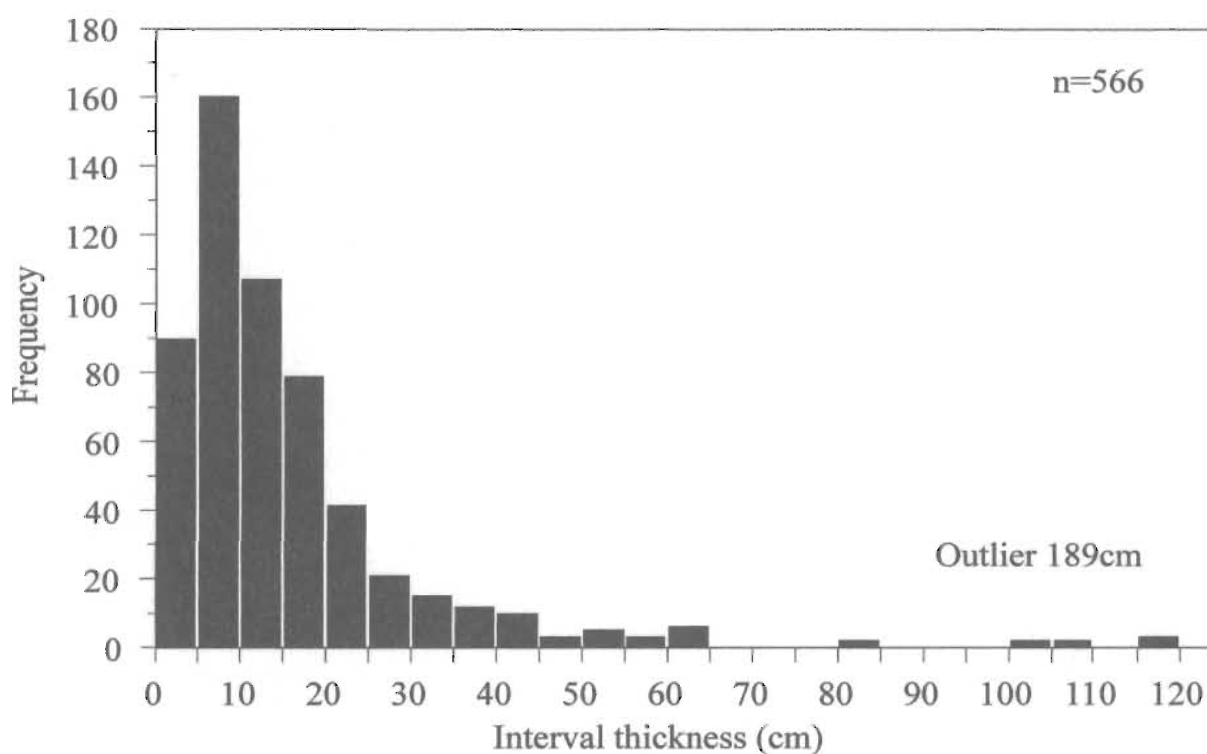


Fig. 3.17. Histogram displaying the frequency of thickness for the 566 intervals in the White Rose A-17 core. Intervals range from a minimum of 0.7 cm to a maximum of 189 cm (outlier). Average interval thickness is approximately 30 cm. Intervals appear to have a log-normal distribution (cf. Drummond and Wilkinson, 1996). Class width is 5cm with data plotted at midpoints.

coarsening-upward trends. They are not found in cored intervals with medium-scale fining-upward and static trends.

#### **3.2.2.6 Interpretation and Implications**

The ungraded intervals in the A-17 core have two probable explanations. They might represent deposition under static conditions, or the sediment available during their deposition was of uniform size even if energy levels fluctuated. In some cases, due to the presence of shells and cements, the ungraded character of some intervals might be a false impression of grain-size variability. Most such intervals, however, are unequivocally ungraded when examined with a binocular microscope.

Normally graded intervals appear to be a result of suspension sedimentation from waning flows. During such processes, particles settle from suspension at different rates. Denser or larger particles settle out first, followed by finer grains. Normally graded beds form in shallow-water settings by sedimentation from suspension clouds generated by storm activity on a shelf, or in deltas with fluctuating fluvial input (Boggs, 1987). During the onset of a storm, large waves put large volumes of seafloor sediment into suspension. When the storm passes, the suspended material returns to the bottom. The larger, heavier grains fall first, followed by the smaller, lighter grains. The abundance of normally graded intervals in the A-17 core implies repeated deposition by decelerating flows, which might be attributed to the onset and passage of storms on a shallow shelf. A shelf setting is interpreted for these deposits based on sedimentological criteria later in this chapter.

Reversely graded intervals are the most difficult of the three to interpret and explain. In the sedimentary record, inverse grading is a relatively rare phenomenon. Boggs (2001) notes that reverse grain-size grading has been attributed to two mechanisms: (1) dispersive pressure and (2) kinetic sieving. Dispersive pressure is believed to be proportional to grain size. Thus, higher dispersive pressures act on the larger particles and tend to force them into the zone of least shear, placing them atop of the finer grains. Kinetic sieving occurs when small grains infiltrate the voids between larger ones. This process presumably takes place in a mixture of grains undergoing agitation. Because reversely graded intervals in the A-17 core are very rare, and the formative mechanism(s) are poorly understood, little significance is placed on these intervals in this thesis.

### **3.3 Contacts and Transitions**

#### **3.3.1 Introduction**

Six hundred and thirty-nine contacts/transitions (minus the 90 discontinuities) with a number of geometries belonging to four principal types were observed and coded in the White Rose A-17 core. Codes distinguish contact geometry. Changes in grain size and permeability across different contact types provide essential data for this study. This section is concerned primarily with the photographic documentation of each principal contact type.

### 3.3.2 Erosive Contacts

The most abundant type of contact in the White Rose A-17 core is erosive.

Erosive contacts are presumed to be bed boundaries. They typically truncate laminae, correspond with marked increases in grain size, and in a number of cases are mantled by bioclasts. Rarely, erosive contacts are draped by fine-grained silty/carbonaceous material. There are 201 erosive contacts in the core.

Erosive contacts have three principal geometries. The first type of erosive contact ranges from very gently to moderately undulatory and is non-inclined (Plate 3.1). There are 76 of these contacts. A range of bioclastic debris may mantle these contacts, including serpulid worm tubes, bivalves, and rarely brachiopods (Plate 3.1, Photos A and C). The amount, density, and diversity of this material is variable. Patches of authigenic siderite cement locally accompany the bioclastic debris (Plate 3.1, Photo A). In other cases bioclastic debris is minimal or absent (Plate 3.1, Photo B). Underlying laminae (typically those highlighted by thin disarticulated bivalves and silty/carbonaceous material) are sometimes unequivocally truncated (Plate 3.1, Photos B and C); in other cases truncation is suspected but uncertain (Plate 3.1, Photo A).

The second type of erosive contact is very gently to moderately undulatory and inclined (Plate 3.2). There are 78 of these contacts. Inclination of these contacts measured relative to a plane perpendicular to the edge of the core ranges from a minimum of 3 ° to a maximum of 12 °, averaging 6 °. The dips of these contacts are apparent dips. As with the non-inclined erosive contacts, the amount, density, and variety of bioclastic debris overlying these contacts is highly variable. The quantity of material may be great (Plate

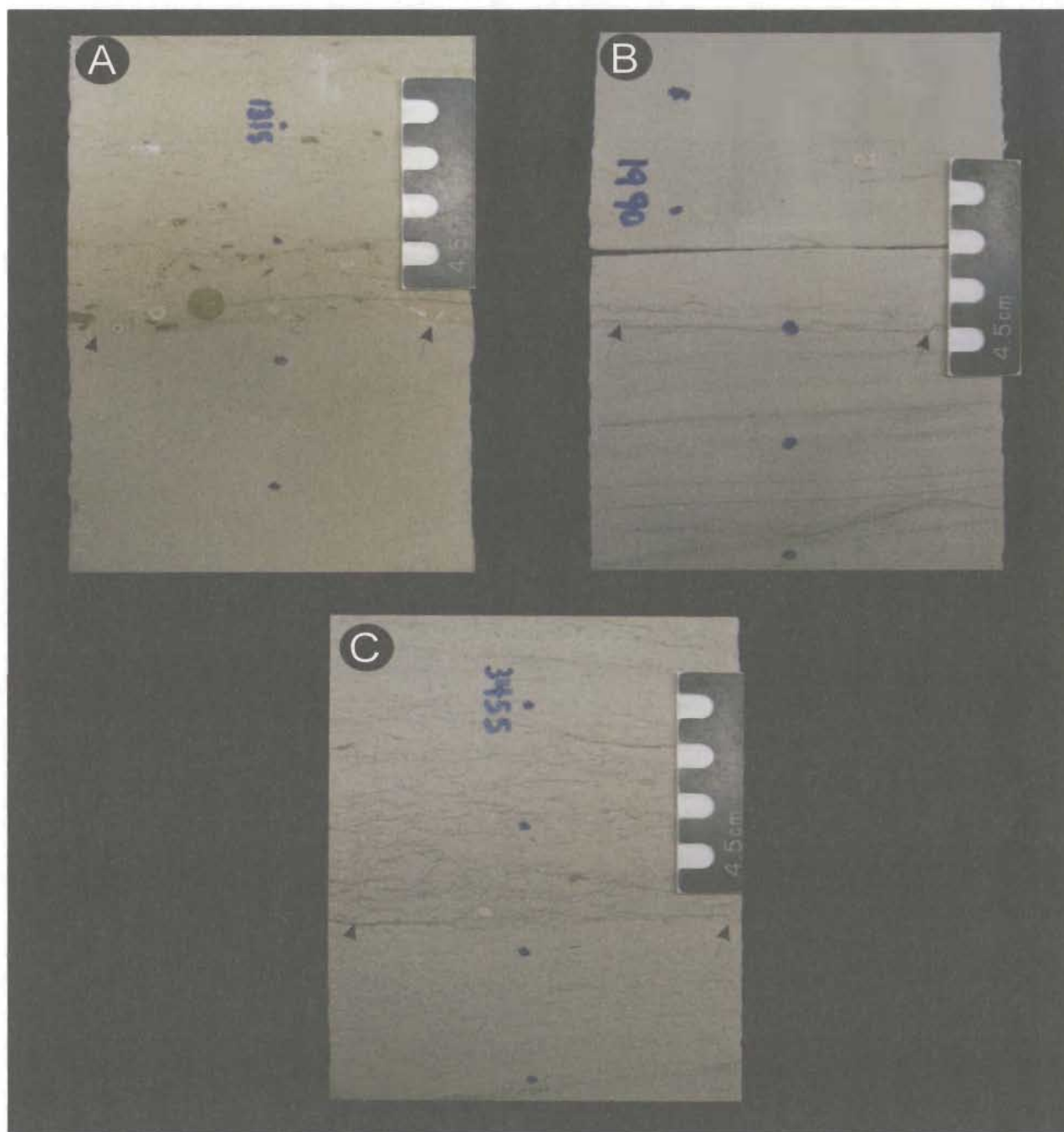


Plate 3.1. Examples of gently to moderately undulatory non-inclined erosive contacts as observed in the White Rose A-17 core. Arrows mark the position of contacts on both sides of each core segment. Depths of the contacts are: A) 2951.20 m, B) 2961.80 m, C) 2979.80 m,

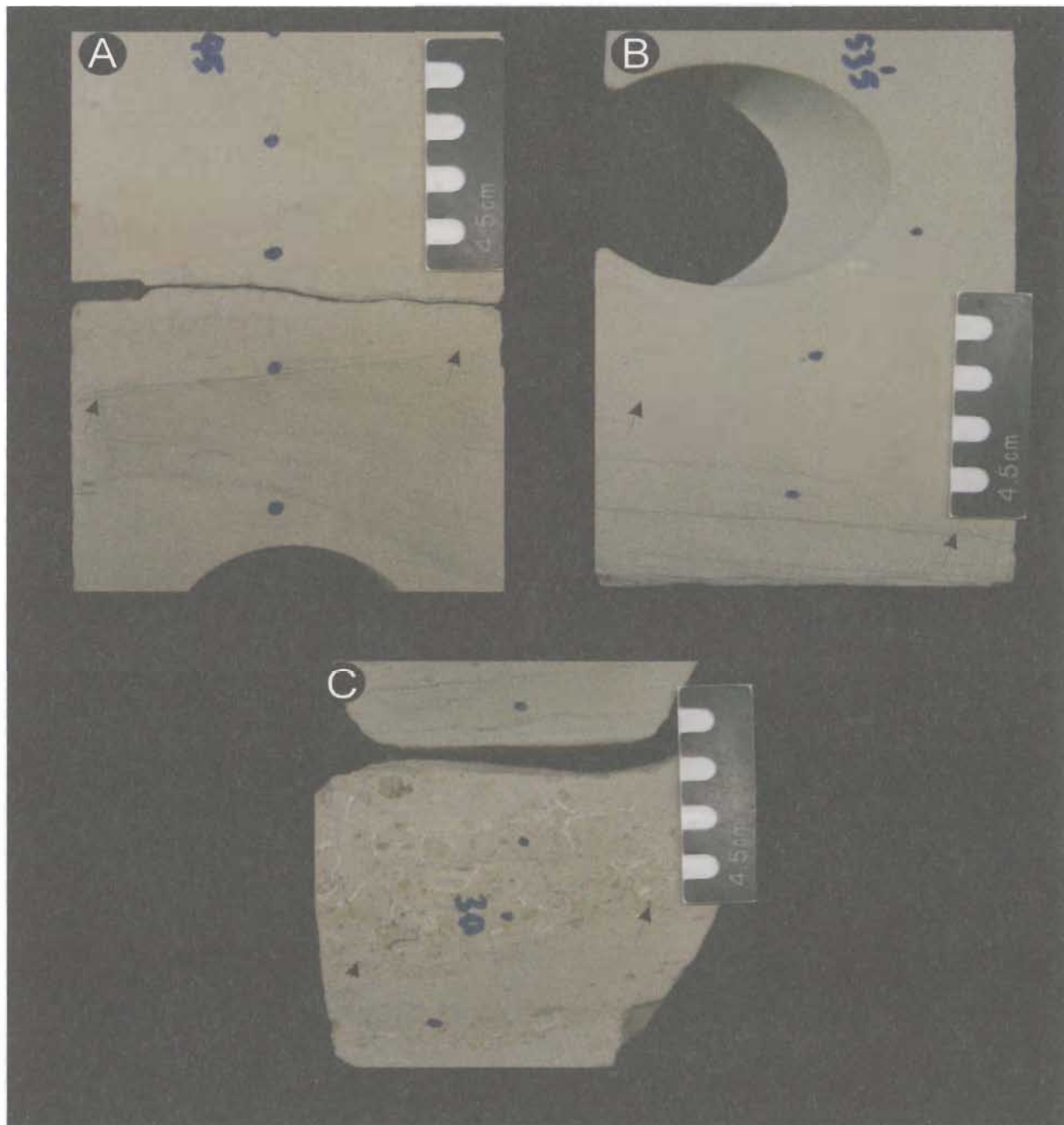


Plate 3.2. Examples of gently to moderately undulatory inclined erosive contacts as observed in the White Rose A-17 core. Arrows mark the position of contacts on both sides of each core segment. Depths of the contacts are: A) 2941.69 m, B) 2949.492 m, C) 2958.356 m.

3.2, Photo C), moderate (not shown) or completely absent (Plate 3.2 Photos A and B). Underlying laminae may be unequivocally truncated (Plate 3.2, Photos A and B) or are very difficult to see (Plate 3.2, Photo C). Spraying of the core with water clarifies that many of the contacts do indeed truncate faint low-angle laminae.

The third and least abundant erosive contact is gently to highly curved, and convex-upward in shape (Plate 3.3). There are 47 such contacts. These contacts are only rarely overlain by bioclastic debris (Plate 3.3, Photos A). Instead, bioclastic debris is typically absent above these contacts (Plate 3.3, Photos B and C). Underlying laminae are typically hard to recognize, but in a few cases are clearly truncated (Plate 3.3, Photo C). In most cases these contacts are overlain by low angle, gently curved, concordant laminae (Plate 3.3, Photos B and C).

### **3.3.3 Abrupt Contacts**

The second most abundant type of contact is abrupt. As with erosive contacts, abrupt contacts have three principal geometries, which total 183 in number. Abrupt contacts occur within beds, between different facies, between zones of the same facies, and above shell accumulations (they do not define bed boundaries). They may be demarcated by thin shell fragments, thin silty/carbonaceous laminae or may be very subtle.

The first type of abrupt contact is very gently to moderately undulatory and non-inclined (Plate 3.4). In the White Rose A-17 core, there are 63 such contacts. In a number of cases, the finer-grained sediment is above the contact (Plate 3.4, Photos A and C); less



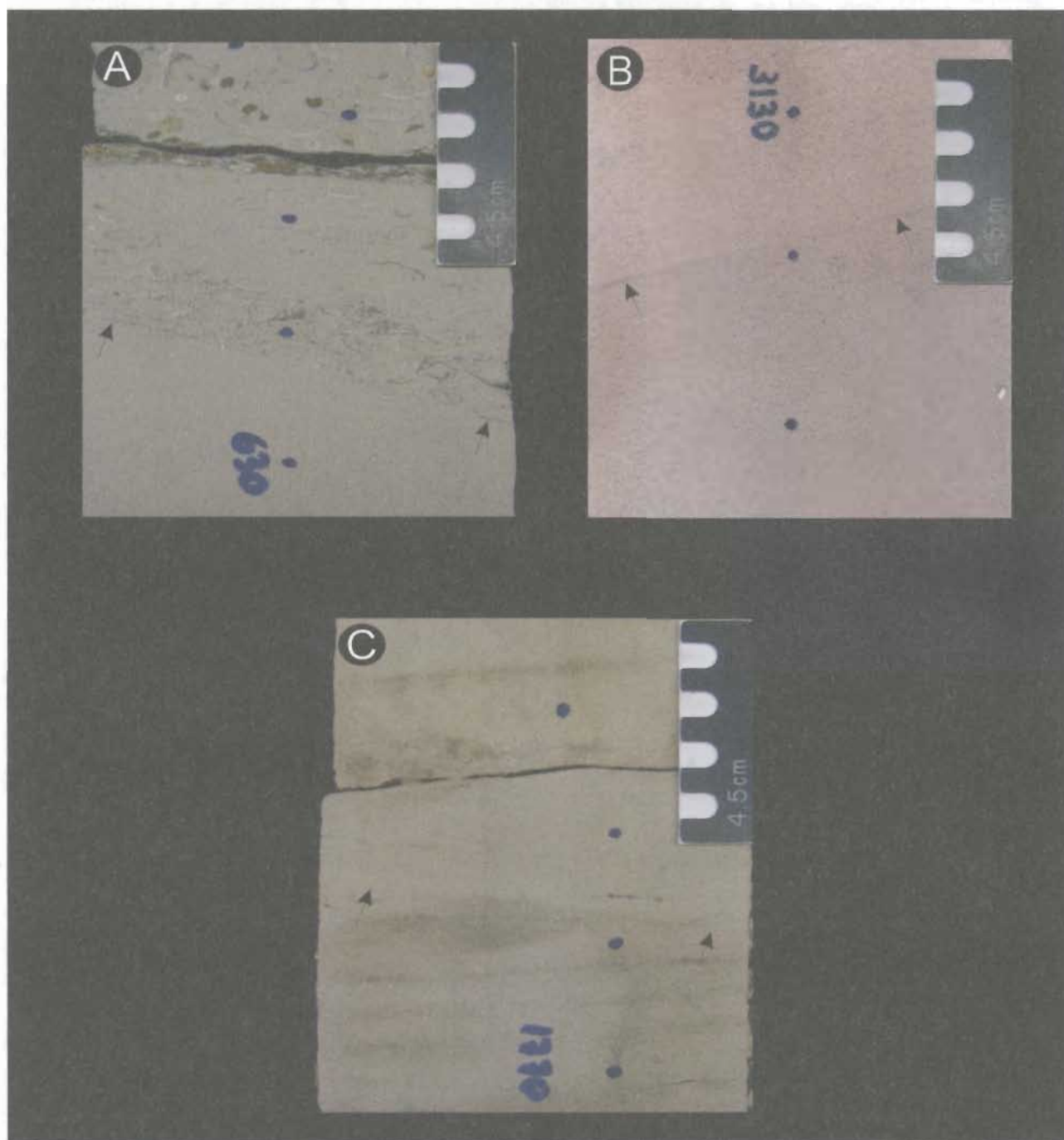


Plate 3.3. Examples of gently to highly curved, convex-up erosional contacts as observed in the White Rose A-17 core. Arrows mark the position of contacts on both sides of each core segment. Depths of the contacts are: A) 2960.82 m, B) 3033.218 m, C) 2995.248 m.

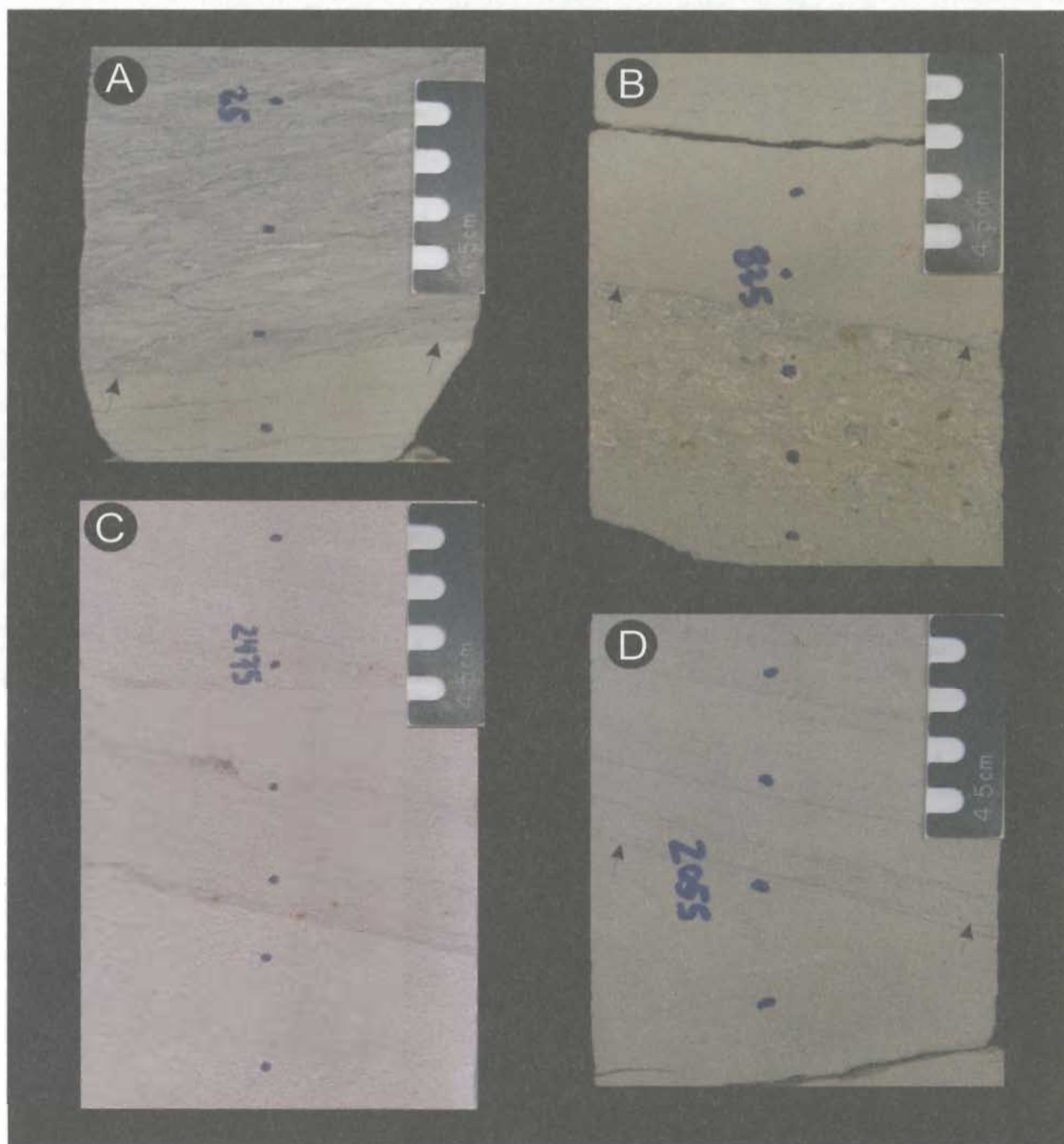


Plate 3.5. Examples of very gently to moderately undulatory inclined abrupt contacts as recognized in the White Rose A-17 core. Arrows mark the position of contacts on both sides of each core segment. Depths of the contacts are: A) 2941.625 m, B) 2966.779 m, C) 2977.16 m, D) 3003.478 m.

commonly, the reverse is true (Plate 3.4, Photo B). These contacts are usually highlighted by thin bioclasts and silt (Plate 3.4 Photos A, B, and C) and are less commonly found directly above bioclastic accumulations (not shown).

The second type of abrupt contact is very gently to moderately undulatory and inclined (Plate 3.5). There are 64 such contacts. These contacts have apparent dips that range from  $2^{\circ}$ - $15^{\circ}$ , and average  $6$ - $7^{\circ}$  measured relative to a plane at right angles to the edge of the core. The variation in the apparent dip of these contacts may be a function of the angle with which the core barrel intersected bedding-bedding dips range from  $0$ - $8^{\circ}$  degrees (Petro-Canada geologists, personal communication, 2005). These abrupt contacts are principally found within beds. They may separate different facies, occurrences of the same facies, and less often they are found above shell accumulations.

The least abundant type abrupt contact is gently to highly curved, and convex-up (Plate 3.6). There are 56 of these contacts in the White Rose A-17 core. These contacts are the most difficult to recognize because there is limited textural contrast associated with them. These contacts range from very gently curved and convex-up (Plate 3.6, Photos A and B) to moderately or highly curved and convex-up (Photo C). Overlying laminae (where present) are usually concordant with these abrupt contacts (Plate 3.6, Photos A and B).

### **3.3.4 Cementation Contacts**

Third in abundance after erosive and abrupt contacts are cementation contacts. There are 90 such contacts. Cementation contacts either separate pervasively cemented

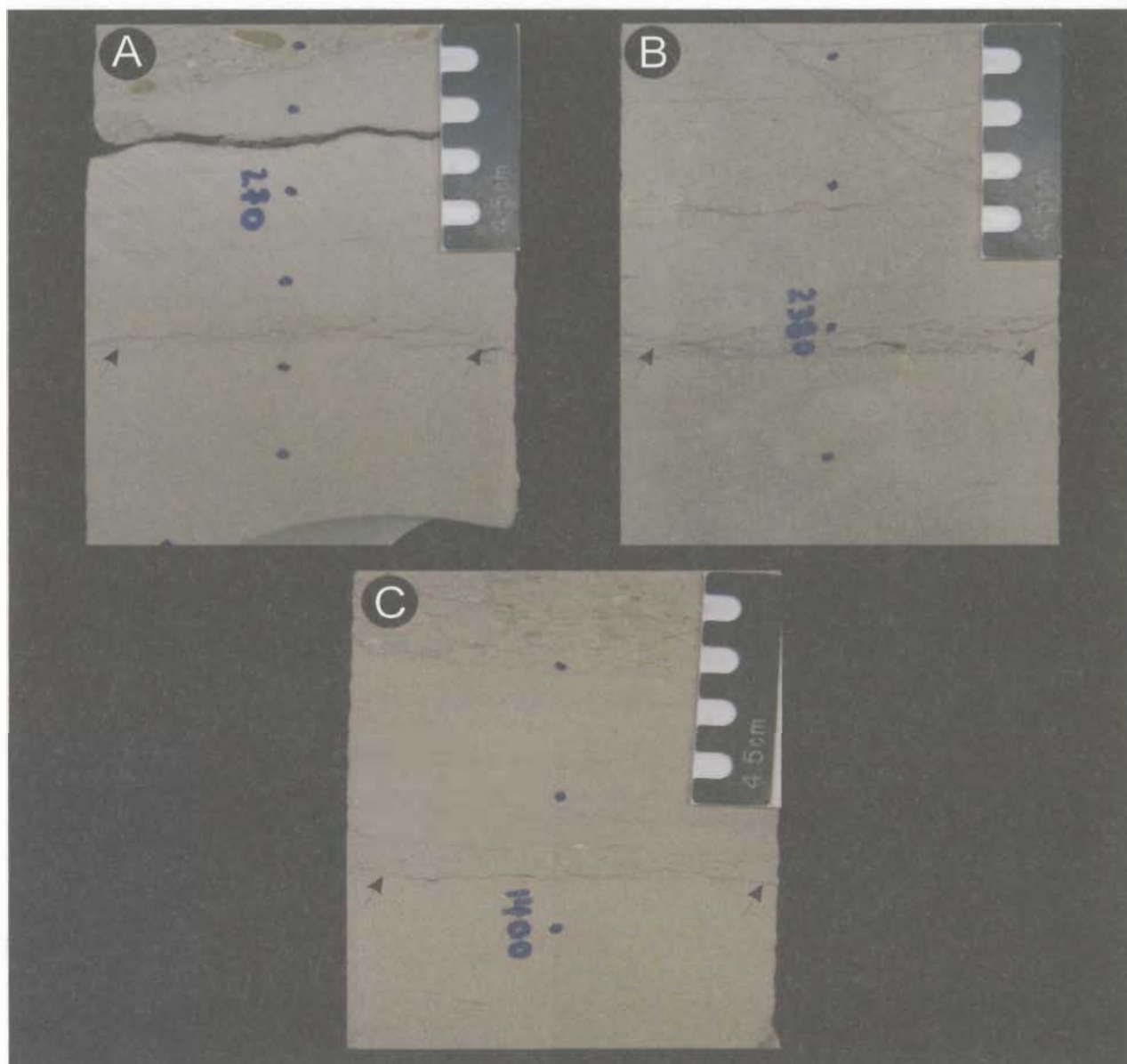


Plate 3.4. Examples of very gently to moderately undulatory non-inclined abrupt contacts as recognized in the White Rose A-17 core. Arrows mark the position of contacts on both sides of each core segment. Depths of the contacts are: A) 2949.505 m, B) 3012.808 m, C) 2982.757 m.

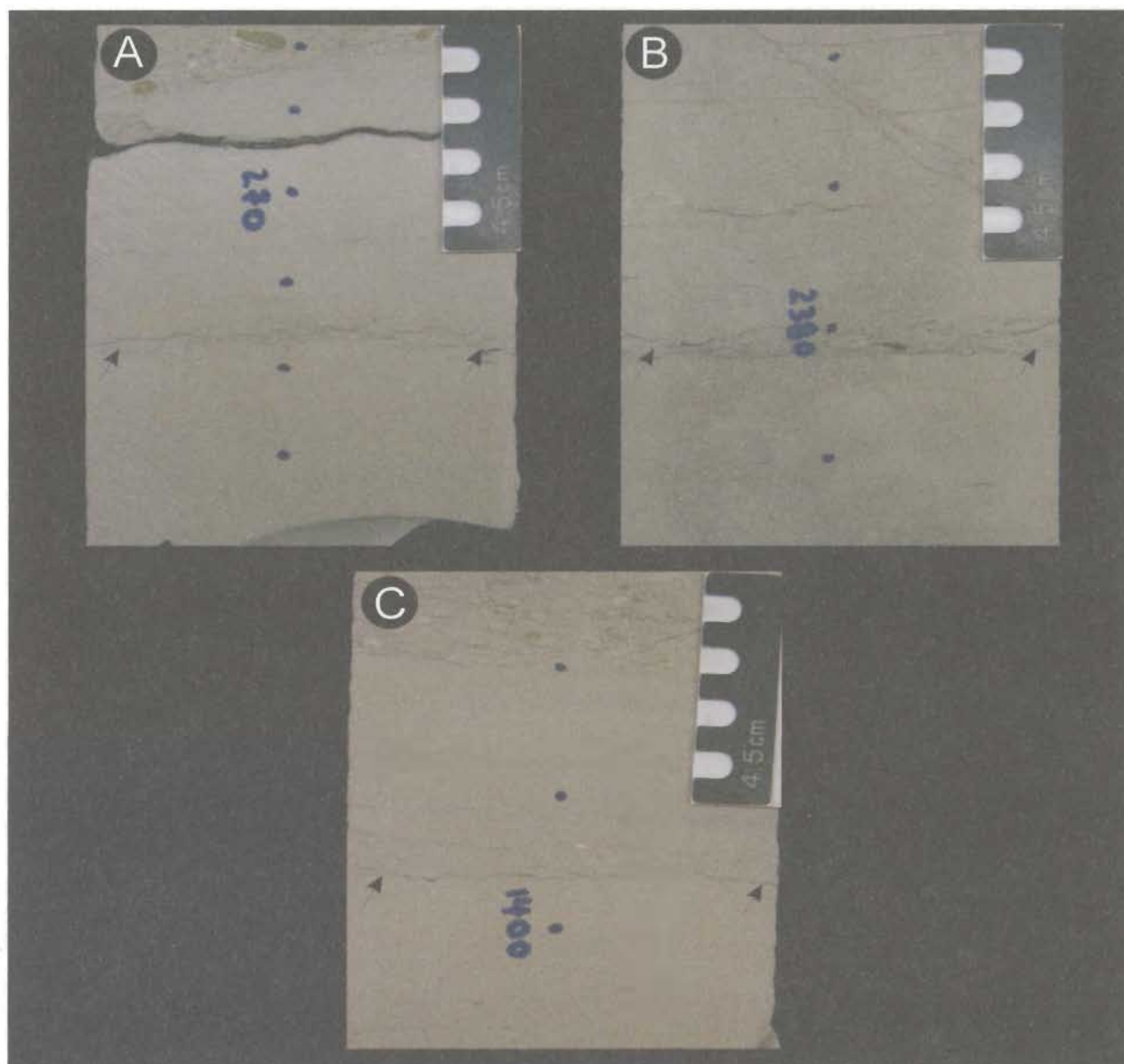


Plate 3.4. Examples of very gently to moderately undulatory non-inclined abrupt contacts as recognized in the White Rose A-17 core. Arrows mark the position of contacts on both sides of each core segment. Depths of the contacts are: A) 2949.505 m, B) 3012.808 m, C) 2982.757 m.



sandstone from more porous sandstone (Plate 3.7, Photos A-F), or separate pervasively calcite-cemented sandstone without bioclasts from those that do contain bioclasts (Plate 3.8, Photos A-D).

Cementation contacts that separate pervasively cemented sandstone from more porous sandstones are always distinct and sharp. Geometrically, they can appear concave-up, convex-up, or moderately undulatory (Plate 3.7, Photos E and F); however, they are most often inclined at angles of 15-30° measured relative to a plane perpendicular to the edge of the core (Plate 3.7, Photos A-D). The fact that these contacts routinely cut across stratification confirms that they are post-depositional features. Their geometry suggests nodular shapes.

Contacts that separate pervasively calcite-cemented zones which do not contain shells from those that do have a multitude of geometries (Plate 3.8, Photos A-D). However, for the purpose of this thesis, they have not been studied in detail because permeability is negligible on either side of these contacts; thus, they have little reservoir significance. Additionally, because there are only 29 of these contacts and their geometries conform to those described for erosive and abrupt contacts, they are believed to add little new to the analysis of the contacts. However, from a stratigraphic point of view they may have significance and thus would require additional investigation, which was not carried out in this thesis.

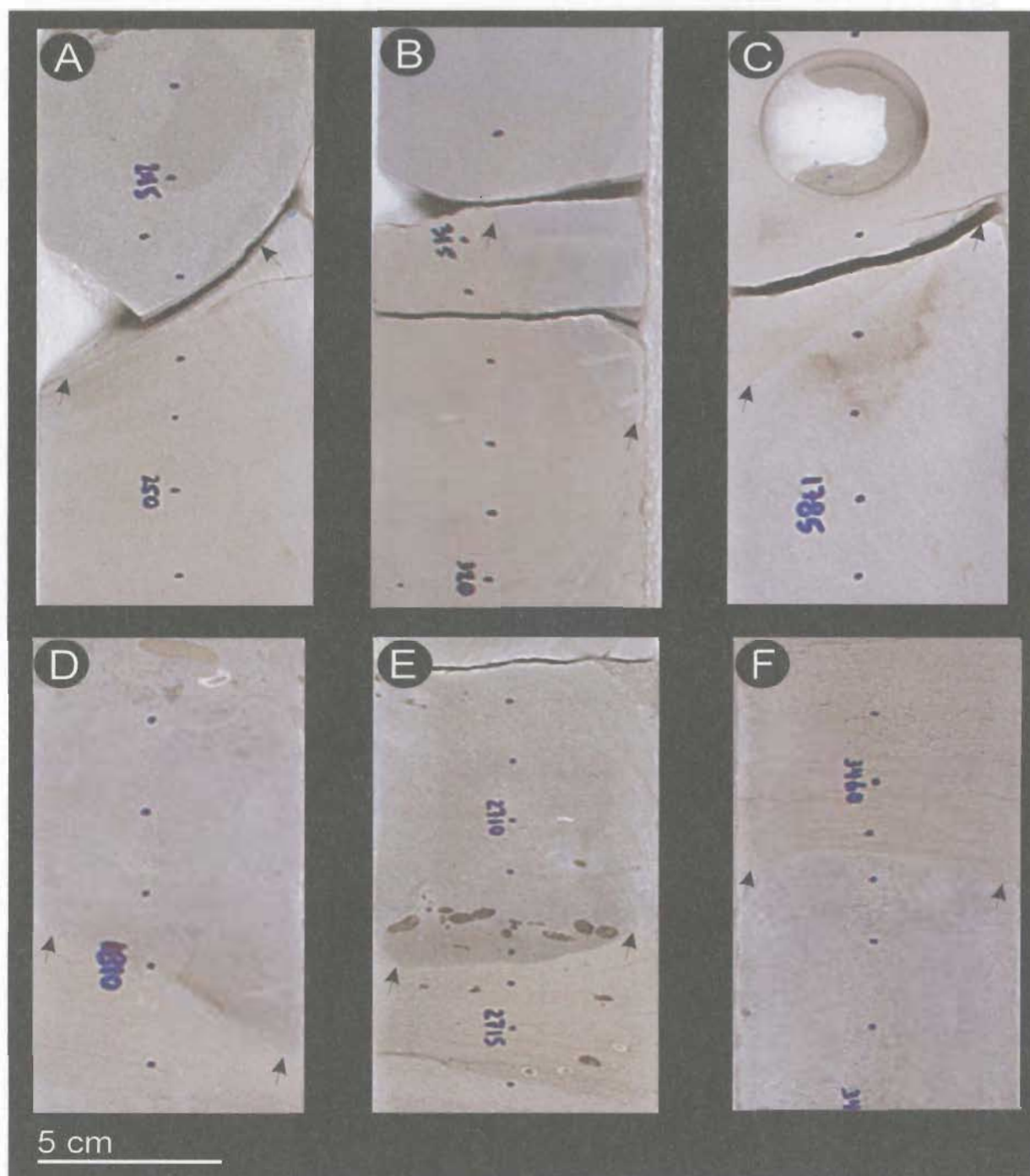


Plate 3.7. Examples of cementation contacts as recognized in the White Rose A-17 core. Arrows mark the positions of contacts on both sides of each core segment. Depths of the contacts are: A) 2978.91 m, B) 2950.873 m, C) 2995.630 m, D) 2996.355 m, E) 3021.18 m, F) 3043.340 m.

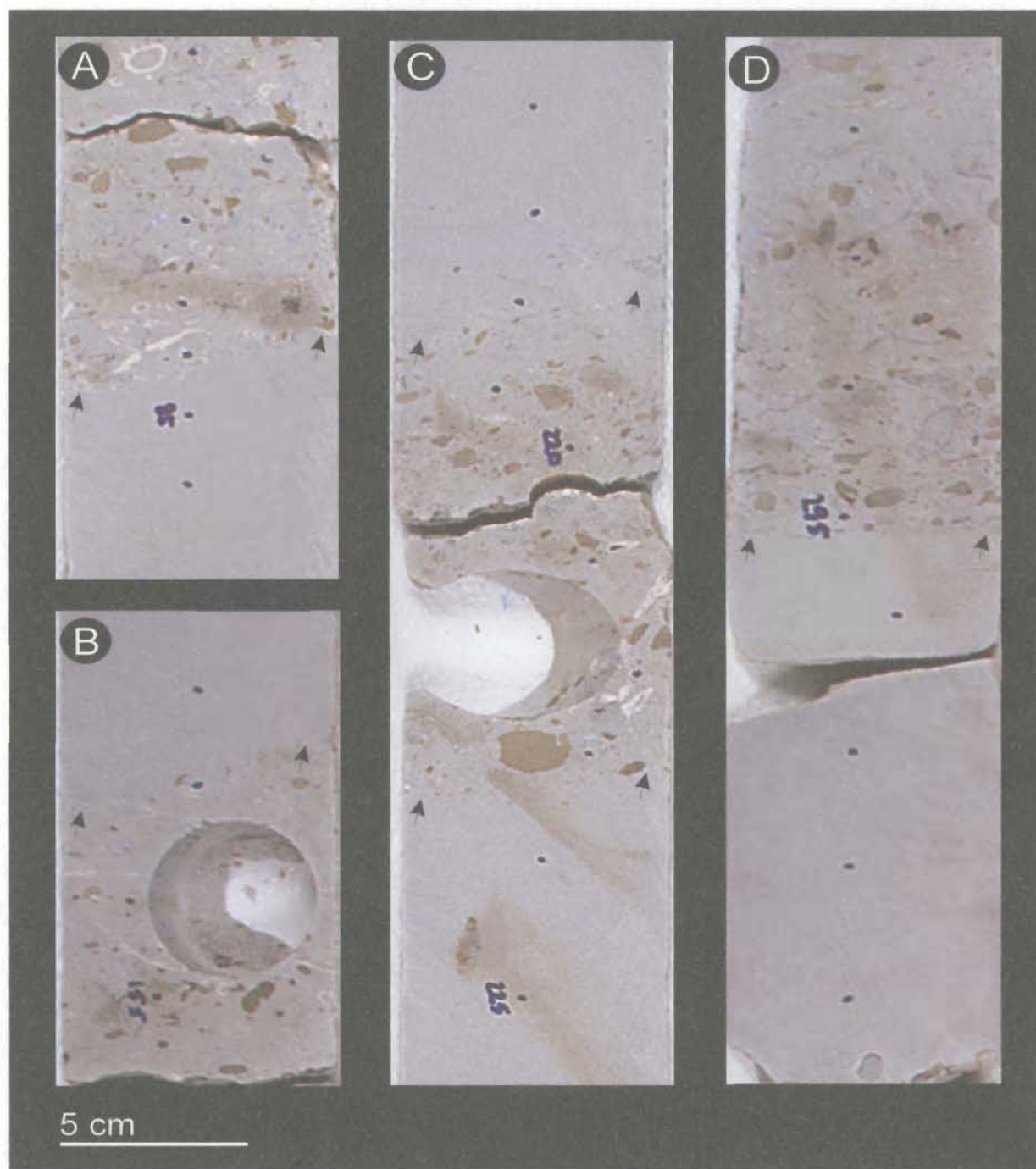


Plate 3.8. Examples of cementation contacts between Facies 5 and Facies 6 as recognized in the White Rose A-17 core. Arrows mark the positions of contacts on both sides of each core segment. Depths of the contacts are: A) 2943.325 m, B) 2945.249 m, C) 2948 and 2948.18 m, D) 2950.16 m.



### 3.3.5 Gradational Transitions

Gradational transitions are relatively uncommon. In total, the size of grains was recorded above and below 64 such transitions. The abundance of bioclasts, authigenic siderite and silt were recorded at the same positions using an ordinal scale.

Gradational transitions most typically occur where bioclasts (of varying abundance) diminish upward away from underlying contacts or where bioclasts, which are aligned with stratification, diminish to zero abundance (Plate 3.9, Photos A and B respectively). Gradational transitions also occur across zones of noticeable change in grain size (Plate 3.9, Photo C). Some gradational transitions occur between unbioturbated and bioturbated zones (Plate 3.9, Photo D), though this is rare.

Grain size, and the abundance of bioclastic debris and authigenic siderite were recorded above and below the top of each gradational transition. This was done to evaluate changes in permeability, discussed in the following chapter. From a sedimentological standpoint, gradational transitions are important because they represent a decrease in energy. The White Rose A-17 core is dominated by small- to medium-scale fining-upward grain-size trends, which internally each have a number of gradational transitions. It is therefore believed that high-energy conditions repeatedly delivered coarser-grained sand and in some cases bioclasts, and that these episodes were followed by waning energy.

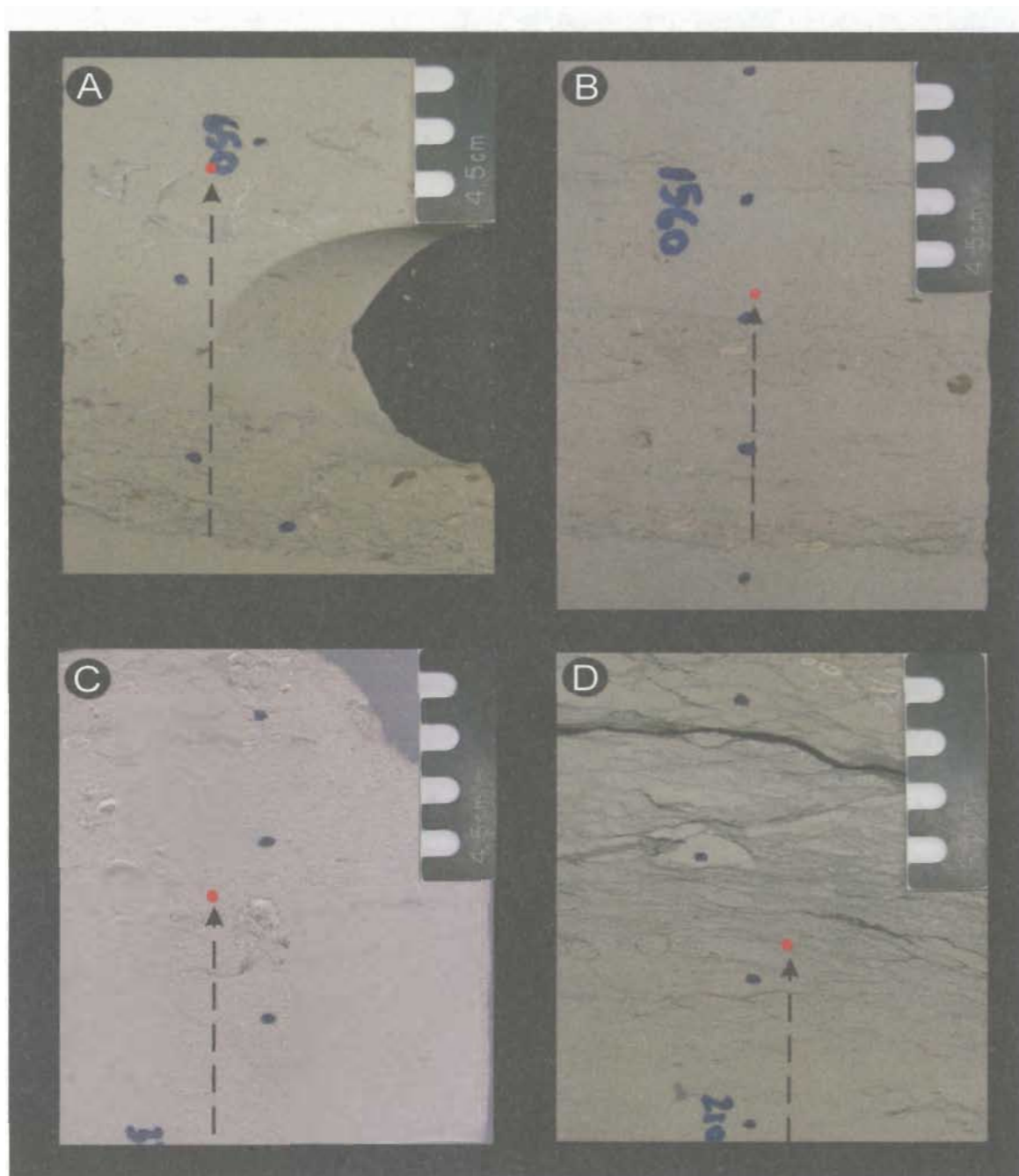


Plate 3.9. Examples of gradational transitions as recognized in the White Rose A-17 core. Dashed arrows represent the gradational intervals. Red dots mark the approximate positions where depth measurements were recorded. Grain sizes were recorded above and below the maximum extent of gradation (i.e. above and below the red dots). Depths for each red dot are: A) 2971.76 m, B) 2988.672 m, C) 3011.323 m, D) 2947.40 m.

### **3.4 Facies**

#### **3.4.1 Introduction**

Based on lithology, sedimentary structures, trace fossils, body fossils and diagenetic components, nine facies are recognized in the A-17 core (Table 3.1). The following subsections define, describe, and provide a process interpretation for each facies. This section will conclude by discussing the most probable depositional environment for the A-17 cored interval, based on facies characteristics and process interpretations.

Some overlap exists between facies. For example, very thin zones of facies 7 and facies 8 identified based upon their shelly components-can appear within facies 1, 2, 3, and 4, which are recognized based upon their characteristic homogeneity or physical sedimentary structures. Specifically, thin-shelled bivalves that characterize facies 8 can occur aligned with stratification in facies 2, 3, and 4. Similarly, these bivalves can occur in facies 7 but are very rare and the zones are so thin that they could not have been shown separately in a graphic column. Additionally, a minor amount of overlap exists between facies 5, which is pervasively cemented by calcite, and facies 9, which is defined by its bioturbation. Zones that are both bioturbated and cemented are included in facies 5. Biogenic traces that are abundant in facies 9 also occur as isolated structures in facies 3, so are discussed under facies 3.

The number of vertical transitions between (a) facies and (b) facies contacts are summarized in Tables 3.2 and 3.3, respectively. Facies associations will be described as part of each facies description.

<b>Facies</b>	<b>Description</b>	<b>Percent of Core</b>	<b>Process Interpretation</b>
<b>Facies 1</b>	Fine- to very fine-grained light gray to beige “clean” homogeneous sandstone	14.7%	Rapid deposition from suspension
<b>Facies 2</b>	Fine- to very fine-grained, planar laminated sandstone	7.0%	Deposition by strong unidirectional or combined-flow currents
<b>Facies 3</b>	Low-angle cross-stratified, fine- to very fine-grained sandstone	53.3%	Product of strong combined-flow currents
<b>Facies 4</b>	Moderately inclined, fine- to very fine-grained sandstone	4.6%	Product of strong combined flow currents
<b>Facies 5</b>	Pervasively calcite-cemented sandstone	12.3%	Dissolution followed by re-precipitation of the shells as calcite cement
<b>Facies 6</b>	Pervasively calcite-cemented sandstone with abundant shelly material	3.1%	Strong erosive currents and rapid deposition. After deposition shells dissolve and re-precipitated as calcite cement.
<b>Facies 7</b>	Shell-serpulid- and siderite-bearing sandstone	2.3%	Erosion, winnowing, and transport followed by mainly rapid deposition
<b>Facies 8</b>	Shelly sandstone	1.4%	Erosion, winnowing, and transport followed by deposition under a strong unidirectional current
<b>Facies 9</b>	Bioturbated sandstone and siltstone	1.3%	Burrowing predominantly by dwelling, deposit- and rare suspension-feeding organisms

Table 3.1. A brief summary of the facies identified in the White Rose A-17 core (left column), the percentage of the core that they occupy (middle column), and their process interpretations (right column).

		F	A	C	I	E	S				
		1	2	3	4	5	6	7	8	9	Total
1		0	10	49	6	4	1	6	2	0	78
F	2	5	0	26	2	0	1	5	1	3	43
A	3	44	26	0	19	5	0	24	14	1	133
C	4	6	2	18	0	3	0	2	0	0	31
I	5	2	0	8	2	0	18	1	2	1	34
E	6	1	0	3	0	17	0	0	0	1	22
S	7	19	3	15	1	1	0	0	0	1	40
	8	2	0	14	1	1	1	0	0	0	19
	9	0	1	0	0	3	2	2	0	0	8
Total		79	42	133	31	34	23	40	19	7	

Table 3.2 Transition matrix for the nine facies identified in the White Rose A-17 core. Facies 1 through 9 are numbered in bold text in the leftmost column and uppermost row. Matrix records the number of upward transitions from one state to the next (in this case the states are facies) when viewing rows. As an example, facies 3 (leftmost column, fourth row) is followed by facies 1 (uppermost row, second column) 44 times. Columns record the number of times a facies succeeds another. In this case, facies 3 succeeds facies 1 49 times (second row, fourth column). Note that most facies are associated with facies 3.

FACIES/CONTACTS																	
F A C I E S / C O N T A C T S		1	2	3	4	5	6	7	8	9	11	12	13	21	22	23	Total
	1	0	5	21	1	4	1	1	1	0	11	11	5	9	10	8	88
	2	0	0	14	0	0	1	1	0	2	9	5	8	9	5	3	57
	3	24	16	0	8	5	0	4	2	0	46	47	29	38	38	37	294
	4	3	0	8	0	2	0	1	0	0	4	4	4	0	7	5	38
	5	1	0	5	1	0	16	0	1	1	0	0	0	0	0	0	25
	6	1	0	3	0	17	0	0	0	1	0	0	0	0	0	0	22
	7	13	3	9	1	0	0	0	0	1	2	5	0	4	3	0	41
	8	1	0	12	1	1	1	0	0	0	0	1	0	2	0	0	19
	9	0	1	0	0	3	2	0	0	0	1	1	0	0	0	0	8
	11	16	9	32	3	0	0	11	4	0	0	0	0	0	0	0	75
	12	7	3	39	6	0	0	16	4	0	0	0	0	0	0	0	75
	13	9	2	25	1	0	0	4	5	0	0	0	0	0	0	0	46
	21	10	11	38	1	0	0	1	0	1	0	0	0	0	0	0	62
	22	3	4	43	8	0	0	2	2	2	0	0	0	0	0	0	64
	23	0	2	45	7	0	0	0	0	0	0	0	0	0	0	0	54
	Total	88	56	294	38	32	21	41	19	8	73	74	46	62	63	53	

Table 3.3 Transition matrix for the nine facies (1-9 bold text highlighted blue), the three types of erosive (11-13 bold text highlighted yellow), and the three types of abrupt contacts (21-23 bold text highlighted yellow). Cementation contacts, gradational transitions and core breaks are not represented in this matrix. As an example, erosive, very gently to moderately undulatory, non-inclined erosive contacts (11, in the leftmost column) are followed by facies 3 (third column uppermost row) 32 times. Erosive, very gently to moderately undulatory, non-inclined contacts succeed facies 3 a total 46 times (fourth row, twelfth column). Note that most facies and contacts are associated with facies 3.

To clarify, the use of the term interval(s) in the rest of this chapter, and in the remainder of this thesis is not used in the same sense as it was in Chapter 2 and in section 3.2 regarding grain-size trends. For the purposes of facies descriptions, it refers to a section where a particular facies occurs and implies thickness. For the remainder of the thesis it implies thickness, and it is used independently of contacts and surfaces.

### **3.4.2 Facies 1- Fine- to Very Fine-Grained, Well-Sorted, Structureless Sandstone**

Facies 1 consists chiefly of very fine-grained, clean, mineralogically and texturally mature, light gray to beige quartz arenites (Plate 3.10, Photos A, B, and C). It represents ~14.7% of the core. The average thickness of facies 1 is 17.5 cm; they range from 1.1 to 115.6 cm thick. Based on 158 measurements made in intervals of facies 1 (Figure 3.18), grain sizes range from a minimum of 75  $\mu\text{m}$  (~3.74  $\phi$ ) to a maximum of 214  $\mu\text{m}$  (~2.22  $\phi$ ), and averages 119  $\mu\text{m}$  (~3.0  $\phi$ ). Rock fragments and matrix are almost non-existent giving facies 1 an exceptionally “clean” appearance. The only discernable accessory mineral is glauconite, which occurs as very small (<1 mm) pellets that can only be seen with the aid of a microscope. Intervals of facies 1 display no evidence of traction-produced sedimentary structures and appear to be completely homogeneous. X-radiographs confirmed that these intervals are indeed massive and that laminations are not present. No biogenic sedimentary structures are present. Shells are diminutive; however, where present, shells exist as small, thin, disarticulated fragments showing no preferred orientation. These are likely bivalve fragments similar to those observed in

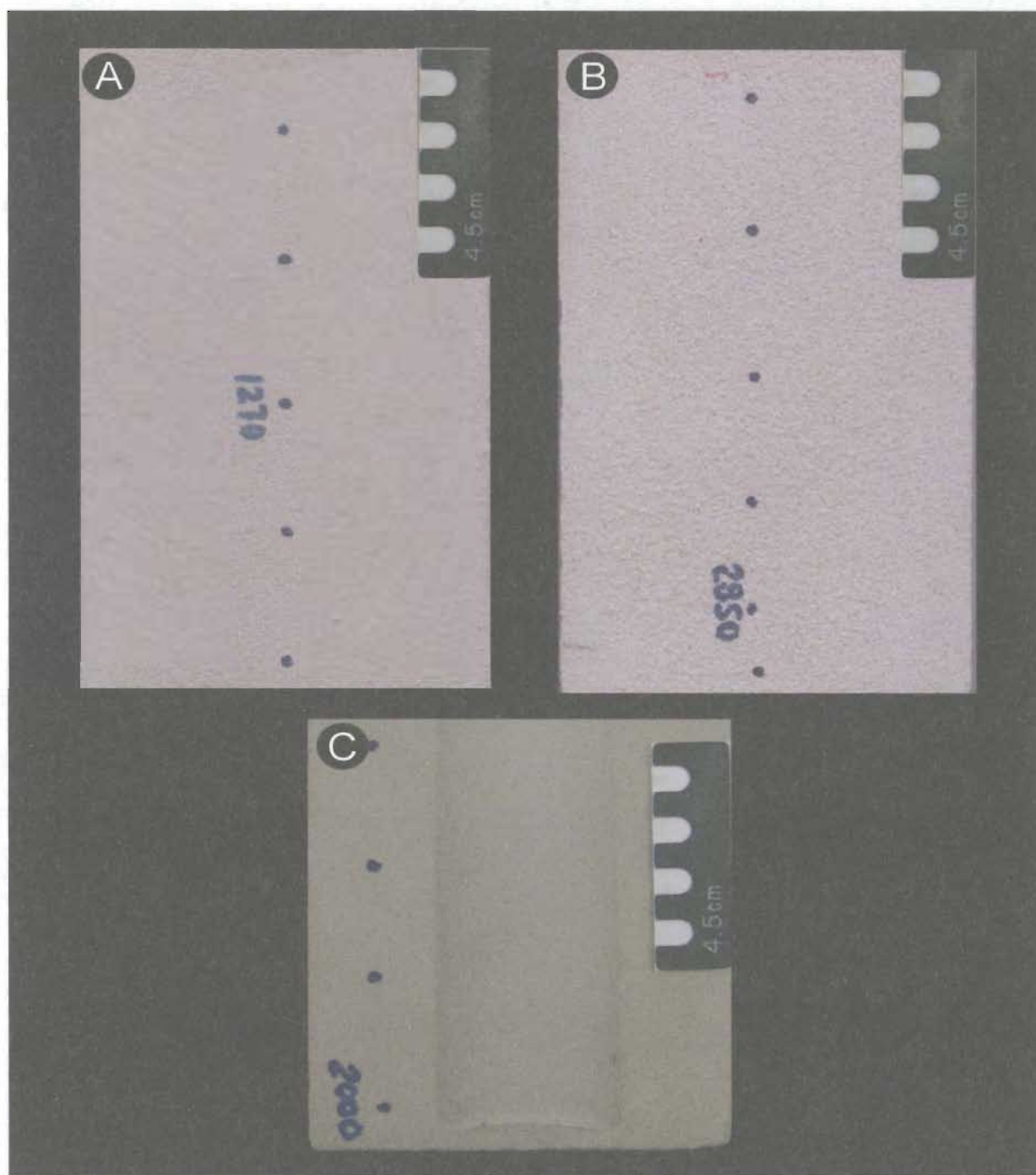


Plate 3.10. Examples of Facies 1 - Fine- to very fine-grained structureless sandstone. Depths are given for the base and top of each core segment. A) 2981.466-2981.341 m, B) 3004.244-3004.119 m, C) 2991.739 - 2991.655 m.



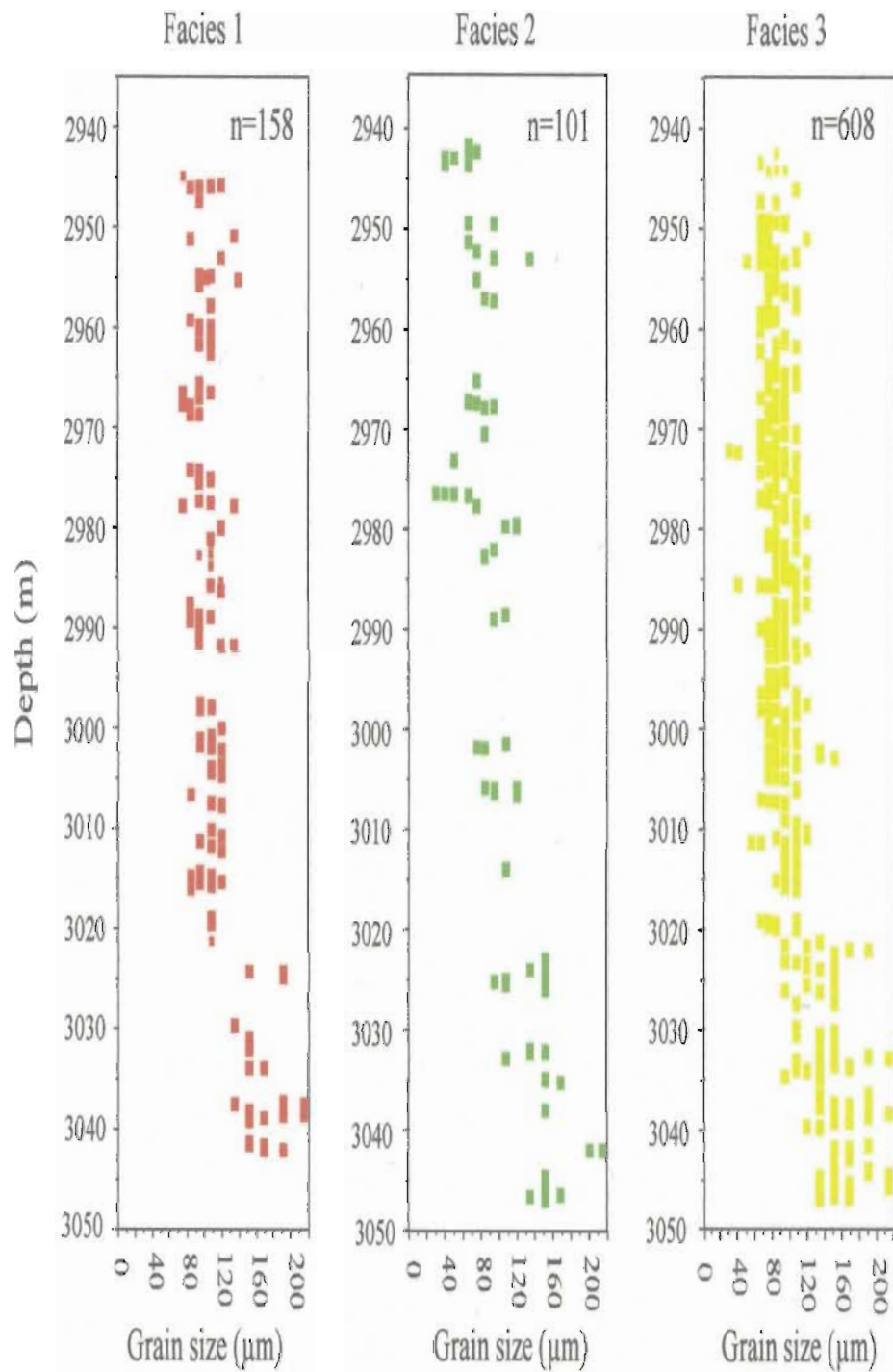


Fig. 3.18 Grain size (μm) vs. Depth (m) for facies 1, 2, and 3. Each graph illustrates the range of grain sizes for the facies and the generalized vertical distribution of the facies in the cored interval. Where there are gaps, the facies is not present.

other sections of the core. Siderite is extremely rare and appears as small (<3 mm) round to oval patches.

Vertically, facies 1 is strongly associated with facies 3 and to a lesser degree facies 2 and 7 (Table 3.2). It is frequently bounded at its base by erosive surfaces and to a lesser degree, abrupt surfaces (Table 3.3). At its top it is bounded by a variety of erosive and abrupt contact types almost equally (Table 3.3). All other facies have minimal affiliation with facies 1.

#### **3.4.2.1 Process Interpretation for Facies 1**

The origin and significance of sandstones that appear to be structureless have been matters of speculation (Hamblin, 1965). Some authors (Allen, 1970; Longwell and Flint, 1962) reason that stratification results from changes that occur during the process of sedimentation, and that homogeneous beds represent a special environment in which sedimentary processes are uniform and free of change. Others point out that structureless intervals may arise because the rate of sedimentation is too rapid for the particles to be sorted out into layers (Geikie, 1903; Arnott and Hand, 1989) or that the material being delivered to the depositional environment is so uniform that textural layering is impossible (Gilluly et al., 1959). Arnott and Hand (1989), through a number of flume experiments, showed that abundant sediment fallout provides an adequate explanation for a lack of lamination in massive deposits. Other explanations for massive bedding include diagenesis (Selley, 1988) and intense burrowing by organisms (Pettijohn, 1957; Frey, 1990; Boggs, 1987; Pemberton et al., 2001). Burrowing by organisms has been regarded

as a major contributor to the homogeneity of sediments, because organisms can disrupt sediment after stratification forms. In Hibernia K-14 and B-27 cores from the Ben Nevis interval, Pemberton et al. (2001) note that some of the well-sorted, massive sandstone intervals are most likely cryptobioturbated. Bioturbation by microorganisms or meiofauna (Pemberton et al., 2001) is not considered likely in facies 1 for the following reasons:

- 1) There is no visual evidence to suggest that micro-organisms disrupted the sediment;
- 2) The homogeneous intervals are essentially devoid of silty or carbonaceous material to provide a food source and materials for constructing burrows.

Therefore, it seems a reasonable conclusion that the homogeneous intervals were rapidly deposited from a highly concentrated suspension cloud. Arnott and Hand (1989) concluded that suppression of laminae at high fallout rates results in reduced lateral segregation due to quick burial and therefore limited traction. In addition, the exceptionally limited textural and color contrast and good sorting in Facies 1 would make any subtle layering imperceptible. Although rapid fallout of grains from highly concentrated suspension clouds and the mineralogical and textural maturity of Facies 1 provides the best explanations for the absence of laminations, some uncertainty remains. A lack of structures is actually negative evidence against, rather than positive evidence for, a particular process.

It was considered that cementation might be responsible for the structureless appearance of facies 1. However, this seems unlikely because other intervals and facies in the core are much more cemented yet laminae are readily discernable.

### **3.4.3 Facies 2 – Fine- to Very Fine-Grained, Planar Laminated Sandstone**

Facies 2 is composed of very fine- to fine-grained, moderately to well sorted, planar laminated quartzose sandstone (Plate 3.11). Approximately 7% of the core is represented by facies 2. Intervals of facies 2 range in thickness from a minimum of 2.2 cm to a maximum of 51.1cm, and average ~ 12.9 cm thick. Based on 101 measurements made in intervals of facies 2 (Figure 3.18), grains are primarily restricted to the very fine-grained sand size class ranging from 62  $\mu\text{m}$  (~4.0  $\phi$ ) to 214  $\mu\text{m}$  (~2.22  $\phi$ ), with an average size of 109  $\mu\text{m}$  (~3.20  $\phi$ ). Lithic fragments (typically <1mm) are more common in facies 2 than in facies 1. They appear as dispersed flecks only weakly controlled by the stratification. Accessory minerals represent less than one percent of facies 2 and include both glauconite and pyrite. Matrix, in the form of silt and carbonaceous material, is uncommon. Some intervals of facies 2 display low to moderate amounts of patchy calcite cement, often associated with very thin, fragmented, bivalves (Plate 3.11, Photos B and C).

Planar stratification differentiates facies 2 from all other facies. Stratification is mostly in the form of laminae that range in thickness from 0.1 to 0.9 mm, with an average of 0.5 mm. One to two centimeter-thick beds are present but uncommon. In clean, well-sorted intervals, minimal textural and color contrast make laminae faint and almost

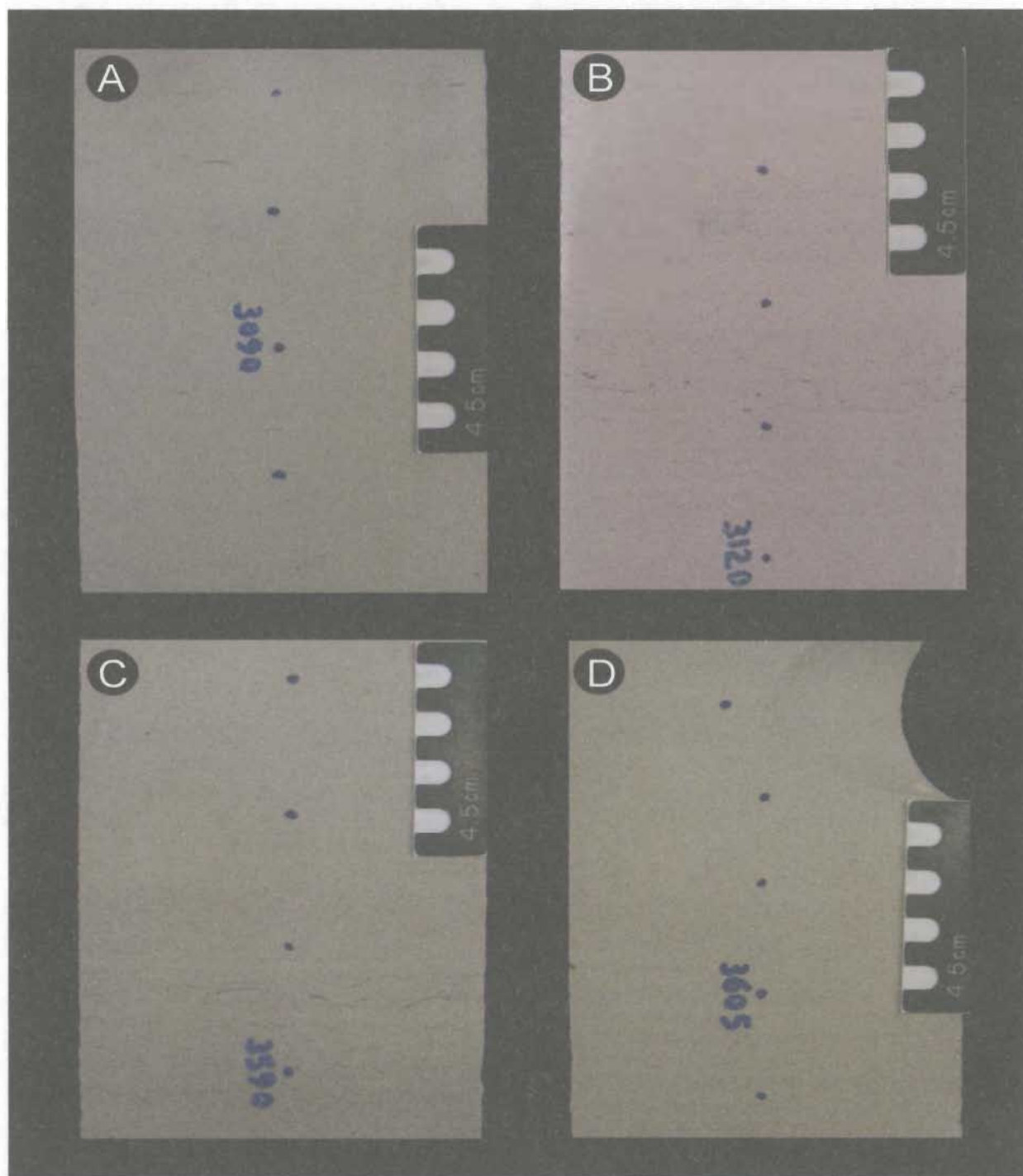


Plate 3.11. Examples of Facies 2 - Very fine- to fine-grained planar laminated sandstones. Depths are given for the base and top of each core segment. A) 3025.31 - 3025.198 m, B) 3032.55 - 3032.438 m, C) 3046.60 - 3046.50 m, D) 3047.00 - 3046.90 m. Note that the planar laminations are very faint.

indiscernible (Plate 3.11, Photo A). More often, laminae are highlighted by very thin (~1 mm, small bivalve fragments, which display preferential horizontal alignment (Plate 3.11, Photos B and C), though these fragments are often difficult to discern. Small, millimeter-sized siderite specks and serpulid worm tubes also accompany shells and highlight the laminae, but are very uncommon. Planar laminations are also made apparent by thin silt laminae; however, this is rare and restricted to the uppermost 10 m of the core. Ungraded and normally graded intervals are most common while reversely graded intervals are very rare. Change in color from light beige to gray is often a reliable indicator of grain-size grading.

Vertically, facies 2 occurs throughout the entire core; however, there are a number of gaps in its distribution (see Figure 3.18). Facies 2 is most commonly associated with facies 3 and less commonly with facies 1 (refer to Table 3.2). Only rarely is it in transition with other facies. All erosive and abrupt contact types are associated with facies 2 (refer to Table 3.3).

#### **3.4.3.1 Process Interpretation for Facies 2**

Planar stratification is the simplest of all sedimentary structures (Nichols, 1999). It is a sedimentary structure that forms under both lower and upper flow regimes. A bedform stability diagram has two regions where plane (i.e. flat) beds are stable (Figure 3.19). Lower flow-regime flat beds in sand finer than 0.6mm (600  $\mu\text{m}$ , or  $\sim 0.75 \phi$ ) are unstable, and any small irregularity on the bed grows into a ripple. In coarse sand, ripples cannot form so lower flow-regime flat beds occur and are stable. Upper flow-regime flat

beds are principally restricted to sands finer than 0.3 to 0.4 mm mean grain size (Figure 3.19). When the mean velocity is greater than or equal to  $\sim 1$  m/s, ripples and dunes are destroyed and are reworked into parallel bedding during the upper flow-regime stage of flow (Boggs, 2001). The upper flow regime is distinguished by sheet-like, rapid flow of water. It occurs under shooting flow or transitional flow with a Froude number of  $\sim 1$ .

Harms et al. (1982) present a range of conditions for which oscillatory flows can produce a plane bed. Flat and/or parallel bedding is favored by fine grain sizes and short wave periods with orbital velocities equal to or in excess of 1.0 m/s. Harms et al. (1982) note that beaches, and other nearshore settings where strong shoaling waves prevail are typical places where flat beds may exist.

The planar laminations of facies 2 are interpreted to represent deposition under either unidirectional or oscillatory upper flow-regime conditions, during the plane-bed stage of flow. This is strongly supported by the flume experiments conducted by Bouguchwal and Southard (1990), where they show that sediment finer than  $\sim 0.4$  mm ( $1.25 \phi$ ) subjected to a mean flow velocity greater than or equal to 1 m/s invariably develops planar laminations. Both unidirectional and oscillatory conditions are considered equally plausible for the formation of the planar stratification because both types of flow are common in shallow-marine settings. It would likely only be possible to distinguish these two possibilities by undertaking fabric analysis on samples from oriented cores. Such studies have been conducted on outcrops (e.g. Shelton and Mack, 1970; Cheel, 1991; Yagishita et al., 1992; Yokokawa, 1995).

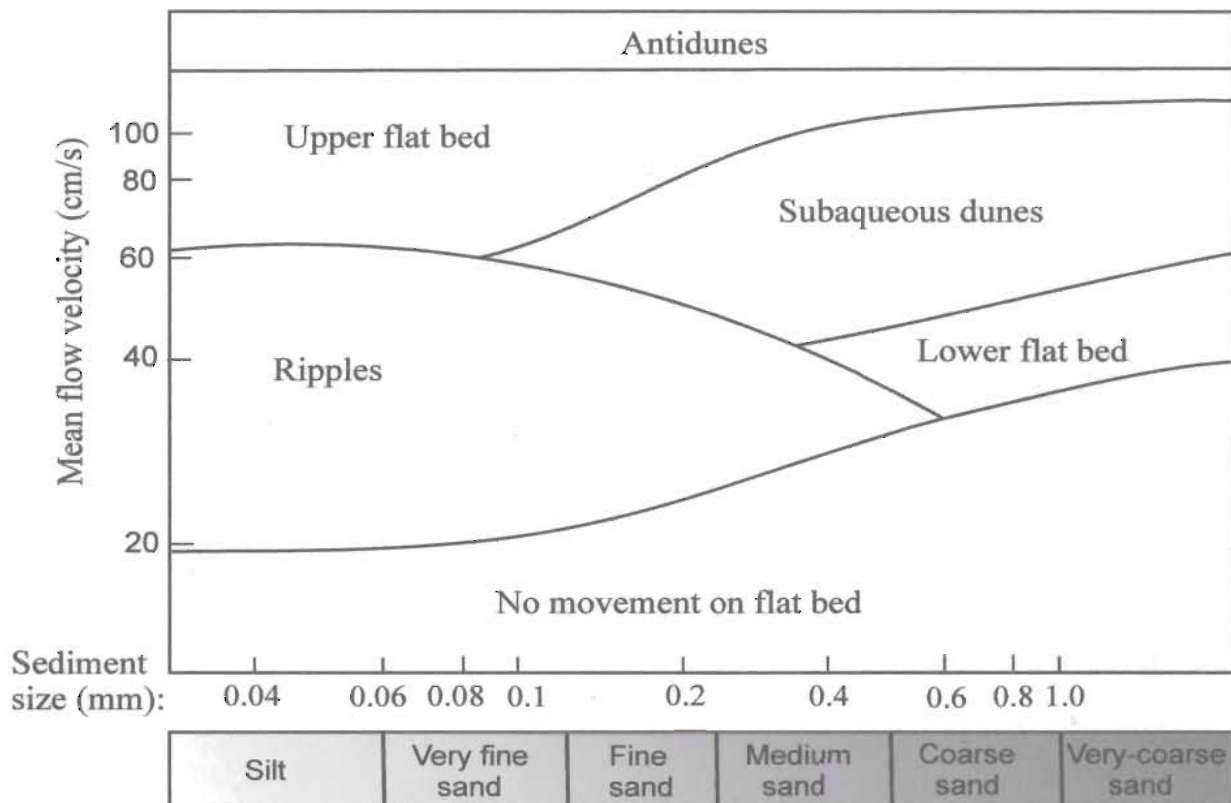


Fig.3.19. A bedform stability diagram showing the stability fields of different bedforms in sediment of different grain sizes at different flow velocities in ~40 cm flow depth. Modified from Harms et al. (1975).



#### 3.4.4 Facies 3 - Low angle Cross-Stratified, Fine- to Very-Fine Grained Sandstone

Facies 3 is the most abundant facies in the White Rose A-17 core, representing approximately 53.3% of the core. Intervals of facies 3 range from 1 to 317 cm in thickness, averaging 35cm. Sandstones of facies 3 consist of fine- to very fine-grained, moderately to well sorted quartzose sandstone. They contain low angle stratification, and are light gray to beige in color (Plate 3.12). Quartz grains range from a minimum of 62  $\mu\text{m}$  ( $\sim 4.0 \phi$ ) to a maximum of 214  $\mu\text{m}$  ( $\sim 2.22 \phi$ ), with a mean size of 102  $\mu\text{m}$  ( $\sim 3.3 \phi$ ), or very fine-grained sand. In total, 608 estimates of grain size (quartz) were recorded within intervals of facies 3 (Figure 3.18). Accessory minerals include trace amounts of glauconite, pyrite, and heavy minerals. Lithic fragments (commonly <1 mm in diameter) are present in trace amounts. Facies 3 is exceptionally “clean” in that carbonaceous and silty material are minor in most samples (Plate 3.12, Photos A, B and C). Some intervals of facies 3 contain low to moderate amounts of calcite cement, which has a patchy distribution. This cement is usually associated with thin bioclasts although these are rare and limited to the lowermost 10 m of the core. Most intervals of facies 3 are ungraded to normally graded; however, textural gradation is generally moderate to weak. The average difference in grain size from the base to the top of intervals of facies 3 is generally less than 20  $\mu\text{m}$  but can be as high as 50  $\mu\text{m}$ .

Low-angle, gently curved laminations distinguish facies 3 from other facies (Plates 3.12 and 3.13, all photos). Laminations are primarily convex-upward, rarely concave-upward and have an average apparent dip of around 5 ° (range 2-9°) measured relative to a plane perpendicular to the edge of the core. The angle of apparent dip of

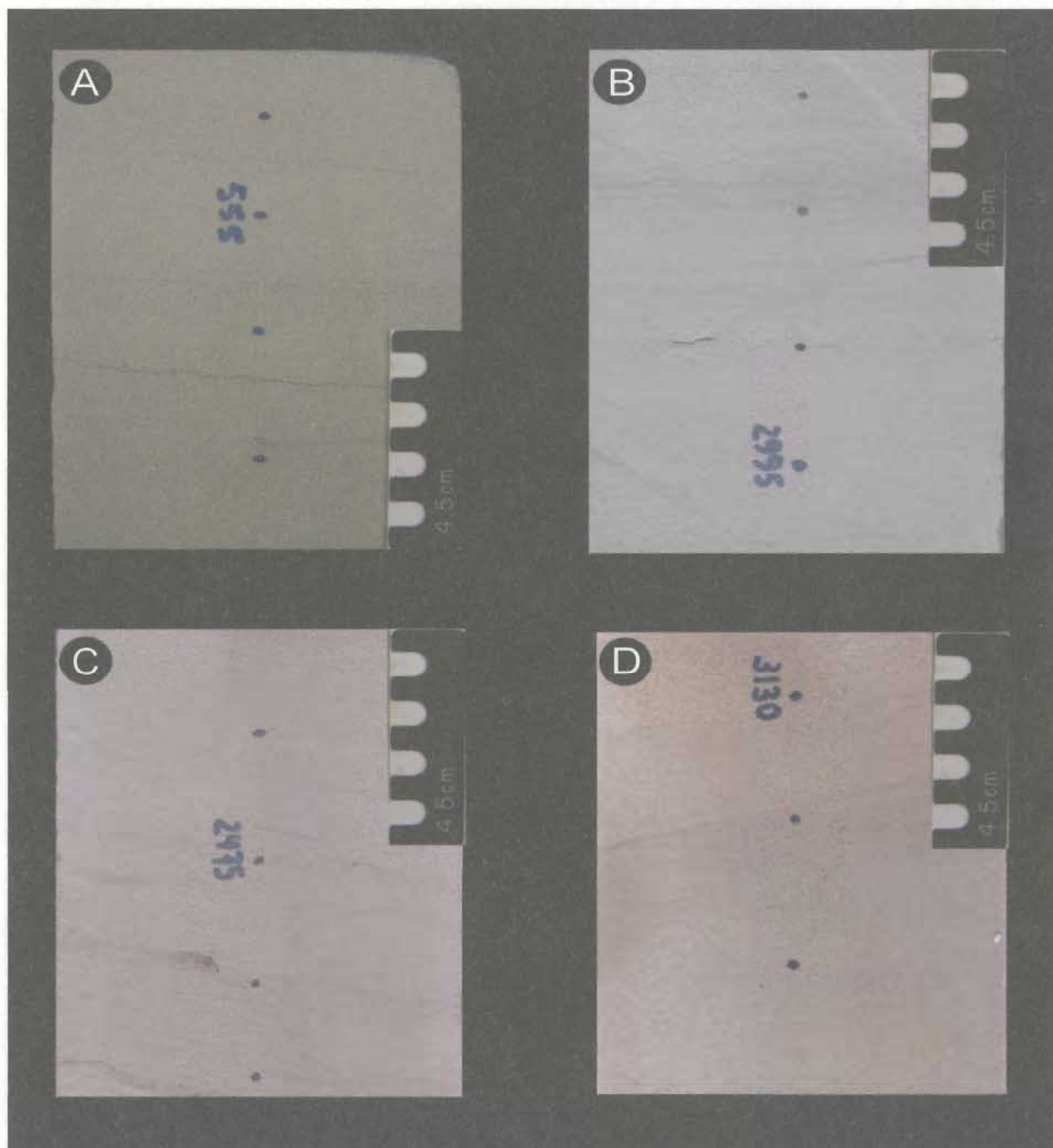


Plate 3.12 Examples of Facies 3 - Low angle cross-stratified fine- to very-fine grained sandstone. Depths are given for the base and tops of each segment. A) 2958.99 - 2958.885 m, B) 2997.00 - 2996.90 m, C) 2984.48 - 2984.375 m, D) 3015.285 - 3015.185 m.

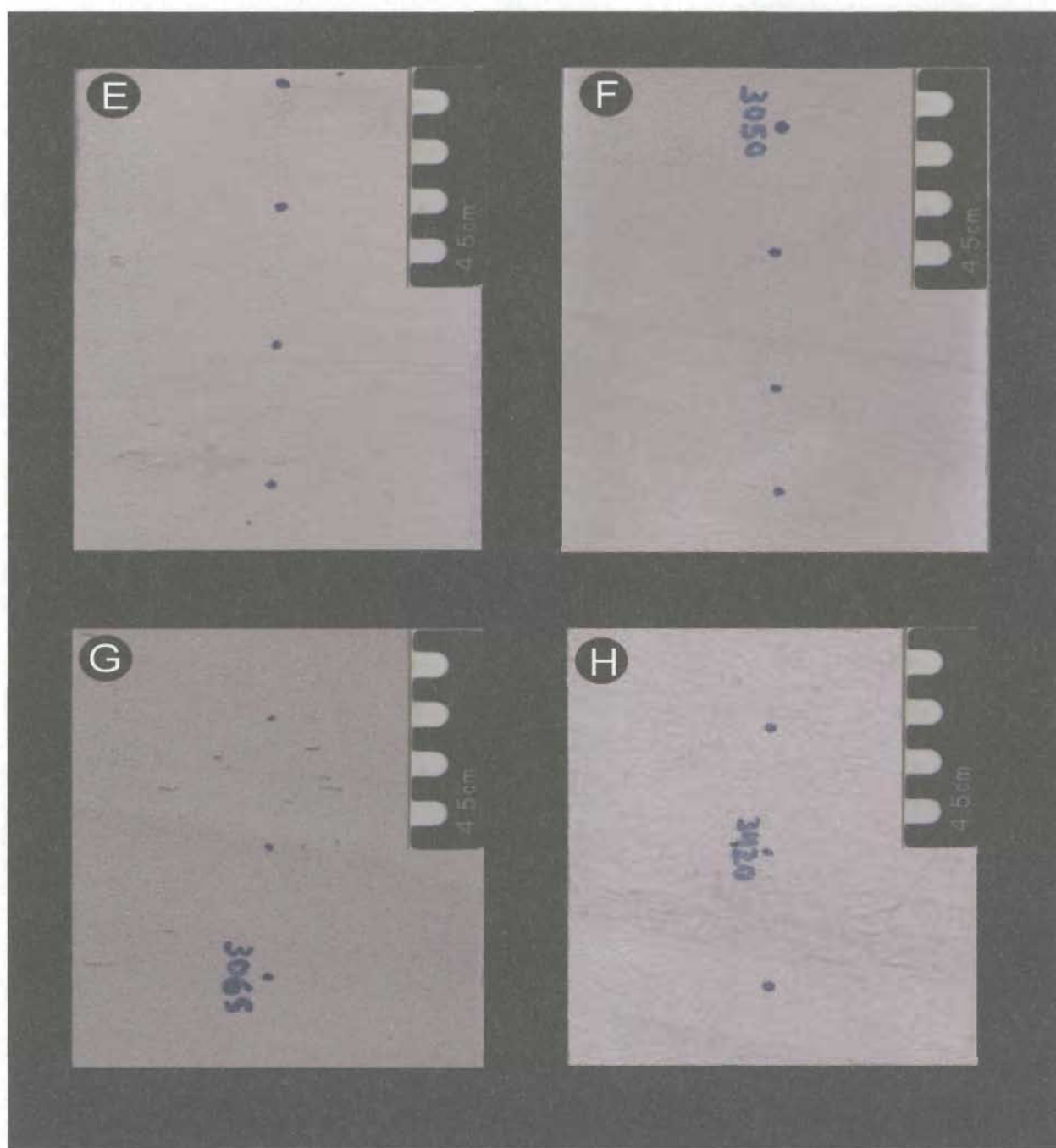


Plate 3.13 Examples of Facies 3 - Low angle cross-stratified fine- to very fine-grained sandstone. Depths are given for the base and top of each segment. E) 2998 - 2997.895 m, F) 3014.56-3014.455 m, G) 3015 - 3014.91 m, H) 3031.30 - 3031.21 m.

these laminations can change by as much as 5 degrees through an interval; however, this is relatively rare and might be a function of how the core intersects bedding. Laminae range from 0.1 to 0.9 cm thick with an average thickness of 0.4 cm. Only on one occasion (Plate 3.13, Photo E) do laminae appear to thicken across the face of the core. In addition, laminae are remarkably consistent in their apparent dip orientation (Plate 3.12 and 3.13, all photos except Plate 3.12, Photo A). Laminae commonly are concordant with abrupt surfaces, including those that display a convex-up or hummocky morphology (Plate 3.12, Photo D and Plate 3.13, Photo F and G). This makes the bounding surfaces sometimes hard to recognize.

Frequently, laminae are subtly developed due to the textural and mineralogical maturity of the sandstones and the limited color contrast. However, in the lowermost 20-30 meters of the core, low-angle laminae are accentuated by thin (<2 mm), short (<5 mm), and discrete, disarticulated shell fragments (Plate 3.13, Photos H). Small (<3 mm), specks of siderite found with the shells also emphasize laminae, although only locally.

Biogenic sedimentary structures are extremely uncommon in facies 3. Only a few *Ophiomorpha* traces were identified. These occur in the uppermost 10m of the core.

Facies 3 is present throughout the core (Figure 3.18). It is associated with all facies but is most strongly associated with facies 1 and 2 (Table 3.2). It is generally associated with both abrupt and erosive surfaces (Table 3.3).

#### **3.4.4.1 Process Interpretation for Facies 3**

The processes that form low-angle bedforms are not fully understood and are rarely discussed in sedimentology texts, except for hummocky cross-stratification (HCS).

Abbot and Francis (1977) recognize stages of sediment transport intermediate between bed-load transport and suspension as defined by Bagnold (1973). At higher stages of transport, because of higher shear stress, grains rise higher from the bed and travel farther in the water column, thus suppressing slip-face avalanching, resulting in lower-angle stratification. Allen and Underhill (1989) note that when suspended-load transport is relatively important, foreset angles of dunes are low.

The low-angle cross-stratification which dominates the A-17 cored interval is not interpreted to represent the migration of a two-dimensional unidirectional dune-scale bedform. Unidirectional bedforms form where bedload transport and unidirectional currents are dominant. Grains of sand are transported up the stoss side of the bedform and avalanche down the lee side. Such cross beds/laminae mostly lie at the angle of rest of the sand, except for asymptotic toesets if suspension fallout is considerable (Allen, 1982). Unidirectional dune-scale bedforms form in fine- to very coarse-grained sand and gravel but are not found in very fine-grained sands (Figure 3.19) A very important aspect of HCS is the grain size in which it most commonly occurs. Various authors (Dott and Bourgeois, 1982; Duke, 1985a; Brenchley, 1985; Swift et al., 1987) note that this grain size varies from coarse silt to fine sand. HCS in coarser sediment is relatively rare but has been reported.

Potter and Pettijohn (1977) have recorded a wide range in the angle of foreset dip for unidirectional bedforms. These dips have a mode from 20-25 degrees, with dips as high as 30 degrees in some instances. These foreset dip angles far exceed the 2-10 degree dip angles in facies 3. Hence, it is concluded that the stratification in facies 3 was not produced by the migration of unidirectional dune-scale bedforms.

Based upon the geometry of laminae, dip angles and internal textural grading, intervals of facies 3 most commonly resemble what is termed hummocky cross-stratification (Harms et al., 1975). It is worth mentioning that some of what has been called hummocky cross-stratification in the White Rose A-17 core may instead be swaley cross-stratification (for an example see Leckie and Walker, 1982). However, because a vast majority of the stratification and abrupt contacts are in the convex-upward position, the term hummocky cross-stratification will be used throughout the remainder of this chapter. Distinction between HCS and SCS is problematic when viewing cores because of the large scale of each of these bedforms.

Controversy surrounds the exact process responsible for the formation of HCS (Allen, 1985). Because HCS has not actually been observed to form in nature, ideas on its mode of formation are inferred from its association with other sedimentary structures and from flume experiments. The form of HCS is highly variable, suggesting that there might be several possible types and modes of formation.

Most early workers consistently attributed HCS formation to powerful oscillatory conditions (e.g. Harms et al., 1975). This mode of formation is apparently favored when laminae are both conformable and symmetric, and display random dip directions (e.g.

Yagishita et al., 1992). Swift et al. (1983) thought that such stratification is formed under the influence of oscillatory and unidirectional currents. Nottvedt and Kresia (1987) also proposed that HCS is the product of combined flows. They showed a conceptual bedform phase diagram (Figure 3.20) in which spectrums of oscillatory-unidirectional currents were proposed. As an example, they suggested that in the case of fine-grained sands and intermediate flow energy, combined flow with a less intense unidirectional current may produce classical hummocky cross-stratification, whereas combined flow with a slightly more vigorous unidirectional flow may produce low-angle megaripples in which the laminae have a tendency to dip in a preferred orientation. Arnott and Southard (1990) and Southard et al. (1990) were able to produce structures under purely oscillatory conditions which closely resemble HCS; with only a minor unidirectional flow component the bedforms became asymmetrical.

In the A-17 core, grain size, concordant surfaces, laminae, and textural grading closely resemble the characteristics of HCS. The differences in laminae dip and dip direction can best be explained by suggesting that these intervals formed under both oscillatory and unidirectional flows (combined flows). Some authors suggest that the variable dip directions recorded in some HCS beds are the result of the complex orbital nature of waved-induced currents. With the introduction of a unidirectional flow component, it seems probable that bedforms would tend to migrate rather than just aggrade vertically, and that laminae would have a tendency to dip in a preferred direction.

The *Ophiomorpha* traces found in intervals of facies 3, are indicative of the *Skolithos* ichnofacies (Pemberton et al., 1992). *Ophiomorpha* is believed to represent the

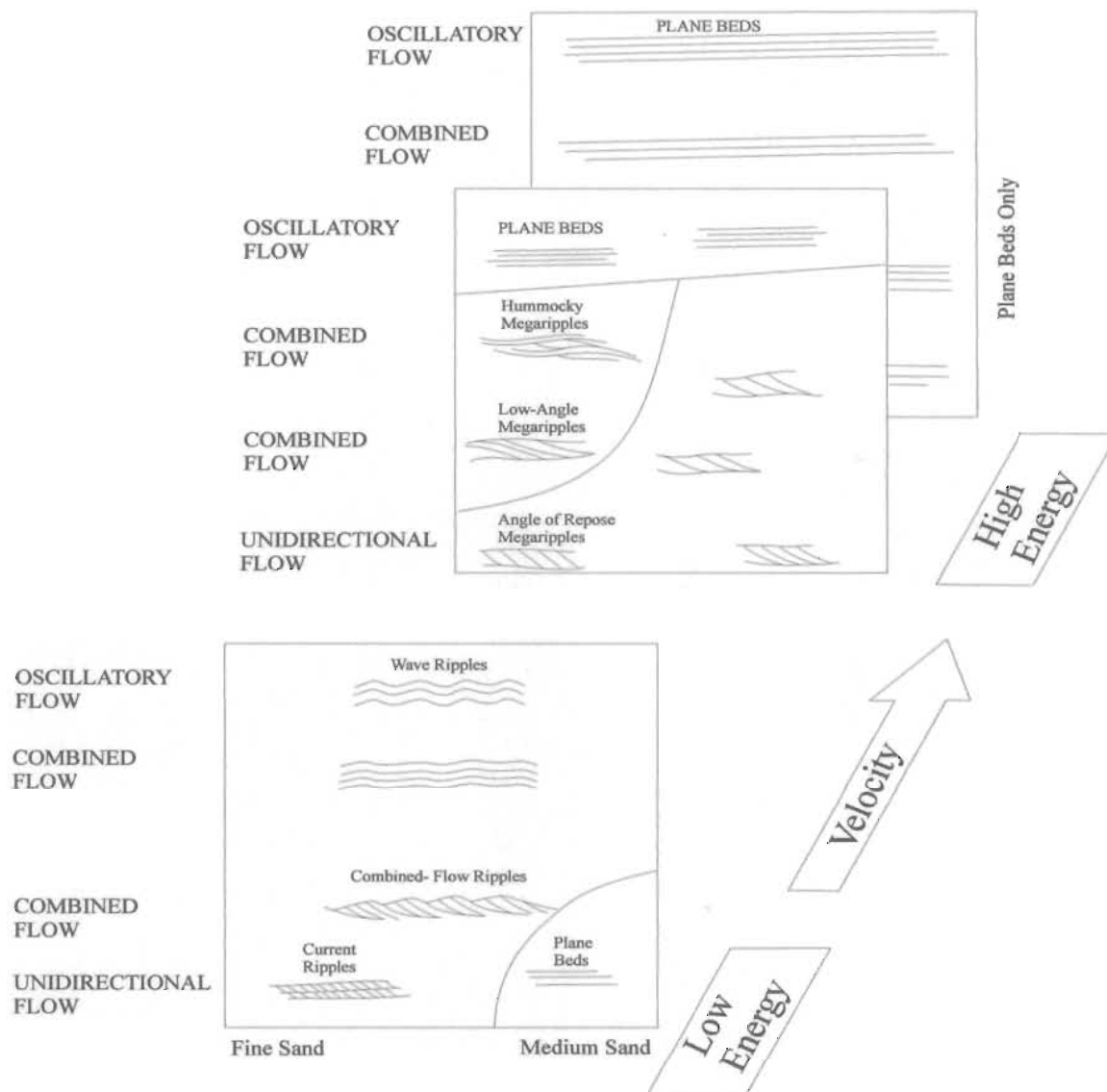


Fig.3.20. Conceptual bedform phase diagrams for variable current type, current velocity, and grain size. Modified from Nottvedt and Kresia (1987). Fine-grained sand under low energy conditions and unidirectional flow will form small-scale current ripples. With increasing energy and the addition of an oscillatory component, combined flow ripples will form. Under purely oscillatory flow, wave ripples are produced. Passage from angle-of-repose, to low-angle, to classical hummocky megaripples is transitional and marked by gradual decrease in foreset inclination and appearance of numerous internal truncation surfaces. For increased velocities, upper-stage plane beds will develop, regardless of the relative importance of oscillatory and unidirectional components.



dwelling burrow of a suspension feeding crustacean (Pemberton et al., 2001). Its pelletal burrow lining suggests that reinforcement to the burrow wall was required to maintain an open burrow in a high-energy setting with a shifting substrate. These traces can be prolifically abundant in marine shoreface settings, particularly in the middle to lower shoreface.

#### **3.4.5 Facies 4 - Moderately Inclined Cross-Stratified, Fine- to Very Fine-Grained Sandstone**

Facies 4 represents only a small proportion (~4.6%) of the cored interval. It generally consists of very fine- to fine-grained, moderately to well sorted, light beige to gray quartzose sandstone. Facies 4 comes in two forms. Type 1 (Plate 3.14) is the more common form. It is typically coarser grained and contains little to no carbonaceous material. Type 2 (Plate 3.15) is less common. It contains abundant thin (<1mm thick) wispy carbonaceous and silty laminae and always occurs in finer-grained intervals.

In the coarser-grained intervals Type 1, grains range in size from 75  $\mu\text{m}$  (3.75  $\phi$ ) to a maximum of 168  $\mu\text{m}$  (~2.6  $\phi$ ), and average 98  $\mu\text{m}$  (~3.25  $\phi$ ). In the finer-grained intervals Type 2 grains range from a minimum of 62  $\mu\text{m}$  (~4.0  $\phi$ ) to a maximum of 84  $\mu\text{m}$  (~3.58  $\phi$ ), and average 78  $\mu\text{m}$  (~3.7  $\phi$ ). In total, the sizes of quartz grains in 68 intervals of facies 4 were recorded (Figure 3.21). As is other facies, lithic fragments are present but very minor. Accessory minerals include trace amounts of glauconite, pyrite, and heavy minerals. Serpulid worm tubes and patches of authigenic siderite cement are rare in facies 4 Type 1, and are absent in facies 4 Type 2.

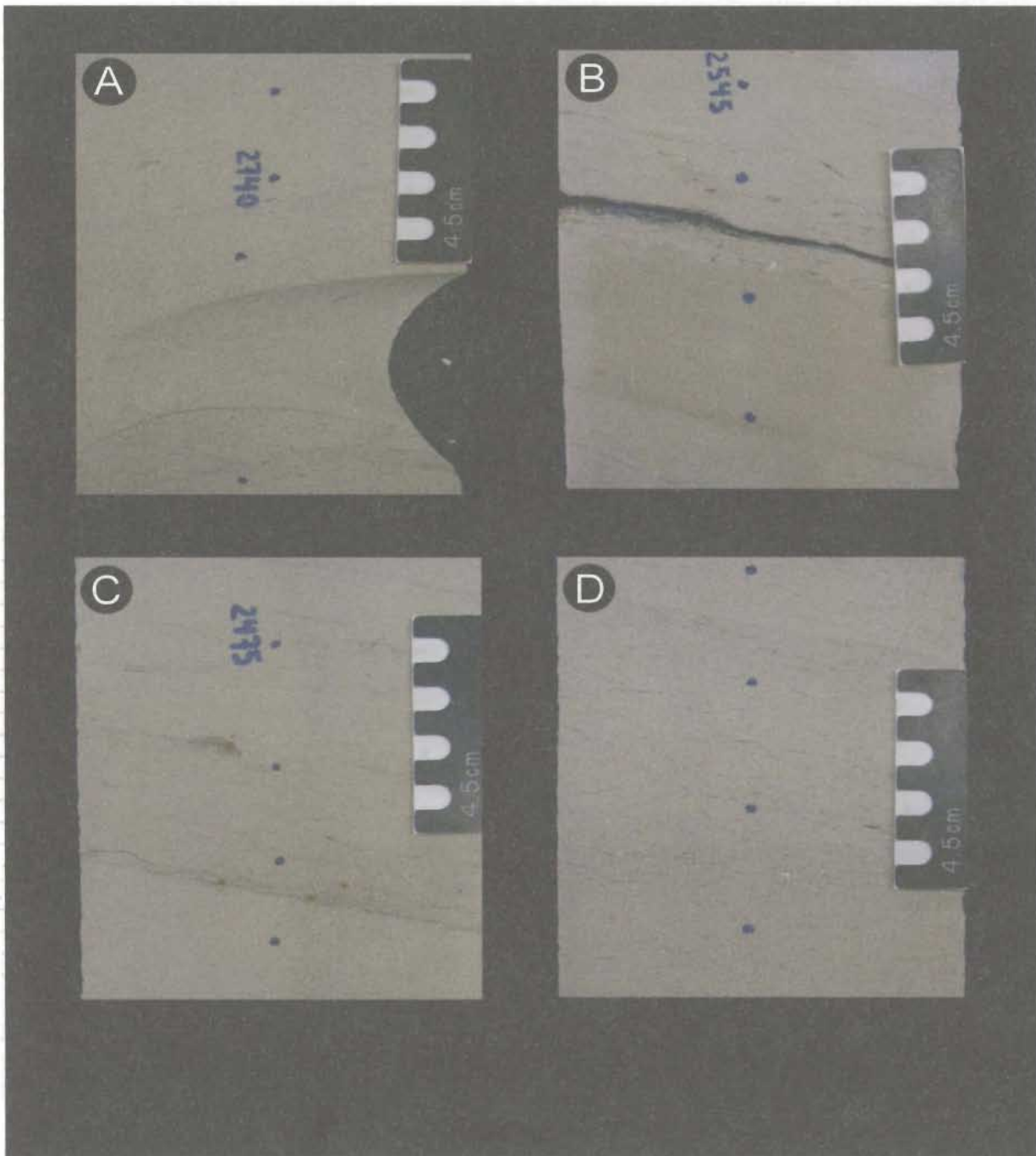


Plate 3.14. Examples of Facies 4 Type 1- Moderately inclined, cross-stratified fine- to very fine-grained sandstone. Depths are given for the base and top of each segment. A) 2987.14-2987.04 m, B) 2984.76-2984.66 m, C) 2983.585-2983.50 m, D) 2999.78-2999.679 m.

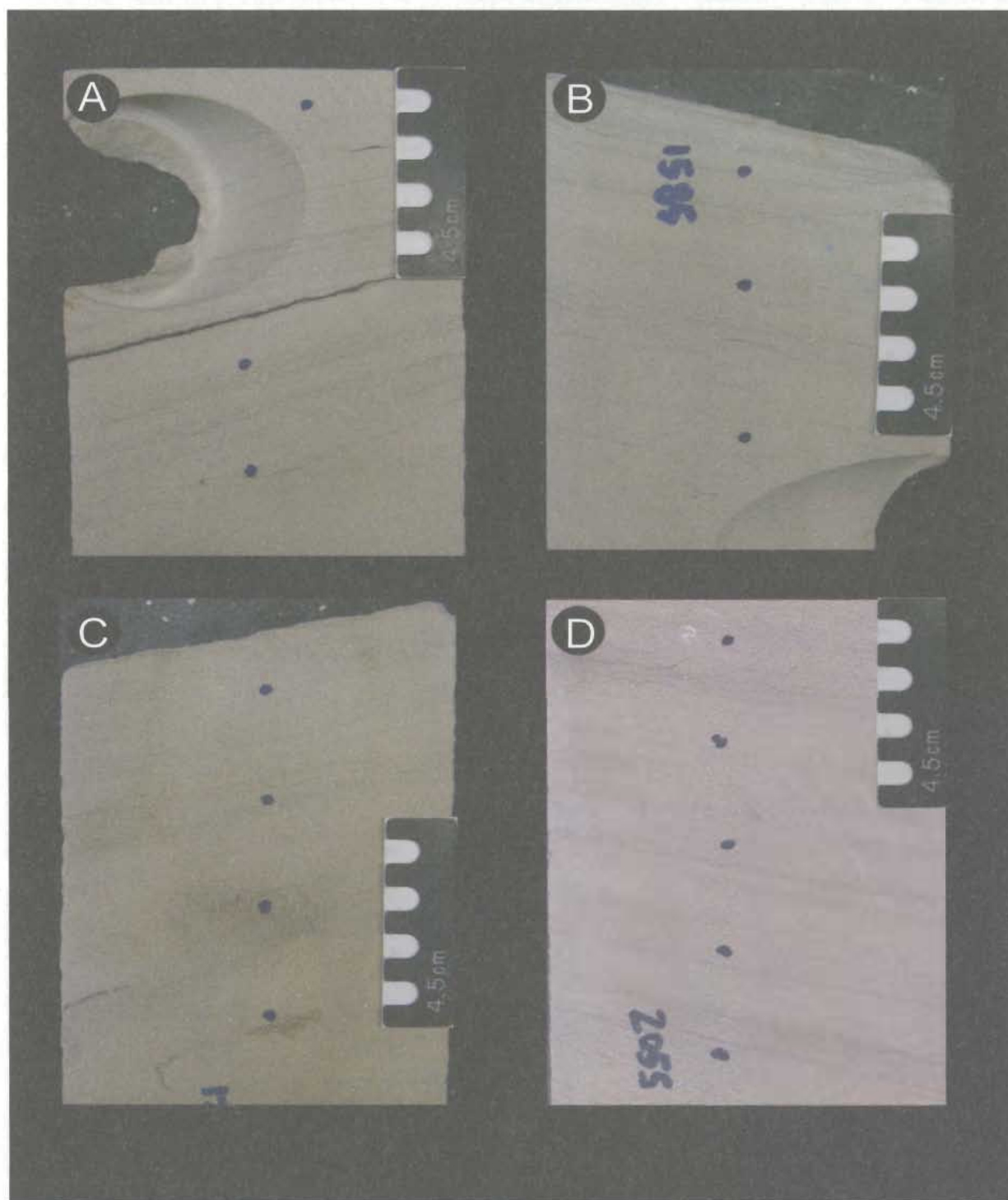


Plate 3.15. Examples of Facies 4 Type 2 - Moderately inclined very fine-grained cross-stratified sandstone with abundant carbonaceous and silty debris. Depths are given for the base and top of each segment. A) 2982.384 - 2982.283 m, B) 2978.375 - 2978.36 m, C) 2995.128 - 2995.018 m, D) 3003.478 - 3003.373 m.

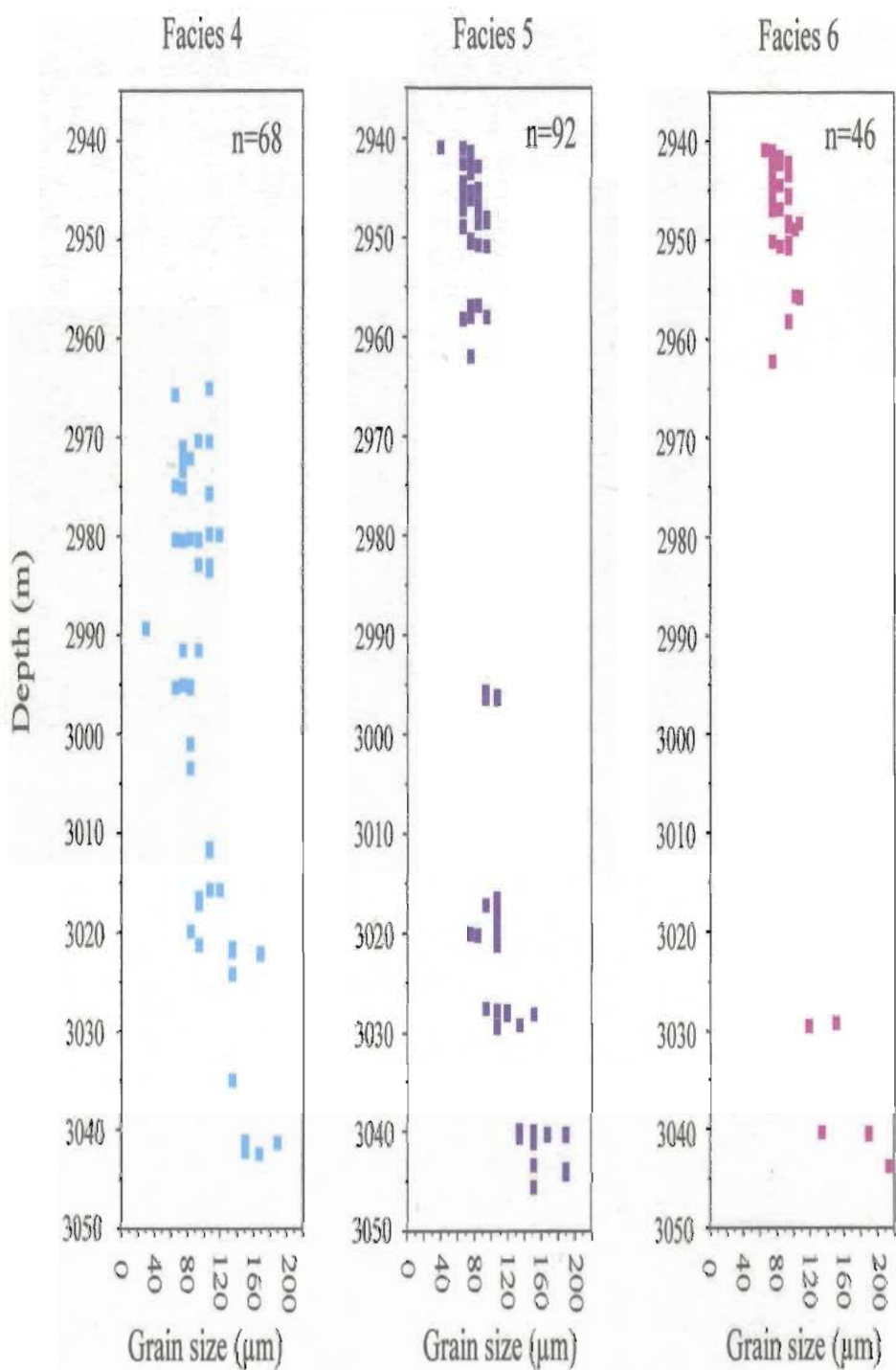


Fig. 3.21. Grain size ( $\mu\text{m}$ ) vs. Depth (m) for facies 4, 5, and 6. Each graph illustrates the range of grain sizes for the facies and the generalized vertical distribution of the facies in the cored interval. Where there are gaps, the facies is not present.

Moderately inclined (10-15°) cross-stratification distinguishes facies 4 from other facies. For Type 1, laminae typically dip (apparent dip) at ~12 ° (range 10-15°), and appear almost planar or gently convex-up (Plates 3.14 and 3.15, all photos). The angle with which the core barrel intersected the bedding in the reservoir interval may have had an effect on these apparent dip angles. Inclined planar laminae are subordinate to the convex-up type. Laminae may be almost very faint (Plate 3.14, Photo A), may be highlighted by thin (<2mm), short (<5mm), broken, disarticulated shells strewn in a discontinuous manner (Plate 3.14, Photos C, and D) or in a very few cases are highlighted by small sideritized shell fragments in combination with thin, broken, bivalve fragments (Plate 3.14, Photo C). Laminae in type two are very similar to those of Type 1, with the exception that they are easily identifiable because they are highlighted by abundant wispy carbonaceous and silty material (Plate 3.15, all photos). Again, a convex-up geometry is the most common form; concave-up and planar varieties are subordinate. Laminae for each type average ~0.5 cm-thick, perhaps a little thinner for type two. Rare 2 cm-thick beds are found in facies 4 Type 1. Intervals of facies 4 range in thickness from 2.4-35.5 cm, and average ~14.25 cm thick.

Facies 4 is limited to 3042-2965 m depth (Figure 3.21) with a number of gaps where the facies is absent. Facies 4 is almost exclusively associated with facies 3 and to a lesser degree facies 1 (Table 3.2). It is bounded by mostly abrupt and erosive contacts, and rarely by erosive convex-up and abrupt undulatory non-inclined contacts. It is succeeded by most contact types, though not by the abrupt undulatory non-inclined type (Table 3.3). A key characteristic of facies 4 Type 2 is that it is always separated at its

base from facies 4 Type 1 by an abrupt surface. Laminae are always concordant with the basal abrupt surfaces.

#### **3.4.5.1 Process Interpretation for Facies 4**

Because of the geometrical similarities and co-occurrence with facies 3, a similar process is interpreted for facies 4. The greater apparent dip angles (10-15°) likely represent different parts of hummocky bedforms. The abundant carbonaceous material, which differentiates Type 2 from Type 1, implies either a change in sediment source, or a less vigorous set of hydrodynamic conditions in which finer-grained sediment was able to settle and accumulate. Both of these hypotheses are plausible, as sand grains in facies 4 Type 2, are typically finer than those which occur in other facies.

#### **3.4.6 Facies 5 - Pervasively Calcite-Cemented Sandstone**

Facies 5 is one of two diagenetic facies present in the A-17 cored interval. It represents ~12.3% of the total core. Intervals of facies 5 range from 1.8-75 cm, and average ~32.7 cm thick. These intervals are found primarily in the lowermost 30 m and uppermost 20 m of core, and occur only sparsely throughout the rest of the core (see Figure 3.21). Facies 5 consists of fine- to very fine-grained quartzose sandstone completely cemented with calcite, giving it a distinct light gray to bluish-gray appearance (Plate 3.16). Calcite cement was confirmed with 10% hydrochloric acid (HCl). The dominant and only easily recognizable framework grain in this facies is quartz. Only occasionally were accessory minerals recognized. These include a minute fraction of



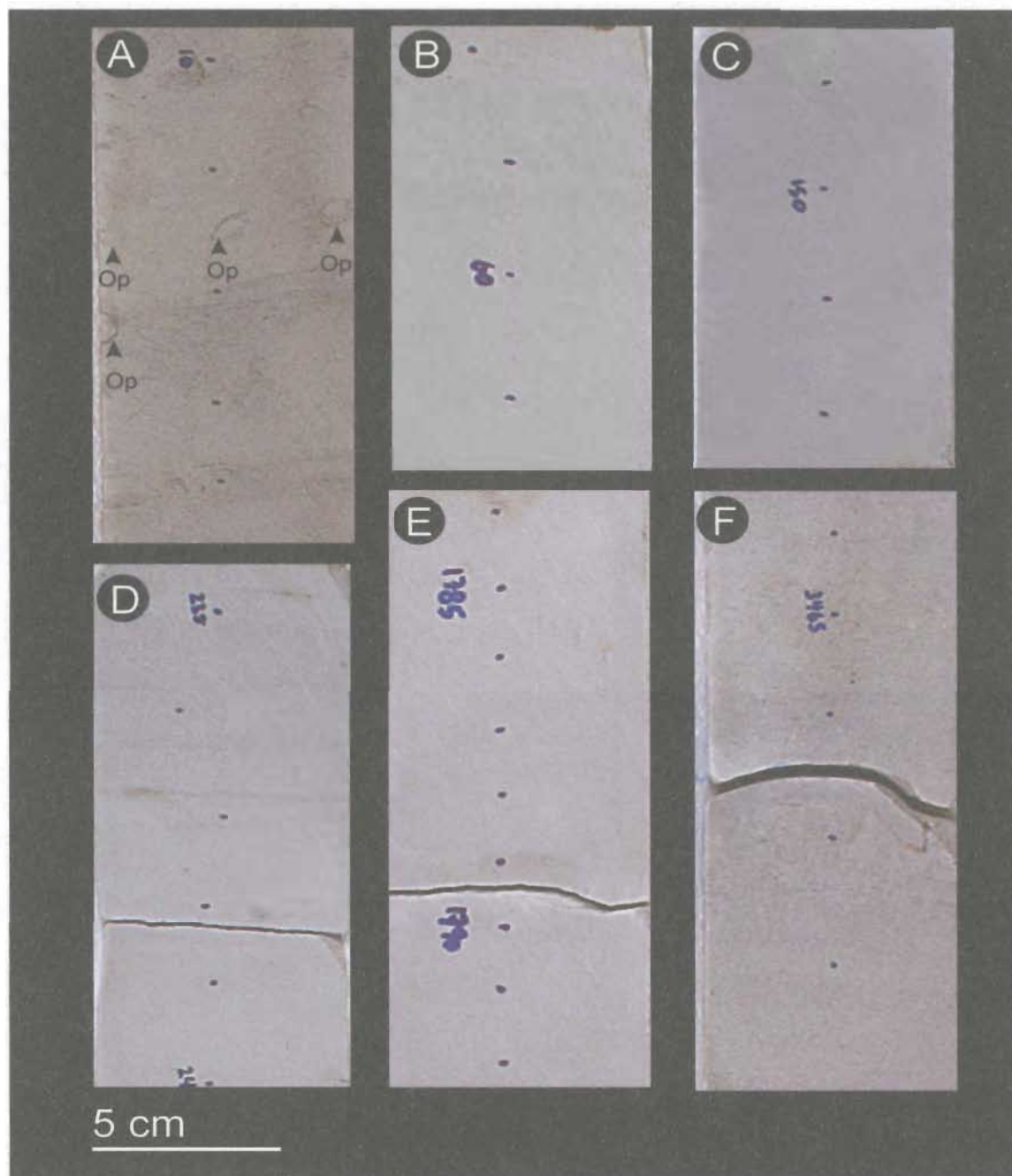


Plate 3.16. Examples of Facies 5 - Pervasively calcite-cemented sandstone. Arrow heads mark the position of traces and letters are abbreviations for trace fossil names. Depths are given for the base and top of each interval. A) 2941.285 - 2941.135 m, B) 2942.75 - 2942.625 m, C) 2944.24 - 2944.115 m, D) 2940.70 - 2940.548 m, E) 2995.92 - 2992.748 m, F) 3043.60 - 3043.428 m. Op = *Ophiomorpha*.

disseminated carbonaceous material, glauconite, and pyrite. Because grain boundaries are obscured by the presence of calcite cement, the absolute grain size could not be confidently determined. However, measurements done to the best of the present author's ability revealed grains from  $\sim 40 \mu\text{m}$  ( $\sim 4.65 \phi$ ) to  $214 \mu\text{m}$  ( $\sim 2.22 \phi$ ) in size, averaging  $114 \mu\text{m}$  ( $\sim 3.13 \phi$ ). Thus, it is apparent that this diagenetic facies is not restricted to any particular grain size, and spans the range of grain sizes observed elsewhere in the core. In total, the sizes of quartz grains in 92 intervals of facies 5 were measured and recorded (see Figure 3.21). Grain-size grading was particularly hard to identify in facies 5. Tentatively, it is thought that these intervals display only weak normal grading.

Intervals of facies 5 display faint, low angle ( $<10^\circ$  apparent dips), gently curved, convex-up laminations (Plate 3.16 Photos A and D), and less commonly planar laminations. Moderately inclined ( $10\text{-}15^\circ$ ) laminations are exceptionally rare. Only in the upper 5-6 m of the core can laminae be unquestionably identified because there they are highlighted by silty and/or carbonaceous material. In this same interval, the trace fossil *Ophiomorpha* is present and easily identifiable (Plate 3.16, Photo A). These traces range from 1-2 cm in diameter, have distinct bulbous outer linings and are generally spaced 2-5 cm apart.

Facies 5 is invariably associated with facies 6 (Table 3.2 and Figure 3.21). These facies are always bounded by cementation contacts. When facies 5 underlies or overlies more porous sandstone cementation contacts are in several cases abrupt, steeply dipping, highly arcuate and cut through stratification (Plate 3.6). Facies 5 is infrequently affiliated with other facies in the core.



### 3.4.6.1 Interpretation of Facies 5

The pervasively calcite-cemented intervals are interpreted to have been deposited under similar conditions to those inferred for facies 1, 2, 3, and 4. A detailed explanation of the diagenetic processes responsible for the calcite cement in facies 5 will not be given here, as it is beyond the scope of this thesis. A more thorough account of the types of cements and processes can be found on the Husky White Rose website ([www.huskywhiterose.com](http://www.huskywhiterose.com)).

Plint (1999) postulates that much of the cement in the calcite-cemented intervals, which he refers to as concretions (based upon FMI images and contact relationships), was provided by the dissolution of aragonite shells dispersed throughout the cored interval. This is logical, as the associated facies 6 contains numerous bioclasts. Alternatively, the bioclasts might have provided a nucleation site for calcium and bicarbonate ions in the pore water.

The *Ophiomorpha* traces, like those in facies 3, are believed to represent the dwelling burrow of a suspension feeding crustacean (Pemberton et al., 2001). Its pelletal burrow lining suggests that energy conditions were relatively high and that reinforcement was required to survive and feed in a high-energy setting within a shifting substrate. These traces can be prolific in post Paleozoic marine shoreface settings, particularly in the middle to lower shoreface (Pemberton et al., 2001).

### 3.4.7 Facies 6 - Pervasively Calcite-Cemented Sandstone with Abundant Shelly

#### Material

Facies 6 is similar to facies 5 in that it is pervasively cemented. However, it contains an assortment of bioclastic debris (Plate 3.17). Hence, it is both a distinct sedimentary and a diagenetic facies. Facies 6 represents only a small percentage (~3.1%) of the cored interval. Intervals of facies 6 range in thickness from a minimum of 2.2 cm to a maximum of 22.4 cm. The average interval thickness is ~10.5 cm. Facies 6 consists of fine- to very fine-grained quartzose sandstone. Lithic grains and accessory minerals were difficult to identify and estimate; however, minor amounts of glauconite and pyrite are associated with the shell fragments. Quartz grains range from 66  $\mu\text{m}$  (~3.92  $\phi$ ) to a maximum of 214  $\mu\text{m}$  (~2.22  $\phi$ ), and average 109  $\mu\text{m}$  (~3.2  $\phi$ ). Quartz grains were measured at 46 points in facies 6 (Figure 3.21). Coarser grained (fine sandstone) intervals are principally restricted to the lowermost 20 m of the core and very fine-grained intervals are primarily situated in the uppermost 10 m of the core (Figure 3.21). Grain size trends were difficult to identify. It is thought, however, that some intervals display weak normal grading. Facies 6 does not possess any detectable physical or biogenic sedimentary structures. The amount and type of shell material changes vertically throughout the core (Plate 3.17 all photos). For example, in the lowermost sections of the core, shell fragments are limited to bivalves, a few gastropods and a potentially a few brachiopods (Plate 3.17 Photo F). In the upper portions of the core, where facies 6 is considerably more abundant, intervals are thicker, and are host to a wider variety of shell types. These include brachiopods, bivalves, oysters, and gastropods (Plate 3.17, Photos

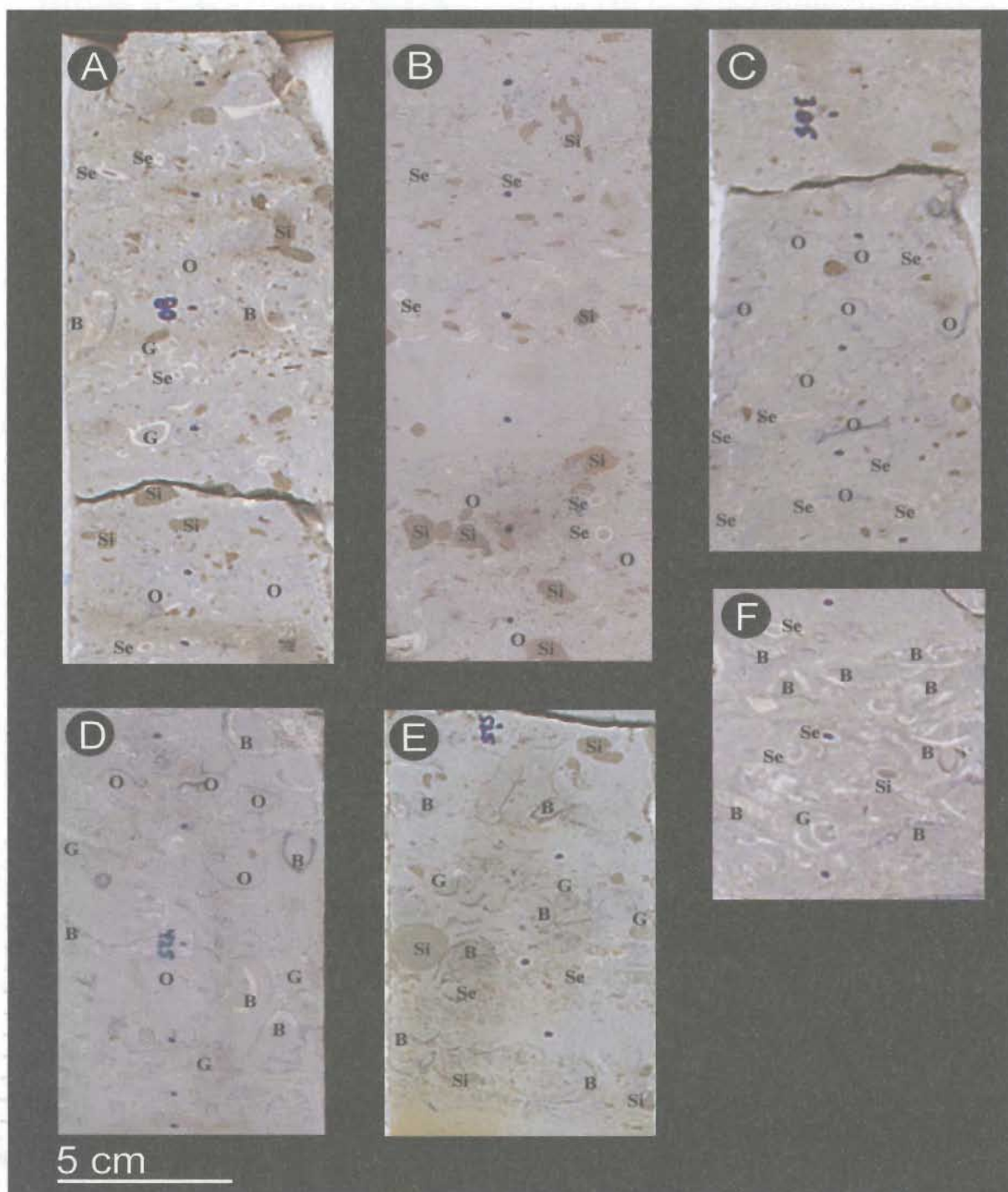


Plate 3.17. Examples of Facies 6 - Pervasively calcite-cemented sandstone with abundant shelly material. Abbreviations are used to highlight the various bioclasts and the authigenic siderite cement found in this facies. Depths are given for each interval. A) 2943.32 - 2943.13 m, B) 2946.895- 685 m, C) 2950.69 - 2950.525 m, D) 2955.69 - 2955.56 m. E) 2958.092 - 2957.962 m, F) 3040.52 - 3040.427 m. B=bivalve fragment, G= gastropod fragment, O= oyster fragment, Se= serpulid worm tube fragment, Si= authigenic siderite cement.

A, B, and C). In these uppermost occurrences of facies 6, shell fragments (bivalves, oysters and gastropods) and serpulid worm tubes are nearly always accompanied by siderite cement (Plate 3.17, Photos A, B, C) as 0.5-3.0 cm, irregularly shaped, circular to oval blotches.

In most cases, bioclasts of facies 6 are poorly sorted and display no preferential orientation. However, in some cases shells are relatively intact (Plate 3.17). Shell debris is generally dispersed in a matrix of very fine sand but is locally clast-supported. The size, orientation and morphology of shell debris can differ markedly from one interval to the next. Serpulids, in particular, show an assortment of sizes, shapes, and orientations. They may be almost completely whole and circular, oval, or appear as tiny (<1 mm) fragments. Oyster fragments, which are prevalent in the uppermost intervals, display a wide range of orientations, but do not appear in the hydrodynamically stable (convex-up) position. They range in size from 0.1-0.3 mm thick, and from 1.0-3.5 cm in length.

Facies 6 is principally restricted to the lowermost and uppermost 20 m of core. Facies 6 is generally intercalated with facies 5 and only rarely with other facies (see Table 3.2).

#### **3.4.7.1 Process Interpretation for Facies 6**

The mechanisms responsible for the development of facies 6 are thought to have occurred in three phases. Firstly, strong currents (either unidirectional or combined flow) eroded, winnowed, and then concentrated the shelly material. Secondly, the shelly material was transported to the depositional site, likely as bedload. Thirdly, the shelly

material was rapidly deposited. This interpretation is strongly supported by the character of the shells and serpulid worm tubes. In all cases, the shells, and in most instances the serpulid worm tubes, are disarticulated or broken. This strongly suggests that the shells and serpulid worm tubes were eroded and underwent sufficient transport to become broken before being deposited. Furthermore, the shell and serpulid worm tube fragments are not size sorted. This implies that intervals of facies 6 were rapidly deposited and that they were not deposited by waning flows, which would have instead have provided more time to sort the shells. Additionally, the shells and serpulids display no preferential orientation. Thus, it is highly unlikely that these deposits were reworked by subsequent unidirectional currents or combined flows. Lastly and perhaps most important is the fact that intervals of facies 6 are bounded at their bases by erosive surfaces which are highly cemented. This last point strongly supports the notion that high-energy conditions prevailed during deposition.

#### **3.4.8 Facies 7- Shell-, Serpulid- and Siderite-Bearing Sandstone**

Facies 7 occupies ~2.4% of the core. It is defined by its shells (principally thin, broken bivalve fragments), serpulid worm tubes, patchy authigenic siderite cement, and moderate to rare oyster fragments (Plate 3.18). These constituents, however, do not always occur together and vary in proportion throughout the uppermost 80 m of core A-17. Facies 7 is different and thus is described independently of facies 6 because its intervals are not pervasively calcite-cemented, they are always thinner than intervals of

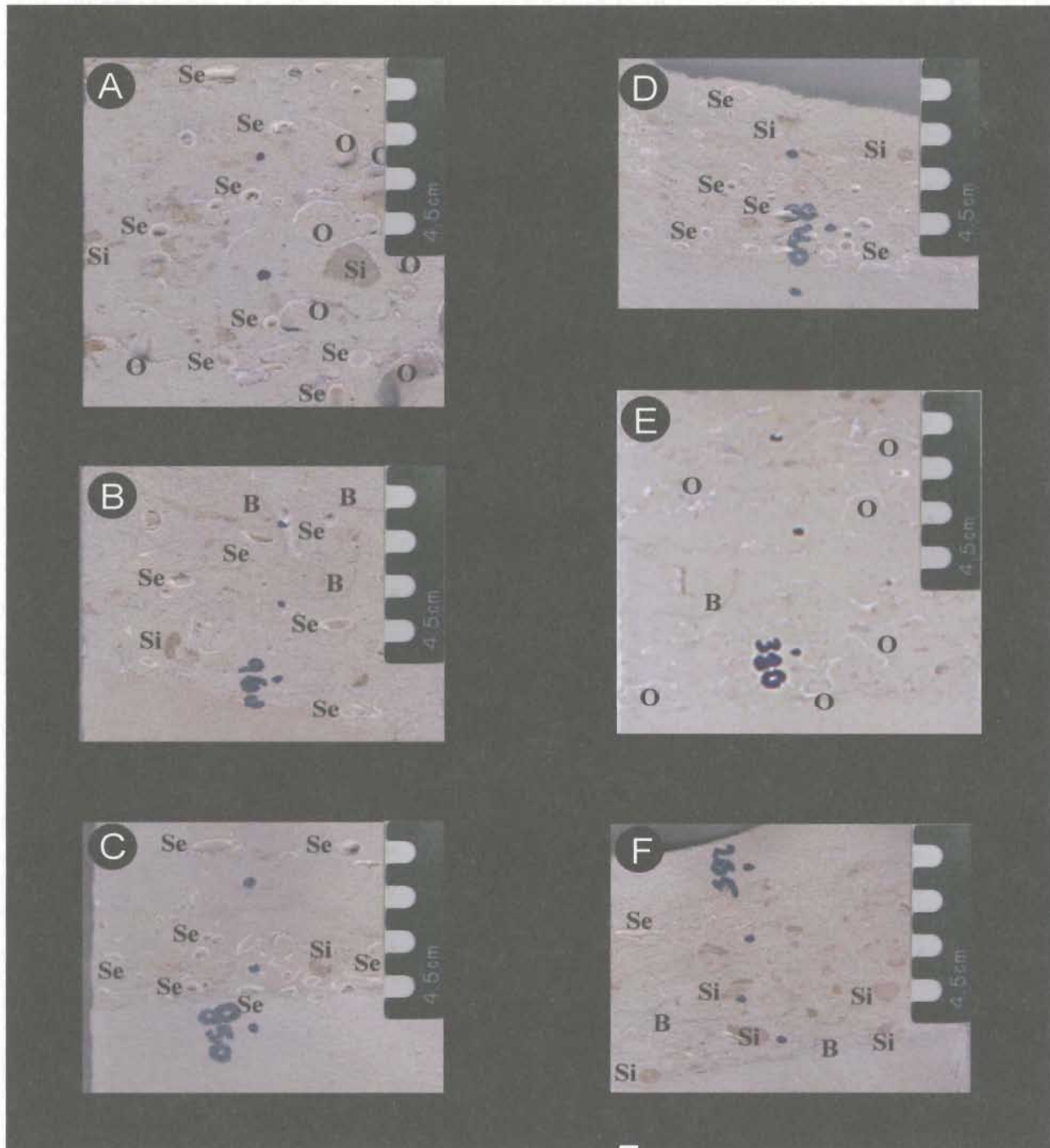


Plate 3.18. Examples of Facies 7 - Shell-serpulid-and siderite-bearing sandstone. Abbreviations are used to exemplify the presence of bioclasts and authigenic siderite in this facies. A) 2987.669 - 2987.59 m, B) 2970.43 - 2970.368 m, C) 2967.02 - 2966.96 m, D) 2996.87 - 2996.815 m, E) 2953.425 - 2953.347 m, F) 2949.45 - 2945.39 m. B = bivalve fragment, O = oyster fragment, Se = serpulid worm tube fragment, Si = authigenic siderite cement.



facies 6, and do not contain gastropod fragments; however, their process interpretations are quite similar.

Facies 7 consists chiefly of very fine-grained quartzose sandstone. The sediment is moderately to well sorted. Accessory minerals include very small amounts of glauconite and pyrite; the pyrite is associated with the shell matter. Quartz grains in facies 7 range from 66  $\mu\text{m}$  ( $\sim 3.92 \phi$ ) to 134  $\mu\text{m}$  ( $\sim 2.9 \phi$ ), and average 98  $\mu\text{m}$  ( $\sim 3.35 \phi$ ). Only a few intervals contain fine-grained quartz. Quartz grains belonging to 60 intervals of facies 7 were measured and recorded (Figure 3.22).

In facies 7, the nature, proportion and abundance of bivalve fragments, serpulid worm tube fragments, oyster fragments, and authigenic siderite change considerably throughout the core. Intervals may be dominated by serpulid worm tubes of varying sizes, shapes and orientations with only a few bivalves and minor amounts siderite (Plate 3.18, Photos C and D). Others are dominated by randomly orientated oyster fragments with only minor serpulids (Plate 3.18, Photo E), or may have similar proportions of bivalve fragments and serpulids, with a variety of sizes and orientations (Plate 3.18, Photos A and B). Bioclasts in facies 7 range from less than 2 mm to a maximum of 1.5 cm in length. Most are broken (Plate 3.18, Photos B and F) while the oyster shells are better preserved (Plate 3.18, Photos A and E), though are broken. Bioclasts in facies 7 are both matrix and clast supported. When oyster fragments are abundant, matrix support is most common (Plate 3.18, Photo E).

Intervals of facies 7 range from 1.2-32 cm, and average  $\sim 6.4$  cm thick. They are limited to 3015-2942 m depth, and are absent from the lowermost 30 m of the core

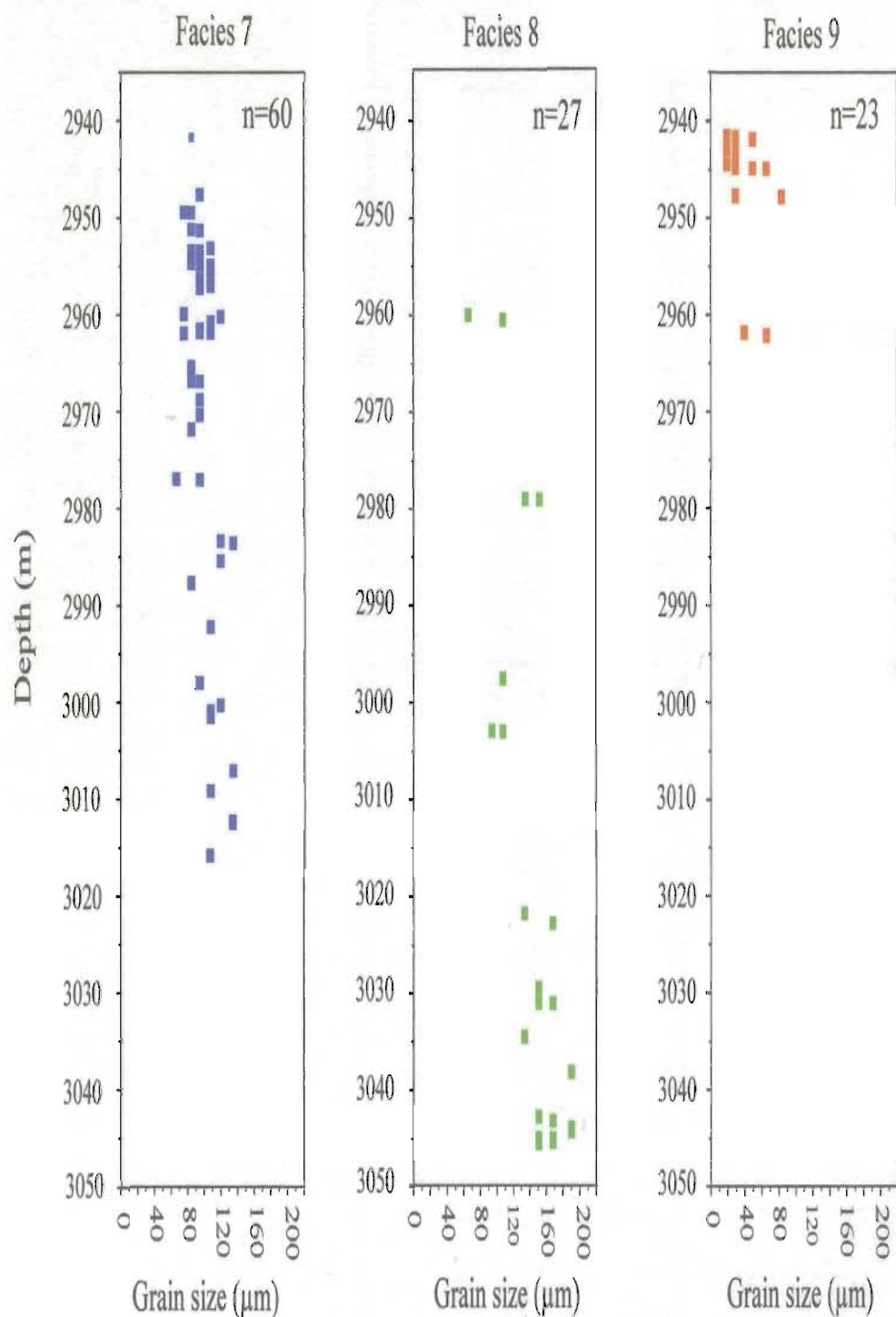


Fig. 3.22. Grain size ( $\mu\text{m}$ ) vs. Depth (m) for facies 7, 8, and 9. Each graph illustrates the range of grain sizes for the facies and the generalized vertical distribution of the facies in the cored interval. Where there are gaps, the facies is not present.



(Figure 3.22). Intervals of facies 7 become more closely spaced upward in the core (see Figure 3.22). Facies 7 is mostly strongly associated with facies 3 and facies 1 (Table 3.2). Erosional surfaces frequently bound facies 7 (Table 3.3), much more often than do abrupt surfaces.

#### **3.4.8.1 Process Interpretation for Facies 7**

It is considered that unidirectional or combined flow currents first eroded, winnowed, transported, and then deposited the bioclastic material, which constitutes facies 7.

The shells are disarticulated and the serpulid worm tubes primarily occur as fragments because of current reworking. In some instances, unidirectional and/or combined-flow currents aligned the bioclastic material. Where oyster fragments are dominant, rapid deposition is inferred because they display no preferential alignment, and are not size-sorted. However, another possibility is that their irregular shape made it less likely for them to become oriented under the influence of a combined/unidirectional current.

#### **3.4.9 Facies 8 - Shelly Sandstone**

Facies 8 occupies ~1.3% of the core and is comprised principally of fine-grained, texturally submature to mature, quartzose sandstone. Intervals of facies 8 are relatively thin. They range in thickness from 3-10 cm and average 5-6 cm. Facies 8 contains numerous thin, disarticulated bivalves (Plate 3.19, all photos). Although many other

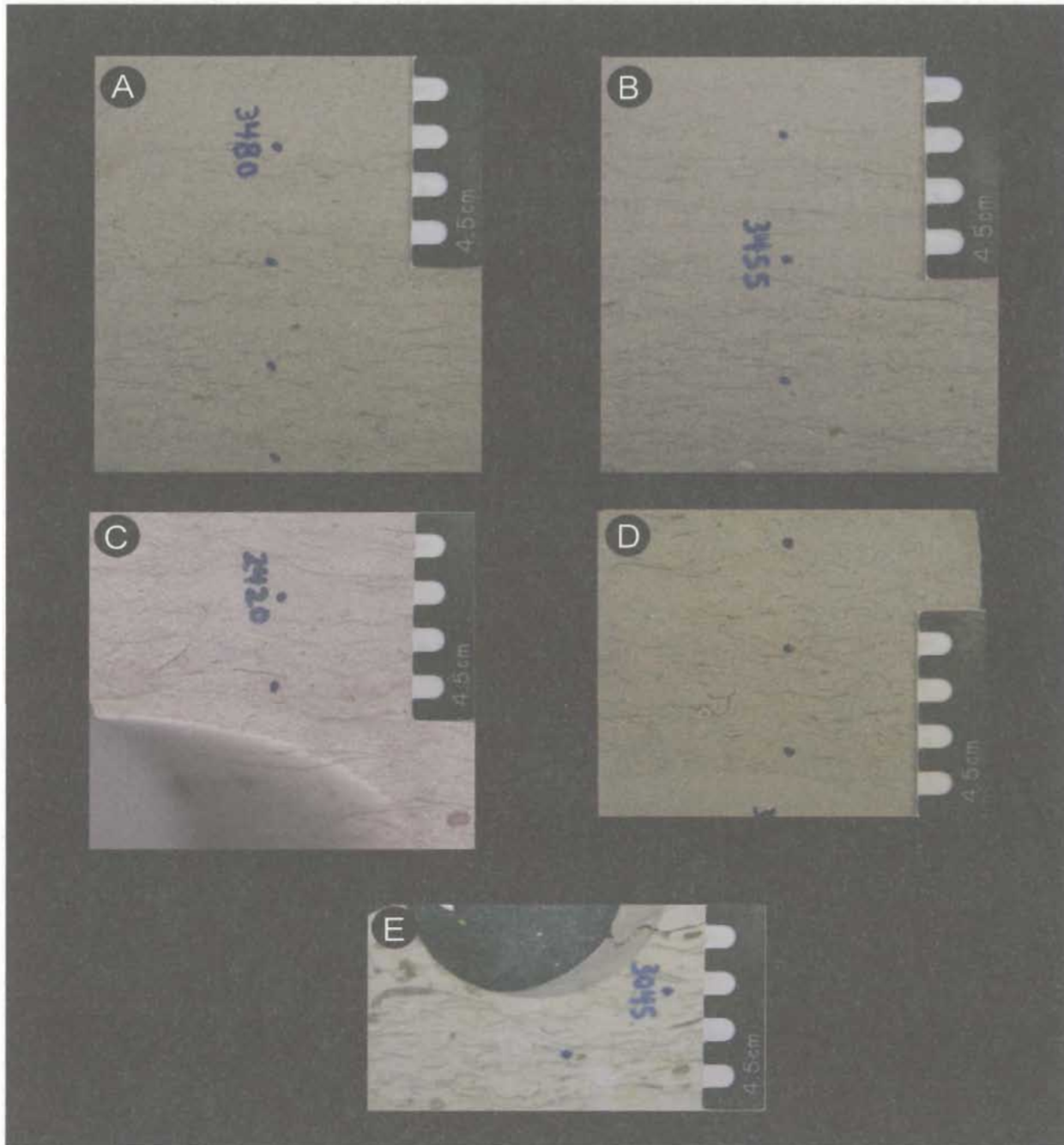


Plate 3.19. Examples of Facies 8 - Shelly sandstone. Depths given refer only to shelly intervals. A) 3044.08- 3043.99 m, B) 3043.89 - 3043.80 m, C) 2982.75- 2982.675 m, D) 3045.032 -3045.962 m, E) 3031.14 - 3031.065 m.

facies in the core possess thin disarticulated bivalves very similar to those in facies 7, facies 8 is distinguished by its distinctive shell accumulations.

Intervals of facies 8 and its shells have the following defining characteristics:

- 1) Bivalves are in every case disarticulated and thin (Plate 3.19, all photos);
- 2) Shells are typically highly concentrated and occur over thin intervals of core);
- 3) Shells locally display a strong horizontal to sub-horizontal alignment, some of which are in the convex-upward (hydrodynamically stable) position (Plate 3.19, all photos);
- 4) Intervals of facies 8 rarely possess serpulid worm tubes or siderite and, if present, their size is small and amounts are very minor (Plate 3.19, Photos C and E);
- 5) The majority of intervals of facies 8 occur in the lowermost 30 m of core A-17 where the sediment is fine grained sand;

Quartz grains in facies 8 range in size from  $84\ \mu\text{m}$  ( $\sim 3.57\ \phi$ ) to  $190\ \mu\text{m}$  ( $\sim 2.40\ \phi$ ).

They average  $\sim 135\ \mu\text{m}$  ( $\sim 2.89\ \phi$ ), making them predominantly fine-grained. Quartz grains were measured at 27 positions, mostly in the lowermost 27 m of the core below 3020 m depth (Figure 3.22). This is the only facies in the core, which is dominantly fine grained rather than very fine grained. Identifiable accessory minerals include very small amounts of pyrite and glauconite. Silty and carbonaceous material is not present in facies 8.

Facies 8 is predominantly restricted to depths below 3020 m with only a few occurrences between 3020-2960 m (see Figure 3.22). Facies 8 is most strongly associated

with facies 3 (Table 3.2) and is frequently bounded by erosive contacts and to a lesser degree abrupt contacts (Table 3.3).

#### **3.4.9.1 Process Interpretation for Facies 8**

The shells scattered through facies 8, were eroded, winnowed then transported to their site of deposition by strong unidirectional and/or combined-flow currents. A majority of the shells in this facies are orientated in the hydrodynamically stable (convex-upward) position (Plate 3.19). Shells in facies 8 underwent significantly more transportation than those in facies 6 and facies 7. They were subjected to considerable winnowing, so are typically highly concentrated.

#### **3.4.10 Facies 9 - Bioturbated Very Fine-Grained Sandstone and Siltstone**

Bioturbated intervals are exceptionally rare in the A-17 core. They represent only 1.2% of the total core and are found primarily in the uppermost 6-7 m (Figure 3.22). These intervals range in thickness from 2.3 to 35.0 cm, and average ~ 11 cm thick. Bioturbated intervals have no visible primary sedimentary structures. Sandstone intervals that contain biogenic traces as well as primary sedimentary structures are not included in this facies; they are assigned to other facies (principally facies 3). Biogenic traces occasionally occur in facies 5 as well.

Bioturbation occurs principally, and is most intense, in the silty sandstone and siltstone intervals. These intervals range from moderately to extensively bioturbated (Plate 3.20, all Photos, Photo A in particular). Recognizable traces include abundant

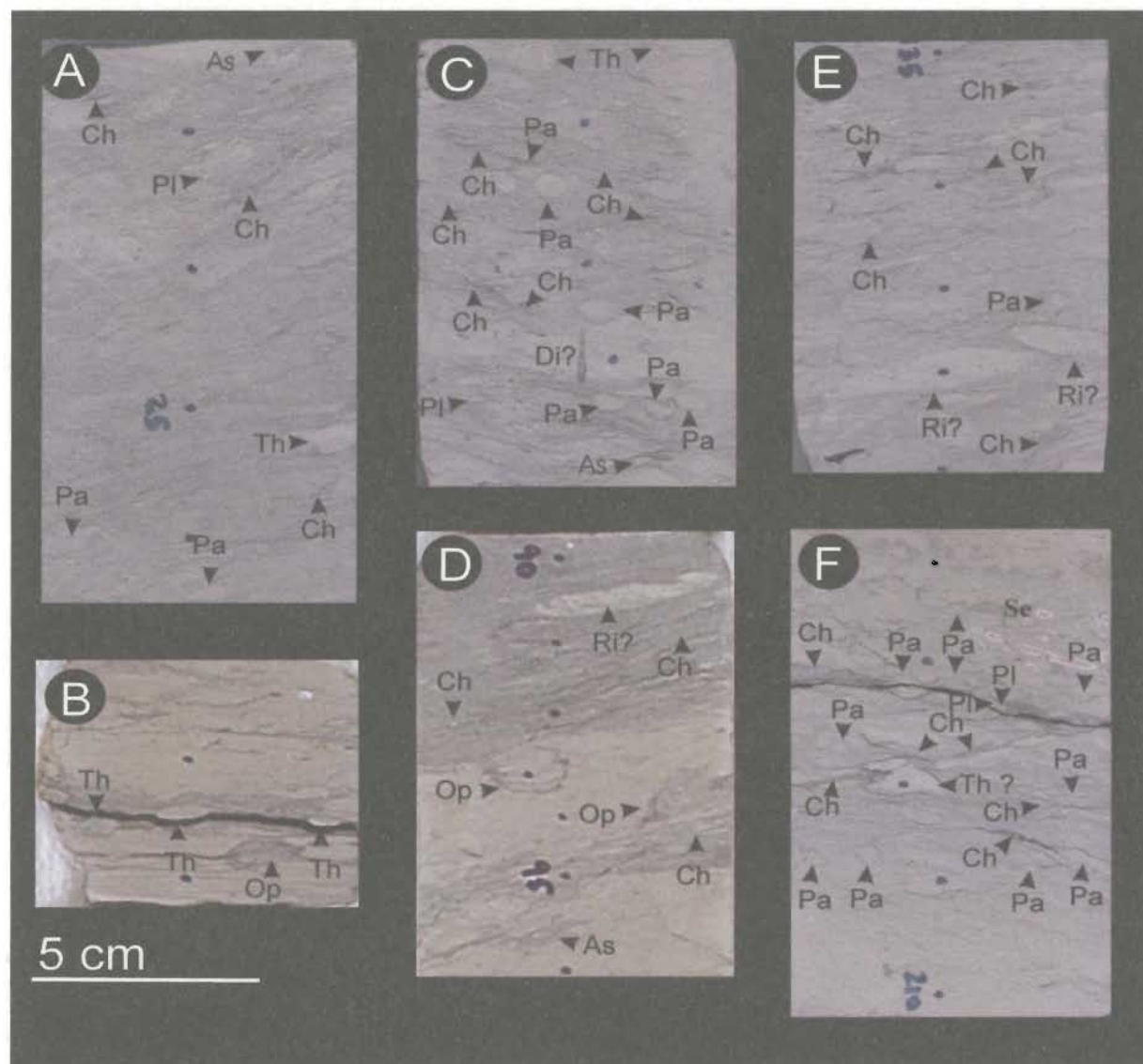


Plate 3.20. Examples of Facies 9 - Bioturbated very fine-grained sandstone and siltstone. Arrowheads mark the position of traces, and abbreviations are used for the names of traces. Depths are given for the base and top of each core segment. A) 2941.615 - 2941.475 m, B) 2941.785 - 2941.725 m, C) 2941.92 - 2941.91 m, D) 2943.61 - 2943.50 m, E) 2944.78 - 2944.67 m, F) 2947.75 - 2947.63 m. As = *Asterosoma*, Ch = *Chondrites*, DI = *Diplocraterion*, Op = *Ophiomorpha*, Pa = *Paleophycus*, Pl = *Planolites*, Th = *Thalassinoides*, Ri = *Rhizocarillium?*, Se = serpulid worm tube fragments.

*Chondrites*, *Paleophycus*, *Planolites*, with rare *Asterosoma*, *Rhizocorallium*?, and *Thalassinoides* (Plate 3.20). The common similarity between these traces is that they are almost all horizontal.

Sections through abundant *Chondrites* traces occur as an array of tiny (~1-2 mm) elliptical sand filled specks and are most common in dark siltstone horizons (Plate 3.20, Photos C, D, E, and F). *Paleophycus* traces are particularly abundant in some of the silty sandstone intervals (see Plate 3.20, Photo F). They are typically small and cylindrical in shape and have a sediment fill identical to the host stratum. Thin walls of *Paleophycus* burrows are distinctly lined by silty material. *Planolites* traces are small, circular in cross-section, unlined, sand-filled, smooth-walled, and are filled with a different lithology than the host rock (Plate 3.20, Photos C and F). *Rhizocorallium* traces were identified by their retrusive spreiten and sub-horizontal inclination (Plate 3.20, Photos D and E). *Thalassinoides* traces are typically semi-circular to oval in shape, are sand-filled, and are contained in black siltstone (see Plate 3.20, Photos B). Rare *Asterosoma* and traces are identified in cross-section by their small circular sand-filled arms surrounded by a silt packing (Plate 3.20, Photos A and D).

Some intervals are so thoroughly bioturbated that biogenic traces are not discernable (see Plate 3.20, Photo A). Locally there are oyster and serpulid worm tube fragments, although this is rare. The majority of the bioturbated intervals overlies cleaner, fine-grained, low angle cross-stratified sandstones, which in some cases overlies centimeter-thick bioclastic lags. A few of the bioturbated intervals have distinct, abrupt, lower contacts; the majority of lower contacts are gradational because of the intrinsic

nature of infaunal tiering. In other instances, the nature of the contact is uncertain because of a break in the core. Very rarely, biogenic traces are seen directly above erosional surfaces.

#### 3.4.10.1 Interpretation for Facies 9

*Paleophycus* traces represent the dwelling burrow of a predaceous polychaete (Pemberton and Frey, 1984). This interpretation is inferred from their passively filled burrows. *Paleophycus* is generally associated with the *Skolithos* ichnofacies. It is found in both high- and-low energy shoreface environments. It can also be found in episodic storm sands (tempestites) and brackish-water assemblages (Frey, 1990). The *Skolithos* ichnofacies is generally indicative of relatively high levels of wave or current energy, and is typically developed in clean, well sorted, loose or shifting particulate substrates (Pemberton et al., 1992a). In such environments, sudden changes in the rates of deposition, erosion and physical reworking are frequent. The traces recognized in the very fine-grained sandstone are thus interpreted to represent the dwelling and feeding behaviors of organisms adapted to a high-energy, presumably shoreface setting (Figure 3.23).

The numerous horizontal, predominantly unlined burrows found in the silty sandstone and siltstone intervals are representative of the *Cruziana* ichnofacies (Figure 3.23) although *Planolites* can be found in virtually all environments from freshwater to deep marine (Pemberton et al., 1992a). *Chondrites* are a common element of the *Cruziana* ichnofacies. The *Chondrites* trace fossil is interpreted to represent a complex

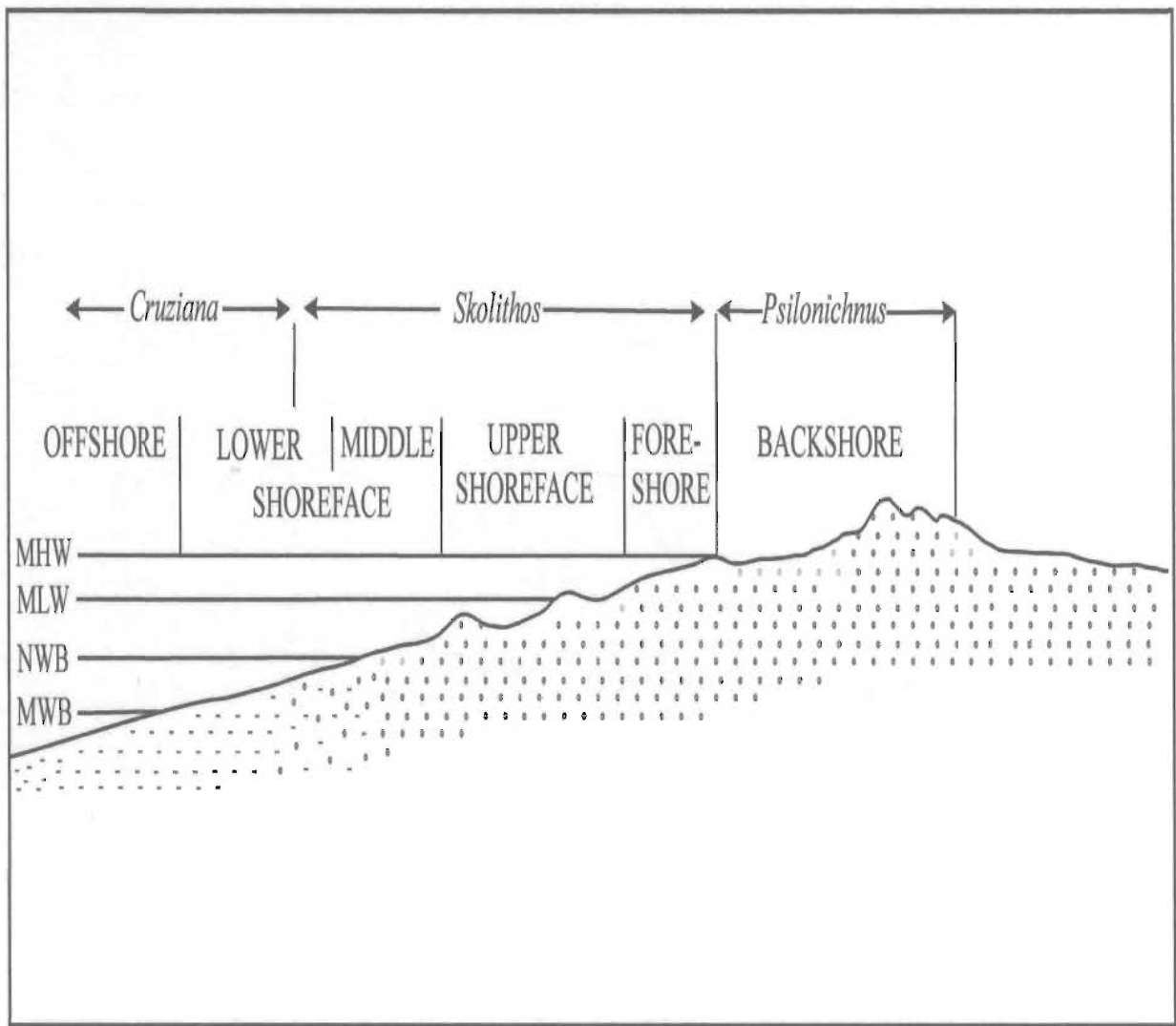


Fig.3.23. Shoreface settings and position of characteristic shallow-marine ichnofacies. Modified from Pemberton et al. (2001). The *Skolithos* ichnofacies is generally restricted to the foreshore through to the upper lower shoreface. The *Cruziana* ichnofacies typically begins in the middle-lower shoreface and proceeds distally to the offshore zone. MHW = Mean High Water, MLW = Mean Low Water, NWB = Normal (fairweather) Wave Base, MWB = Maximum (storm) Wave Base.



deposit-feeding strategy of a siphunculid worm, and is therefore commonly associated with fully marine conditions (Simpson, 1957). In recent literature, Chondrites have been described from brackish environments or in brackish water deposits (Pemberton et al., 2001). *Thalassinoides* is a domicile (dwelling burrow) in which a crustacean filters food out of the water column (suspension feeder) (Bromley and Frey, 1974). Some authors also consider the organism that produces *Thalassinoides* to be a predator. The main significance of *Thalassinoides* is that, because it is a sharp smooth-walled burrow, the sediment in which it appears was stable (non-shifting). This implies that the organism did not have to support the burrow with a lining. Because *Thalassinoides* represents feeding/dwelling behavior, it fits best with the Cruziana ichnofacies. *Teichichnus*, which is commonly found in lower shoreface to offshore environments, is also associated with the Cruziana ichnofacies (Figure 3.23). It is interpreted to represent the dwelling/feeding burrow of a deposit-feeding organism (Frey, 1990). The few *Asterosoma* traces identified in the core are also a common element of the Cruziana ichnofacies. These traces represent the specialized feeding structures of a worm which are generally found in the upper lower shoreface. *Rhizocorallium* is interpreted to represent deposit-feeding behavior and is a common element of the Cruziana ichnofacies (Pemberton et al., 2001).

Conditions for the Cruziana ichnofacies typically range from moderate energy levels in shallow water, below fair-weather wave base but above storm wave base, to lower energy in deeper, quieter water (Pemberton et al., 1992). Sedimentation rate in such a setting is inferred to be moderate.

The horizontal traces found in the silty sandstone and siltstone intervals represent more specialized feeding/deposit-feeding behavior in a quieter, lower-energy setting opposed to those in the sandier intervals, which are less burrowed.

### **3.5 Depositional Environment**

#### **3.5.1 Previous Interpretations**

. This section will begin by presenting the interpretations proposed by Plint (1999), the only person to have published information regarding the A-17 core.

Plint (1999) recognized and described ten facies in White Rose cores. Three of these facies occur in the A-17 core. These are his facies 2, 4, and 5 as described in Plint (1999). His classification of facies is different from that presented in this thesis. The differences are attributed to the different aims of the research. This thesis is focused on the affect of facies characteristics on permeability; therefore, a more detailed classification scheme is used.

Plint's facies 2 (similar to facies 9 in this thesis) consists of centimeter-scale, sharp-based beds of very fine- to fine-grained sandstone, interbedded with and grading upwards into centimeter- to decimeter-scale beds of bioturbated silty mudstone. Physical structures range from fine parallel lamination, to low-angle inclined lamination, to massive bedded. The basal portion of these beds commonly contains layers of bioclasts. The silty/muddy portion of each bed is thoroughly bioturbated. Plint (1999) interpreted this facies as storm deposits on a low-energy muddy shelf in water depths of 20-50 m.

This is based on the trace-fossil assemblage and the lack of evidence of fair-weather deposits.

Plint described his facies 4 (facies 3 in this thesis) as being very fine-grained, clean, well sorted sandstone that generally contains millimeter- to centimeter-scale parallel to low angle (typically  $<10^\circ$ ), planar to gently curved lamination. He noted that beds are occasionally massive, and that burrows are neither large nor abundant. Amalgamated beds separated by subtle erosional surfaces are common. This facies was interpreted by Plint (1999) to represent deposition in a shoreface setting during intense storms. Individual laminated sandstone units were interpreted as single or possibly amalgamated storm events. Plint (1999) noted that the absence of mud laminae in this facies suggests that deposition took place in an environment in which all traces of mud deposited during times of fair-weather were removed by storms.

Facies 5 of Plint (1999) (facies 7 in this thesis) is rich in serpulid worm tubes and various species of bivalves, including several species of oysters, with rare brachiopods. Shells are generally dispersed through a matrix of very fine-grained sandstone but are occasionally clast supported. These beds can range from one shell thick ( $<5\text{mm}$ ) to typically 5-30 cm thick. Calcite concretions are invariably associated with these shell horizons. Calcite commonly extends several decimeters above and below the shell beds, sometimes resulting in several shell beds being incorporated into one large concretion. Plint interpreted the shell beds of his facies 5 to be basal lag deposits genetically related to the laminated and massive sandstones of his facies 4. Each lag was interpreted to represent a major storm event. From the interpretations of Plint (1999), it is apparent that

most of the A-17 core represents deposition in a high-energy storm-dominated shoreface setting. The bioturbated intervals represent periods of fair weather deposition, during which there was enough time for organisms to rework the sediment.

A number of other cores from the Ben Nevis formations have similar characteristics to the White Rose A-17 core.

Harding (1988) described facies and depositional environments recorded in the North Ben Nevis M-61 well taken from the Lower Cretaceous Ben Nevis Formation. His shoreface facies association resembles parts of the White Rose A-17 core. The sandstone layers are very fine-grained, sharp based and commonly contained aligned intraclasts. Sandstone units were interpreted to contain hummocky cross-stratification of very low relief. Harding (1988) states that long-wavelength, low-relief hummocks have been inferred from the Ben Nevis Formation in the cored intervals of other Grand Banks wells.

A number of cores from the Ben Nevis Formation have been described and interpreted by Sinclair (1988). He noted that the Ben Nevis Formation consists of a large percentage of normally graded sandstones. The quartzose sandstones typically grade upward from clean and fine grained to argillaceous and very fine grained in the Ben Nevis 1-45 well (Mobil Oil Canada, 1981). Intervals of abundant calcite cement occur throughout these sandstones. In places, the calcite-cemented zones are associated with beds of shell debris, and in other places, the cemented zones apparently contain no shell debris. The contacts separating these zones from more porous sandstone cut steeply across bedding planes (Sinclair, 1988). In a number of wells (e.g. North Trinity H-71)

sandstones are clean, fine to very fine grained, massive and/or low-angle cross-bedded and contain lag deposits.

Pemberton et al. (2001) have described several cores from the Avalon and Ben Nevis formations, taken from the Hibernia, South Mara, and Ben Nevis fields. A number of these cores contain intervals very similar to parts of the White Rose A-17 core. Their facies 13 belongs to the Ben Nevis Formation. This facies is present in a number of wells including South Mara C-13, North Ben Nevis M-61 and Hibernia B-27. It consists of amalgamated, scour-based, fine to very fine-grained sandstone, which completely lacks bioturbation and carbonaceous particles. Bivalve debris and sideritic mud clasts are found above erosive surfaces (Pemberton et al., 2001, their figure 203). Massive beds are common. Cementation by calcite occurs throughout some intervals of core (up to 2 m). Pemberton et al. (2001) interpret this facies to be indicative of deposition by high-energy waves and currents. The abundance of scours overlain by mud and shell rip-up clasts, as well as the amalgamation, were attributed to repetitive storm deposition in a shoreface environment. The absence of biogenic activity in the clean sandstones stems from the low amount of organic material (i.e., food) and, the high-energy depositional conditions (Pemberton et al., 2001).

It is apparent that the descriptions provided by other authors have a number of striking similarities to the facies recognized and described in the White Rose A-17 core. In all of the descriptions, sediment is fine to very fine grained, laminations are typically of very low angle, and sharp bed bases are commonly overlain by shell accumulations.

### 3.5.2 Interpretation Developed for this Thesis

The cored interval from the A-17 well is interpreted to represent deposition in a high-energy, shoreface setting, which experienced intense and/or frequent storm activity with a subordinate amount of normal, fair-weather activity. The overall upward fining grain-size trend and change in lithology imply a shift in the depositional environment through time from a more proximal to a more distal shoreface setting.

Numerous lines of evidence support the proposed environmental interpretation. They are itemized below.

- 1) The A-17 core consists almost exclusively of amalgamated fine- to very fine-grained sandstones grading upward (over ~100 m) into very fine-grained sandstones interbedded with siltstones.
- 2) Erosional surfaces mantled by bioclastic debris are frequent.
- 3) Low relief cross-stratification is the dominant bedform.
- 4) Silt, carbonaceous material and biogenic sedimentary structures are almost completely absent, with the exception of a few intervals and the uppermost 5-6 m of the studied core.
- 5) Rapid deposition is indicated by the common homogeneous intervals.
- 6) Normal grain-size grading.
- 7) Only the uppermost 5-6 m of the core contain interbedded siltstone with biogenic structures.

This evidence suggests that deposition was restricted primarily to a high-energy, storm-influenced, marine depositional setting. Two settings where such criteria are met

are the middle and lower shoreface. The middle shoreface (Figure 3.23) is defined as an area that extends over the zone of shoaling and initial breaking of waves (Reinson, 1984). Storms have a strong influence on the middle shoreface (Pemberton et al., 2001). Sandstones in the middle shoreface tend to be well sorted, well winnowed, and medium to fine grained with only minor shale and siltstone.

The lower shoreface extends downward from fair-weather to storm-weather wave base (Reinson, 1984). Most structures reflect storm deposition including hummocky cross-stratification, rarer swaley cross-stratification and quasi-planar stratification (Pemberton et al., 2001). Intervals not dominated by erosional amalgamation may show waning-stage oscillation ripples or combined-flow ripples capping the low-angle structures. Hummocky cross-stratification has been widely reported in wave-dominated settings, and it is inferred to represent storm-wave deposition above storm wave base (Harms et al., 1975; Dott and Bourgeois, 1982; Hunter and Clifton, 1982).

Many authors have suggested that HCS is often encountered in middle to lower shoreface settings below fair-weather wave base (Harms et al., 1975; Dott and Bourgeois, 1982; Brenchley and Newall, 1982; Brenchley et al., 1982; Duke et al, 1991). Because the A-17 core is dominated by HCS (or a variant thereof) it is logical to suggest that it too formed in a high-energy middle to lower shoreface setting. HCS in the A-17 core is primarily erosively amalgamated with little to no intervening silt/mudstone layers, fair-weather sedimentary structures, or bioturbated intervals. This is almost certainly a function of the intensity or frequency of storm activity and the position/setting in which sands were deposited. Only in the uppermost few meters of the core are sandstone and

siltstone interbedded, and trace fossils become common. Amalgamated HCS is characterized by thick (up to several tens of meters) sandstone deposits and differs from the other HCS associations by the lack of mudstone and absence of a preferred sequence of structures. Duke (1985a) notes that beds in such associations are in erosional contact with underlying beds and that erosion locally eliminates the upper parts of the previously emplaced sandstone/mudstone layer. Occurrences of such amalgamated deposits have been interpreted as representing highly agitated, shallow- marine environments that experienced either extremely energetic or frequent storm activity. The lateral variability of HCS beds has been documented by relatively few authors (e.g. Dott and Bourgeois, 1982; Brenchley, 1985). Based upon their description, from proximal to distal settings the following generalizations and relation to the A-17 cored interval can be made.

- 1) Thicker sandstone beds occur in proximal settings: amalgamated HCS sandstones grade laterally into discrete HCS beds in more distal deposits. This onshore-offshore trend is seen in the A-17 core, which consists predominantly of amalgamated HCS grading upward into discrete HCS beds.
- 2) Grain size decreases distally. This fits with observations from the A-17 core, because grain size decreases vertically in the core, which is interpreted to represent deposition in more distal settings due to progressive relative sea level rise.
- 3) There is decreasing sandstone to siltstone ratio distally.



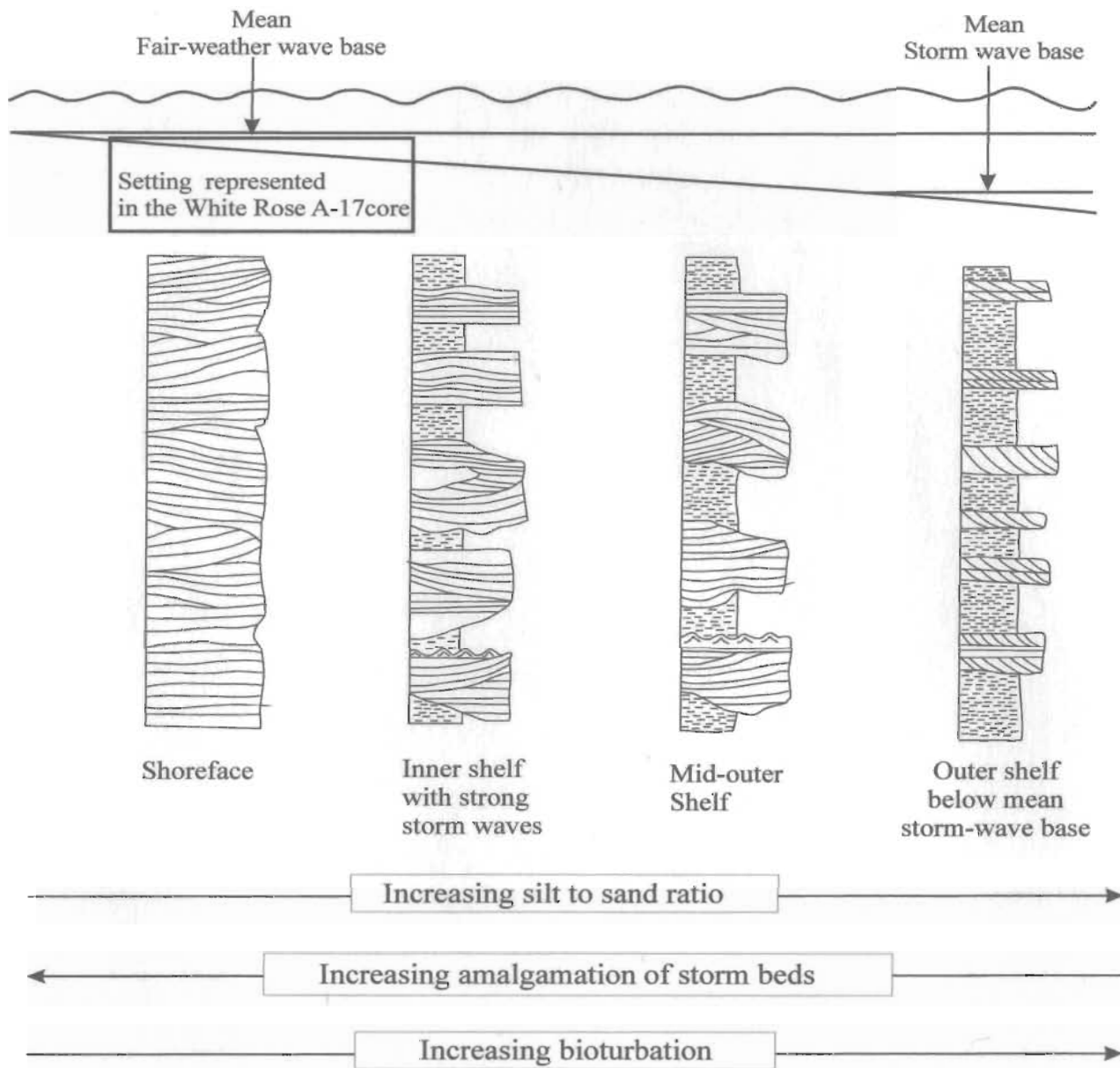


Fig.3.24. Schematic of a shoreline cross-section used to illustrate the proximal to distal relationships of HCS beds. Modified from Brenchley (1985). As distance from the shoreface increases, the amount of interbedded silt and sand increases, the abundance of erosively amalgamated HCS beds decreases, and bioturbation increases. Below mean storm wave base, extreme events still deposit tempestites. The boxed in area represents the depositional setting interpreted for the A-17 cored interval.

- 4) There are more prominent gutter casts distally. Gutter casts were not observed in core, but this is not surprising because of the limited width of the core. Some of the undulatory contacts might be cross-sections of gutter casts.
- 5) There is a distal increase in the abundance of wave ripples passing into current ripples, and, lastly into graded-beds. Nowhere in the core are there small-scale wave or current ripples recorded.
- 6) Normal grain-size grading does dominate intervals of the A-17 core, but because of the limited grain-size range, it does not appear that normal grading is better developed in any particular section of the A-17 core. However, in the uppermost few meters, very fine-grained sandstones does grade into bioturbated siltstone.
- 7) Moving distally, there is an increase in intensity of bioturbation, particularly at the tops of HCS beds. This is true for the A-17 core. The tops of beds in the uppermost 5-6 m are bioturbated.

Brenchley (1985a) provides a shoreline cross-section (Figure 3.24), which illustrates the proximal to distal relationships in HCS beds. In this diagram, it is clear that in more proximal shoreface settings, storms have a significant influence on the stratigraphy. Beds of HCS tend to be amalgamated, and show little to no preservation of interbedded silt/mudstone nor bioturbation. As distance from the shoreface increases, interbedded HCS sandstone and siltstone beds increase. Additionally, fair-weather sedimentary structures, including current ripple cross-lamination and wave-ripple cross-lamination increase, as does the degree of bioturbation.

For the A-17 cored interval, deposition is inferred to have taken place mainly in a high-energy, middle to lower shoreface setting. Through time, possibly because of transgression, mean grain size decreased gradually from fine- to very fine-grained sand and eventually to silt. This decrease in grain size and the change in lithology point to a relative sea level rise and a shift in sedimentary environments. From this it is inferred that the uppermost 5-6 m of the core represent deposition in a more distal setting, possible lower shoreface. The change from unburrowed fine-grained sandstone to burrowed silt and silty sandstone in the uppermost 5-6 m represents a transition to deposition under normal fair-weather offshore conditions where organisms had ample time to construct domiciles and feed upon the sediments.

### **3.5.3 Problems with the Depositional Model**

Though most of the deposition is thought to have occurred predominantly in a high-energy middle to lower shoreface setting, a number of enigmas still surround the interval represented by the A-17 core. Firstly, it is difficult to understand why there are absolutely no small-scale wave-produced sedimentary structures when the dominant bedform is interpreted to be the result of wave activity. Did all the deposition occur below fair-weather wave base, or were all fair-weather structures completely eradicated by the passage of the next storm? Secondly, how is it that 100<sup>+</sup> m of shallow-marine sandstone contains virtually no silt-sized particles or carbonaceous material? Was the water column so agitated that such material could never settle and accumulate, or if it did, was it eroded and transported away by the passage of the next major storm? Thirdly, what

Thirdly, what set of conditions allowed for the 100<sup>+</sup> meters of fine- to very fine-grained sandstone to be deposited in virtually the same setting with no evidence for a major discontinuity? What were the roles of basin subsidence, relative sea-level change, eustatic sea-level change, and sediment supply in ensuring such thick aggradation? Additional analysis of several of the White Rose cores in conjunction with seismic and structural analysis and interpretation are required if these questions are to be answered. This additional work is beyond the scope of this thesis.

## **CHAPTER 4**

### **LINKS BETWEEN GRAIN SIZE, FACIES, AND PERMEABILITY**

#### **4.1 Introduction**

The principal objective of this chapter is to investigate and interpret relationships between the sedimentological and permeability data in the White Rose A-17 core. This is because: 1) there are a large number of permeability measurements available for comparison with the sedimentological data, and 2) these relationships have not been previously investigated in this, and in other White Rose cores.

This chapter is divided into four main sections. The first section will explain a number of aspects of permeability including what it is, why it is important, and what factors influence and/or control it. The second section is concerned with presenting and discussing the permeability data and grain-size versus permeability relationships. Section three focuses on changes in permeability and grain-size across the main types of contacts and boundaries. The fourth and final section is concerned with investigating and interpreting lithofacies-specific permeability trends and the relationship(s) between permeability and grain-size for each of the nine facies in the core.

#### **4.2 Permeability: Definition, Importance, and Controls**

##### **4.2.1 Definition**

Permeability is defined as the ability of a fluid to pass through a porous material, or the rate at which it passes through a material (Selley, 1998). In clastic rocks, permeability is determined by the size of pore throats present in the rocks and by the number of connected pores (Evans et al., 1997). The unit of measurement is the Darcy,

named after the French engineer who investigated the flow of water through filter beds near Dijon France in 1856. Muskat and Botset (1931), Botset (1931), and Muskat (1937), further developed the work of Darcy and formulated Darcy's Law. Darcy's Law is as follows:

$$Q = \frac{k(P_1 - P_2)A}{\mu L}$$

where

Q = rate of flow

k = permeability

(P<sub>1</sub>-P<sub>2</sub>) = pressure drop across the sample

A = cross-sectional area

L = length of the sample

μ = viscosity of the sample

Rearranging for permeability the equation becomes:

$$k = \frac{Q\mu L}{(P_1 - P_2)A}$$

One Darcy is defined as the permeability that will permit a fluid of one centipoise (cP) viscosity to flow at a rate of one cubic centimeter per second through a cross-sectional area of one square centimeter when the pressure gradient is one atmosphere per centimeter (Selley, 1988). In practical units, one Darcy will yield a flow of approximately one barrel per day of one centipoise oil through one foot of formation thickness in a well bore when the pressure differential is one pound per square inch (psi) (Simpson, personal communication, 2004). Darcy's law is valid assuming that: 1) the fluid in question is under laminar flow conditions; 2) there is no reaction between the fluid and the rock, and 3) only one fluid phase is present. These conditions are seldom satisfied; thus, variations

of the Darcy equation are required. In dual porosity systems where, for example, rocks with fractures and vugs occur, more complex relationships exist than those that can be accurately expressed by Darcy's law (Selley, 1998). Reservoirs typically have permeabilities less than a Darcy, and for that reason, the millidarcy (mD) is most often used ( $1\text{D} = 1000\text{ mD}$ ). Permeabilities in clastic reservoirs can range from  $<0.1\text{ mD}$  to  $>10\text{ Darcys}$  (Evans et al., 1997), although average permeabilities in reservoirs are typically in the range of 5 to 500 mD (Selley, 1998).

#### **4.2.2 Importance**

Permeability is a key parameter influencing the economic value of a hydrocarbon accumulation (Evans et al., 1997), and according to Dryer et al. (1990) it is the single most important factor influencing fluid flow in a reservoir. The spatial variation of permeability significantly influences the migration and distribution of fluids and gases and determines the ability of a reservoir to release its fluids and gases (Pryor, 1973).

#### **4.2.3 Controls**

A number of factors are known to control the magnitude and distribution of permeability. The most important ones are grain-size, sorting, compaction, and cementation (Cade et al., 1994) (Figure 4.1). In addition, grain shape and grain packing also influence permeability (Beard and Weyl, 1973; Selley 1998). Because several of these parameters are in turn regulated by depositional environments, previous authors have related permeability distributions to depositional facies (Jones et al., 1985;

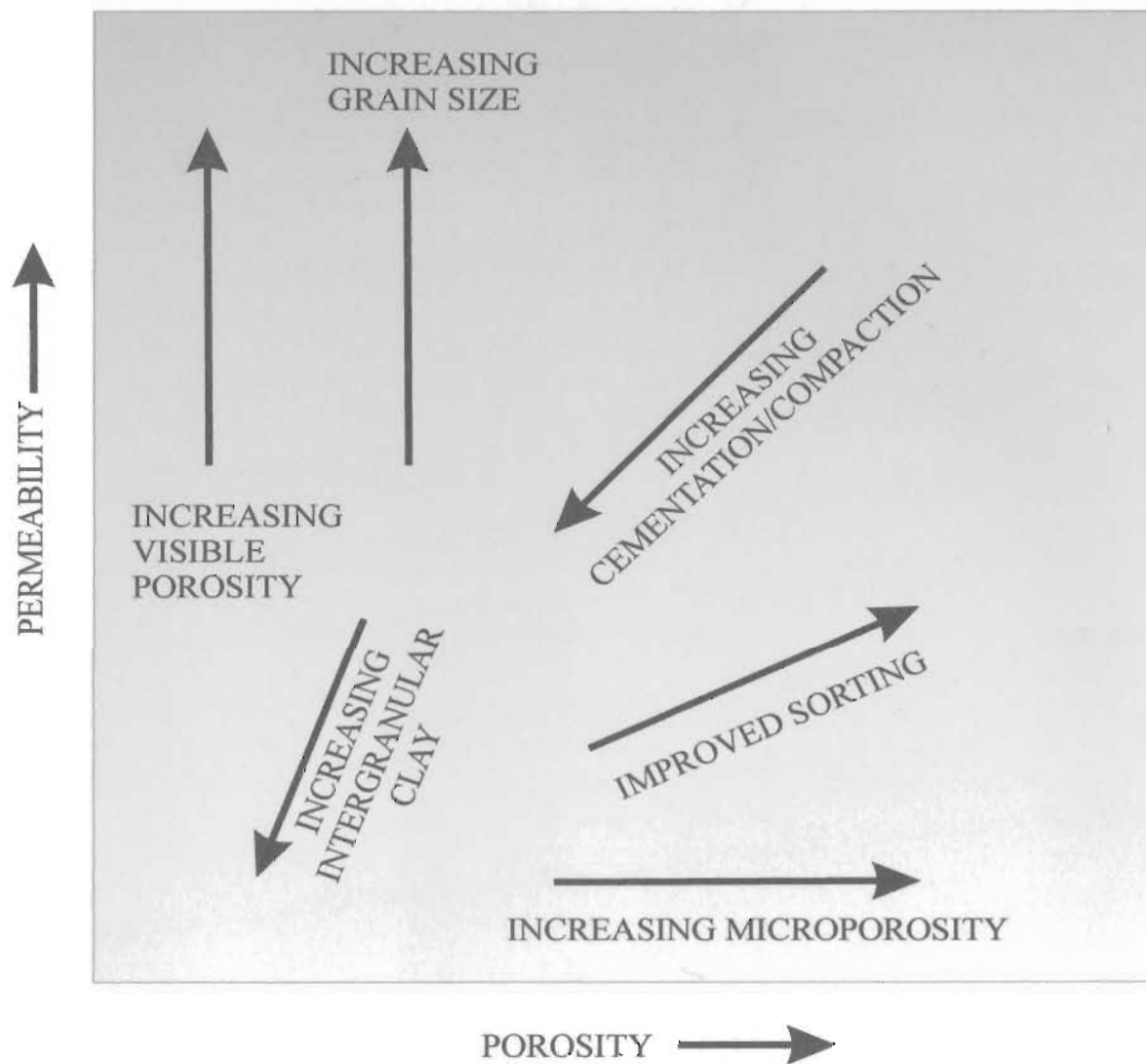


Fig.4.1. An interpretation of the effects of various controls on porosity and permeability. Modified from Ethier and King (1991).



Haldorsen, 1986; Hearn et al., 1986; MacMillan et al., 1986; Stalkup et al., 1986; Weber, 1986).

The following text will briefly describe how compaction and cementation affect permeability. This is followed by a much more thorough explanation of how textural factors, particularly grain-size and sorting, influence permeability. Grain shape was not considered for this study because little comparative data exists. Next, sedimentary structures, trace fossils, and depositional environments are discussed with reference to their relationship(s) to permeability.

#### **4.2.3.1 Compaction and Cementation: Their Affect on Permeability**

Compaction will always have an adverse effect on reservoir quality, particularly permeability (Evans et al., 1997). During compaction, pore-throat sizes are reduced as grains become more tightly packed, which leads to a gradual decline in permeability with a reduction in porosity (Selley, 1998).

Cementation usually brings about permeability reduction (Ehrlich et al., 1997) by constricting pore throats and reducing pore-throat size. Reduction of pore-throat size increases capillary pressure and decreases permeability.

Unquestionably, in consolidated sandstones, diagenesis (compaction and cementation) has an important effect on permeability. The precise effect on permeability depends on the amount of compaction and distribution of the cements. Increasing compaction and cementation alters or obscures the relationship between texture and

permeability but appears to never completely eliminate the influence of the original syndepositional texture (Ehrlich et al., 1997).

#### **4.2.3.2 Textural Controls on Permeability**

The texture of sediment is closely correlated with its porosity and permeability (Selley, 1998). As noted by Beard and Weyl (1973), past investigations have shown that the most important textural properties of natural clastic sediments are: 1) grain size, 2) sorting, 3) grain shape (sphericity), 4) roundness (angularity), and 5) packing. Of these, grain size and sorting are the most important with respect to porosity and permeability while sphericity, roundness, and packing are of lesser importance. Grain orientation (another characteristic of fabric) also has an influence on permeability (Mast and Potter, 1963; Pryor, 1973; Selley, 1988). The text to follow provides a summary of how each of these parameters relate to permeability.

##### **4.2.3.2.1 Grain size and Permeability**

It is imperative to note that relationships between grain size and permeability are only documented for unconsolidated sands (Shepard, 1989). Lithification tends to reduce permeability regardless of grain size, but little is known concerning details of this relationship in consolidated sandstones (Ehrlich et al., 1997). A major element of this thesis is to investigate and describe the relationships between permeability and grain size in well-consolidated sandstones.

In unconsolidated sands and gravels, strong correlations exist between permeability and grain size (Ehrlich et al., 1997). Shepard (1989) states that permeability is an exponential function of grain size, with the relationship proportional to grain size raised to the power 1.3 to 2 in well-sorted sands. Work done by Beard and Weyl (1973) shows that for any given porosity, permeability will systematically increase with grain size. Conversely, permeability declines with decreasing grain size because pore diameters decrease and capillary pressures increase.

#### **4.2.3.2.2 Sorting and Permeability**

Another important textural control on permeability is sorting (Beard and Weyl, 1973). Both Krumbein and Monk (1942), and Beard and Weyl (1973) demonstrated that greater sorting correlates with greater permeability. As an example, Selley (1988) states that well sorted sand has a high proportion of detrital grains to matrix (particles  $< 62\mu\text{m}$ ) as opposed to poorly sorted sand, which has a low proportion of detrital grains to matrix. The finer grains of the matrix fill the pores and obstruct pore-throat passages within the framework, thus reducing porosity and inhibiting permeability. This heterogeneity diminishes permeability by increasing the tortuosity of the pore system. Similarly, rocks with poorer sorting will have smaller mean pore-throat diameters and, therefore, lower permeability than better sorted rocks with the same mean grain size (Evans et al., 1997). Kegley et al. (1994) analyzed the texture and made 4200 permeability measurements in Eocene and Miocene units in the Mixed Waste Disposal (MWD) area at the Savannah River Sites in South Carolina. They concluded that the distribution of permeability is

primarily controlled by mud (silt and clay) content of the sediment. Units with low mud content have a higher permeability than those with high mud content. The distribution of permeability is also more variable with varying mud content, compared to units with uniform mud content.

Sorting will differ from reservoir to reservoir and the degree of sorting will depend upon a number of factors including sandstone composition and the environment of deposition. For texturally and mineralogically mature sandstones deposited in virtually a fixed setting, such as those from the Ben Nevis Formation in the South White Rose field, sorting has a very limited range; therefore, its affect on permeability is rather difficult to address. Nevertheless, a few comments on the sorting data at its relationship to permeability are made and, as well, general remarks regarding the effect with which bioclasts and silt have on permeability are made. The latter remarks have no quantitative backing.

#### **4.2.3.2.3 Grain Shape, Fabric, and Permeability**

Very little is known of the relationship between grain shape (roundness and sphericity), packing, and permeability due to lack of relevant data. Fraser (1935) noted that porosity might decrease with increasing sphericity because spherical grains potentially pack more tightly than subspherical ones. He did not discuss the relation between sphericity and permeability.

The relationship between grain fabric and permeability is more straightforward. In sediments, grains are normally deposited with a statistically preferred long axis because:

1) grains are most often deposited under the influence of a unidirectional current, and 2) clastic grains are rarely spherical. It can be predicted that fluid flow is less tortuous and that permeability is greater parallel to the fabric alignment. Selley (1988) notes that most sand grains in planar laminated sediments are elongated parallel to the current direction, and that this direction coincides with maximum permeability. This relationship has been seen in planar-bedded sandstones in fluvial and turbidite sections (Shelton and Mack, 1970; Martini, 1971; Von Rad, 1971).

#### **4.2.3.3 Sedimentary Structures and Permeability**

A number of authors have investigated the relationships between sedimentary structures and permeability. Most of these studies involve fluvial cross-bedding.

One of the earliest studies was conducted by Mast and Potter (1963). They demonstrated the relations amongst cross-stratification, grain orientation, and permeability. They found that permeability in sandstones is greatest in the plane parallel to the foresets of cross-stratification. Hewitt and Morgan (1965) determined that horizontal permeabilities were at a maximum parallel to the trough axis of cross-bedding and minimum permeabilities were documented perpendicular to the laminae of the crossbed sets. Dodge et al. (1971) also concluded that permeabilities are higher parallel to the dip directions of cross-bedding than in the strike directions. Pryor (1973) concluded that permeability in modern fluvial deposits is highest in the deepest and central part of trough cross-beds parallel to grain orientation. Selley (1988) notes, that for cross-bedded sandstones, grain-size variations appear to exert more of an influence on permeability

than grain orientation. For example, in fluvial cross-bedding, permeability will decrease as grain size decreases from the foresets to toesets. Weber (1982) reports that, in the case of festoon cross-bedding, the important elements are the bottomset and foreset laminae with the lowest permeabilities occurring in the bottomsets. He also noted that variability in permeability was more pronounced within sedimentary structures than between them. Another thorough account of permeability variation within sedimentary structures, mainly cross-bedding, has been given by Hurst and Rosvoll (1991). They, like Weber (1982) determined that the main source of permeability variation in sandstones exists within sedimentary structures.

For bioturbated facies, permeability is most often hindered by the presence of silt particles infilling pores and obstructing pore throats (Weber, 1982). It is common, however, to find permeable streaks, especially if there are a number of sand-filled burrows.

#### **4.2.3.4 Depositional Environments and Permeability**

As with sedimentary structures, there have been some studies of the relationships between permeability and depositional environments. One of the earliest was conducted by Pryor (1973). He determined porosity, permeability, and textural parameters for 992 oriented, undisturbed sand samples from Holocene river-bar, beach, and dune deposits. Sand bodies from the various depositional environments exhibit well-organized and different spatial patterns of permeability. Results from Pryor (1973) are taken to indicate that the largest variation in permeability of the three environments studied was in

river point bars. Permeability ranged from 4 millidarcies to 500 Darcies with an average of 93 Darcies. Beach sands had the second broadest permeability distribution with a range of 3.6 to 166 Darcies and an average of 68 Darcies. Dune sands had the least variation in permeability with a range of 5 to 104 Darcies and an average of 54 Darcies. Of these three environments, river point bars are the most heterogeneous and have the widest variation in texture whereas dune deposits are the least heterogeneous and contain the least variation in texture. Weber et al. (1982) examined the permeability distribution of unconsolidated Holocene channel-fill sands. They found that permeability was highest near the center of the channel-fill and gradually decreased towards the channel edges. Chandler et al. (1989) and Goggin (1988) characterized permeability distributions in the eolian Jurassic Page Sandstone. They found a close correlation between strata type and permeability, and determined that the average permeability of each lithology was significantly different from other types. For instance, grain-flow, wind-ripple, interdune, and extra-erg (non-eolian) deposits have progressively poorer reservoir characteristics. The study of Dryer et al. (1990) documented a close connection between depositional facies and permeability. Based on their data, five permeability classes were distinguished corresponding to different depositional environments.

There have been few published examples of the relationship(s) between marine depositional settings and permeability. Nevertheless, a number of generalities can be made. For example, in shallow-marine and shoreline settings the major controls on permeability (before compaction and cementation) should be, by analogy with the previous examples, grain size and the distribution of silts and clays. Factors affecting

these are provenance, depositional energy/setting, and bioturbation. Coarse-grained sediments that are both free from silts/clays are those subject to highest wave energy or tidal action. Such coarse-grained clean sediments are typically deposited in littoral environments where wave and tidal action can be vigorous. The sediments deposited in these settings should have the highest permeabilities. Extensive bioturbation can effectively destroy small-scale permeability trends related to earlier bedding structures. Bioturbation redistributes or mixes finer grained sediments such as silt and clay that might otherwise exist as laminations or beds. In shallow marine settings, permeability likely decreases offshore as finer grained material and bioturbation increase.

It appears that both grain size and sorting significantly influence permeability in both unconsolidated and consolidated sands, irrespective of their environment of deposition. This may be by either increasing or decreasing permeability.

### **4.3 Permeability: Description of the A-17 Core Data and its Relation to Grain Size**

#### **4.3.1 Introduction**

The purpose of this section is to: 1) present and remark on the White Rose A-17 permeability data and, 2) investigate its relation to grain size. The data used in this section include 1176 grain-size and permeability measurements. In this section and the sections to follow the grain size of sandstone is indicated by the characteristic size, in microns, of grains which were measured during core description. For example, a sandstone for which the characteristic size is 84  $\mu\text{m}$  is referred to as a sandstone of 84  $\mu\text{m}$



grain size, even though the sediment is not all of identical size (i.e. sandstones in the cored interval are not perfectly sorted).

This section will begin by presenting the White Rose A-17 permeability data in both profile and histogram format. This is done so the reader can obtain a sense of the nature of the permeability population and how it is distributed stratigraphically. Next, the relationship(s) between grain size and permeability is investigated at various scales. This is somewhat similar to how grain-size trends were treated in Chapter 3. The first is at the scale of the entire cored interval. Next, grain size and permeability are compared with one another in each unit. Finally, smaller-scale relationships are investigated. Vertical profiles and cross plots are used to highlight the findings in the data.

#### **4.3.2 Permeability Data**

Permeability in the White Rose A-17 core ranges from a minimum of ~0.001 mD to a maximum of 451 mD, and averages ~75 mD (Figure 4.2A). When the dataset is ‘clipped’ by excluding values less than 1 mD (most of which correspond to facies 5 and facies 6) the average permeability is ~85 mD (Figure 4.2 B). These ‘clipped’ permeability data approximate a log-normal distribution (c.f. Drummond and Wilkinson, 1996). This is confirmed when the logarithms of each value greater than 1 mD are plotted (Figure 4.3). The result is a somewhat negatively skewed distribution, with a tail of small permeability values; however, it approximates a normal distribution (c.f. Drummond and Wilkinson, 1996).

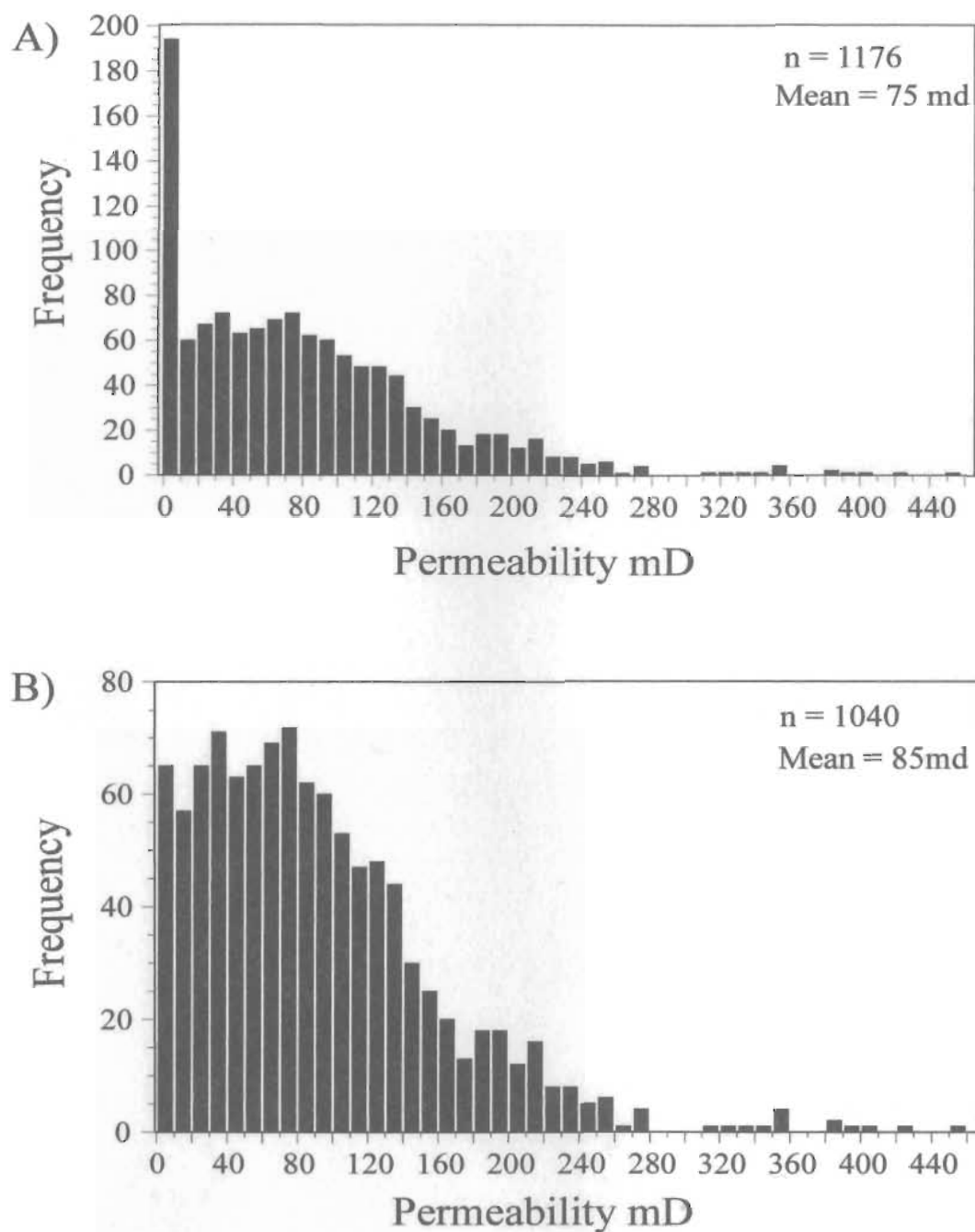


Fig.4.2. Permeability frequency distributions for the White Rose A-17 cored interval with all data (A), and minus permeabilities from Facies 5 and Facies 6 (B). The mean is ~10 mD higher for (B) when pervasively calcite-cemented intervals are eliminated. The distribution of the data in (B) approximates a log-normal distribution (c.f. Drummond and Wilkinson, 1996). Bin size is 10 mD with data plotted at midpoints.

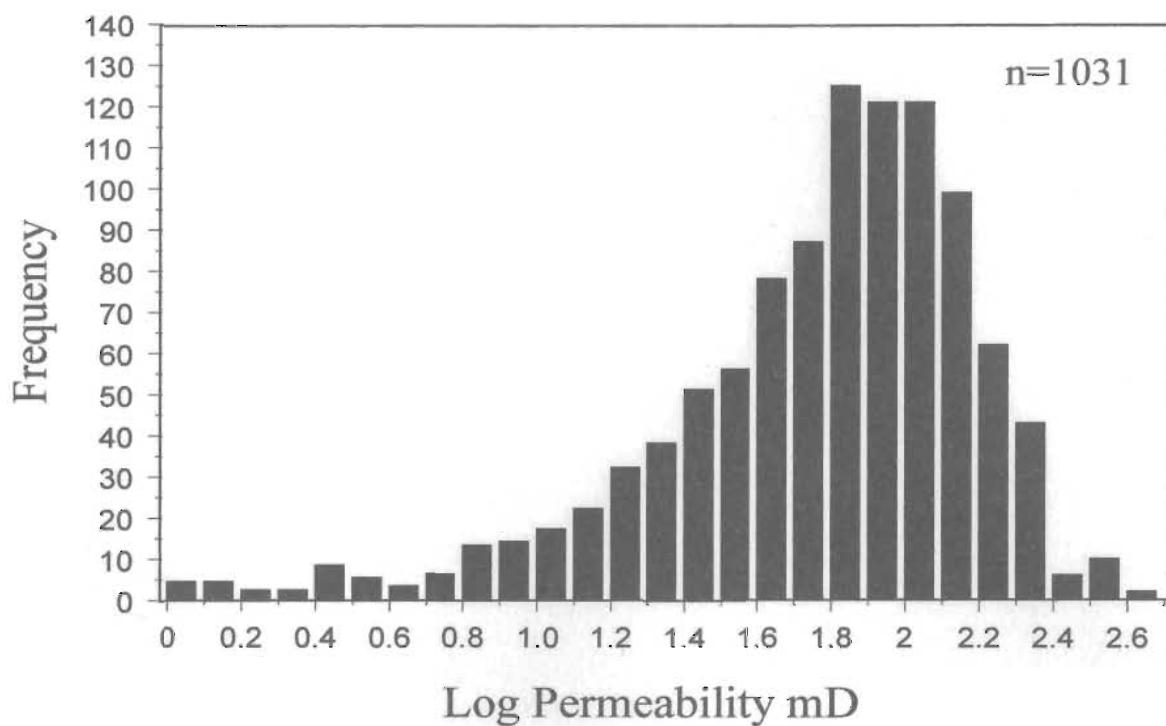


Fig.4.3. Frequency distribution of the logarithms of all permeabilities greater than or equal to 1mD. Permeabilities less than 1 mD are excluded because their log values are negative. This plot confirms that permeability is best approximated by a log-normal distribution (c.f. Drummond and Wilkinson, 1996). Bin size is 0.1 log units with data plotted at midpoints.

A vertical permeability profile demonstrates that the data are highly variable within the A-17 core (Figure 4.4). There are few if any consistent trends in the data. Permeabilities higher than 85 mD (the mean ignoring permeability data from facies 5 and 6) occur mostly between 3019-2996 m and 2990-2979 m. Low permeabilities of <50 mD occur intermittently throughout the cored interval but are particularly common from 2955-2940 m. Zones of extremely low permeability (i.e. <1 mD) appear mostly in the upper 10 m and lower 30 m of the core. These correspond mostly with pervasively calcite-cemented intervals (see Appendix B).

From the data, it appears that texturally and mineralogically mature shallow-marine sandstones of the White Rose A-17 cored interval have a log-normal permeability distribution and highly a variable vertical permeability profile.

### **4.3.3 Permeability and its Relationship(s) to Grain size**

#### **4.3.3.1 For the Entire Cored Interval**

For unconsolidated sands, Beard and Weyl (1973) demonstrated that there is a close relation between grain size and permeability. As grain size increases, permeability increases. The relation between grain size and permeability in the White Rose A-17 cored interval is not so straightforward. To illustrate this, vertical grain-size and permeability profiles are overlain for comparison (Figure 4.5). Over the whole interval, these two variables do not appear to track one another closely (i.e. they do not co-vary strongly). This indicates, at least at this scale, that grain size and permeability are not closely related.

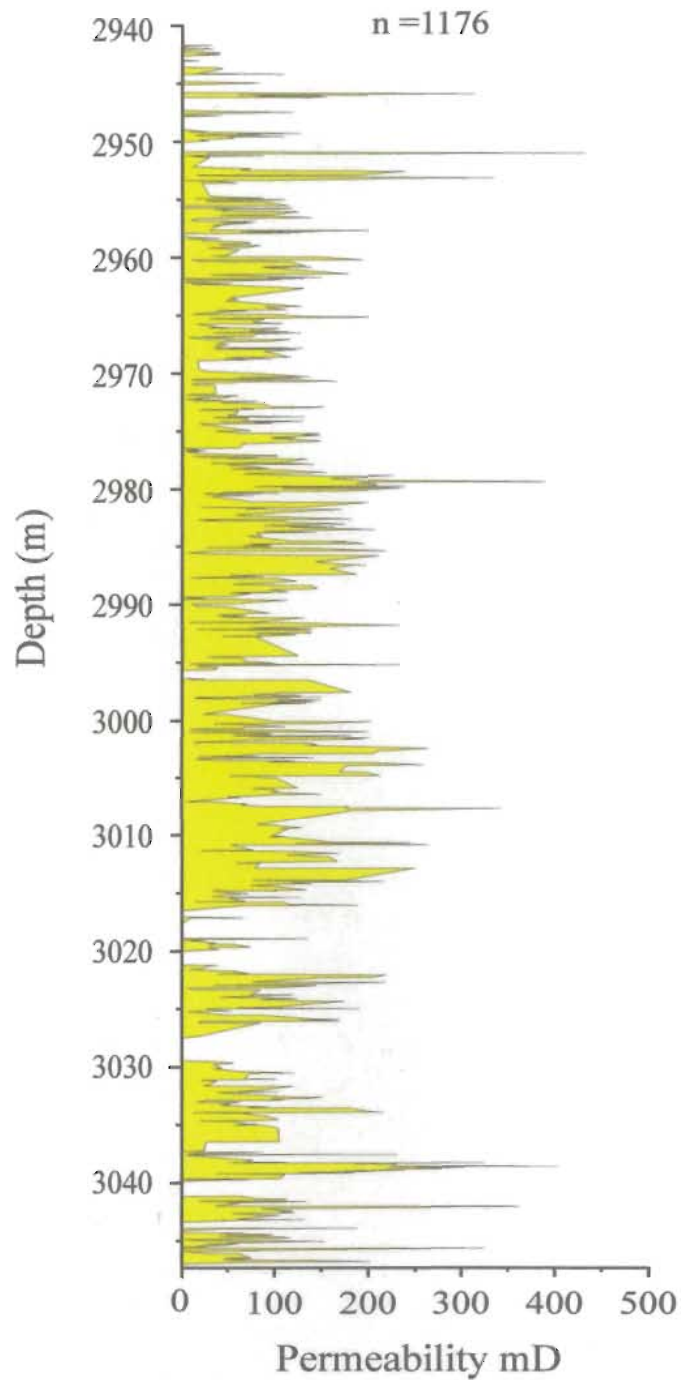


Fig.4.4. Vertical permeability profile for the White Rose A-17 cored interval. Data used for the construction of this vertical permeability profile is raw; it has not be modified.

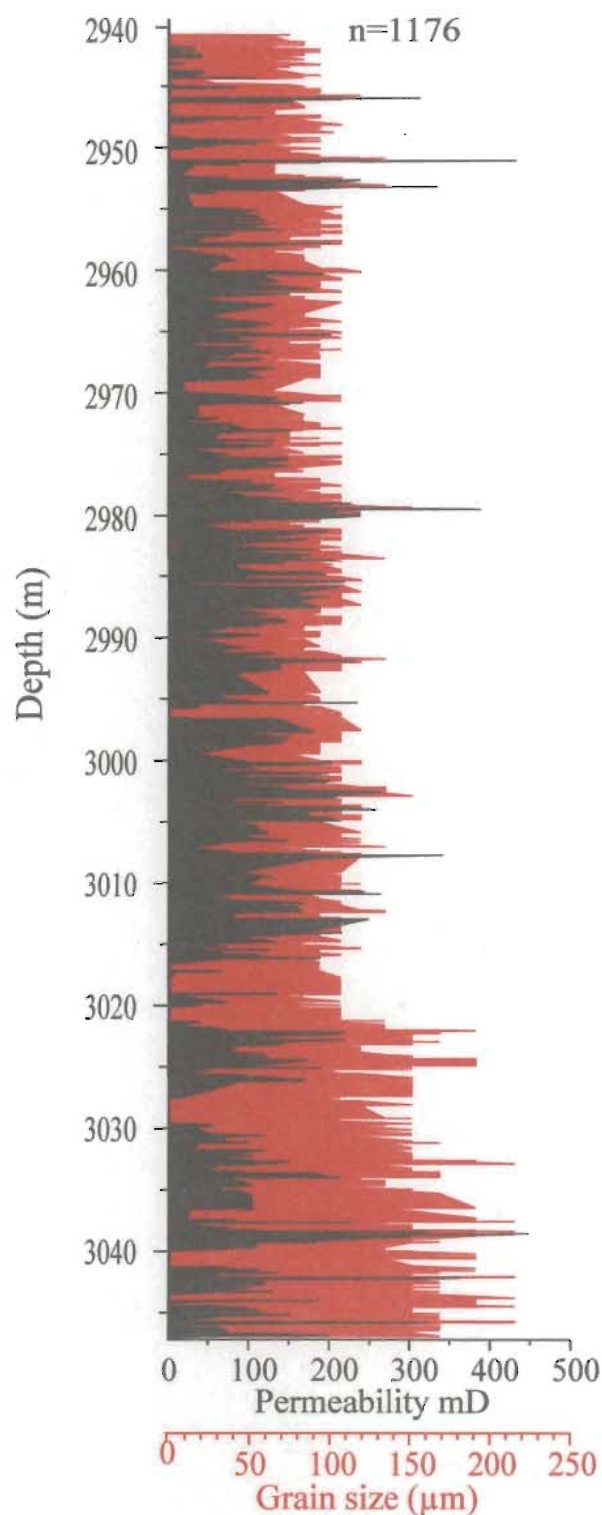


Fig.4.5. Vertical permeability profile (black) and vertical grain-size profile (red) for the White Rose A-17 cored interval overlain for purposes of comparison. Note that these data do not correlate strongly. The data used for the construction of these vertical profiles has not been modified.

When grain-size and permeability measurements are cross-plotted (Figure 4.6), relationships amongst the data are clearer and a number of inferences can be made. Firstly, the relationship between grain size and permeability is not linear, which means that the data do not cluster around, or cannot be defined by a straight trend line. For any given grain size there is a broad range of possible permeabilities. The relationship amongst these variables is best defined by a surface that envelops maximum permeabilities (data envelope), with the exception of a few 'high' permeability outliers (Figure 4.6). In general, for each increase in grain size the range of associated permeabilities increases. For example, sandstones of 66  $\mu\text{m}$  grain size correspond to permeabilities which range from  $\sim 0.008$  mD to 75 mD. Sandstones of 94  $\mu\text{m}$  grain size correspond to permeabilities which range from  $\sim 0.005$  mD to  $\sim 250$  mD, and sandstones of 134  $\mu\text{m}$  grain size correspond to permeabilities which range from  $\sim 0.001$  mD to 265 mD (excluding the few outliers). Above a grain size of 134  $\mu\text{m}$ , the range of permeabilities no longer increases with increasing grain size. In fact, maximum permeabilities are slightly lower (excluding the few outliers) than those associated with sandstones of 107 to 134  $\mu\text{m}$  grain size. From this it can be deduced that the coarsest-grained sandstones do not correspond with the highest permeabilities. Equally high and higher permeabilities are associated with sandstones of significantly finer size. In addition, it is clear that minimum permeabilities are essentially the same ( $\sim \leq 0.01$  mD) irrespective of grain size (Figure 4.6). These findings demonstrate that grain size (particularly above 134  $\mu\text{m}$ ) is not the only factor controlling permeability in the White Rose A-17 core. Other factors such as compaction and

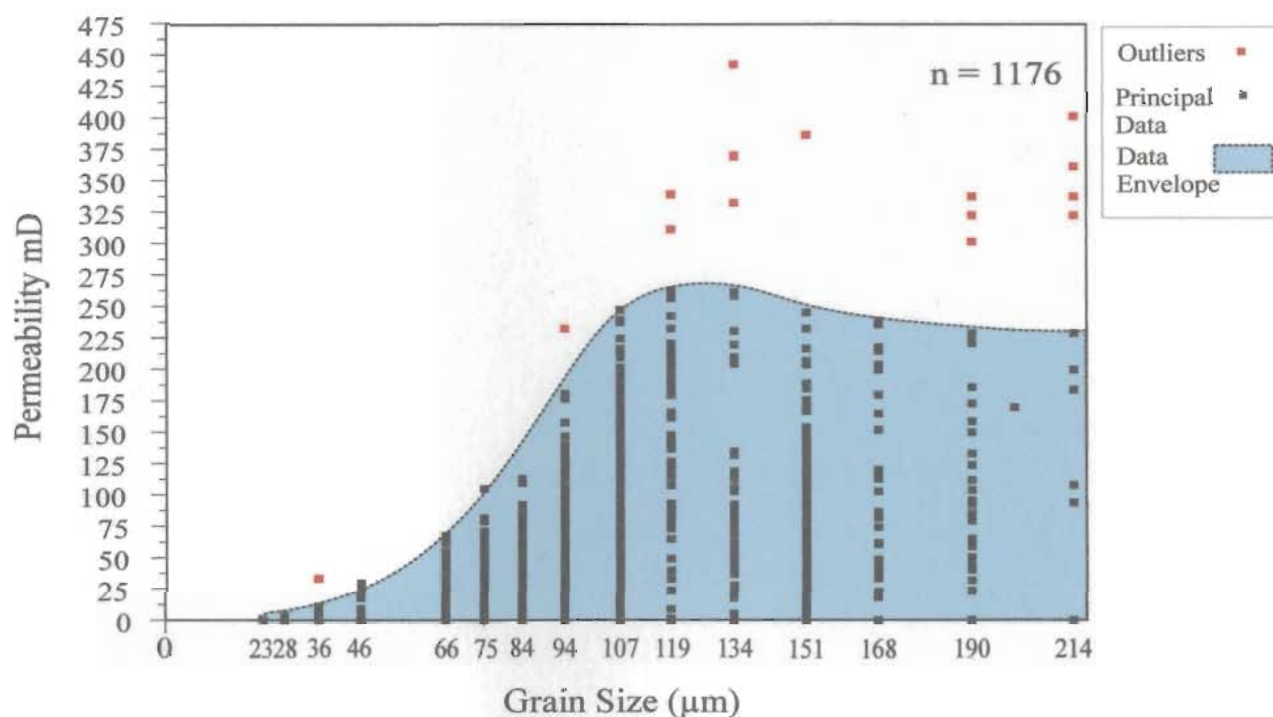


Fig.4.6. Grain size ( $\mu\text{m}$ ) vs. Permeability mD for the White Rose A-17 cored interval. Red dots are considered outliers where data is sparse, black dots are the principal data points, and dashed-line encompassing the principal data points is the data envelope. Note that there is a great deal of overlap in the principal data points giving the impression that these data points form lines; this is not so. It is a result of the large number of data points and the size of the character used to represent them.



cementation (see Figure 4.1) are likely also significant, obscuring the direct relationship between grain size and permeability demonstrated by Beard and Weyl (1973) from unconsolidated sands. Grain-size sorting is not interpreted to be an important factor influencing permeability over the cored interval as sorting values are essentially the same (Table 4.1) and, with the exception of one sample, can all be described as well sorted according to the terminology of Folk and Ward (1957).

#### **4.3.3.2 For the Three Units**

The cored interval is divisible into three units based upon dominant grain-size class and lithologies (refer to Figure 3.4). As a result, cross plots of grain size and permeability were constructed for each unit (Figure 4.7). Though each cross plot is somewhat similar to the global cross plot in Figure 4.6, (i.e. as grain size increases the range of associated permeabilities increase) there are fundamental differences, which otherwise would not have been recognized without stratigraphically segmenting the data.

Ranges in permeability for sandstones with equal maximum grain size differ between units, as do average permeabilities (Table 4.2). The largest range of permeabilities and highest average permeabilities for sandstones with equal grain sizes occur in the middle unit; followed by the upper unit then the lower unit. Ranges in permeability also increase with grain size at different rates. The fastest rate corresponds to the middle unit, followed by the upper unit, and then the lower unit (Figure 4.7). For both the lower and middle unit, permeability stops increasing beyond a certain grain size.

Facies	Depth(m)	Unit	Average Sorting	Term used according to Folk and Ward (1957)
2	2942.22	Upper	0.37753	Well Sorted
3	2962.11	Upper	0.34730	Very well sorted
3	2984.02	Middle	0.37511	Well Sorted
1	2997.14	Middle	0.38258	Well Sorted
1	3004.04	Middle	0.36333	Well Sorted
4	3021.69	Lower	0.40468	Well Sorted
3	3033.33	Lower	0.41032	Well Sorted

Table 4.1 Sorting values from the seven analyzed thin-sections. The sorting values were obtained using the procedures outlined in chapter 2. Note that only one analyzed sample (thin-section) is very well sorted and the rest are well sorted according to the terms as per by Folk and Ward (1957).

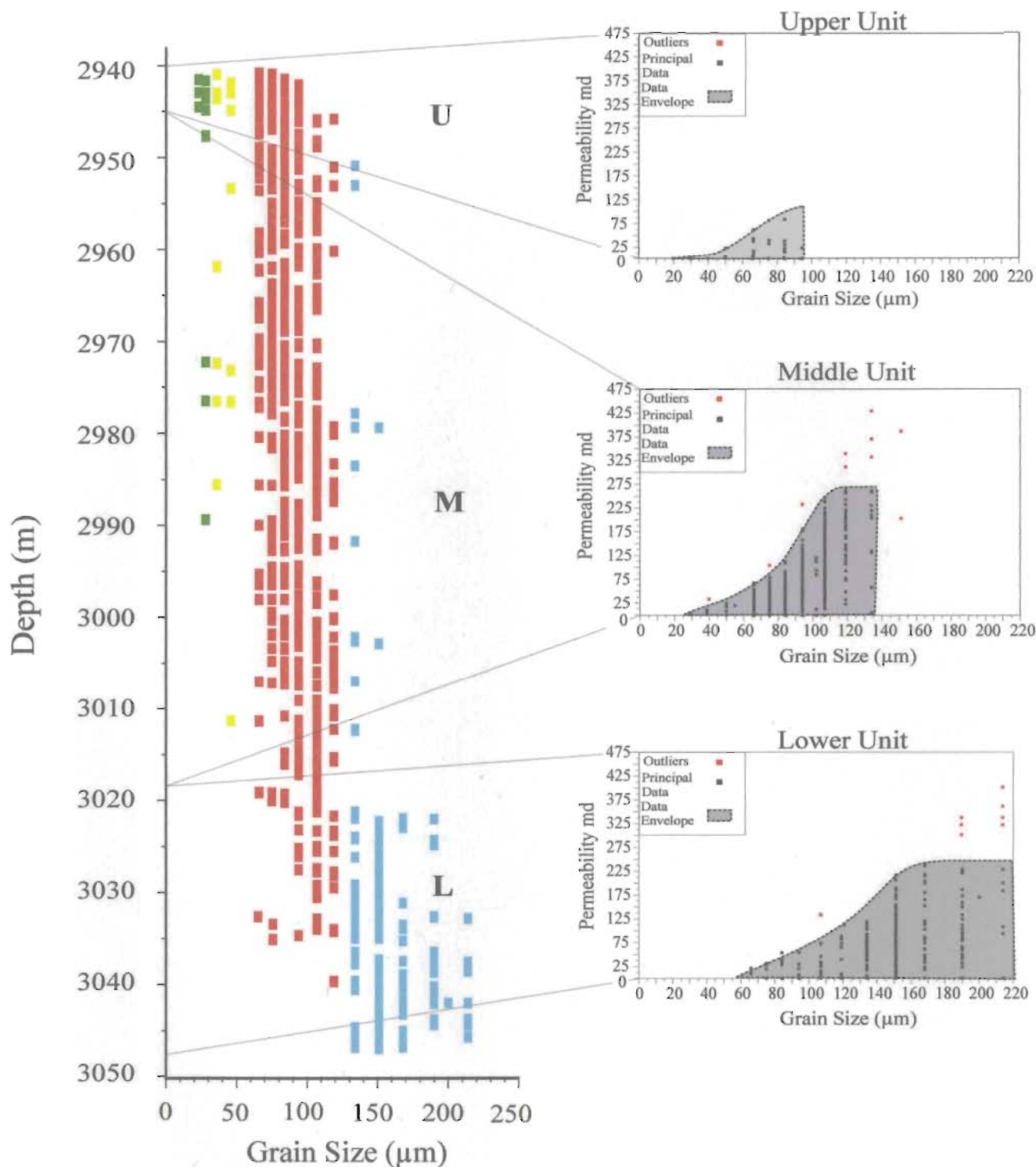


Fig.4.7. Grain Size ( $\mu\text{m}$ ) vs. Permeability mD cross plots for the lower (L), middle (M), and upper (U) units of the White Rose A-17 core.. Note the different ranges of permeability for grains of the same size between units as well as the rate at which permeability increases with increasing grain size between the units.

	Upper Unit			Middle Unit			Lower Unit		
Grain size $\mu\text{m}$	K Min mD	K Max mD	K Avg mD	K Min mD	K Max mD	K Avg mD	K Min mD	K Max mD	K Avg mD
38	0.001	0.001	0.001	3	20	11.5			
84	16	40	34	3.5	113	56	0.05	50.5	32
94	0.003	108	33	0.6	245	88	8	55	23
107				1.2	248	125	1.0	78	47

Table 4.2. Examples used to demonstrate the broad range of permeabilities and different average permeabilities for sandstones of the same grain size between the different units. Empty cells imply that there is no data.

In the lower unit this is 168 microns; in the middle unit this is 119 microns. The corresponding maximum permeabilities are 250 mD and 275 mD respectively. From these observations, it is clear that grain size is not the only factor controlling permeability in the White Rose A-17 core; therefore, other factors must be involved.

The most probable explanation for the range of permeabilities between units is the amount of cement. Sandstones with low amounts of cement normally have higher permeabilities (for any given grain size) than sandstones with abundant cement. For each of the three units, larger ranges of permeability imply higher maximum permeabilities. This is because minimum permeabilities for all grain sizes are essentially zero; therefore, the maximum value determines the range. Since all grain sizes in the middle unit are associated with higher maximum permeabilities compared with the upper and lower units it is likely that, on average, sandstones in the middle contain less cement. Conversely, because the lower and upper units have both lower maximum and average permeabilities than the middle unit (Table 4.2), they likely contain more cement.

The influence of sandstone grain-size sorting on permeability is (if at all) interpreted to be minor for and between each of the three units. These is because sorting values are very similar and, with the exception of one sample, are all classified as well sorted according the terminology of Folk and Ward (1957).

The rate at which permeability ranges increase with increasing grain size for and between each unit cannot be explained based on the data collected; therefore, it is beyond the scope of this thesis and additional work is required.

#### 4.3.3.3 For Small-Scale Intervals

The previous two sub-sections have presented permeability and grain-size data for the entire cored interval and for the lower, middle, and upper units. At these scales, it is clear that: 1) the relationship between grain size and permeability is not linear, 2) this relationship is best defined by a data envelope that defines the maximum permeability for a given grain-size range, 3) the maximum range in permeability is generally associated with sandstones of 119 to 134  $\mu\text{m}$  grain size, 4) ranges in permeability are different for sandstones of the same grain size, and 5) these ranges differ according to depth.

The intention of this sub-section is to investigate four small-scale (1-5m) intervals where grain size and permeability trends appear concordant. Investigation at smaller scales is important because at larger scales (as discussed in the above text) the correlation between grain size and permeability is limited. The selection of smaller intervals was done without adopting statistically-based sampling methods; therefore, they are somewhat subjective. However, covariation between grain size and permeability is rare, and in the cored interval only four somewhat convincing examples were noted (Figure 4.8). Comparisons of grain size and permeability at 10 m intervals can be made by examining the logs in Appendix B.

The relationship between grain size and permeability for the small-scale intervals is different from the relationships that characterize the entire cored interval and the three units. Firstly, grain size and permeability appear to track one another closely when plotted side by side (Figure 4.8). When grain size increases permeability generally increases, and when grain-size decreases permeability generally decreases. Secondly,

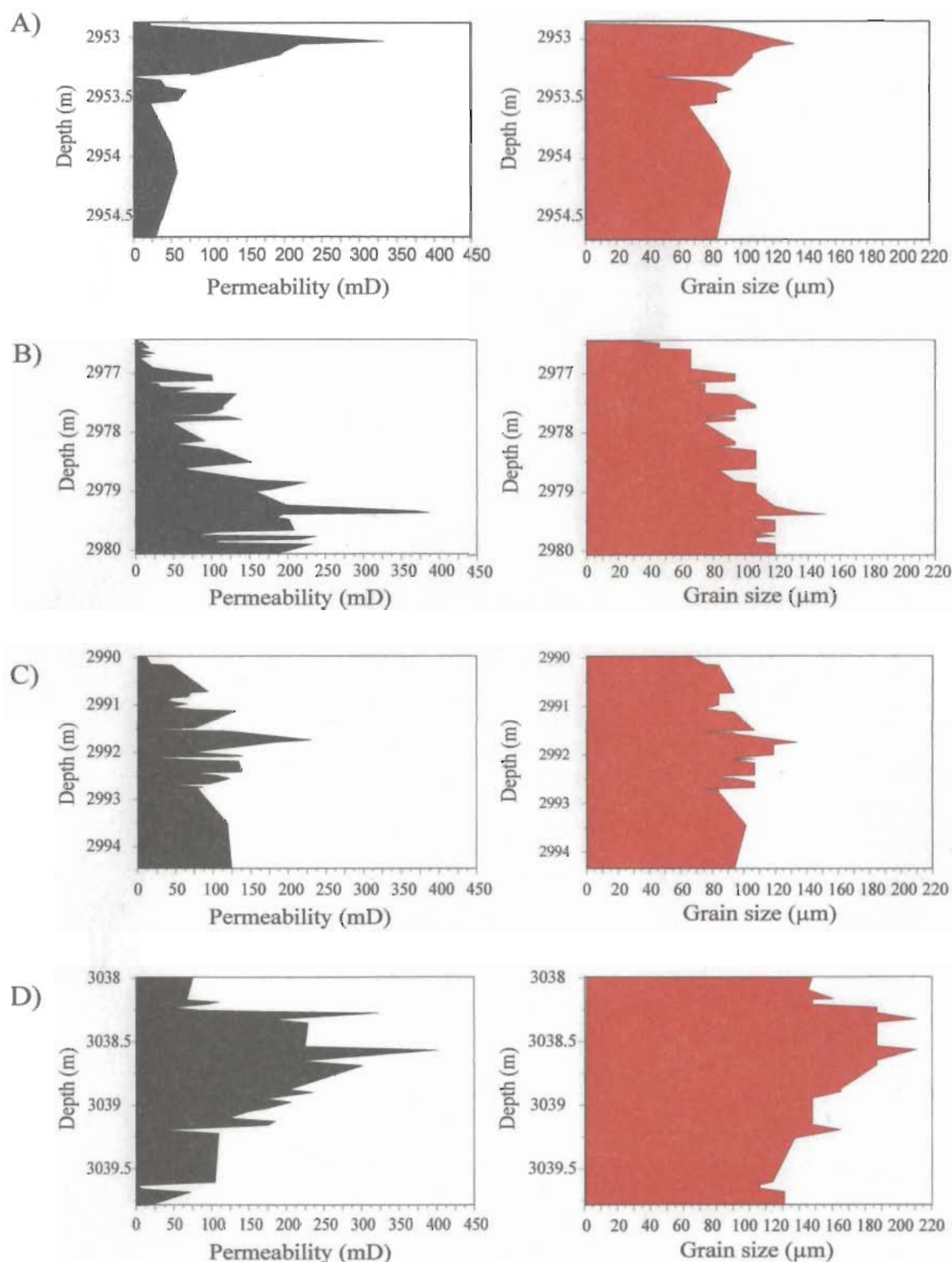


Fig.4.8. Selected intervals to demonstrate the apparent close relationship between grain size (red fill) and permeability (black fill). Vertical permeability profiles are on the left, and vertical grain-size profiles are on the right. Note that vertical scales are not the same amongst examples. Depth ranges for each example are: A) 2952.85-2954.70 m, B) 2976.755-2980 m, C) 2990-2994.40 m, D) 3038-3039.80 m.

increases in grain-size do not necessarily correspond with increasing ranges of permeability (Figure 4.9, left diagrams). Instead, the relationship between grain-size and permeability can be closely approximated by a best-fit line in these small-scales intervals (though perhaps not for Figure 4.9 D). However, dependent upon the scale and stratigraphic position of examination (refer to Fig.4.8) the strength of the relationship between grain size and permeability between the small-scale intervals differ. This is because best-fit lines to the data have different correlation coefficients. This might indicate that the degree of cementation is different between these small-scale intervals.

Though the relationship(s) between grain size and permeability seem quite different at smaller scales, there is a fundamental similarity between these and the larger data sets; that is, there still exists a range (though smaller) of permeabilities associated with most grain sizes (Figure 4.9). This implies that: 1) maximum grain size cannot explain all of the variation in permeability regardless of the vertical scale at which they are compared, 2) grain size might explain more of the variation in permeability if it is measured at a more refined scale, and 3) there are other factors, such as compaction, cementation, and facies type, that in combination with grain size influence and/or control permeability. These outstanding issues could likely be resolved by thin section analyses. Again, sandstone grain size sorting is thought to have little influence on the permeability values in the A-17 core, as sorting values are essentially the same (see Table 4.1).



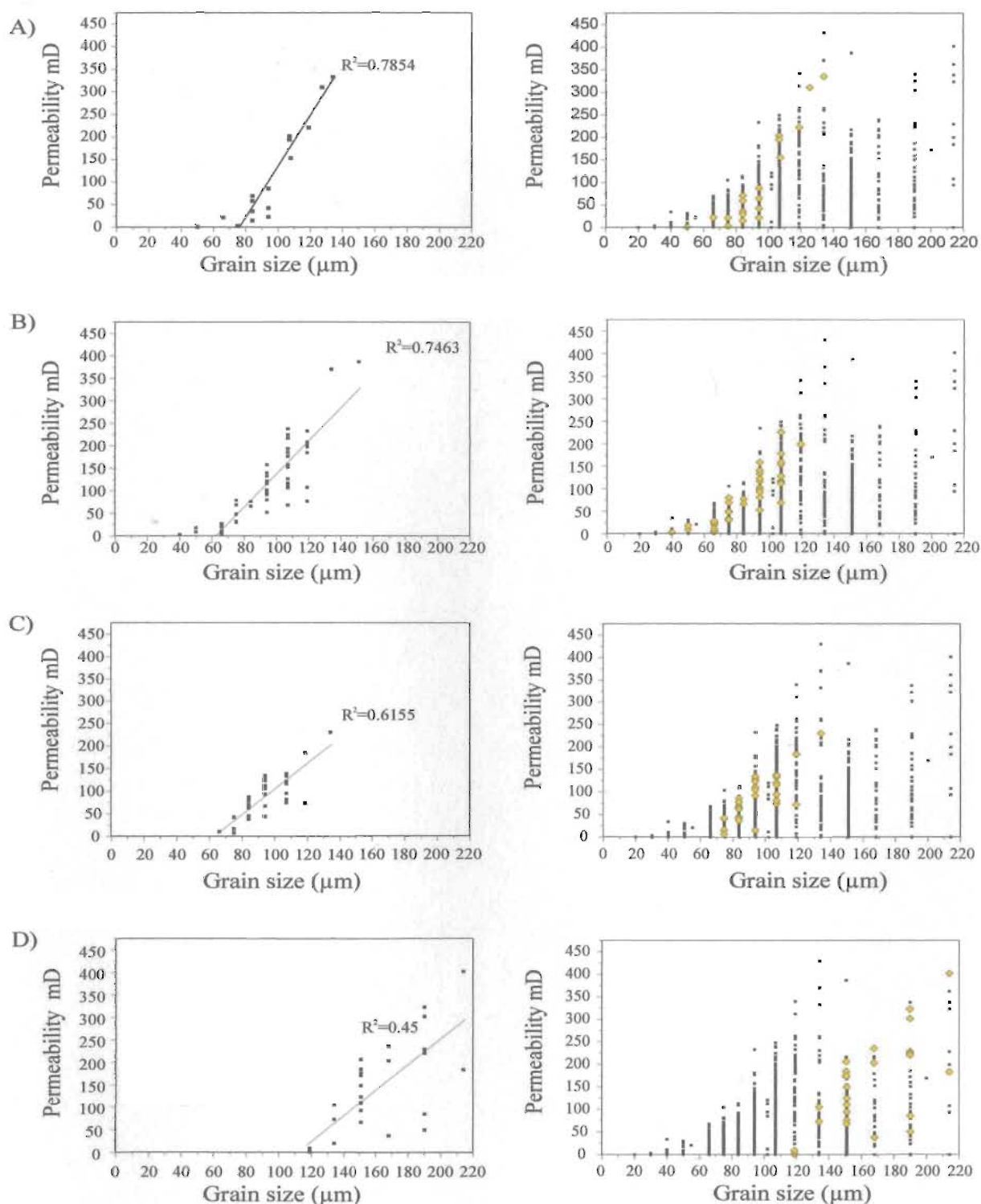


Fig.4.9. Grain size ( $\mu\text{m}$ ) vs. Permeability mD cross plots for the four small-scale intervals selected to demonstrate the apparent close relationship between grain size and permeability. Graphs on the left display data points for the selected intervals, while graphs on right display all of the 1176 data points (the yellow diamonds being those data points from the selected intervals). Note the different slopes and correlation coefficients between intervals.

#### **4.4 Parallel and Unrelated Changes in Both Permeability and Grain size Across Contacts and Gradational Transitions**

The intent of this section is to demonstrate and comment briefly on the changes in both permeability and grain size across most of the major contacts and boundaries in the White Rose A-17 core. Permeability and grain-size measurements were collected below and above each contact; therefore, changes in these variables across contacts can be evaluated. To the knowledge of this author, an analysis of this type has never been undertaken for consolidated sediments.

Upward changes in grain size or permeability across contacts can be positive, negative, or essentially zero (i.e. no real change). There are therefore nine possible upward changes in the pair (grain size, permeability): (+, +), (+, 0), (+, -), (0, +), (0, 0), (0, -), (-, +), (-, 0), and (-, -). Three of these are called “parallel changes” [(+, +), (0, 0), (-, -)], whereas the others correspond to a change in one variable that is not reflected in a corresponding predictable change in the other. These are called “unrelated” changes.

Because of the numerous contact subtypes (refer to Table 2.2), changes in permeability and grain size across them, as well as comparisons between them (the subtypes) might be difficult to establish; therefore, all subtypes are grouped under each major contact type. As well, because changes in grain size almost certainly do not influence permeability across cementation contacts (i.e. from “less cemented” to pervasively cemented intervals) they are ignored.

It is not the intent of this section to investigate or explain all of the positive, negative, as well as the highly variable combinations of changes (parallel and unrelated)

in both permeability and grain size across each contact; this would be extremely difficult. Therefore, only general relationships are listed and only a few inferences are made.

Across erosive and abrupt contacts and gradational transitions, the following generalities with respect to permeability and grain size can be made.

- 1) A single, easily defined pattern or rule-of-thumb to predict changes in either permeability or grain size across any of the contacts and/or boundaries is not recognized (Figures 4.10, A, B, and C).
- 2) Changes in permeability (both positive and negative) need not be accompanied by parallel changes in grain size, nor are changes in grain size (both positive and negative) typically accompanied by parallel changes in permeability (Figures 4.10, A, B, and C).
- 3) The magnitude (amount) and direction of change (i.e. positive, negative, or any combination thereof) for both permeability and grain size are highly variable across the range of recognized contacts and boundaries (Figures 4.10 A, B, and C). The largest amount of change in permeability occurs across erosive contacts, followed by abrupt contacts and then gradational transitions (Figures 4.10, A, B, and C).
- 4) In the absence of simultaneous changes in grain size (i.e., when  $\Delta$  grain size = 0), upward changes in permeability across erosive contacts are mostly negative. For abrupt contacts these changes are somewhat more positive than negative, and for gradational transitions these changes are mostly positive (Figures 4.10, A, B, and C).

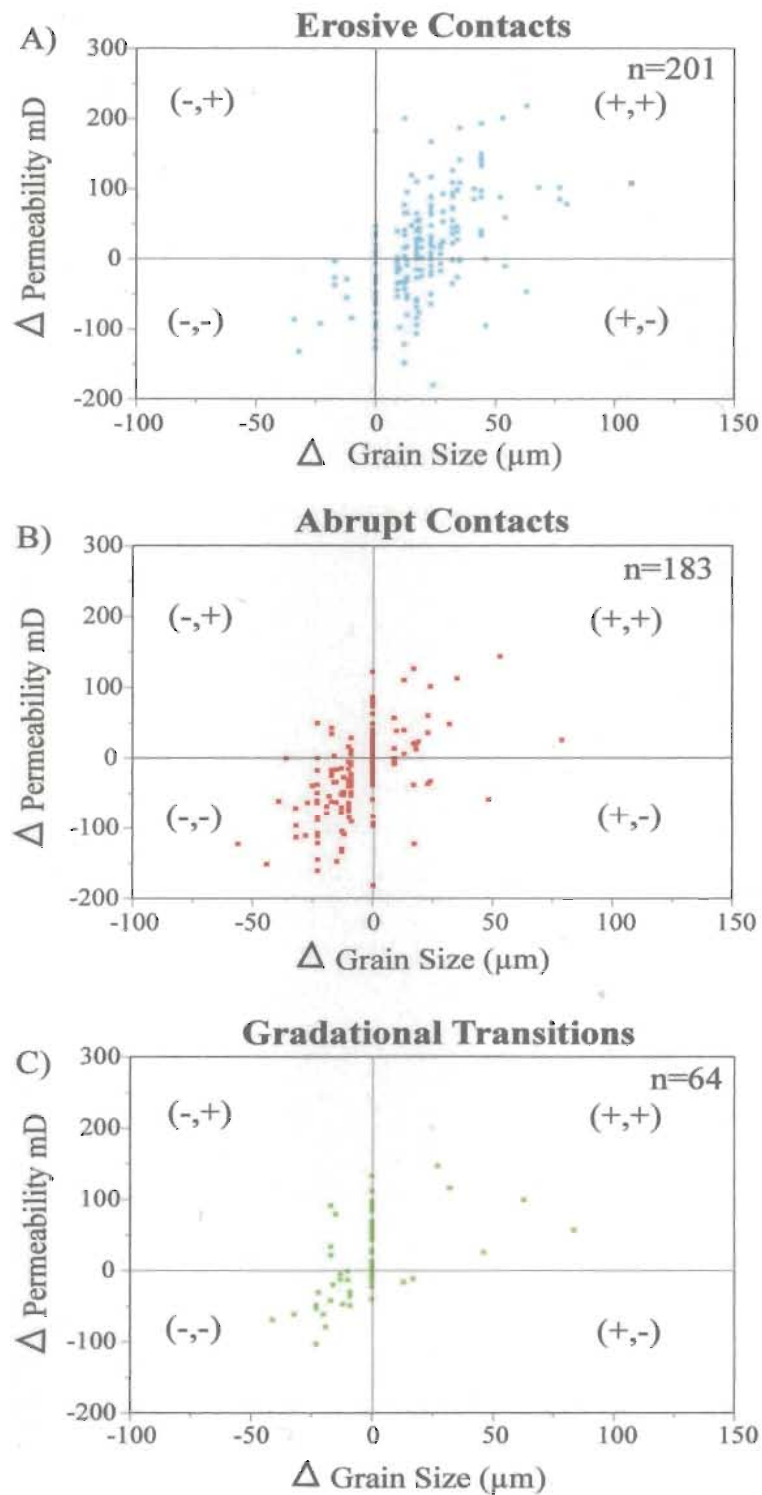


Fig. 4.10. Plots of change in Grain size ( $\mu\text{m}$ ) vs. change in Permeability mD across erosive and abrupt contacts and gradational boundaries.  $\Delta$  = "change in". See text for details.

- 5) Across each type of contact and gradational transition, changes in grain size (both positive and negative) are typically accompanied by a wide range of changes in permeability (Figures 4.10, A, B, and C).
- 6) Across erosive contacts, changes in grain size are mostly positive; they are rarely negative. Associated changes in permeability are both positive and negative, though with increasingly positive changes in grain size, changes in permeability tend to be more positive (Figure 4.10 A).
- 7) Across abrupt contacts and gradational transitions, most changes in grain size are negative, as are changes in permeability. For abrupt contacts, there are a few cases where positive increases in grain size are accompanied by positive increases in permeability (Figures 4.10, B and C).
- 8) Across abrupt contacts and gradational transitions, some decreases in grain size are accompanied by increases in permeability; this does not occur across erosive contacts (Figures 4.10, B and C).

From the above list and from Figures 4.10 A, 4.10 B, and 4.10 C, it is clear that across contacts and/or boundaries, the amount of change in both permeability and grain size is highly variable and that changes in permeability and grain size do not strongly correlate with one another. Increases in grain size do not always imply increases in permeability or vice-versa. As well, a particular amount of change in maximum grain size across a contact and/or boundary does not imply an equivalent degree of change in permeability, whether positive and negative.

The variety of changes (parallel and unrelated) in both permeability and grain size across erosive and abrupt contacts and gradational transitions is likely the result of a number of factors. For example, the wide range of increases in permeability which accompany each increase in grain size across erosive contacts might be the result of dissimilar amounts of cement, variable amounts of bioclastic material and/or authigenic siderite, or the juxtaposition of different facies below and above these contacts. The wide range of decreases in permeability accompanied by increases in grain size across erosive contacts might occur for similar reasons. The large degree of scatter in permeability across erosive contacts without accompanying changes in grain size is further evidence that grain size and permeability are not strongly correlated with one another.

The abundance of positive increases in grain size across erosive contacts also supports the notion that erosive contacts demarcate bed boundaries. This is because, in Chapter 3, it was determined that beds in the White Rose A-17 core are almost always coarser at their base and finer at their top. The few decreases in grain size might mean that depositional events were less vigorous or only finer material was available.

Across abrupt contacts and gradational transitions, changes in permeability, which cannot be explained by changes in grain size, might also be the result of variable amounts of cement, bioclastic material and authigenic siderite, or the juxtaposition of different or similar facies below and above these “surfaces”. The fact that there are a variety of changes in permeability (both positive and negative) for each change in grain size across these contacts and boundaries further supports the notion that permeability and grain size are not strongly correlated with one another. Because grain size either decreases or does

not change at all across most abrupt contacts and gradational transitions, it is fair to conclude that such surfaces indeed do represent internal surfaces and not bed boundaries. This is because: 1) bed boundaries are most often demarcated by an increase in grain size and, 2) beds are ungraded or normally graded; therefore, within beds, decreases or no changes in grain size are expected until the next overlying bed boundary is reached.

Since a large number of the changes in permeability across the various contacts and boundaries cannot be explained by grain size alone, and because the degree to which other factors such as cementation affect these changes is not known, further analysis is required.

#### **4.5 Relationships between Grain Size, Permeability, and Facies**

The purpose of this section is to: 1) examine and discuss the grain-size versus permeability relationships for the nine facies recognized in the core, 2) examine the permeability distributions for each facies and, 3) provide geological explanations for some of the findings. Similar to the last section, data are discussed separately for the lower and middle units. Because only a small amount of data (permeability and grain-size measurements) comes from the upper unit, and because it consists mostly of bioturbated and pervasively calcite-cemented facies, it is not considered in depth. It is worth noting that mostly qualitative inferences about the relationship(s) between permeability and facies are made. This is because sample sizes and permeability variances from facies to facies are quite different; therefore, statistical tests were not applied.

Most investigations regarding the relationship between depositional facies and permeability have been conducted on either unconsolidated sands or outcrops. The examination of permeability and facies in this thesis is considerably different from previous (published) studies for the following reasons: 1) this investigation involves core data, 2) this study has a large number of grain-size measurements accompanying each permeability measurement which can be related to facies, 3) the range of grain sizes in each facies is limited, and 4) the depositional environment is restricted to a shallow-marine, high-energy, storm-influenced middle shoreface setting.

#### **4.5.1 Grain-size Versus Permeability Relationships for Facies in the White Rose A-17 Core**

Most facies in the White Rose A-17 core have similar grain-size versus permeability relationships (Figure 4.11). That is, ranges in permeability generally increase with increasing grain size, and above 107-119  $\mu\text{m}$  grain size, maximum permeabilities cease to climb. This is similar to the global data set (see Figure 4.6), and is particularly true for facies 3. However, for facies 8 and facies 9, which contain abundant shelly material and moderate to abundant amounts of bioturbation respectively, this is not the case. In each of these facies, ranges in permeability do not increase systematically with increasing grain size. For facies 1, 2, 3, 4, and 7, increasing ranges of permeability are generally well established for sandstones  $\leq 107 \mu\text{m}$  grain size (Figure 4.11); however, for facies 1, this trend is well pronounced for sandstones  $\leq 119 \mu\text{m}$  grain size. In fact, very fine-grained sandstones in intervals of facies 1 correspond with most of the highest



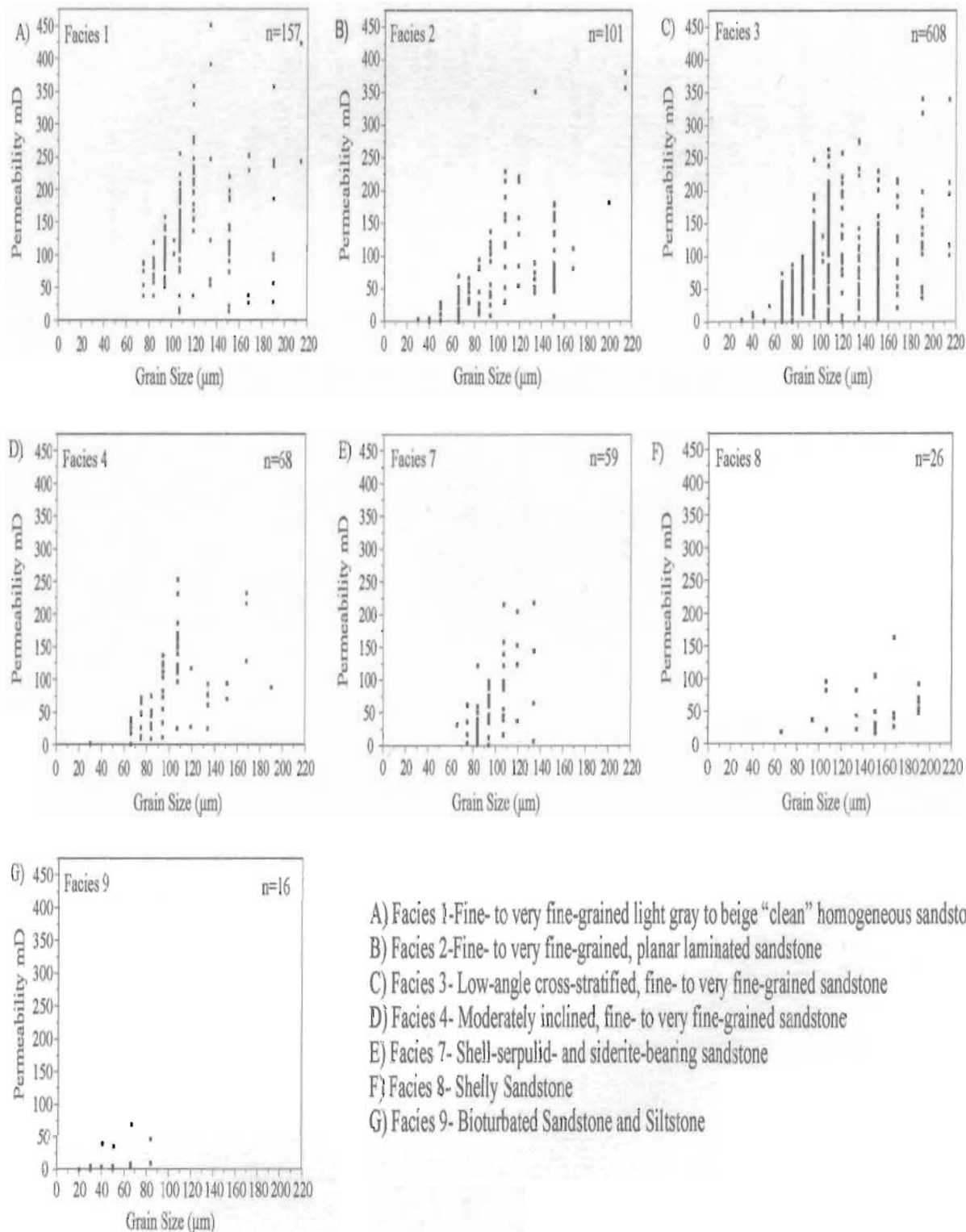


Fig 4.11. Grain ( $\mu\text{m}$ ) size vs. Permeability mD cross plots for Facies 1, 2, 3, 4, 7, 8, and 9. Facies 5 and 6 are omitted because they have negligible permeabilities. Note that for Facies 1, 2, 3, 4, and 7, each increase in grain size is generally accompanied by an increase in the range of permeabilities. This is not true for Facies 8 and 9 where the data points are scattered. Note that in a few of these graphs there is a great deal of overlap in the principal data points giving the impression that these data points form lines; this is not so, and is a result of the large number of data points and the size of the character used to represent them..

permeabilities. Conversely, fine-grained sandstones in each facies do not correspond with well-defined increases in permeabilities. In fact, maximum permeabilities in fine-grained intervals remain somewhat constant (facies 1 and facies 7), decrease (facies 3), or are scattered and show no trends at all (facies 2 and facies 4). The exceptions to these generalities are the few outliers.

In each facies, minimum permeabilities in very fine-grained sandstones and coarse to medium-grained siltstones are mostly negligible with the exception of facies 1. In facies 1, minimum permeabilities which correspond to grains of the very fine-grained size class generally increase with increasing grain size (Figure 4.11, graph A). For example, sandstones of 75  $\mu\text{m}$  grain size correspond to a minimum permeability of ~38 mD, sandstones of 94  $\mu\text{m}$  grain size correspond to a minimum permeability of 52 mD, and sandstones of 119  $\mu\text{m}$  grain size correspond to minimum permeabilities mostly >125 mD (Figure 4.11, graph A). Increases in minimum permeabilities occur in facies 2, 3, 4, and 7, but are mostly restricted to sandstones of 100  $\mu\text{m}$  grain size and greater; however, these trends are neither well defined nor do they occur over limited grain-size ranges. For facies 8, minimum permeabilities regardless of grain size are generally no greater than 25 mD, and for facies 9 they are approximately 1 mD.

#### **4.5.2 Grain-size Versus Permeability Relationships for Facies in the Lower and Middle Parts of the White Rose A-17 Core**

Facies 1, 2, 3, 4 and 8 (excluding facies 5 and facies 6) occur in the lower and middle units of the core consist of both very fine- and fine-grained sandstones (Figures 3.18, 3.22, and 3.23). When grain size and permeability data for each facies are separated stratigraphically (Figure 4.12) each increase in grain size in the middle unit is accompanied by an increase in the range of permeabilities; this relationship is well defined for each facies with the exception of facies 8. Minimum permeabilities are similar to those of the entire dataset (refer to Figure 4.6) with the exception is facies 3. Above a grain size of 84  $\mu\text{m}$  minimum permeabilities in facies 3 generally increase with increasing grain size.

For the lower unit, increasing ranges of permeability with increasing grain size are best defined for facies 3. For facies 1 and 2, this relationship is not as well defined, though maximum permeabilities generally increase with increasing grain size; again with some exceptions (Figure 4.12). These relationships are much less clear for facies 4 and 8, as there are few data points and they are scattered. The stratigraphic subdivision of data reveals that, for the lower unit, minimum permeabilities are no different from those observed when all the data are examined (Figure 4.11).

Maximum permeabilities for sandstones of the same grain size are different between the middle and lower units (Figure 4.12). This is most apparent in facies 3. For example, the maximum permeability for sandstones of 84  $\mu\text{m}$  grain size in the middle unit is 105 mD and only 60 mD in the lower unit. Similarly, the maximum permeability

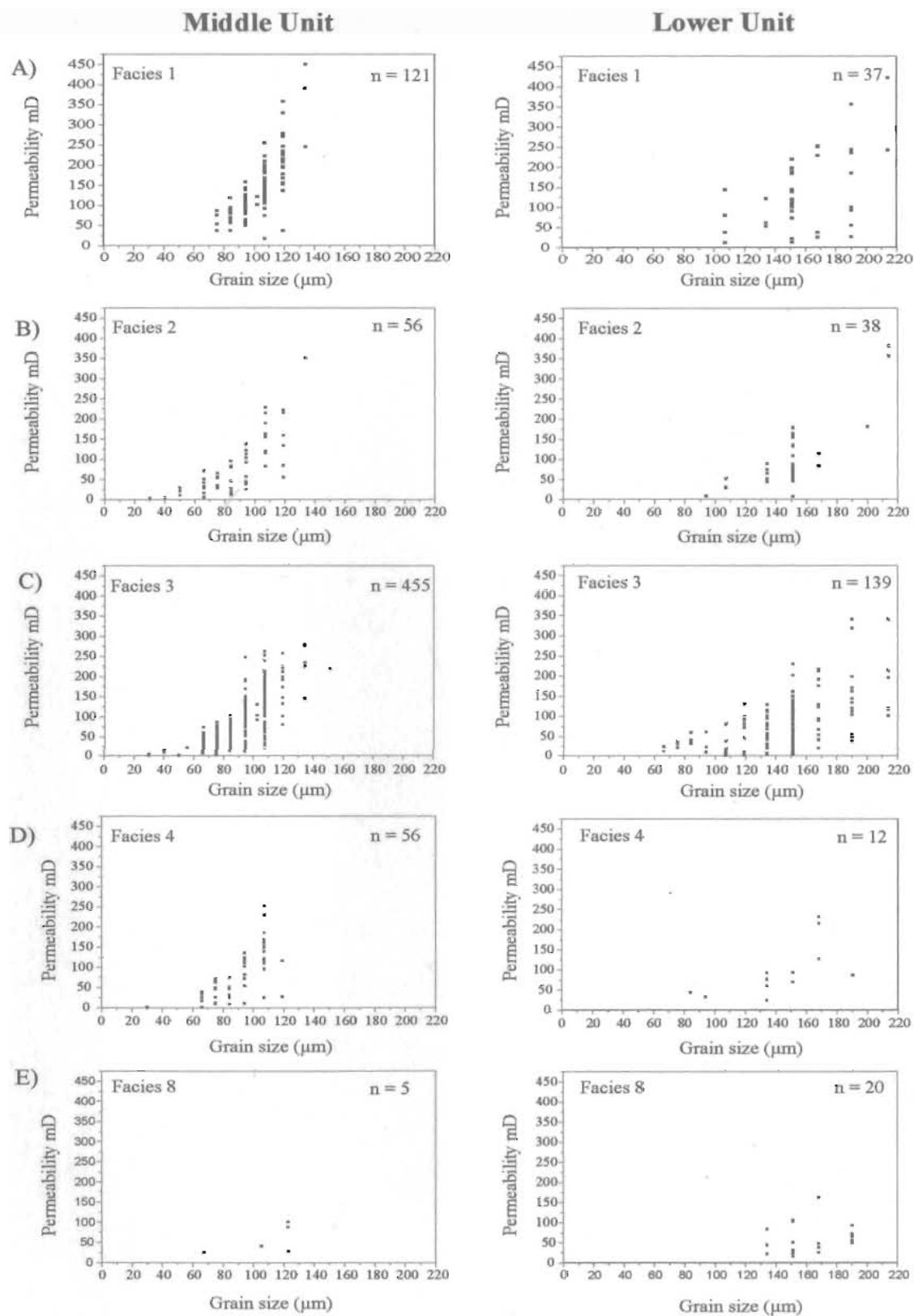


Fig.4.12. In descending order, Grain size ( $\mu\text{m}$ ) vs. Permeability mD cross plots for facies 1,2,3,4, and 8. Cross plots on the left display facies data for the middle unit and cross plots on the right display facies data for the lower unit.

for sandstones of 107  $\mu\text{m}$  grain size is nearly 275  $\mu\text{m}$  in the middle unit and of only 75 mD in the lower unit. This reinforces the conclusion drawn in the previous section; that is, permeabilities for sandstones of the same grain size are less in the lower unit than in the middle unit. As well, it would appear that facies have little influence on this relationship. The lower permeability values, in the lower unit, might be attributed to more extensive cementation or different cementation patterns.

#### **4.5.3 Distribution of Permeabilities for Each Facies**

High permeabilities (those greater than 300 mD) occur in facies 1, 2, and 3 with the highest values belonging to facies 1 (Figure 4.11, graph A). Facies 1 also has the largest number of permeabilities greater than 200 mD. This is followed by facies 3 and 2 (Figure 4.11, graphs C and B). Facies 4 and 7 have only a few values higher than 200 mD while facies 8 and 9 have none (Figure 4.11, graphs F and G). Facies 1 has the largest percentage of values in excess of 200 mD, followed in order of decreasing percentage by facies 4, 3, 2, 7, 8, and 9 (Figure 4.11, all graphs). Most facies have a number of permeabilities equal to or in excess of 100 mD though this is quite uncommon for facies 8 and is not true for facies 9 (Figures 4.11, graphs F and G). Facies 3 has the largest number of values in excess of 100 mD. This is followed by facies 1, 2, 4, 7, 8 and 9. Facies 1 also has the highest percentage of permeabilities in excess of 100 mD. This is followed by facies 4, 3, 2, 7, 8, and then 9.

Minimum permeabilities are generally the highest and exhibit the most pronounced trend in facies 1 for very fine-grained sandstones (Figure 4.11, graph A). For

fine-grained sandstones, minimum permeabilities are as high as 200 mD but this is rare; they are generally less than 20 mD. For facies 2, minimum permeabilities are very low for both siltstones (<3-5 mD) and most very fine-grained sandstones. For sandstones of 107 to 134  $\mu\text{m}$  grain size, minimum permeabilities range from 25-50 mD, decrease to 0.01 mD at 151  $\mu\text{m}$ , then increase rapidly to a maximum of 340 mD at 214  $\mu\text{m}$  grain size (Figure 4.11, graph B). Minimum permeabilities in facies 3 are negligible for most grain sizes, but increase from ~20 mD to a maximum of ~100 mD for the coarsest fine-grained sandstones (Figure 4.11, graph C). For facies 4 minimum permeabilities are very low (<10 mD) for sandstones <100  $\mu\text{m}$  grain size, increase and remain constant at ~20-25 mD for sandstones of 107 to 134  $\mu\text{m}$  grain size, and then increase linearly to a maximum of ~115 mD at 168  $\mu\text{m}$  grain size (Figure 4.11, graph D). Minimum permeabilities for facies 7 are generally very low (<10 mD); however, values as high as 30 mD do exist (Figure 4.11, graph E). Minimum permeabilities for facies 8 are remarkably constant at ~15 mD, with minor exceptions (Figure 4.11, graph F). Minimum permeabilities for facies 9 remain constant, and are low (~1 mD) irrespective of grain size (Figure 4.11, graph G).

In the White Rose A-17 core, mean permeabilities for facies 1 and 9 are significantly different from all other facies. Facies 1 has the highest mean permeability, and facies 9 has the lowest (Figure 4.13). Although the range of permeabilities and number of permeability measurements for facies 2, 4, 7, and 8 and facies 2, 3, and 4 are somewhat different, there is no reason to suggest that their mean permeabilities are significantly different from one another because 95% confidence intervals about their means overlap. This signifies that there is more than 1 chance in 20 that the facies share

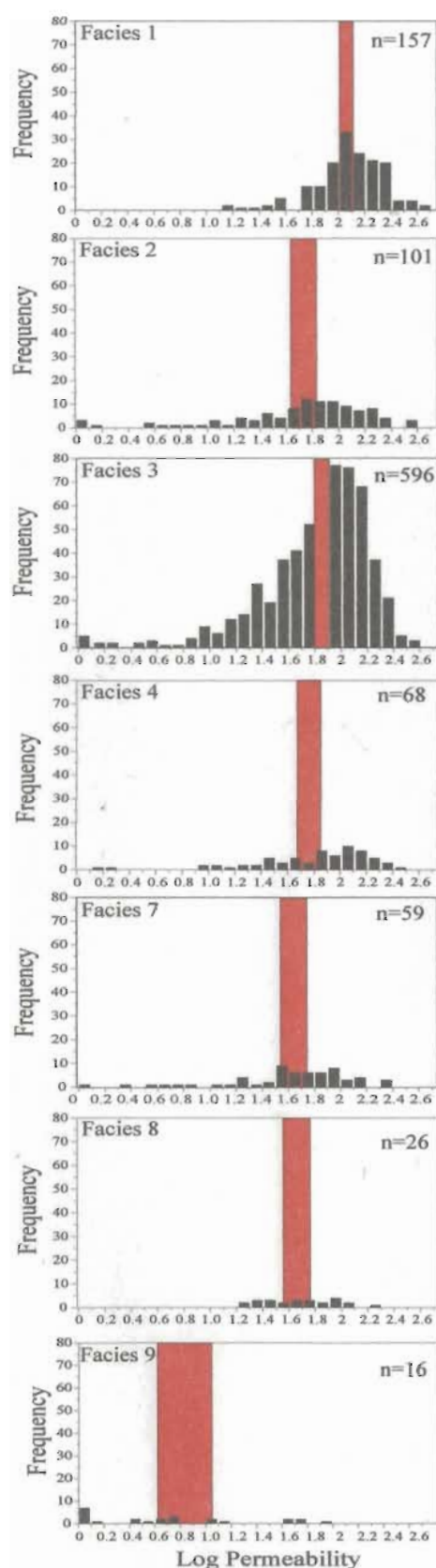


Fig.4.13. Permeability frequency distributions for Facies 1, 2, 3, 4, 7, 8, and 9. Facies 5 and 6 are excluded because their permeabilities are negligible. The red bands on each figure represent the 95% confidence interval about the mean. This implies that there is a 95% chance that the mean value lies within the red band (confidence interval), and a 1 in 20 chance that it does not. The mean permeabilities for facies 1 and 9 are significantly different than for all other facies. Facies 1 has the highest mean permeabilities, and facies 9 has the lowest. The mean permeability for facies 2, 4, 7, and 8 do not significantly differ from another because there is overlap of their confidence intervals. This is also true for facies 2, 3, and 4. However, facies 3 has overlapping confidence intervals with two groups of facies, and only misses overlapping with facies 7 and 8 by a small amount. Because the individual distributions are not exactly log-normal, this marginal lack of overlap is not taken as strong enough evidence to separate facies 3 from facies 7 and facies 8.

the same mean value of permeability. A probability of less than 1 in 20 is generally needed to reject the hypothesis that the means are the same.

Discrimination between mean permeabilities was determined by calculating the 95% confidence intervals about the means for facies 1, 2, 3, 4, 7, 8 and 9 (Figure 4.13). This was not done for facies 5 and facies 6 because their permeabilities are insignificant. A 95% confidence interval about the mean implies that there is 95% chance that the mean falls within the determined range (confidence interval), and a 5% chance that it does not. This is true for normally distributed populations/samples and therefore was applied to these data because the logarithms of permeabilities for facies with  $n > 25$  are approximately normally distributed (Figure 4.13). Because there is overlap between confidence intervals amongst facies 2, 3, and 4 it is concluded that the mean permeabilities for those facies are not significantly different. The same is true for facies 2, 4, 7, and 8. However, facies 3 has overlapping confidence intervals with two groups of facies, and only misses overlapping with facies 7 and 8 by a small amount. Because the individual distributions are not exactly log-normal, this marginal lack of overlap is not taken as strong enough evidence to separate facies 3 from facies 7 and 8. Therefore, only facies 1 and 9 are concluded to have significantly different mean permeabilities than the rest of the facies.

Caution is advised when making inferences using the distribution of the data from the confidence limits about the mean. Overlapping confidence intervals can arise even if other population parameters are clearly different. This is well exemplified for facies 8



where the confidence interval about the mean is similar to most other facies; however, from Figure 4.11 it is very clear that the range of its permeabilities are much less.

#### **4.5.4 Interpretation of the Permeability Data for Each Facies**

The purpose of this subsection is to discuss and provide some geological explanations for the permeability distributions in each facies. Because of the large range of permeabilities that occur in most facies, interpretation of all the data is beyond the scope of this thesis. As a result, mostly high, low, and average values are discussed. Additionally, because bioclasts, authigenic siderite, and serpulid worm tubes are best represented in facies 7, their affect on permeability is described under that facies. These three components are dispersed in varying abundance throughout the core, though not to the same extent as in facies 7. Thorough representations of their abundance, stratigraphic positions, and relation to facies, grain size, and permeability can be found in Appendix B. However, a thorough examination of their influence on permeability other than in facies 7 is not covered in the following text.

In the White Rose A-17 core, facies 1 is the most permeable. It has the highest mean permeability, the highest permeability values, the highest percentage of permeabilities above 100 mD and 200 mD, and the largest minimum permeabilities (specifically for very fine-grained sandstones). There might be a number of reasons for this; however, based upon the available data it appears that facies 1 absence of stratification is the most probable.

Laminations are typically distinguished by silty material, bioclastic debris, and heavy minerals. These features may inhibit fluid flow across laminae. This is because of 1) decreased sorting and 2) packing differences. Both of these factors likely increase the tortuosity of fluid movement and as a result, reduce permeability. The higher permeability of facies 1 might indicate that there are packing or pore-to-pore-throat connectivity differences associated with homogeneous sandstones which are not found in the other facies. Petrographic and/or image analysis would be required to investigate and prove such a hypothesis. Table 4.1 would suggest that the higher permeabilities associated with facies 1 is not a function of sorting as values amongst the facies are very similar. However, that being said, it is possible that additional thin-section analysis could prove otherwise.

Although facies 1 is generally more permeable than other facies, it still contains a wide range of permeabilities. Because this cannot be explained by differences in grain size and sorting alone, other factors must also be significant. A probable explanation for the range of permeabilities would be the degree, type, and spatial distribution of cement. These characteristics likely vary throughout the cored interval; therefore, dependent upon the location of each probe permeameter measurement, different values will arise.

The stratified units, which include facies 2, 3, and 4, possess similar permeability characteristics since their mean permeabilities are similar and cross plots of grain size and permeability for each of these facies are comparable (refer to Figures 4.13 and 4.11). These similarities might be the result of their analogous sedimentological characteristics. Each of these facies are moderately to well-sorted, they are stratified, and possess

variable amounts of carbonaceous and silty detritus, bioclastic material, serpulid worm tube fragments, along with authigenic siderite.

Differences in permeability distributions between the stratified facies are not easily explained since only a limited number of variables were examined. Nevertheless, reasons for some of the differences can be inferred. As an example, the large number of permeabilities  $\geq 150$  mD in facies 3 (Figure 4.11) might be a function of the abundance of this facies in the core. Facies 3 accounts for approximately 53% of the cored interval; therefore, the probability of obtaining a larger number of values  $\geq 150$  mD is higher for facies 3 than for any other facies. Conversely, these higher values might be the result of different cementation patterns. In general, these high values correspond with zones that do not bioclastic material or authigenic siderite cement (see Appendix B). The influence that sandstone grain size sorting has on these permeabilities is interpreted to be minimal as sorting values (see Table 4.1) for each of the stratified facies are very similar. The affect that the minor differences in sorting values has on permeability is difficult, if not impossible, to interpret.

A few of the low permeabilities in facies 4 correspond well with those intervals where stratification is highlighted by abundant amounts of carbonaceous and silty material (Figure 4.14). These intervals constitute facies 4 (Type 2) (Chapter 3; Plate 3.15). Presumably, the carbonaceous material has a similar affect on permeability as does silt laminae; it reduces vertical permeability. This theory was not tested using thin-section

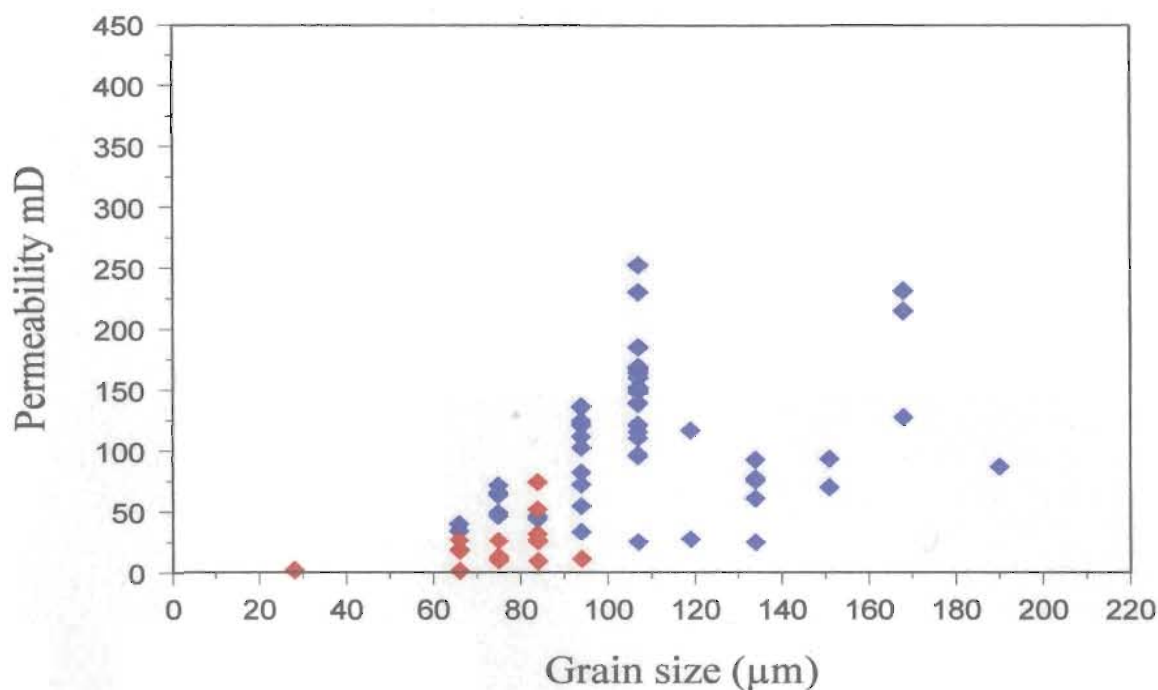


Fig.4.14. Grain Size ( $\mu\text{m}$ ) vs. Permeability mD cross plot for Facies 4 (Type 1) and (Type 2). The blue diamonds correspond to data from Facies 4 Type 1 and the red diamonds correspond to data from Facies 4 Type 2. It is evident from the separation of data points in this cross plot that most of the low permeabilities occur where there is abundant carbonaceous material (red-diamonds) and high permeabilities occur where there is no such material; however, it must be kept in mind that the low permeabilities associated with the carbonaceous material might also reflect the fine grain sizes associated with the carbonaceous material.

analysis as silty sandstone intervals have polymodal grain size distributions. Analyzing such samples is not accounted for in the Folk and Ward (1957) equation. The range of permeabilities associated with intervals that contain carbonaceous material might be a function of its abundance and distribution because these two parameters differ between intervals. The alternative to these statements is that the very-fine grain sizes associated with the carbonaceous material (Figure 4.14) account for these low permeabilities. Differentiation of these two theories would require petrographic (thin section) or image analysis.

The range of permeabilities in each of the stratified facies, which cannot be accounted for by grain size and sorting, is likely the result of variable amounts of cement. It might also be that the small amount of bioclastic material and siderite cement in these facies influence some of these values (refer to Appendix B); however, without further data this is difficult to establish. Confirmation of this would likely require detailed petrographic or image analysis.

The negligible permeabilities associated with facies 5 and facies 6 are attributed to pervasive calcite cementation. The near-zero permeabilities imply that intervals of these facies have almost no ability to transmit fluids (in this case air). Cementation reduces pore-throat size, which means that capillary pressures increase, and, as a result—permeability decreases.

Facies 7, which is characterized by variable amounts of bioclastic debris and authigenic siderite, has an overlapping 95% confidence interval with those for facies 2, 4, 8, and nearly facies 3 (Figure 4.13). Additionally, facies 7 is similar to facies 1, 2, 3, and

4, given that their grain-size versus permeability cross plots are comparable (though permeabilities in facies 7 are somewhat lower) (see Figure 4.11). This would suggest that shells, serpulid worm tubes, and authigenic siderite do not affect permeability much more than if they were rare or not present at all. However, because higher permeabilities in facies 7 are clearly associated with low amounts of shell material and low- to very low permeabilities are associated with abundant shelly material (Figure 4.15) it appears that the amount of shell material does influence permeability (in combination with other factors including serpulid worm tubes and authigenic siderite cement). This result indicates that the range of permeabilities for sandstones of equal grain size between facies 7 and facies 1-4 arise for different reasons; permeabilities in facies 7 are a result of variable amounts and combinations of shell fragments, serpulid worm tubes, authigenic siderite and poor sorting. Conversely, the range of permeabilities in facies 1-4 is most likely the result of variable amounts of cement, and to a lesser degree, bioclastic material and carbonaceous/silty material.

Facies 7 differs from facies 1, 2, 3, and 4 in that permeabilities  $\geq 150$  mD are rare; most of the maximum permeabilities are generally no greater than 100 mD. This lower limit to maximum permeabilities might be the result of poorer sorting compared with other facies due to the bioclastic material (shell and serpulid worm tube fragments). Patches of authigenic siderite also likely limit the attainment of higher permeabilities by infilling pores and blocking pore throats. Again, this would require petrographic analysis.

The near-equal range of permeabilities for each grain size in facies 8 suggests that factors other than grain size are important in controlling permeability (Figure 4.11). The

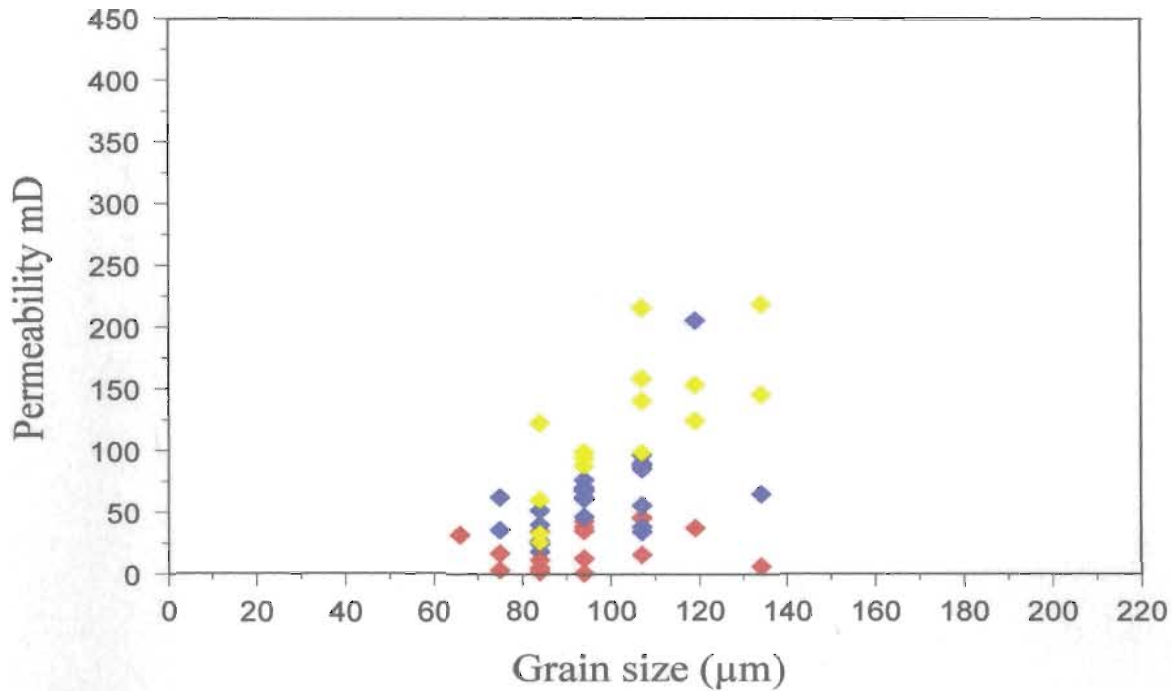


Fig.4.15. Grain size ( $\mu\text{m}$ ) vs. Permeability (mD) cross plot for Facies 7. The differently colored data points (diamonds) represent different amounts of shelly material. For instance, yellow colored diamonds represent low amounts of shelly material (1 on the ordinal scale), blue colored diamonds represent moderate amounts of shelly material (2 on the ordinal scale), and red colored diamonds represent abundant amounts of shelly material (3 on the ordinal scale). Note the somewhat well-defined separation of data points suggesting that the amount of shelly material influences permeability.

absence of high permeabilities (e.g. those over 100 mD) and limited range of permeabilities in facies 8 as compared with facies 1-4 and 7 is either a result of the stratigraphic position of facies 8 in the core (see below) or the abundant shelly material that it contains.

Facies 8 is principally restricted to depths below 3020 m, in the lower unit of the core. Through a number of examples in the above text, it was determined that permeabilities for sandstone of the same grain size in a number of different facies are typically less in the lower unit as compared to the middle unit. This is taken to suggest that (in the absence of additional information) the degree of cementation is greater in the lower unit and as a result, permeabilities are lower. Similar to facies 6, it is also possible that shells in facies 8 acted as both nucleation sites for calcite cement or dissolved and re-precipitated as calcite cement. This might explain the absence of the high permeabilities and limited range of permeabilities in this facies. However, petrographic analysis would be required to investigate and resolve this issue.

In addition to the greater amount of cement presumably associated with facies 8, the tightly packed nature and preferred orientation of the shelly material (Plate 3.19) might be responsible for the generally low permeabilities. The high concentration of shells likely inhibits fluid flow into and around the pores and pore-throat networks by partially blocking them. Some of the permeabilities in facies 8 might be lower than those in facies 7 because of the orientation of the shelly material. Shells in facies 7 are typically randomly orientated whereas those in facies 8 have a preferred sub-horizontal to horizontal orientation. Sub-horizontally to horizontally oriented shell fragments could



affect the way in which fluid travels outward from the tip of the probe permeameter, in a way different to the case of randomly oriented shell fragments. However, experiments would have to be designed to test such an hypothesis.

The very low to low permeabilities associated with facies 9 are most likely the result of the very fine grain sizes and poorer sorting that characterizes this facies. For almost all facies, it has been shown that the finest grain sizes correspond to both low permeabilities and limited permeability ranges. Because facies 9 consists of very fine-grained sandstone and siltstone, it is not surprising that it has very low permeabilities. Poor sorting also likely contributes to these low permeabilities. Burrowing organisms redistribute silt and sand, which would have otherwise existed in separate layers (laminae or beds). They bioturbate sediments causing heterogeneity at varying scales. This mixing causes silt particles to infill pores and block pore throats, which inhibits permeability (Weber, 1982). The higher permeability values in facies 9 correspond to those areas where there is a higher degree of sorting (more uniform grain sizes and less silt), where there are sand-filled burrows, and where there are unburrowed very fine-grained sandstones. The range of permeabilities for each grain size in facies 9 might imply that sorting differs from one probe permeameter measurement position to the next, or that the amount and distribution of cement is variable.

## CHAPTER 5

### CONCLUSIONS, RECOMMENDATIONS, AND IMPLICATIONS

#### 5.1 Introduction

This study was undertaken to address two issues with respect to the White Rose A-17 cored interval and, in general the White Rose field. The first was to test aspects of the depositional model currently in use by industry geologists and the second was to investigate the influence of the sedimentology on reservoir fluid flow. These issues are important for two reasons. First, a principal function of a depositional model is to provide a predictor in new geological situations; therefore, if a more accurate model is formulated it might be used to better predict the distribution and/or geometry of the reservoir facies in other parts of the White Rose field. Secondly, permeability is the single most important factor influencing fluid flow in a reservoir; consequently, if sedimentological characteristics can be related to permeability, prediction of permeability using these characteristics might be possible. Addressing these issues might aid in the future development and/or expansion of this field.

This chapter pulls together the most important conclusions of this study, provides recommendations for future work on White Rose and other cores, and highlights some of the implications of the results of this study to the White Rose oilfield.

## 5.2 Inventory of the Main Conclusions

The following conclusions with regards to the sedimentology of the White Rose A-17 cored interval, the depositional environment represented by the cored interval, and relationships between the sedimentology and permeability can be made.

### 5.2.1 Sedimentology and Depositional Environment

- Grain size in the White Rose A-17 cored interval ranges from a minimum of 23  $\mu\text{m}$  ( $\sim 5.44 \phi$ ) to a maximum of 214  $\mu\text{m}$  ( $\sim 2.22 \phi$ ), with an average grain size of 107  $\mu\text{m}$  ( $\sim 3.22 \phi$ ). These are very fine-grained sandstones.
- Grain-size trends are recognized at different scales: 1) the entire cored interval, 2) the bed-set scale, and 3) the bed and interval scales. At the scale of the entire cored interval, grain size overall fines upward. At the bed-set scale, fining-upward trends are the most common. At the bed and interval scale, static trends then fining-upward trends are most common.
- The cored interval is divisible into three distinct units based upon dominant grain-size class and lithology. The lowermost 20 m consists predominantly of moderately to well sorted fine-grained quartzose sandstone; the middle unit which spans  $\sim 75$  m consists chiefly of very fine-grained sandstones, and the upper unit consists of interbedded/ interlaminated very fine-grained sandstone and siltstone.
- Four principal types of contacts/transitions are recognized in the A-17 cored interval. The most abundant type of contact is erosive. This is followed by abrupt and cementation contacts, then gradational transitions. Erosive contacts represent

bed boundaries; abrupt contacts represent internal surfaces within beds.

Cementation contacts either separate pervasively cemented intervals from more porous sandstone, or separate facies 5 from facies 6, where facies 5 is pervasively calcite-cemented, and facies 6 is similar but contains abundant bioclastic material.

Gradational transitions are uncommon and typically represent a decrease in grain size or the upward reduction of bioclastic debris. Contacts do not appear to be organized vertically nor do they have preferred associations with facies in the core. Facies 3, which constitutes over half of the core by volume, is the exception.

- Based on physical and biogenic sedimentary structures, diagenetic features and shelly components, nine facies are recognized in the A-17 cored interval. Fine- to very fine-grained, low angle cross-stratified sandstone (facies 3, 53.3%) and structureless sandstone (facies 1, 14.7%) are the most abundant facies types, whereas planar laminated (facies 2, 7.0%), moderately inclined cross-stratified (facies 4, 4.6%), pervasively calcite-cemented (facies 5 and 6, combined 15.4%), shell-bearing sandstones (facies 7 and 8, combined 3.7%) and bioturbated, intercalated very fine-grained sandstones and siltstones (facies 9, 1.3%) are less abundant. As with contacts, facies are not well organized stratigraphically. In addition, facies associations are poorly developed, with the exception of facies 5 and facies 6.
- Facies 1 represents deposition from highly concentrated suspension clouds. Facies 2 reflects deposition under either unidirectional or oscillatory upper flow-regime conditions, during the plane-bed stage of flow. Facies 3 is interpreted as

hummocky cross-stratification formed under the combined influence of oscillatory and unidirectional currents. Because of the geometrical similarities and co-occurrence with facies 3, a similar process is interpreted for facies 4, which – due to greater apparent dip angles – likely represents different parts (locations within) hummocky bedforms. Dissolution and re-precipitation of bioclastic components as calcite cement is the most plausible explanation for the cement in facies 5 and 6. Erosion, winnowing, and transport, followed by mainly rapid deposition is interpreted for intervals of facies 7, while erosion, winnowing, and transport followed by deposition under a strong unidirectional current is interpreted for intervals of facies 8. The trace fossils that characterize facies 9 mostly represent specialized feeding/deposit-feeding behavior.

- The White Rose A-17 cored interval represents deposition in a high-energy middle to lower shoreface setting, which experienced frequent and/or intense storm activity. This is based on the abundance of well sorted, very fine-grained quartzose sandstones, repeated fining-upward grain-size trends, a predominance of low-angle, gently curved, convex-up laminations, structureless beds, numerous erosional contacts overlain by transported bioclastic debris, rare mud and siltstone laminae, and limited biogenic structures. However, through time the depositional environment gradually shifted from a more proximal to distal environment, as indicated by a change in lithology and the occurrence of biogenic sedimentary structures which are represented in the upper unit of the core.

### 5.2.2 Sedimentology and its Relation to Permeability

- Over the entire cored interval, permeability measurements are not strongly correlated with grain size. Only in rare cases can linear correlations be established. The relationship between grain size and permeability is best defined by a data envelope that defines the maximum permeability for a given grain-size range. All grain sizes are associated with a range of possible permeabilities; (and) these ranges generally increase with increasing grain size. These observations suggest that grain size (particularly above 134  $\mu\text{m}$ ) is not the only factor controlling permeability and that other factors such as compaction, cementation, and sorting (are also significant).
- For all grain sizes, the middle unit has the largest range of permeabilities and the highest average permeabilities. This is followed by the upper unit, then the lower unit. This is somewhat of a surprise, because the lower unit is the coarsest, with a characteristic size of fine sand. The rate at which permeability increases with increasing grain size is fastest for the middle, followed by the upper and lower units. These observations demonstrate that the middle unit is the most homogeneous with respect to permeability.
- For the middle and lower units, the maximum permeability ceases to increase with increasing grain size beyond a certain size; these sizes are different for each unit. In the middle unit, this limiting size is 119  $\mu\text{m}$ ; in the upper unit it is 134  $\mu\text{m}$ . Different maximum permeabilities associated with these grain sizes, from unit to unit, demonstrates that grain size and permeability are not strongly related

to one another. Other factors such as compaction, cementation, and sorting likely obscure the direct relationship between grain size and permeability that is well documented for unconsolidated sands.

- Changes in grain size and permeability across contacts and boundaries, can be linked (i.e., both parameters increase or decrease), or seemingly unrelated to one another. Changes in permeability across contacts can occur independently of grain size; however, where there is a grain-size change there is typically a change in permeability. Most increases in permeability that are accompanied by increases in grain size occur across erosive contacts. Most permeability decreases accompanied by decreases in grain size occur across abrupt contacts and through gradational intervals.
- The abundance of increases in grain size across erosive contacts provides additional support that erosive contacts demarcate bed boundaries. Conversely, because the grain size either decreases or does not change at all across most abrupt contacts and gradational boundaries, it is reasonable to conclude that such surfaces represent internal surfaces and not bed boundaries.
- The largest permeabilities (those greater than 300 mD) occur in facies 1, 2, and 3 with the highest values in facies 1. Facies 1 also has the largest number of permeabilities greater than 200 mD. This is followed by facies 3 and 2. Facies 4 and 7 have only a few values higher than 200 mD, while facies 8 and 9 have none. Permeabilities equal to or greater than 100 mD in facies 8 are uncommon, and in facies 9 are non-existent.

- Facies 1 and facies 9 have distinctly different mean permeabilities from all other facies in the core. Facies 1 has the highest mean permeability whilst facies 9 has the lowest (excluding tightly cemented facies 5 and facies 6). Mean permeabilities of all other facies have overlapping 95 % confidence limits about their means (the exception being facies 3, though it only misses overlapping by a very small amount).
- High permeabilities, particularly those in facies 1, 2, and 3, appear to be a function of good sorting, and in the case of facies 1, the absence of stratification. Low permeabilities, especially those in facies 4 (Type 2), facies 7, facies 8, and facies 9, appear to be a function of poor sorting associated with carbonaceous material or silt, bioclasts, and bioturbation. For each facies, the range of permeabilities that cannot be explained by grain size and sorting is likely a function of variable amounts and distributions of cement.

### **5.3 Recommendations for Future Studies**

- Instead of using a grain-size comparator card positioned adjacent to core slabs under a binocular microscope; an ocular micrometer on a petrographic microscope could be used to measure grain sizes. Because there are different levels of magnification on a petrographic microscope, the sizes of very fine-grained sandstones and siltstones would likely be easier to determine. However, difficulty arises when trying to place core slabs on such microscopes.



- Fabric analysis on samples from single pieces of core could be used to distinguish whether or not the planar laminated sandstones of facies 2 were produced under unidirectional or oscillatory flow conditions. Within a single piece of core, the mutual relative orientation of each fabric sample would be known, even if the absolute orientation is not. Similarly, this technique could be applied to the low angle cross-stratified sandstones of facies 3 to determine whether they were produced under purely oscillatory or combined-flow conditions.
- A more comprehensive x-radiography analysis could be undertaken to determine if the structureless intervals (facies 1) are, throughout the core, devoid of stratification.
- More cores from the north, south, and west White Rose pools could be logged and interpreted in a similar manner to that of the A-17 core to confirm or challenge the depositional model, and to evaluate the lateral and vertical continuity of the various reservoir facies.
- Other variables known to have an effect on permeability, particularly cement, should be quantified and incorporated into future studies. This is because grain size in the White Rose A-17 cored interval is not strongly correlated with permeability.
- To evaluate the type(s), spatial distributions(s), and amount of cement, petrographic and/or image analysis techniques could be utilized.
- Thin-sections of core slabs could be cut around the localities of probe permeability measurements. If the position of a permeability measurement on a

thin-section were known, it would greatly enhance the ability to determine what factors control the magnitude of that measurement.

- A suite of logs (e.g. gamma, spectral gamma, neutron-density, resistivity etc.), could be compared visually with vertical permeability profiles and/or statistically with permeability measurements. Correlations might exist which otherwise could not be recognized/determined through a conventional core-based analysis.
- A more in-depth examination of the sorting and its relationship with permeability could be undertaken utilizing thin-sections.

#### **5.4 Implications for the Future Development and/or Exploration of the White Rose Oilfield**

- Results of this study demonstrate that for the White Rose A-17 cored interval, and potentially the White Rose field, a middle to lower shoreface depositional model is appropriate for future development and/or exploration.
- The A-17 cored interval is divisible into three units. The middle unit, which represents depths from ~3018-2945 m, is on average the most permeable of the three units. Reservoir models should incorporate this observation.
- The pervasively calcite-cemented intervals represented by facies 5 and facies 6 have mostly nodular geometries; thus, they are unlikely to be laterally continuous and should not significantly affect the vertical migration of fluids.
- Grain size can be used as a predictor of maximum permeability for given reservoir facies though permeability could be much less. In addition, maximum

permeabilities for each facies differ between the lower, middle, and upper units of the core.

- Most facies have overlapping grain-size versus permeability distributions, hence, the prediction of facies type using grain size and permeability alone is likely not possible.
- Structureless, fine- to predominantly very- fine grained quartzose sandstones of Facies 1 have the highest mean permeability and are the most permeable for any given grain size. A better understanding of the origin and geometry of Facies 1 would be beneficial to production and reservoir modeling teams.

## REFERENCES CITED

- Abbott, J. E., and J. R. D. Francis, 1977, Saltation and suspension trajectories of solid grains in a water stream: *Philosophical Transactions of the Royal Society of London, Series A*, 284, p. 225-254.
- Allen, J. R. L., 1970, *Physical Processes of Sedimentation; an Introduction*: London, Allen & Unwin, 248 p.
- Allen, J. R. L., 1982, *Sedimentary Structures: Their Character and Physical Basis*: New York, Elsevier, v. 1, 594 p., v. 2, 644 p.
- Allen, P. A., 1985, Hummocky cross-stratification is not produced purely under progressive gravity waves: *Nature*, v. 313, p. 562-564.
- Allen, P. A., and J. R. Underhill, 1989, Swaley cross-stratification by unidirectional flows, Bencliff Grit (Upper Jurassic), Dorset, U.K: *Journal of the Geological Society*, v.146, p. 241-252.
- Arnott, R. W. C., Hand, B.M., 1989, Bedforms, primary structures and grain fabric in the presence of suspended sediment rain: *Journal of Sedimentary Petrology*, v.59, p. 1062-1069.
- Arnott, R. W. C., and J. B. Southard, 1990, Exploratory flow-duct experiments on combined-flow bed configurations, and some implications for interpreting storm-event stratification: *Journal of Sedimentary Petrology*, v. 60, p. 211-219.
- Bagnold, R. A., 1973, The nature of saltation and bed-load transport in water: *Proceedings of the Royal Society of London*, v. 332, 473 p.
- Beard, D. C., and P. K. Weyl, 1973, Influence of texture on porosity and permeability of unconsolidated sand: *American Association of Petroleum Geologists Bulletin*, v.57, p. 349-369.
- Bernoulli, D., 1984, Sedimentary evolution of passive margins of Mesozoic Tethys: *American Association of Petroleum Geologists Bulletin*, v.68, 793 p.
- Boggs, S., 1987, *Principles of Sedimentology and Stratigraphy*: New York, MacMillan Publishing Company, 784 p.
- Boggs, S., 2001, *Principles of Sedimentology and Stratigraphy*: Upper Saddle River, Prentice Hall, 726 p.

- Botset, H. G., 1931, The measurement of permeability of porous aluminum discs of water and oils: *Review of Scientific Instruments*, v.2, p.84-95.
- Bouguchwal, L. A., and J. B. Southard, 1990, Bed configurations in steady unidirectional water flows. Part 1. Scale model study using fine sands: *Journal of Sedimentary Petrology*, v.60, p. 649-657.
- Brenchley, P. J., G. Newall, 1982, Storm influenced inner-shelf sand lobes in the Caradoc (Ordovician) of Shropshire, England: *Journal of Sedimentary Petrology*, v. 52, p. 1257-1269.
- Brenchley, P. J., 1985, Storm influenced sandstone beds: *Marine Geology*, v.9, p. 69-396.
- Bromley, R. G., and R. W. Frey, 1974, Re-description of the trace fossil *Gyrolithes* and taxonomic evaluation of *Thalassinoides*, *Ophiomorpha*, and *Spongiomorpha*: *Geological Society of Denmark Bulletin*, v. 23, p. 311-335.
- Cade, C. A., J. Evans, and S. L. Bryant, 1994, Analysis of permeability controls: a new approach: *Clay Minerals*, v.29, p.491-501.
- Chandler, M. A., G. Kocurek, D. J. Goggin, and L. Lake, 1989, Effects of stratigraphic heterogeneity on permeability in eolian sandstone sequence, Page Sandstone, northern Arizona: *American Association of Petroleum Geologists Bulletin*, v. 73, p.658-668.
- Cheel, R. J, 1991, Grain fabric in hummocky-stratified storm beds: genetic implications: *Journal of Sedimentary Petrology*, v. 61. p. 102-110.
- C-NOPB, 2001, Decision 2001.01, Canada-Newfoundland Offshore Petroleum Board, St. John's, 185 p.
- DeSilva, N. R., 1994, "Submarine fans on the northeastern Grand Banks, offshore Newfoundland", *Submarine Fans and Turbidite Systems*, The Fifteenth Annual Research Conference of the Society of Economic Paleontologists and Mineralogists Foundation.
- DeSilva, N. R., 2004, Application of petroleum system logic to Jeanne d'Arc Basin Offshore Newfoundland, in R.H. Hiscott and A. Pulham, eds., *Petroleum Resources and Reserves of the Grand Banks, Eastern Canadian Margin*: Geological Association of Canada, Special Paper 43, p. 1-10.
- Dodge, C. F., D. P. Holler, and R. L. Meyer, 1971, Reservoir heterogeneities of some Cretaceous sandstones: *American Association of Petroleum Geologists Bulletin*, v. 55, p. 1814-1828.

- Dott, R. H. Jr., and J. Bourgeois, 1982, Hummocky stratification: Significance of its variable bedding sequences: *Geological Society of America Bulletin*, v. 93, p. 663-680.
- Duke, W. L., 1985a, Hummocky cross-stratification, tropical hurricanes, and intense winter storms: *Sedimentology*, v. 32, p. 167-194.
- Duke, W. A., W. Arnott, and R. J. Cheel, 1991, Shelf sandstones and hummocky cross-stratification: New insights on a stormy debate: *Geology*, v.19, p. 625-628.
- Driscoll, N. W., and Hogg, J. R., 1995, Stratigraphic response to basin formation; Jeanne d'Arc Basin, offshore Newfoundland, *in* J. J. Lambiase, ed., *Hydrocarbon Habitat in Rift Basins: Geological Society of London Special Publication 80*, p. 145-163.
- Drummond, C.N., and Wilkinson, B.H., 1996, Strata thickness frequencies and the prevalence of orderedness in stratigraphic sequences: *Journal of Geology*, v. 104, p.1-18.
- Dryer, T., A. Scheie, and O. Walderhaug, 1990, Minipermeameter-Based study of permeability trends in channel sand bodies: *American Association of Petroleum Geologists Bulletin*, v. 47, p. 359-374.
- Ehrlich, R., M. C. Bowers, V. L. Riggert, and C. M. Prince, 1997, Detecting permeability gradients in sandstone complexes-quantifying the effect of diagenesis on fabric, *in* J. A. Kupez, J. Gluyas, and S. Bloch, eds., *Reservoir quality prediction in sandstones and carbonates : American Association of Petroleum Geologists Memoir 69*, p. 103-114.
- Enachescu, M. E., 1987, Tectonic and structural framework of the northeast Newfoundland continental margin, *in* C. Beaumont and A.J. Tankard, eds., *Sedimentary Basins and Basin Forming Mechanisms: Canadian Society of Petroleum Geologist Memoir*, v. 12, p. 117-146.
- Enachescu, M. and Dunning, G., 1994, Grand Banks Basin, Canada, *Basin Monitor. Book*, 85 p., 16 figures, published by PetroConsultants, Geneva, Switzerland.
- Ethier, V.G., and H. R. King, 1991, Reservoir quality evaluation from visual attributes on rock surfaces; methods of estimation and classification from drill cuttings or cores: *Bulletin of Canadian Petroleum Geology*, v.39, p. 233-251
- Evans, J., C. Cade, and S. Bryant, 1997, A Geological Approach to Permeability Prediction in Clastic Reservoirs: *in* J. A. Kupez, J. Gluyas, and S. Bloch, eds., *Reservoir quality prediction in sandstone and carbonates: American Association of Petroleum Geologists, Memoir 69*, p .91-101.

- Folk, R.L., and Ward, W.C., 1957, Brazos River Bar: A study in the significance of grain size parameters: *Journal of Sedimentary Petrology*, v. 27, no. 1, p. 3-26.
- Fraser, H. J., 1935, Experimental study of the porosity and permeability of clastic sediments: *Journal of Geology*, v.43, p. 910-1010.
- Frey, R. W., 1990, Trace fossils and hummocky cross-stratification, Upper Cretaceous of Utah: *Palaios*, v. 5, p. 203-218.
- Geikie, A., 1903, *Textbook of Geology*, London, Volume 2, MacMillan Publishing Company.
- Gilluly, J., A. C. Waters, and A. O. Woodford, 1955, *Principles of Geology*: San Francisco, W. H. Freeman & Co.
- Goggin, D. J., 1988, Geologically sensible modeling of the spatial distribution of permeability in eolian deposits: Page Sandstone (Jurassic) northern Arizona: Unpublished Ph.D. dissertation, University of Texas at Austin, Austin, Texas, 417 p.
- Grant, A. C., K. D. McAlpine and J. A. Wade, 1986, The Continental Margin of Eastern Canada: Geological Framework and Petroleum Potential, *in* M. T. Halbouty, ed., *Future Petroleum Province of the World*: American Association of Petroleum Geologists, Memoir 40, p. 177-205.
- Haldorsen, H. H., 1986, Simulation parameter assignment and the problem of scale in reservoir engineering: in *Reservoir characterization*, *in* L. W. Lake and H. B. Carroll Jr., eds., *Reservoir Characterization*: Orlando, Florida, Academic Press, p. 341-372.
- Hamblin, W. K., 1965, Internal Structures of "Homogeneous" sandstones: *Kansas Geological Survey Bulletin*, v. 175, pt. 1, p. 1-37.
- Harding, S., 1988, Facies Interpretation of the Ben Nevis Formation in the North Ben Nevis M-61 Well, Jeanne d'Arc Basin, Grand Banks, Newfoundland, *in* D.P. James, D. A. Leckie, eds., *Sequences, Stratigraphy, Sedimentology : Surface and Subsurface*: Canadian Society of Petroleum Geologists, Memoir 15, p. 291-306.
- Harms, J. C., J. B. Southard, D. R. Spearing, and R. G. Walker, 1975, Depositional environments as interpreted from primary sedimentary structures and stratification sequences: *Society of Economic Paleontologists and Mineralogists Short Course 2*, p. 1-161.
- Harms, J. C., J. B. Southard, and R. G. Walker, 1982, Structures and sequences in clastic rocks: *Society of Economic Paleontologists and Mineralogists short course 9*, 161p.
- Haworth, R. T. and Keen, C. E., 1979, The Canadian continental margin: a passive continental margin encompassing an active past: *Tectonophysics*, v. 59, p. 83-126.



- Hearn, C. L., J. P. Hobson, and M. L. Fowler, 1986, Reservoir characterization for simulation, Hartzog Draw field, Wyoming, *in* L. W. Lake and H. B. Carroll Jr., eds., *Reservoir Characterization*: Orlando, Florida, Academic Press, p. 341-372.
- Hewitt, C. H., and J. T. Morgan, 1965, The fry *in situ* combustion test—reservoir characteristics: *Journal of Petroleum Technology*, v. 13, p. 223-230.
- Hubbard, R. J., J. Pape, and D. G. Roberts, 1985a, Depositional sequence mapping as a technique to establish tectonic and stratigraphic framework and evaluate hydrocarbon potential on a passive continental margin, *in* Berg, O. R. and D. Woolverton, eds., *Seismic Stratigraphy II: An Integrated Approach to Hydrocarbon Exploration*: American Association of Petroleum Geologists Memoir 39, p. 9-91.
- Hunter, R. E., H. E. Clifton, 1982, Cyclic deposits and hummocky cross-stratification of probable storm origin in Upper Cretaceous rocks of the Cape Sebastian area, southwestern Oregon: *Journal of Sedimentary Petrology*, v. 52, p. 127-143.
- Hurst, A., and K. J. Rosvoll, 1991, Permeability variations in sandstones and their relationship to sedimentary structures: *Reservoir Characterization 2*.
- Husky Energy, “White Rose Project” 2004, [<http://www.huskywhiterose.com>] (29 January 2004).
- Jansa, L. F., and J. A. Wade, 1975, Geology of the continental margin off Nova Scotia and Newfoundland: *Geological Survey of Canada Paper* 74-30, p. 51-105.
- Jansa, L. F., P. Enos, B. E. Tucholke, F. M. Gradstein, and R. E. Sheridan, 1979, Mesozoic–Cenozoic sedimentary formations of the North American Basin, western North Atlantic, *in* M. Talwani W. Hay, and W. B. F. Ryan, eds., *Deep Drilling Results in the Atlantic Ocean: Continental Margins and Paleoenvironment*: American Geophysical Union, Maurice Ewing Ser, v. 3, p. 1–57.
- Jenkyns, H. C., 1980, Tethys; past and present: *Proceedings of the Geologists Association*, v.91, Parts 1-2, p. 107-118.
- Jones, J. R., Jr., A. J. Scott, and L. W. Lake, 1985, Reservoir characterization for numerical simulation of Mesaverde Meanderbelt sandstone, northwestern Colorado: *Society of Petroleum Engineers Paper* 13052, p. 1-14.
- Jones, S.C., 1992, The Profile Permeameter: A new, fast, accurate minipermeameter: Paper presented at the 67<sup>th</sup> Annual Technical Conference and Exhibition of the Society of Petroleum Engineers, Washington, DC, October, SPE 24757, p.973-983.



- Keen, C. E., and D. L. Barrett, 1981, Thinned and subsided continental crust on the rifted margin of eastern Canada: crustal structure, thermal evolution and subsidence history: *Geophysical Journal of the Royal Astronomical Society*, v. 65, p. 443–465.
- Keen, C. E., R. Boutilier, B. de Voogd, B. Mudford, and M.E. Enachescu, 1987, Crustal Geometry and extensional models for the Grand Banks of eastern Canada: constraints from deep seismic reflection data, *in* Beaumont, and A. J. Tankard, eds., *Sedimentary Basins and Basin-Forming Mechanisms: Canadian Society of Petroleum Geologists Memoir 12*, p. 101-115
- Kegley, W. A., W. C. Fallaw, D. S. Snipes, S. M. Benson, and V. Price Jr, 1994, Textural factors affecting permeability at the MWD well field, Savannah River Site, Aiken, South Carolina: *Southeastern Geology*, v. 34, p. 139-161.
- Krumbein, W. C., and G. D. Monk, 1942, Permeability as a function of the size parameters of sedimentary particles: *AIME Tech. Pub.* 1432, p. 1-11.
- Kumar, N., and J. E. Sanders, 1976, Characteristics of shoreface storm deposits: modern and ancient examples: *Journal of Sedimentary Petrology*, v. 46, p. 145-162.
- Leckie, D. A., and R. G. Walker, 1982, Storm-and tide-dominated shorelines in Cretaceous Moosebar-Lower Gates interval – outcrop equivalents of deep basin gas trap in western Canada: *American Association of Petroleum Geologists Bulletin*, v. 66, p. 138-157.
- Leckie, D. A., and Krystinik, L. F, 1989, Is there evidence for geostrophic currents preserved in the sedimentary record or inner to middle shelf deposits?: *Journal of Sedimentary Petrology*, v. 59, p. 862-870.
- Lemoine, M., 1983, Rifting and early drifting; Mesozoic Central Atlantic and Ligurian Tethys: *Initial Reports of the Deep Sea Drilling Project*, v. 76, p. 885-89.
- Longwell, C. R., and R. F. Flint, 1962, *Introduction to Physical Geology*: New York, John Wiley & Sons, 504 p.
- MacMillan, J. R., and A. L. Gutjahr, 1986, Geological control on spatial variability for one-dimensional arrays of porosity and permeability normal to layering, *in* L. W. Lake and H. B. Carroll, Jr., eds., *Reservoir Characterization*: Orlando, Florida, Academic Press, p. 265-292.
- Martini, L. P., 1971, Grain size orientation and paleocurrent systems in the Thorold and Grimsby Sandstones (Silurian), Ontario and New York: *Journal of Sedimentary Petrology*, v. 41, p. 425-434.

- Masson, D. G., and P. R. Miles, 1984, Mesozoic sea-floor spreading between Iberia, Europe and North America: *Marine Geology*, v. 56, p. 279-287.
- Mast, R. F., and P. E. Potter, 1963, Sedimentary structures, sand-shape fabrics, and permeability, pt. 2: *Journal of Geology*, v. 71, p. 548-565.
- McAlpine, K. D., 1990, Mesozoic stratigraphy, sedimentary evolution and petroleum potential of the Jeanne d'Arc basin, Grand Banks of Newfoundland: *Geological Survey of Canada Paper* 89-17, 50 p.
- McWhae, J. R. H., 1981, Structure and spreading history of the northwestern Atlantic region from the Scotian Shelf to Baffin Bay, *in* J. W. Kerr and A. J. Ferguson, eds., *Geology of the North Atlantic Borderlands*: Canadian Society of Petroleum Geologists Memoir 7, p. 299-332.
- Mobil Oil Canada, 1981, Well History Report, Mobil et al., Ben Nevis 1-45.
- Muskat, M., and H. G. Botset, 1931, Flow of gas through porous materials: *Physics*, v.1, p.27-47.
- Muskat, M., 1937, "Flow of homogeneous fluids through porous media." New York, McGraw-Hill.
- Nichols, G. A., 1999, *Sedimentology and Stratigraphy*: Oxford, Blackwell Science, 355 p.
- Nottvedt, A., and R. D. Kresia, 1987, Model for the combined-flow origin of hummocky Cross-stratification: *Geology*, v. 15, p. 357-361.
- Pemberton, S. G. and R. W. Frey, 1984, Ichnology of storm-influenced shallow marine sequence: Cardium Formation (Upper Cretaceous) at Seebe, Alberta: *in* D. F. Stott and D. L. Glass eds., *The Mesozoic of Middle North America* :Canadian Society of Petroleum Geologists, Memoir 9, p. 281-304.
- Pemberton, S. G., J. A. MacEachern and R. E. Frey, 1992a, Trace fossil facies models: environmental and allostratigraphic significance: *in* R. G. Walker and N. P. James, eds., *Facies Models: Response to Sea Level Change* : Geological Association of Canada, Geo- text 1, p. 47-72.
- Pemberton, S. G., M. V. Spila, A. J. Pulham, T. Saunders, J. A. Maceachern, D. Robbins, and I. Sinclair, 2001, Ichnology and sedimentology of shallow and marginal marine systems: Ben Nevis and Avalon reservoirs, Jeanne D'Arc Basin: *Geological Association of Canada Short Course Notes* 15, 353 p.

- Pettijohn, F., 1957, *Sedimentary Rocks* 2<sup>nd</sup> ed: New York, Harper and Brothers, 718p.
- Plint, A.G., 1999, Husky et al White Rose A-17: Preliminary core description and revised stratigraphy for the White Rose area, Jeanne d'Arc Basin, offshore Newfoundland: Confidential report for Husky Oil Operations Ltd., 25 p.
- Potter, P. E., and F. J. Pettijohn, 1977, *Paleocurrents and basin analysis*: New York, Second Edition, Springer-Verlag, 425 p.
- Pryor, W. A., 1973, Permeability-porosity patterns and variations in some Holocene sand bodies: *American Association of Petroleum Geologists Bulletin*, v. 57, p. 162-189.
- Reinson, G. E., 1984, Barrier-island and associated strand-plain systems: *in* R.G. Walker ed., *Facies Models*, Second Edition: Geoscience Canada, Reprint Series 1, Geological Association of Canada, p. 119-140.
- Selly, R. C., 1988, *Applied Sedimentology*: London, Academic Press, 446 p.
- Selly, R. C., 1998, *Elements of Petroleum Geology*: London, Second Edition, Academic Press, 470 p.
- Shelton, J. W., and D. E. Mack, 1970, Grain orientation in determination of paleocurrents and sandstone trends: *American Association of Petroleum Geologists*, v. 54, p. 1108-1119.
- Shepard, R. G., 1989, Correlations of permeability and grain size: *Groundwater*, v. 27, p. 633-638.
- Simpson, S., 1957. On the trace fossil *Chondrites*: *Quarterly Journal Geological Society of London*, 112: 475-499.
- Sinclair, I. K., K. D. McAlpine, D.F. Sherwin, N. J. McMillan, G. C. Taylor, M. E. Best, G. R. Campell, J. P. Hea, D. Henao and R. M. Procter, 1992, Petroleum resources of the Jeanne d'Arc basin and environs, Grand Banks, Newfoundland: Geological Survey of Canada Paper 92-8, 48 p.
- Sinclair, I. K., 1995a, Sequence stratigraphic response to Aptian-Albian rifting in conjugate margin basins: a comparison of the Jeanne d'Arc basin, offshore Newfoundland and the Porcupine Basin, offshore Ireland, *in* R.A. Scrutton, M.S.
- Southard, J. B., J. M. Lambie, D. C. Federico, H. T. Pile, and C. R. Weidman, 1990, Experiments on bed configurations in fine sands under bi-directional purely oscillatory flow, and the origin of hummocky cross-stratification: *Journal of Sedimentary Petrology*, v. 60, p. 1-17.

- Srivastava, S. P., and C. R. Tapscott, 1986, Plate kinematics of the North Atlantic, *in* P. R. Vogt and B.E. Tucholke, eds., *The Geology of North America, Volume M. The western North Atlantic region*: Geological Society of America, Boulder, Colorado, USA, p.379-404.
- Stalkup, F. I., and W. J. Ebanks, 1986, Permeability variation in a sandstone barrier island-tidal channel-tidal delta complex, Ferron Sandstone (Lower Cretaceous), central Utah: Society of Petroleum Engineers Paper 15532, 13 p.
- Storetvedt, K. M., 1985, The pre-drift central Atlantic; a model based on tectonomagmatic and sedimentological evidence: *Journal of Geodynamics*, v. 2, p. 275-290.
- Swift, D. J. P., A. G. Figueiredo, G. L. Freeland, and G. F. Oertel, 1983, Hummocky cross-stratification and megaripples: A geological double standard? : *Journal of Sedimentary Geology*, v. 53, p. 1295-1317.
- Swift, D. J. P., P. M. Hudelson, R. L. Brenner, and P. Thompson, 1987, Shelf construction in a foreland basin: storm beds, shelf sandbodies, and shelf-slope depositional sequences in the Upper Cretaceous Mesaverde Group, Book Cliffs, Utah: *Sedimentology*, v. 34, p. 423-457.
- Tankard, A. J., and H. J. Welsink, 1987, Extensional tectonics and stratigraphy of the Hibernia oil field, Grand Banks, Newfoundland: *American Association of Petroleum Geologists Bulletin*, v. 71, p. 1210-1232.
- Tucholke, B. E., J. A. Jr. Austin, and E. Uchupi, 1989, Crustal structure and rift-drift evolution of the Newfoundland Basin, *in* A. J. Tankard and H. R. Balkwill, eds., *Extensional tectonics and stratigraphy of the North Atlantic Margin*: American Association of Petroleum Geologists Memoir 46, p. 247-263.
- Von Rad, U., 1971, Comparison between 'magnetic' and sedimentary fabric in graded and cross-laminated sand layers, Southern California: *Geologische Rundschau*, v. 60, p. 331-354.
- Wade, J. A., 1981, Geology of the Canadian Atlantic margin from Georges Bank to the Grand Banks, *in* J.W. Kerr and A.J. Fergusson, eds., *Geology of the North Atlantic Borderlands*: Canadian Society of Petroleum Geologist Memoir 7, p. 447-460.
- Walker, R. G., W. L. Duke, D. A. Leckie, R. H. Jr. Duke, and J. Bourgeois, 1983, Hummocky stratification; significance of its variable bedding sequences; discussion and reply: *Geological Society of America Bulletin*, v. 94, p. 1245-1251.

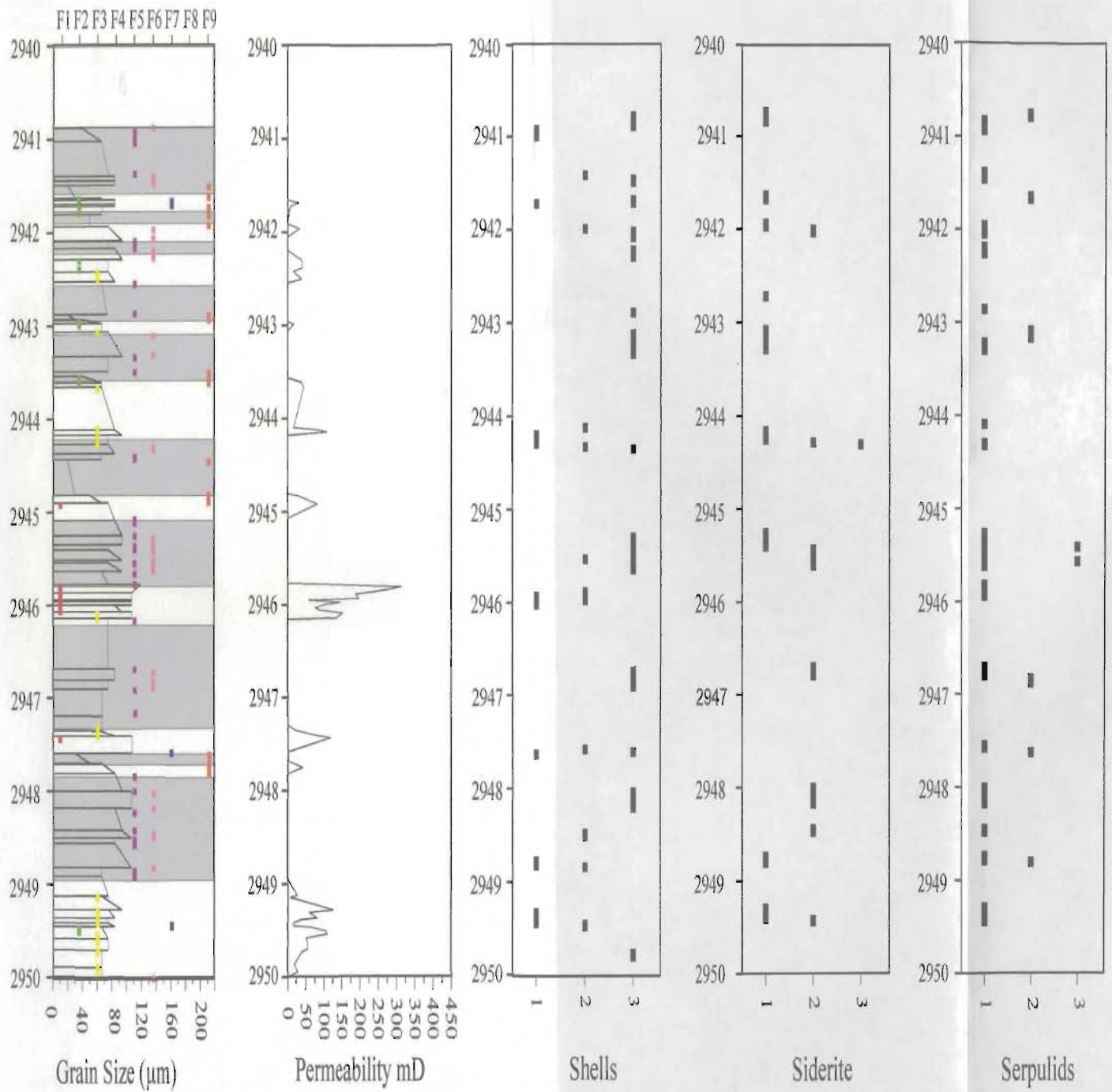
- Walker, R. G., and N. P. James, eds., 1992, *Facies Models: Response to Sea Level Change*: Geological Association of Canada, Geotext 1, 409 p.
- Weber, K. G., 1982, Influence of common sedimentary structures on fluid flow in reservoir models: *Journal of Petroleum Technology*, v.34, p. 665-672.
- Weber, K. J., 1986, How heterogeneity affects oil recovery, *in* L.W. Lake and H.B. Carroll, Jr., eds., *Reservoir Characterization*: Orlando, Florida, Academic Press, p. 487-544.
- Yagishita, K., S. Arakawa, A. Taira, 1992, Grain fabric of hummocky and swaley cross-stratification: *Sedimentary Geology*, v. 78, p. 181-189.
- Yokokawa, M., 1995, Combined-flow ripples: genetic experiments and applications for geologic records: Kyushu University, Faculty of Science, *Memoirs, Series D: Earth and Planetary Sciences*, v. 29, p. 1-38.

#### APPENDIX A

CD with Excel File of the White Rose A-17 Core Sedimentological and Permeability  
Data- Back Cover of Thesis

## APPENDIX B

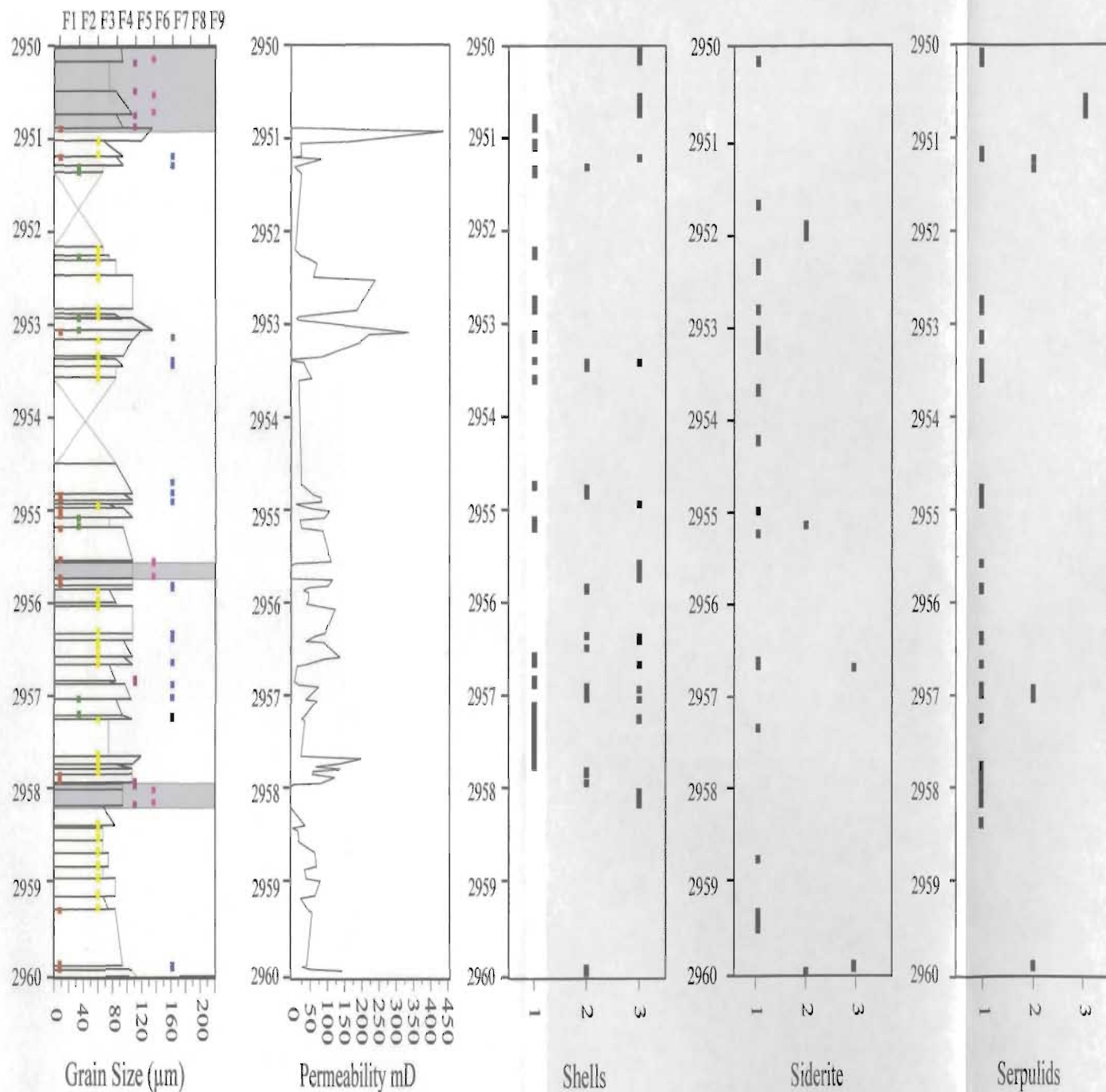
### Logs with Sedimentological and Permeability Data



From left to right, logs displaying grain size, position of facies, permeability, and the abundance of shells (fragments), siderite (authigenic), and serpulid worm tubes (fragments) for the interval between 2950-2940 m, White Rose A-17 core.

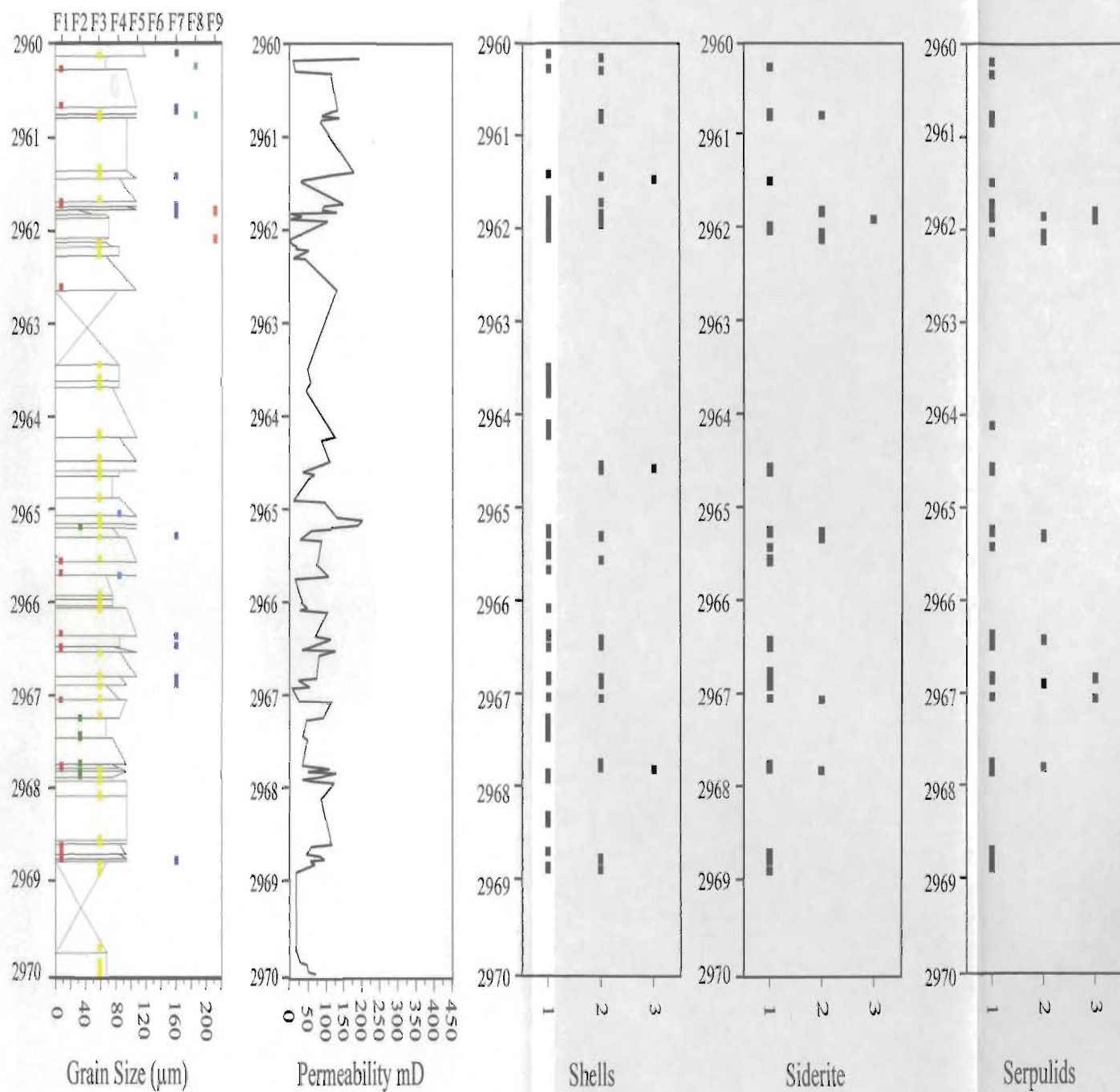
Scale 15mm = 1m





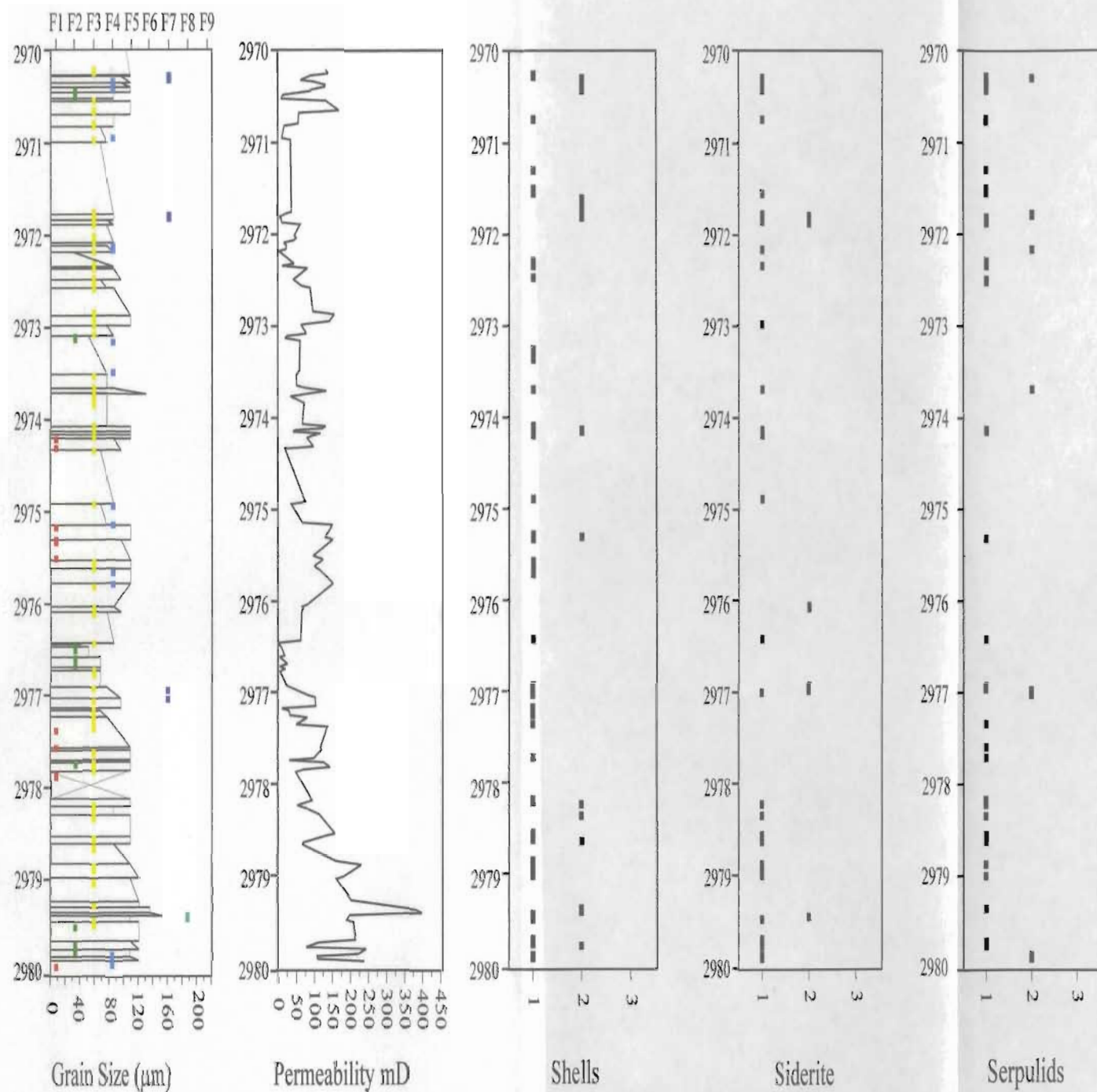
From left to right, logs displaying grain size, position of facies, permeability, and the abundance of shells (fragments), siderite (authigenic), and serpulid worm tubes (fragments) for the interval between 2960-2950 m, White Rose A-17 core.

Scale 15mm = 1m



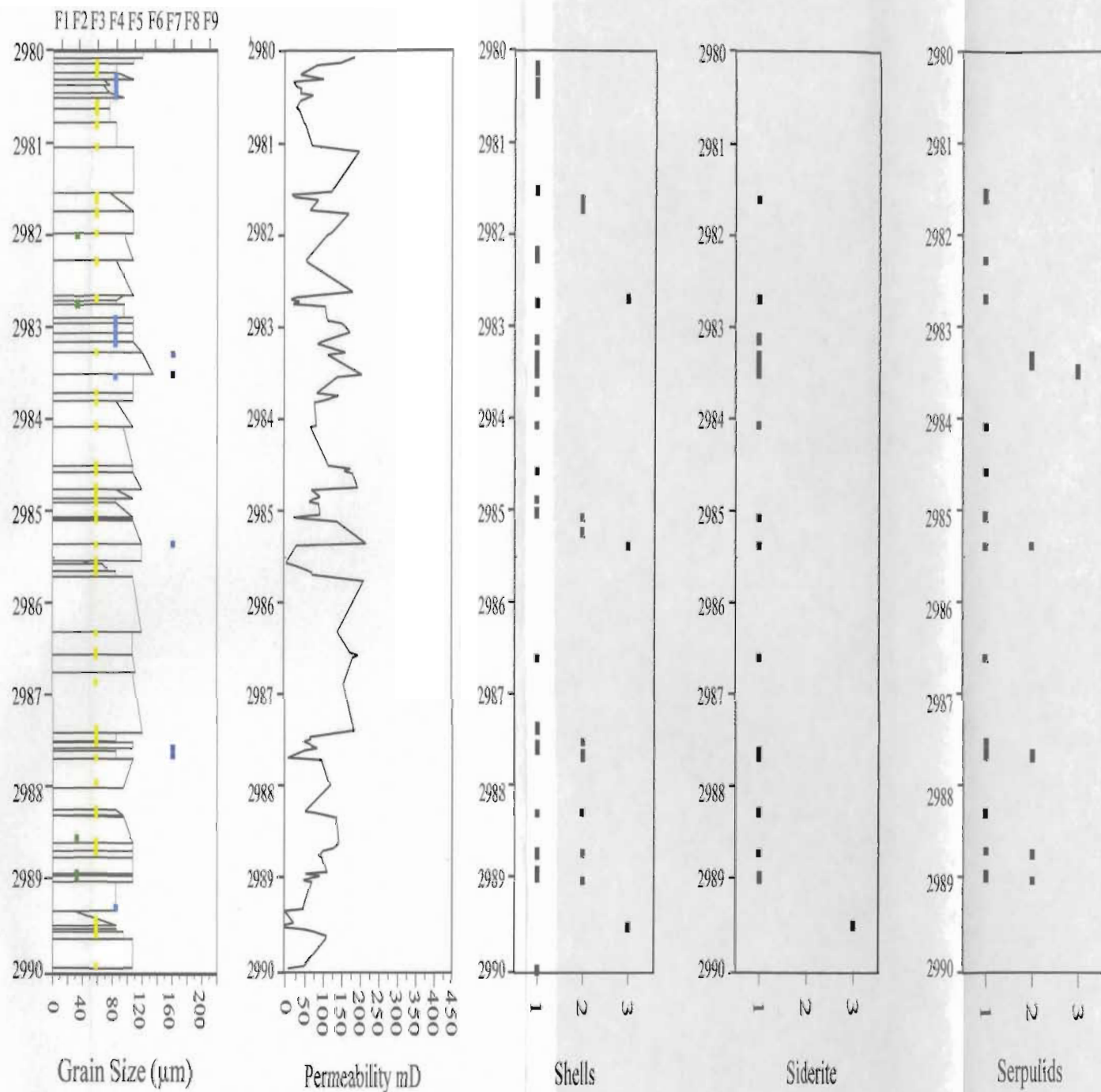
From left to right, logs displaying grain size, position of facies, permeability, and the abundance of shells (fragments), siderite (authigenic), and serpulid worm tubes (fragments) for the interval between 2970-2960 m, White Rose A-17 core.

Scale 15mm = 1m



From left to right, logs displaying grain size, position of facies, permeability, and the abundance of shells (fragments), siderite (authigenic), and serpulid worm tubes (fragments) for the interval between 2980-2970 m, White Rose A-17 core.

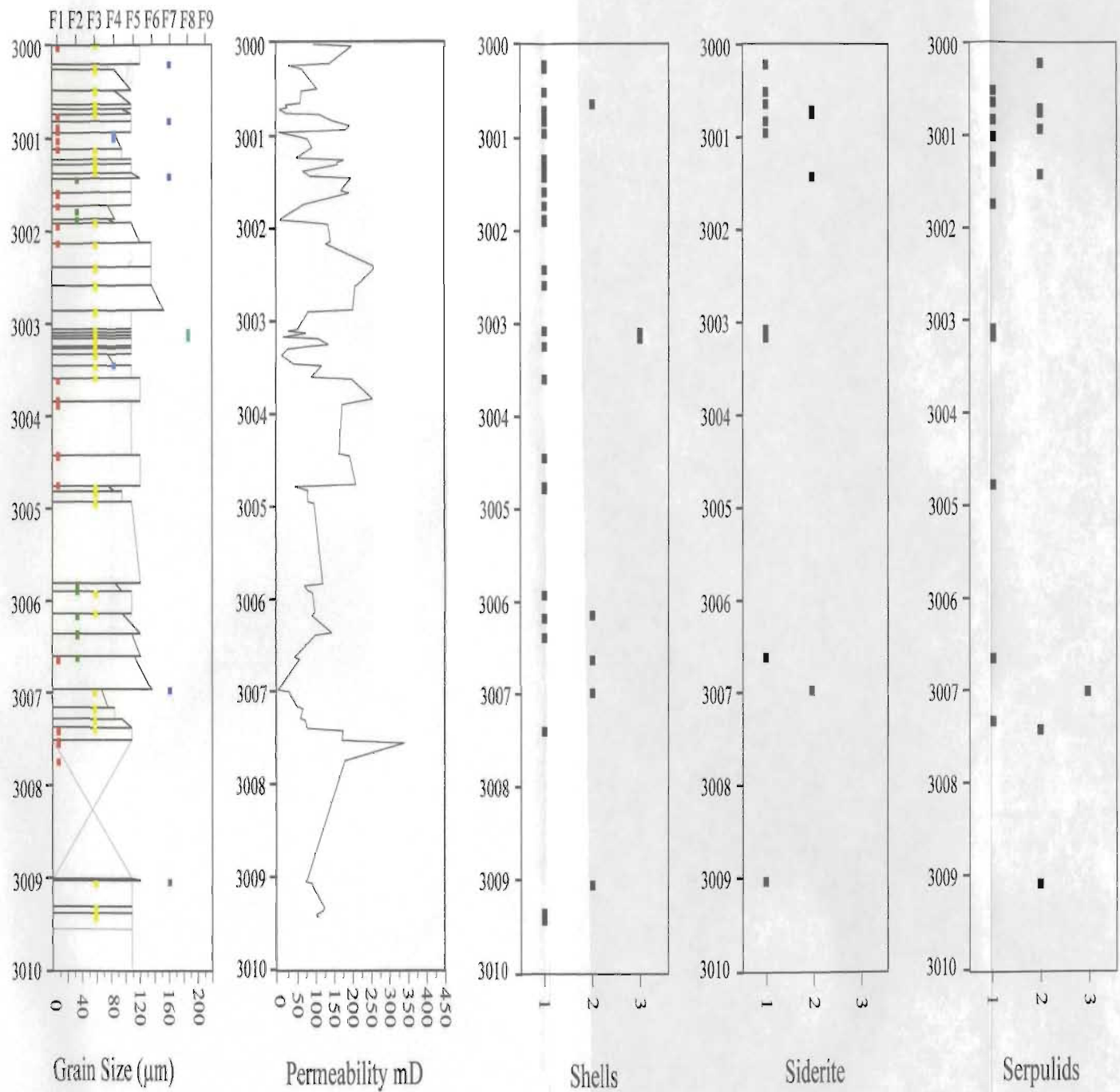
Scale 15mm = 1m



From left to right, logs displaying grain size, position of facies, permeability, and the abundance of shells (fragments), siderite (authigenic) and serpulid worm tubes (fragments) for the interval between 2990-2980 m, White Rose A-17 core.

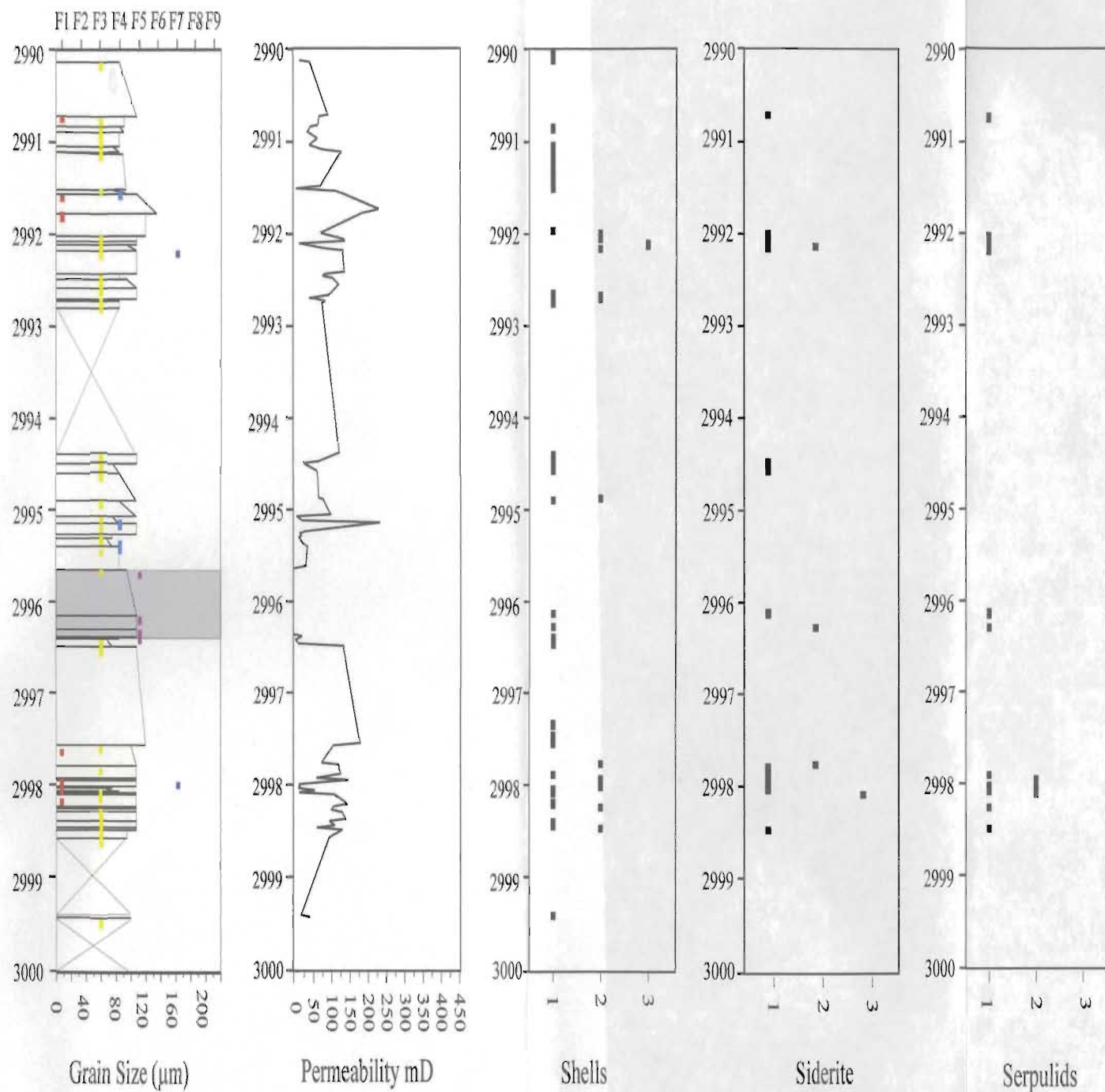
Scale 1.5mm = 1m





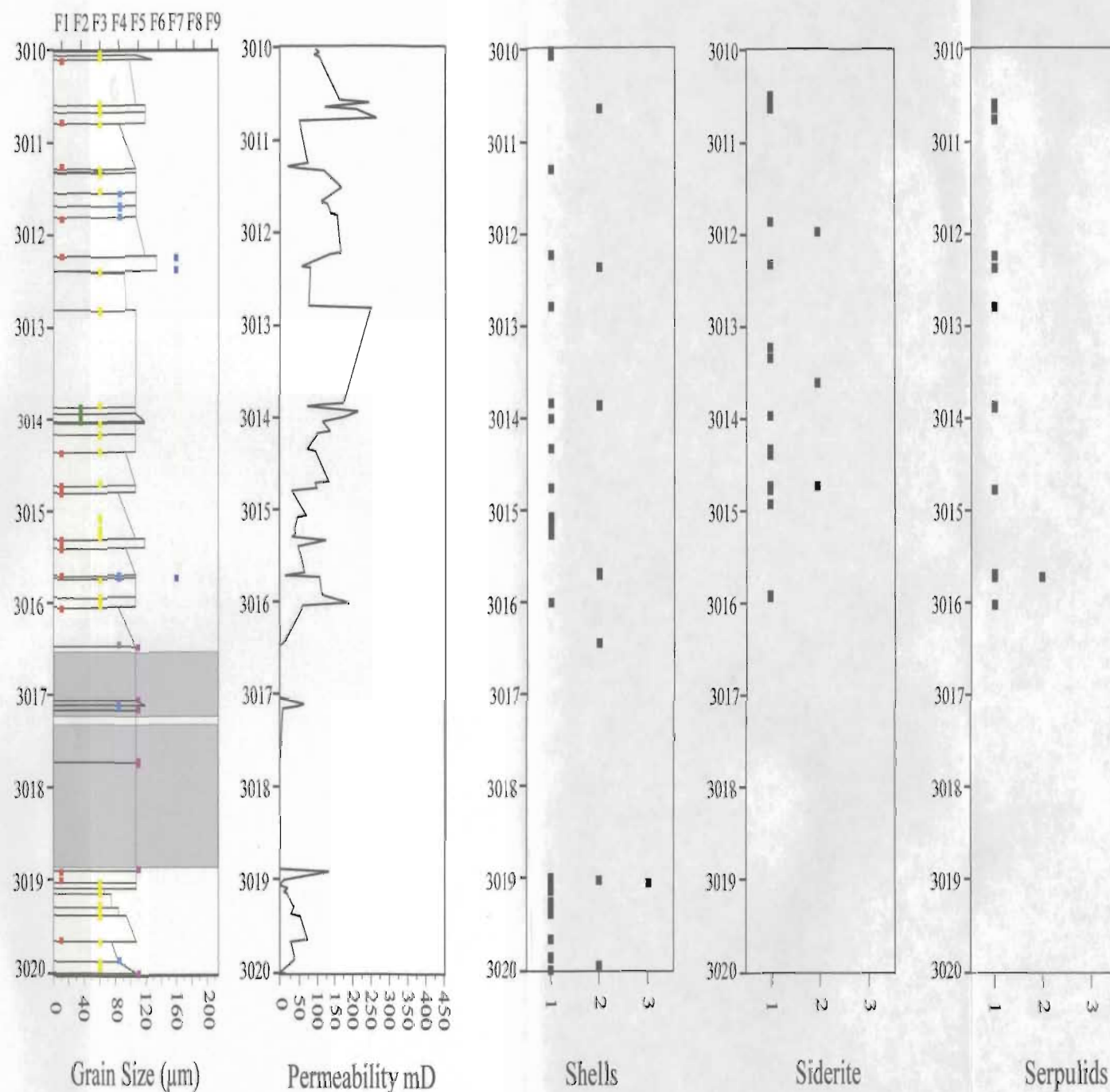
From left to right, logs displaying grain size, position of facies, permeability, and the abundance of shells (fragments), siderite (authigenic), and serpulid worm tubes (fragments) for the interval between 3010-3000 m, White Rose A-17 core.

Scale 15mm = 1m



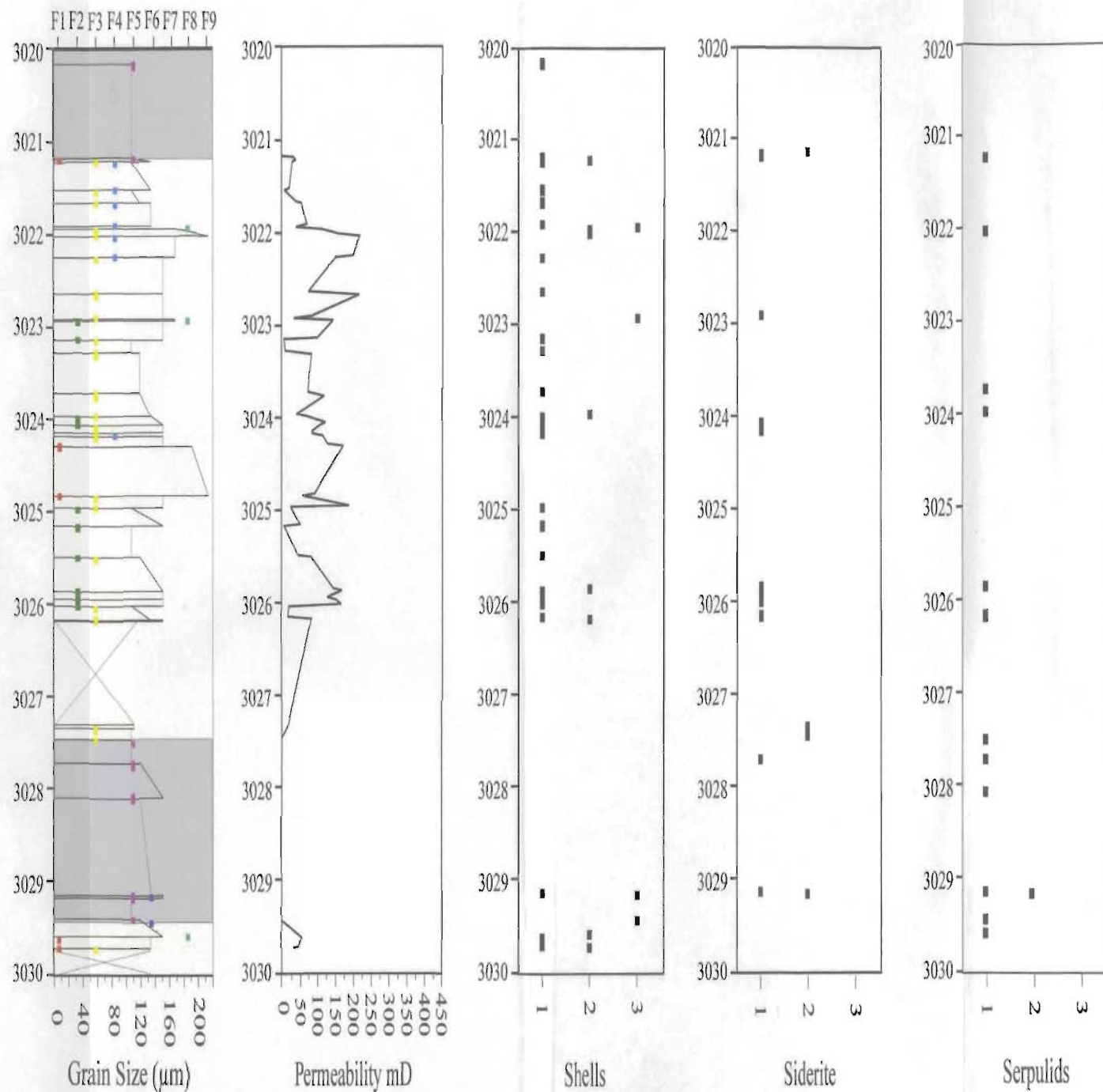
From left to right, logs displaying grain size, position of facies, permeability, and the abundance of shells (fragments), siderite (authigenic), and serpulid worm tubes (fragments) for the interval between 3000-2990 m, White Rose A-17 core.

Scale 15mm = 1m



From left to right, logs displaying grain size, position of facies, permeability, and the abundance of shells (fragments), siderite (authigenic), and serpulid worm tubes (fragments) for the interval between 3020-3010 m, White Rose A-17 core.

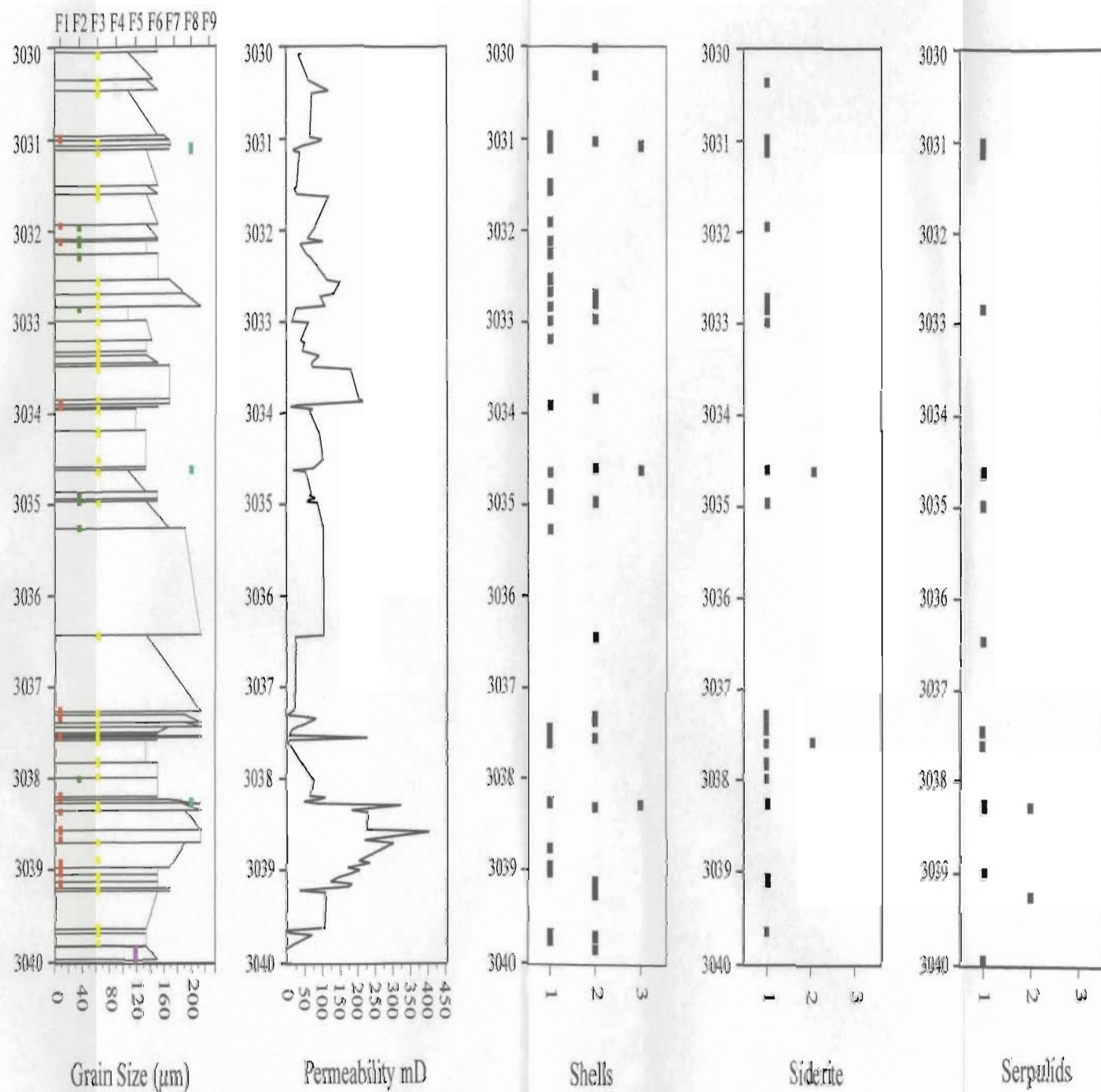
Scale 15mm = 1m



From left to right, logs displaying grain size, position of facies, permeability, and the abundance of shells (fragments), siderite (authigenic), and serpulid worm tubes (fragments) for the interval between 3030-3020 m, White Rose A-17 core.

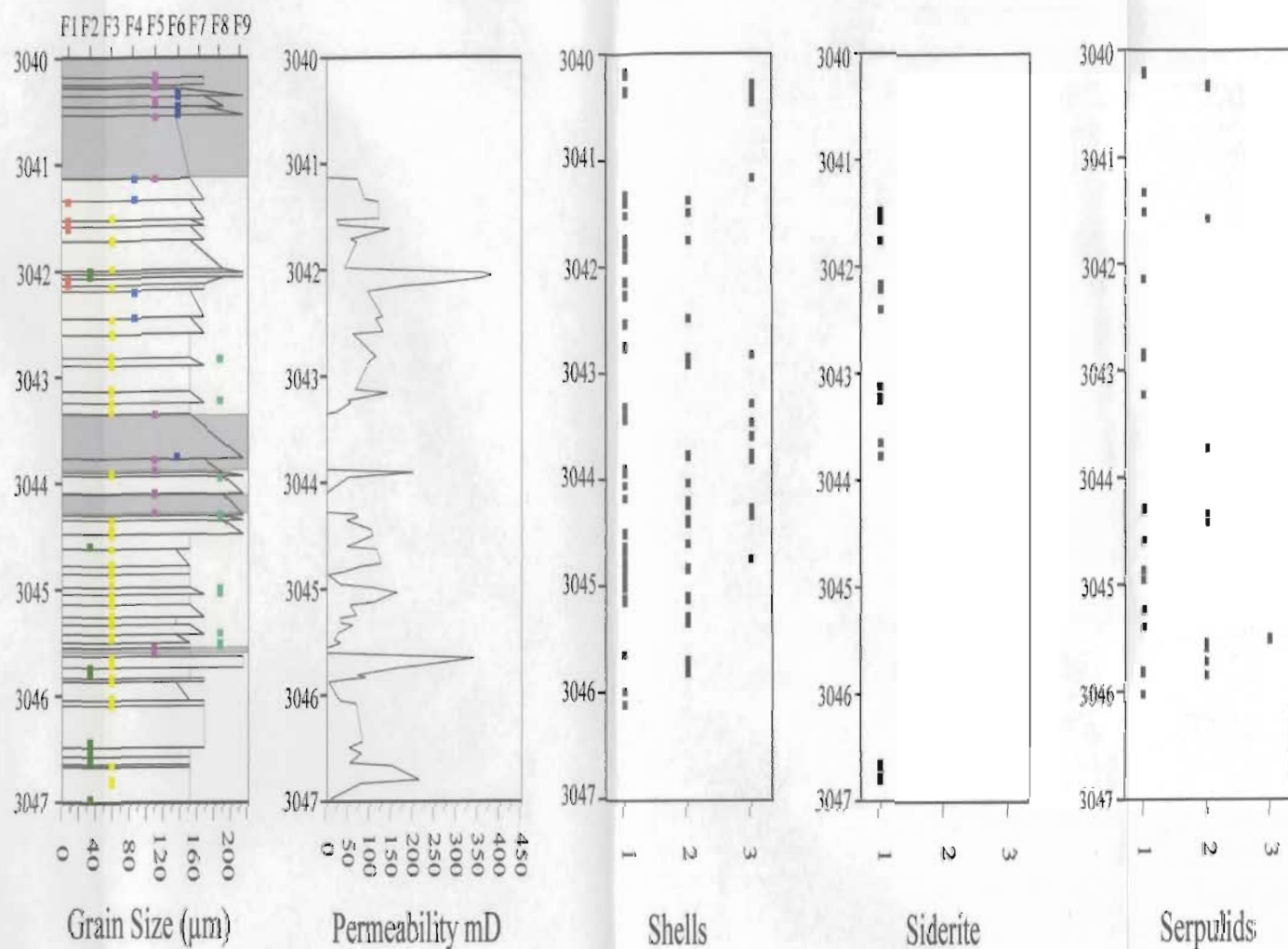
Scale 15mm = 1m





From left to right, logs displaying grain size, position of facies, permeability, and the abundance of shells (fragments), siderite (authigenic), and serpulid worm tubes (fragments) for the interval between 3040-3030 m, White Rose A-17 core.

Scale 15mm = 1m



From left to right, logs displaying grain size, position of facies, permeability, and the abundance of shells (fragments), siderite (authigenic), and serpulid worm tubes (fragments) for the interval between 3047-3040 m, White Rose A-17 core.

Scale 15mm = 1m









